Modular Approach for Characterizing and Modeling Conducted EMI Emissions in Power Converters

Qian Liu

Dissertation submitted to the Faculty of the
Virginia Polytechnic Institute and State University
in partial fulfillment of the requirements for the degree of

Doctor of Philosophy
in
Electrical Engineering

APPROVED:

Dushan Boroyevich, Co-Chairman

Fei Wang, Co-Chairman

Jacobus Daniel van Wyk

Yilu Liu

Guo-Quan Lu

Nov. 10, 2005
Blacksburg, Virginia

Key Words: Modular-Terminal-Behavioral (MTB), Electromagnetic Interference (EMI), Conducted EMI, EMI modeling, EMI Generation, EMI Source, Common-mode (CM), Differential-mode (DM)

Modular Approach for Characterizing and Modeling Conducted EMI Emissions in Power Converters

Qian Liu

Abstract

With the development of power electronics, electromagnetic interference (EMI) and electromagnetic compatibility (EMC) issues have become more and more important for both power converter designers and customers. This dissertation studies EMI noise emission characterization and modeling in power converters.

A modular-terminal-behavioral (MTB) equivalent EMI noise source modeling approach is proposed. This work is the first to systematically develop a 3-terminal EMI noise source model for a switching phase-leg device module. Each module is modeled as pairs of equivalent noise current sources and source impedances. Although the proposed MTB modeling approach applies the linear circuit theory to a semiconductor switching device, which exhibits nonlinear behavior during switching transients, the analysis and experiments show that the nonlinearity has negligible practical effect on the modeling methodology. The validation range of the modeling methodology has been analyzed.

One of the differences between the proposed MTB model and the other state-of-the-art models is that the MTB model characterizes and predicts the CM and DM noise simultaneously. The inseparable high-frequency CM and DM noise characteristics contributed by the source impedance and propagation path are analyzed. A comprehensive evaluation of different EMI noise source modeling approaches according to the criteria of accuracy, feasibility and generality has been presented. Results show that the MTB modeling approach is more accurate, feasible and general than other approaches.

The modular and terminal characteristics of the MTB noise source model are verified in two more complicated cases. One example is the application of the MTB equivalent

source model in a half-bridge AC converter with variable switching conditions. Although the MTB model is derived under a certain operating condition, the models under different conditions can be combined together to predict the EMI noise for the converter with variable switching conditions. Another example is the application of the MTB equivalent source model in multi-phase-leg converters. The EMI noise of a full-bridge converter is predicted based on the MTB equivalent source model of one phase-leg module. The implementation procedures and results for both applications are verified by the experiment. The applicability of the MTB model in different type of converters is discussed.

Based on the MTB model, EMI noise management is explored. The parametric study based on the MTB model is demonstrated by selecting DC-link decoupling capacitors for voltage source converter (VSC). The EMI effect of a decoupling capacitor for a device's safe operation is analyzed, and this analysis shows the terminal characteristics of the MTB model. Both the EMI and voltage overshoot are predicted by the MTB model. A completed converter-level EMI model can be derived based on the noise source model and propagation path model. This model makes it possible to optimize the EMI filter design and study the EMI noise interactions between converters in a power conversion system.

Acknowledgements

I owe an enormous debt of gratitude to my advisors, Dr. Dushan Boroyevich and Dr. Fei Wang, for their support, guidance and encouragement during my study. Their profound knowledge, masterly creative thinking, and consistent encouragement have been my source of inspiration through this work. The most important things I have learned from them are motivation and leadership. Their gentle personalities and rigorous attitude toward research will benefit my career as well as my personal life. I am very lucky to have both professors to mentor me during my time in CPES.

I would like to express my appreciation to my committee member, Dr. van Wyk, who is such an elegant and admirable professor. I enjoyed each meeting and always learned more aspects of power electronics from him. I would also like to thank my other committee members Dr. Yilu Liu and G. Q. Lu for always helping and encouraging me.

I would also like to thank all my colleagues in CPES. Their help, mentorship, and friendship provided a base for the accomplishment of the work. I cherish the wonderful time that we worked together. My life would not have been enjoyable without my friends in CPES. Although this is not a complete list, I must mention some of those who made valuable input to my work. They are Luisa Coppola, Dr. Shuo Wang, Bing Lu, Dr. Wei Dong, Dr. D. Y. Chen, Dr. Rengang Chen, Liyu Yang, Wei Shen, Pengju Kong, and so many others.

I would like to thank the administrative staff members, Marianne Hawthorne, Robert Martin, Teresa Shaw, Trish Rose, Elizabeth Tranter, Michelle Czamanske, Dan Huff, who always smiled at me and helped me to get things done smoothly. Thanks also go to Keara Axelrod, who polished all my publications, including this dissertation.

Special thanks must go to my American host, Jane Maclachlan, who always helped me in different ways, shared many thoughts about the life with me and treated me like her granddaughter and friend. She truly enriched my life in Blacksburg, and beyond.

Nothing can express my gratitude to my family. My dear Dad and Mom always encourage, care for, and support me. I am so proud to be their daughter. I must also thank my sister for supporting me and believing I can finish this work from the first day I came to the US. Deep in my heart are special thanks to my husband Jian for his continuous love, encouragement, understanding and sacrifice. I could not have made all this happen without my family.

This work is primarily supported by the National Science Foundation under Award Number EEC-9731677.

To my husband Jian
and
father Renhui & mother Qiying

Table of Contents

Table of Figures

List of Tables

Chapter 1 Introduction

This chapter starts with the background of conducted electromagnetic interference (EMI) issues in power converters. The state-of-the-art conducted EMI research in power electronics is reviewed. The motivation and objectives of this research work are presented. Finally, an outline of the dissertation is given.

1.1. Background

Electromagnetic interference (EMI) is any electromagnetic disturbance that interrupts, obstructs, or otherwise degrades or limits the effective performance of electronics or electrical equipment [1], [2]. Adopting the practice of electromagnetic compatibility (EMC) controls the effects of EMI. This is defined as "the ability of a device, unit of equipment or system to function satisfactorily in its electromagnetic environment without introducing intolerable electromagnetic disturbances to anything in that environment" [3]. From the point of view of electromagnetic energy transfer, there are four aspects of the EMC problem: conducted emissions, radiated emissions, conducted susceptibility, and radiated susceptibility. The first two aspects describe the ability of electrical and electronic systems to operate without interfering with other systems; the last two describe the ability of such systems to operate as intended within a specified electromagnetic environment. In this dissertation, the conducted EMI emission is the main concern.

Conducted EMI emission is often defined as undesirable electromagnetic energy coupled out of an emitter or into a receptor via any of its respective connecting wires or cables, as shown in Figure 1-1. The source generates the EMI noise, and a coupling path transfers the noise to a receiver through cables or wires. There are three basic ways to prevent interference:

- Suppress the emission at its source.
- Make the coupling path as inefficient as possible
- Make the receptor less susceptible to the emissions.

Figure 1-1 Conducted EMI Emission Illustration

With the continually increasing use of power converters, the resulting electromagnetic inference (EMI) noise is a concern for both power converter designers and consumers. The EMI noise management of converters should be done in order to comply with stringent electromagnetic compatibility (EMC) regulations [4] - [6]. Different EMI standards or regulations exist in different countries. There are three major standards-making bodies: the International Electrotechnical Commission (IEC), the Federal Communications Commission (FCC) in the United States, and the European Committee for Electrotechnical Standardization (CENELEC) and the European Telecommunications Standards Institute (ETSI) in European countries. There are two IEC technical committees devoted full time to EMC work: TC77, who study electromagnetic compatibility between equipment, including networks, and the International Special Committee on Radio Interference (CISPR). The major output of TC77 is various parts of IEC Publication 61000. CISPR publications deal with the limits and measurement of radio interference characteristics or potentially disturbing sources. As of this writing, CISPR publications will continue to co-exist with IEC 61000.

The main basic international standards for conducted emission are listed in Table 1-1. In United States, the limits of conducted EMI noise emissions are based on measuring equipment employing a CISPR quasi-peak detector function. But the emission levels and frequency ranges are different from CISPR, as shown in Figure 1-2 [5]. Another important group of EMI specifications are those issued by the U.S. Department of

Defense (DOD). The testing requirements and limits are contained in MIL-STD-462 and MIL-STD-461 [6].

Table 1-1 International Conducted Emission

Frequency Range: • Band A (9 kHz to 150 kHz), limits only for lighting equipment • Band B (150 kHz to 30 MHz)
Instrumentation and sites (according to CISPR 16-1 standard): • Measuring receiver (quasi-peak and average detectors) • Artificial mains network (LISN) • Voltage probe • Shielded chamber
Main basic standards: • CISPR11, CISPR14, CISPR 15, CISPR22 (standards give information concerning EUT configuration and general measurement conditions)

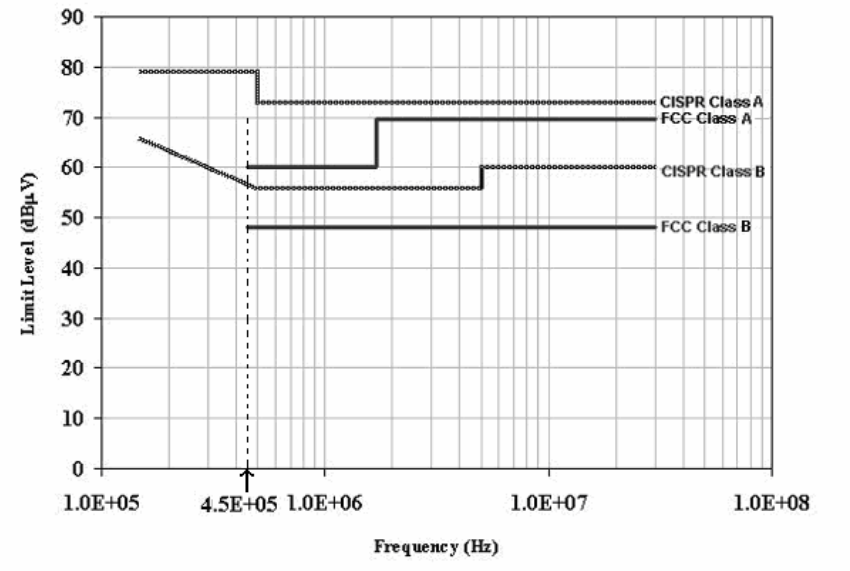

Figure 1-2 Conducted EMI Standards of FCC and CISPR

1.2. Literature Review

The proliferation of power electronics products with fast-switching semiconductor devices has led to concerns and regulation over their generation of electromagnetic interference (EMI) noise. First of all, an accurate EMI noise source model is needed for EMI noise management in converters. EMI management is required in order to comply with EMC standards. EMI suppression components, such as EMI filters, are often necessary additions to power electronics products. Because there are no EMI noise emission models of converters at the design stage, filters usually have to be designed and fine-tuned after converters have been built, which can often lead to a long design cycle and less-than-optimal system designs. Secondly, the state-of-the-art modeling research is still focusing on converters in different applications. But in a large power conversion system, there are multiple power electronic converters with different EMI noise sources. A general modeling approach is desirable for modeling different EMI noise sources in the system. To this end, a hierarchical, modular, standard concept has been introduced in power electronics to efficiently design power conversion systems in the last 20 years [7] - [9]. However, the concept has not been applied in system-level EMI mitigation design. Finally, converter-level solutions for system-level EMI are often inefficient and can be even ineffective due to the lack of consideration of interactions in systems. Understanding and characterizing complex EMI phenomena through accurate converters' EMI noise emission models is a necessary first step for achieving an efficient filtering solution and for effectively managing the EMI/EMC issue in power conversion system. Therefore, it is necessary to review the-state-of-the-art EMI emission modeling first.

There are many criteria for comparing different EMI modeling methodologies. In this dissertation, evaluating different methodologies of EMI modeling and prediction for power converter systems includes the following primary considerations:

1) Accuracy - Since all the EMI management is carried out after predicting the EMI noise level and frequency range based on derived models, such as filter design [10] -[15] and system geometry design, accurate EMI modeling is a key factor. Modeling accuracy of both magnitude and frequency should be

considered because there are different aspects to control and reduce EMI noise level in different frequency ranges.

2) Feasibility - In the last twenty years, different EMI models have been derived for power converters, such as PFC circuits, motor drives and DC-DC converters [16] - [18]. Some of the EMI models are difficult to use because of their complexity. Therefore, the feasibility of EMI models is important for modeling EMI issues in large power conversion systems.

3) Generality - Due to different applications, some of the existing EMI modeling methods are only valid for specific applications. In order to characterize and manage EMI noise in a large converter system, which includes various converters, a generic modeling methodology is indispensable.

The basic EMI modeling process includes two steps: 1) Model EMI noise propagation, 2) Model EMI noise generation.

1.2.1 Modeling of Conducted EMI Noise Propagation

In the EMI modeling process, all connections between the noise receiver and the noise source are considered possible noise propagation paths. The paths could be cables, wires, PCB traces, magnetic components, capacitors, and their parasitics. Research efforts [15], [17] and [19] - [33] have been reported on modeling paths. They can be classified as two approaches: 1) Theoretical models [15], [17], [19] - [24], and 2) Experimental models [25] - [33].

The concept of a theoretical model is to solve Maxwell equations by a known physical structure, material property and geometry information. Finite element analysis (FEA) is one of the most widely-used methods. Now commercial software is available to simulate parasitics [17], [24], [26], such as Ansoft Maxwell Q3D, Maxwell 2D, etc. Some literature, including [19] - [21] and [23], also has simulations of propagation paths based on the partial element equivalent circuit (PEEC) method. The advantage of the theoretical method is that it can obtain path parameters before the entire propagation path

is built up. However, some of the components' characteristics are very complex and need not be simulated. For example, a commercial electrolytic capacitor is very difficult to simulate by users because of its chemical mechanisms. However, its impedance characteristics are relatively simple to measure accurately with instruments.

The other path modeling method used to determine EMI noise propagation is the experimental approach. This includes measuring individual component parameters [26] - [30] and path network characteristics [15], [25] and [31] - [33]. For individual component measurement, the experimental approach gives clear physical characteristics of components, but it is not easy to measure relatively small parasitics, such as the impedance of a screw and a connector. The propagation path can also be modeled as multi-port networks. Measuring path networks can avoid large errors when measuring small parasitics. However, it may not directly give clear insight of the causes of resonances in the network. For the above experimental method, the impedance analyzer can be a useful tool. There is also other equipment based upon different measuring principles used to measure components' parameters [26]. Another such experimental method used is a kind of injection method [33]. It is similar to the measurement of the path network, but the injection source is switching devices instead of equipment. This method can characterize some large signal effects.

In summary, the above path modeling methods described above provide adequate means to obtain noise propagation characteristics. The theoretical and experimental methods can be used together or separately. The choice of which modeling method to use depends on the design and prediction stages and needs.

1.2.2 Modeling of Conducted EMI Noise Generation

Recent research shows that the switching power modules are noise emission sources [16]. Two basic approaches have been used to characterize and model conducted EMI noise sources: device-based models [44], [59], [27], [29], [34], [37], [17], [36], [38], [52],

[54] and behavioral analytical equivalent models [18], [24], [28], [30], [39] - [41], [45] [46], [48], [50], [51], [53], [55] - [58].

Device-based models are widely used in EMI noise prediction process because they have clear physics meaning associated with semiconductor devices. There are three basic categories: 1) Physics-based model [44] [59], 2) Behavioral models provided by device manufacturers [17], [36], [38], [52], [54], 3) Ideal devices with some approximate device impedances [27], [29], [34], [37].

In [44] and [59], physics-based device models are adopted as EMI source models. The device physics-based modeling method depicts devices' switching characteristics through physical equations and associated equivalent circuits. A physics-based model is to consider all the major device physics in a set of nonlinear, high-order, and highly coupled multivariable differential equations. In [44], Hefner's IGBT model [65] [66] is used as the EMI noise source model in the three-phase inverter. Hefner's model has been demonstrated to achieve acceptable accuracy, and such a model has been implemented in the commercial circuit simulator Saber to facilitate the circuit designers' design. However, the associated parameter extraction process requires designated sets of experiments and an elaborate software tool, which makes the model parameter extraction work a very complex task. Furthermore, the parasitics resulted from the device packaging have to be modeled separately, either by simulations or measurements after knowing the detail of the package information.

In [59], the IGBT physics modeling process is improved and simplified. The parameter extraction scheme can extract equivalent parasitics inside the device module based on impedance measurements. The parameter extraction scheme can be used to build the IGBT model in a Saber simulation, but the whole process is still complicated and requires users to have a good understanding of semiconductor devices' physics.

Both models in [44] and [59] are accurate device physics-based models. With the device, impedance models of device packaging and noise propagation path model, the time-domain EMI noise can be predicted fairly accurately. In theory, the physics-based

model can be very accurate with sufficient modeling and parameter details. In practice, the models and associated parameters often have to be tuned through testing for satisfactory results. In addition, even the simplest physics-based model will require some intimate knowledge of the device, such as material properties, structure, and operating mechanism. As a result, a physics-based model is often neither simple nor easy to use. It is especially cumbersome to apply to a converter system with multiple switches or converters, since it is difficult and prohibitively time-consuming to model all the device physical details in the system to achieve sufficient accuracy. Furthermore, there are various time constants of converters within the system. For example, the fundamental period of motor drives and PFC circuits are in milliseconds, while the period of DC-DC converters could be in microseconds. It is difficult to reach the entire system steady-state operating condition with the required simulation steps, such as nanoseconds for accuracy up to 30 MHz. It is clear that the physics-based EMI source model is not suitable as a converter system design tool mainly due to its complexity. Because of the lengthy simulation process, physics-based models are also not suitable for parametric study of the system with respect to propagation path parameters, including the filters.

The second type of device-based model is the behavioral model provided by device manufacturers [17], [36], [38], [52], and [54]. The model can be derived based on the physics-based model and experimental results under a certain test condition. In practice, it is difficult to derive a model, which can be accurate for studying different aspects of device characteristics, such as thermal and high–frequency switching transients. Therefore, the modeling and prediction accuracy of the device manufactures' models is not clear when users obtain the model from manufacturers. Some research work [17] has been done to improve the model applicability in a PFC circuit. This type of model requires a long simulation time because these models are actually collections of circuit equations, which are similar to physics-based models. Furthermore, this kind of device model may not be available for users. Their availability depends on device manufacturers. In fact, the low-availability limits the feasibility and generality of this type model in EMI research.

Generally speaking, the third type of device-based model is a simplification of the physics-based model at a certain operating condition. References [27], [29], [34], and [37] use ideal switches with some approximate device parasitics from a datasheet, such as device output capacitance and turn-on resistance, to replace real devices in converters. In [27], a time-varying resistor is used to simulate device-switching transients. During the process, the accuracy of modeling device impedances is essential. Some parameters are difficult to characterize and change during the switching period and under different load conditions. The other important transients for devices – the turn-on and turn-off slope – cannot be accurately modeled simply by using ideal switches. This type of model can accurately predict the EMI noise up to several MHz. It sacrifices accuracy to obtain an easy-to-use EMI source model. This type of model can be extended to other converters with a good accuracy up to a few MHz.

The behavioral analytical equivalent source models with device parasitics are the other category of EMI noise source models. [18], [24], [28], [30], [39] - [41], [45] [46], [48], [50], [51], [53], [55] - [58]. It is used to represent the commutation transients of a device module via an equivalent current or voltage source. Device parasitic impedances are modeled as part of the noise propagation path. This type of behavioral models employs a time-invariant linear equivalent circuit. They can be easily converted into the frequency domain, which can reduce the EMI computation and simulation time dramatically. This is especially true for converters with variable switching conditions and long system time constants, such as PFC circuits and motor drives. However, because of the simplifications involved, the accuracy of the behavioral models is often compromised. It is also inherently difficult to develop a simple behavior model that is accurate for the entire frequency range and under different operating conditions. For example, one difficulty for the trapezoidal current source approach is to accurately obtain the turn-on and turn-off time, since the device manufacturer usually provides the rising and falling times under certain test conditions, which may not be the same as the real operating conditions. As a result, trapezoidal switching transient waveforms assumed for the equivalent current source models for all the switching conditions are oversimplified. This oversimplification can lead to considerable errors in the high-frequency region.

Another source of error is the simplified assumptions about parasitic impedance or even their total omission. The phenomena of the device parasitics resonance are not easily synthesized. Without modeling device parasitics, the analytical equivalent source model can miss the important resonances between device parasitics and propagation path.

Furthermore, the behavioral analytical equivalent source modeling approach characterizes the EMI noise source into separate common-mode (CM) and differential-mode (DM) noise sources. Although the separation helps to simplify the modeling process and to understand the noise generation and propagation characteristics, this approach is based on the assumption that there are no interactions and transformations between these two mode noises, which may not be valid in practice. Some research [67] [68] has shown the CM and DM noises are inseparable in the off-line converter filter design.

In short, the status of EMI source modeling can be summarized as follows:

1. Present modeling methods, both device-based and behavioral analytical equivalent models, can help predict the conducted EMI noise for converters in a certain frequency range, but none of them can predict the EMI noise in the entire conducted EMI range, especially high-frequency (>5 MHz) EMI noise.
2. Some of the models are too complicated, while other models sacrifice accuracy to achieve simplicity. There is a lack of a general and practical design model.
3. Some important EMI phenomena are not fully explored, such as CM and DM noise interaction. This interaction can change the modes of EMI noises. This type of noise interaction is not easily controlled and suppressed by traditional EMI management.

As shown above, the purpose of modeling the propagation path and noise source is to understand EMI noise characteristics and to manage EMI noise effectively. Therefore,

the modeling research is the foundation for EMI management in power converter systems.

1.3. Motivation and Objectives

From reviewing the results of the existing literature, it is obvious that the state-of-the-art conducted EMI modeling research is still not adequate. Both EMI noise source and propagation path modeling are essential in order to characterize EMI noise. Between these two modeling parts, the EMI noise path modeling is more mature and straightforward. Either the theoretical or experimental method can quite accurately characterize the EMI noise propagation path. The application of these two methods depends on the design stage, propagation characteristics, and the applicability of software and instruments. In this dissertation, the research focus is the EMI noise source modeling since the present modeling methods are relatively inaccurate, and the mechanisms of noise generation are even more unclear.

First of all, an accurate EMI noise source behavioral model for the entire conducted EMI frequency range is not available yet. Most EMI source model can deal with the EMI noise lower than 5 MHz. In the low-frequency range, the noise is controlled or affected by the switching patterns, which are the harmonics of switching frequency. Therefore, improving the accuracy of the EMI source model is necessary and significant for the EMI research. A more accurate modeling methodology is needed to deal with both low and high frequency EMI noise.

Secondly, the state-of-the-art EMI management is still a trial-and-error process. In converter design, EMI management is usually the last step, which can often lead to a long converter design cycle and less-than-optimal system designs. Some efforts [69] - [71] have been made to design a converter system with consideration of the converter's different variables in an optimization program. The thermal and electrical issues can be designed at the design stage based on models, such as the device thermal model, the core material model, etc. But none of them can involve the EMI management at the design

stage because of the unavailability of EMI noise source models. This makes the EMI noise source model a desirable tool for efficient converter designs.

Thirdly, the present modeling research is still at the converter level. Different EMI models are derived for one kind of converter, such as models for PFC circuits, DC-DC converters, inverters, etc. In fact, all of these converters are the EMI noise sources in a large power conversion system. Converter-level solutions for system-level EMI are often inefficient and can be ineffective because of the lack of consideration of interactions in systems. A general modeling approach is desirable for the entire system EMI noise modeling.

The ultimate goal of the conducted EMI research is to understand what the causes of EMI are and how to manage and suppress EMI noise in a systematic way. This dissertation focuses on developing a modular-terminal-behavioral (MTB) EMI noise source model, which can be used to accurately predict EMI noise in the entire conducted EMI range. The main task is to provide a methodology and tool for designing EMI management of a converter at the design stage. Furthermore, the source modeling methodology is not only for one device or one kind of converters. It is intended to be a general method for dealing with EMI issues in different applications. The generality of EMI noise source model is one of the aspects of this research. Based on the MTB source model and the path model, a complete converter-level EMI model can be derived. The noise interactions and suppressions based on the MTB model can be explored.

1.4. Organization of Dissertation

This dissertation presents the modular EMI noise source modeling methodology, and its applications. The following chapters are arranged as follows:

Chapter 2 starts with the fundamental modeling concept – equivalent EMI noise source and source impedance. Given that the importance of modeling the source impedance is not well established as the importance of modeling EMI noise sources, the concept of terminal source impedance is systematically presented in the dissertation. The

main focus of this chapter is to propose a modular-terminal-behavioral equivalent (MTB) noise source modeling approach. The modeling process is presented in detail. The experimental results verify the MTB modeling methodology.

Chapter 3 analyzes the validity of the proposed MTB model and prediction errors existing in the process and measurement. The inseparable high-frequency CM and DM noise characteristics contributed by the source impedance and propagation path are presented in detail. A unified MTB CM and DM model is proposed, which can be used to predict DM and CM noise simultaneously. At the end of the chapter, the proposed methodology is compared with the state-of-the-art methodologies and evaluated according to given evaluation criteria.

Chapter 4 applies the MTB equivalent source model in more complicated converters. Two application examples are presented. One example is the application of the MTB equivalent source model in a half-bridge with variable switching conditions. Another example is to predict the EMI noise of a full-bridge converter based on the MTB equivalent source model. The implementation procedure for each of these converters is described. The noise prediction results are verified by the experimental results. The possible applications of the MTB model to different types of converters are also discussed in this chapter.

Chapter 5 discusses some EMI noise interactions and management based on the MTB equivalent source model. The parametric study based on the MTB equivalent source model is demonstrated through selecting decoupling capacitors for voltage source converter (VSC). A completed converter-level EMI modeling procedure is presented. The applications of the converter-level model are discussed.

Finally, Chapter 6 summarizes the entire dissertation and discusses some ideas for future work.

Chapter 2 Modular-Terminal-Behavioral (MTB) Equivalent EMI Noise Source Modeling Approach

This chapter starts with the fundamental modeling concept – equivalent EMI noise source and source impedance. The concept of equivalent EMI noise source impedance for a device module is proposed and its importance is addressed through examples. The modular-terminal-behavioral (MTB) equivalent noise source modeling methodology is also proposed and the experimental procedure is presented. The MTB modeling is verified by experimental results.

2.1. EMI Noise Source Modeling Concept

EMI and EMC are important issues in a power conversion system with switching devices being used. For example, all AC pulse width modulation (PWM) drives can cause EMI with adjacent sensitive equipment when large quantities of drives are assembled in a concentrated area [16], [75] - [77]. The use of fast switching semiconductor devices in power conversion systems causes more EMI/EMC issues.

In modern switch mode power supplies and motor drive systems, high switching speed semiconductor devices, such as IGBTs and MOSFETs, are widely used. In recent years, the fundamental approach to electronic power processing has steadily moved toward “high-frequency synthesis”, resulting in important improvements in converter performance, size, weight and cost [72] - [74]. However, high switching frequencies require steep switching processes with higher dv/dt and di/dt for lower switch power losses. The increasing switching frequency causes electromagnetic inference to rise simultaneously. This interference can occur as radiated E- and H- field and as conducted interference currents and voltages.

Figure 2-1 is an example of a voltage-fed motor drive system. In order to obtain the desired current and voltage for the load, semiconductor devices are switched according to

a certain switching pattern. Each device's switching behavior could change the circuit energy flowing path, such as energy stored in the load, parasitic inductors, and capacitors, which generate chopped currents on the input side. The voltages on the load side are also abruptly changed, which induce currents to the ground through parasitic capacitors. From the EMI perspective, those currents contribute to the conducted EMI noise, which is caused by the device switching. Without switching, there would be no EMI noise. Therefore, each device under a certain switching condition can be treated as an EMI noise source.

After the conducted EMI noise is generated by an EMI noise source, it propagates through the connectors, cables, and parasitics to the outside of the converter system. In practice, it is difficult to physically separate the noise source and propagation path clearly. For example, half-bridge phase-leg modules, as shown in Figure 2-2, are used in drive systems. Because of the mechanisms of semiconductor device physics and the packaging technology, the devices are not ideal switches. They associate with equivalent impedances of device parasitics, such as device junction capacitors, conducting resistance and lead inductors. Nevertheless, those associated impedances can interact with a noise propagation path outside of the device module. Those interactions are usually in the high-frequency range (>5 MHz) and can generate a large noise peak, which could cause the converter to fail to pass EMI standards and make EMI noise mitigation difficult. Therefore, the contribution of switching phase-leg modules to EMI noise emission is not only as EMI noise sources but also impedances inside the module. The importance of both the noise source and impedance will be addressed in detail in this dissertation.

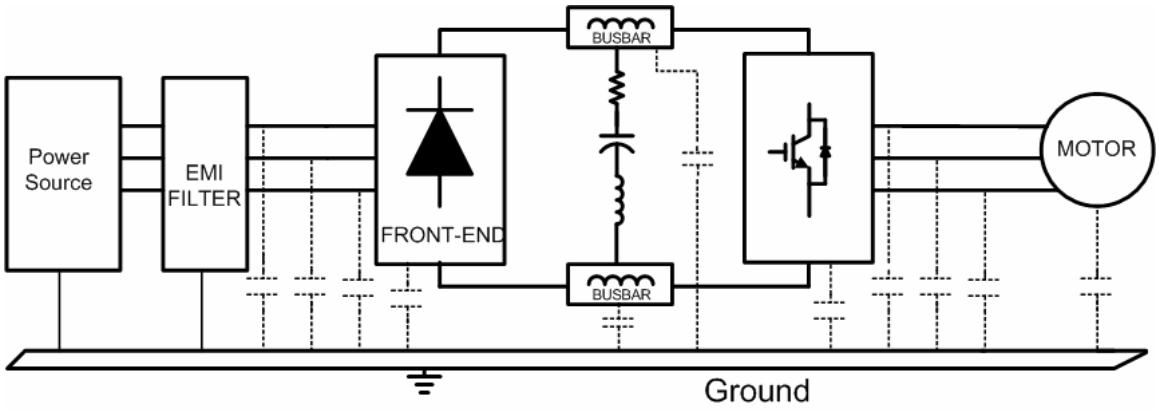

Figure 2-1 Motor Drive EMI Illustration

Figure 2-2 Half-bridge Phase-leg Module

2.1.1. EMI Noise Source

As discussed above, the pulsating current and voltage in a device module, which are modulated by the switching pattern, result in the intrinsic conducted EMI noise in the system. The waveform of the current and voltage consist of pulses with different amplitudes and different durations. The switching current and voltage are conducted through three electrical terminals of one phase-leg module in Figure 2-2. In terms of EMI noise propagation these three terminals conducts two mode noises– CM and DM noise. Based on the mode definition [1], a DM component flows out through one conductor and returns on the other conductor, and a CM component flows out through both conductors and returns through ground. In the state-of-the-art EMI noise source modeling the CM and DM noise source are separated. The three-terminal device module together with earth

ground is modeled as two separately CM and DM noise source, which are simplified as two two-terminal equivalent noise sources. Normally, the current flowing into the module and the voltage from the mid-point to the ground are looked as the DM and CM noise source respectively.

Figure 2-3 shows one phase-leg module in a chopper circuit. Since each switching event in a phase-leg-based converter involves an IGBT and a diode on the same phase leg, a clear understanding of the EMI noise generation mechanisms of a single phase leg is necessary and sufficient to understand multi-phase converters. When triggering the bottom IGBT, the waveform of input current I_{in} flowing into the module is shown in Figure 2-4. I_{in} is often treated as a DM noise source and the voltage jumping between m and ground (omitted in the Figure 2-3) is looked as a CM noise source in the literature. In order to help to understand the basic features of an EMI noise source, the EMI effects of idealized pulse current and voltage waveform without finite slew rate are analyzed first. The amplitude of the waveform is A, period is T_s, and duty cycle is D. The frequency spectrum of the waveform can be represented by Eqs. (2-1) – (2-3)

$$x(t) = A \cdot D + \sum C_n \cdot \cos(n \cdot \omega_o t + \varphi_n) \tag{2-1}$$

$$C_n = 2 \cdot A \cdot D \cdot \left| \frac{\sin(n\pi D)}{n\pi D} \right| \tag{2-2}$$

$$\varphi_n = \pm n\pi D \tag{2-3}$$

where C_n is the amplitude of the nth harmonic, φ_n is the phase angle of nth harmonic.

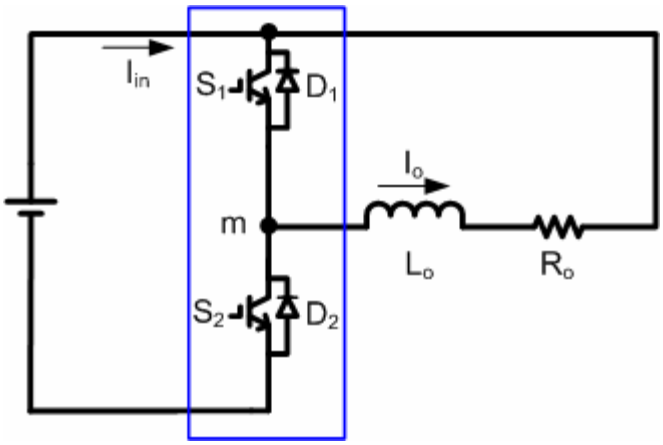

Figure 2-3 One Phase-leg Module in a Chopper Circuit

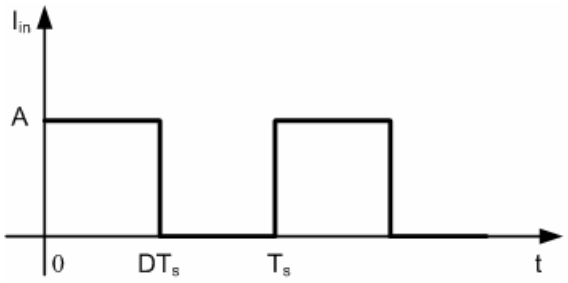

Figure 2-4 Input Current in the Chopper Circuit

Based on Eq. (2-1) - (2-3), the spectrum of the square waveform is illustrated in Figure 2-5. The asymptote of the magnitude can be described as Eq. (2-4) and Figure 2-6. The asymptote includes two slopes: one is 0 dB/dec; the other is –20 dB/dec. The corner frequency is at $1/\pi DT_s$, which indicates that the larger the duty cycle, the lower the corner frequency.

$$C_n = 2AD\left|\frac{\sin(n\pi D)}{n\pi D}\right| \qquad \textbf{(2-4)}$$

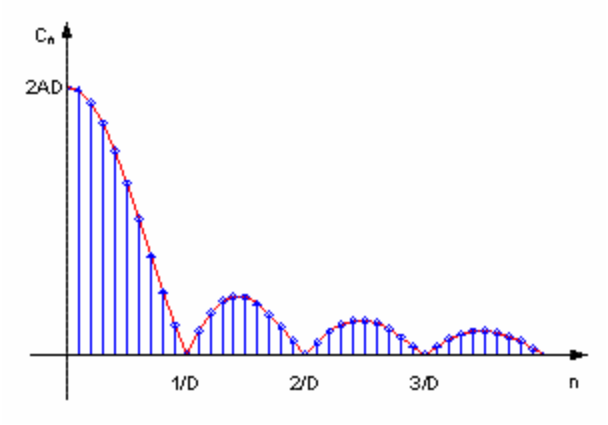

(a) Magnitude Spectrum

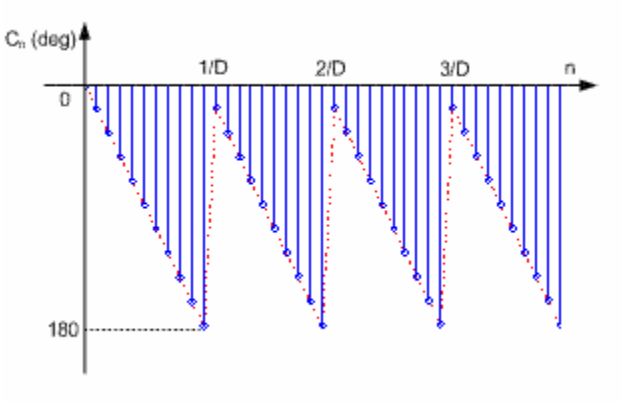

(b) Phase Spectrum

Figure 2-5 Frequency-domain Spectrum of Square Waveform

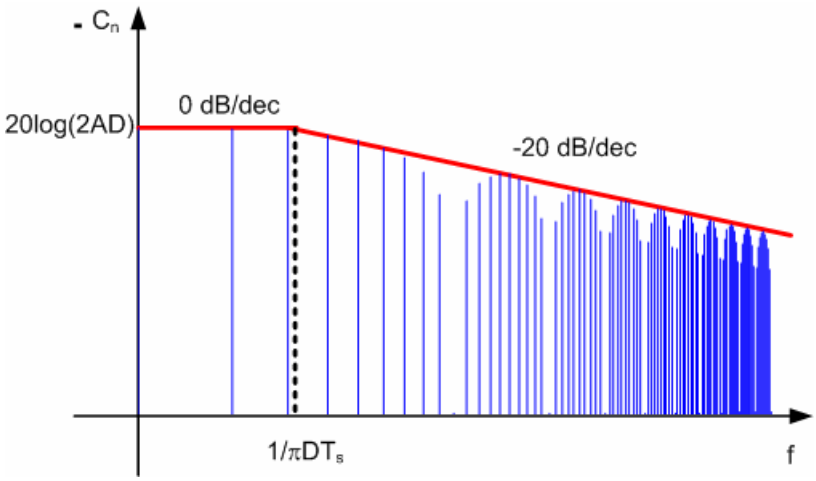

Figure 2-6 Asymptote of Magnitude Spectrum of Square Waveform

For practical cases, semiconductor devices cannot be turned on or off immediately. The trapezoidal waveform, as shown in Figure 2-7, is closer to the real current or voltage waveform. To simplify the analysis, it is assumed that the rising time t_r and falling time t_f are equal. Therefore, the magnitude asymptote of a trapezoidal waveform can be described by Eq. (2-5) and Figure 2-8. In contrast with the spectrum of a square waveform, the spectrum of a trapezoidal waveform has three slopes: the first one is 0 dB/dec, the second is – 20 dB/dec, and the third is – 40 dB/dec, which is caused by the finite rising and falling time. From Eq. (2-5), it is seen that the slower rising and falling time lead to a lower corner frequency, noted as $1/\pi t_r$. and thus the magnitudes of the higher-order signal are smaller.

$$C_n = 2AD\left|\frac{\sin(n\pi D)}{n\pi D}\right| \cdot \left|\frac{\sin(n\pi t_r / T_s)}{n\pi t_r / T_s}\right| \quad \textbf{(2-5)}$$

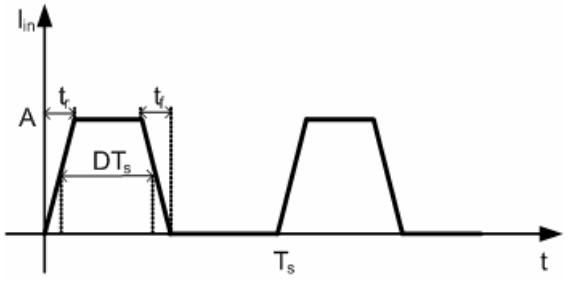

Figure 2-7 Time-domain Trapezoidal Waveform

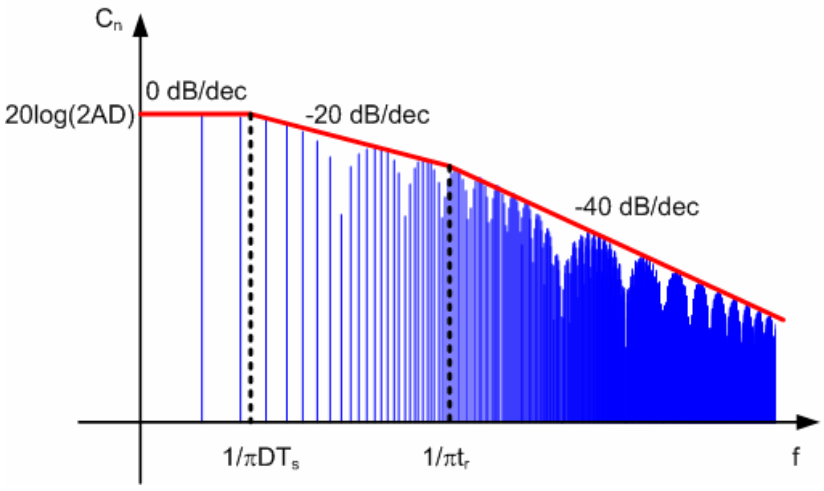

Figure 2-8 Frequency-domain Spectrum of Trapezoidal Waveform

Analysis of the square and trapezoidal waveform provides a basic understanding of the effect of the duty cycle and the rising and falling time on the frequency-domain spectrum. In more practical cases, the slope of device turn-on and turn-off are changing during switching transients, which means several slew rates are included in the rising and falling time period, as shown in Figure 2-9 (curve 2). Compared with two different single-slew-rate waveforms, the asymptote of the magnitude spectrum of the multi-slew-rate waveform is less than the steep asymptote and higher than the slow one in a certain frequency region, as illustrated in Figure 2-10. When frequency increases, the noise level of the multi-slew-rate curve will be the same as the steep slew rate.

Figure 2-9 Multi-slew-rate Time-domain Waveform

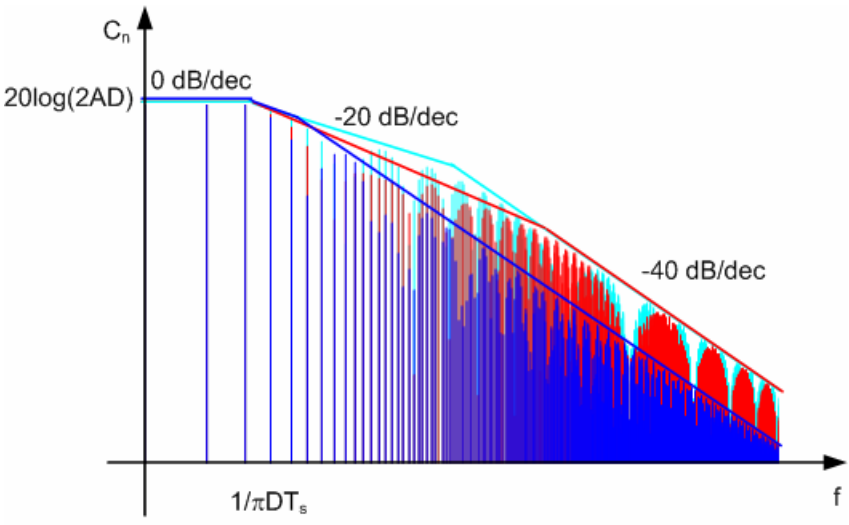

Figure 2-10 Magnitude Spectrum Comparison between Multi-slew-rate and Single-slew-rate Waveform

From the above analysis, it is clear that the accurate model of the source slew rate is important. The simplification of replacing the noise source as square or trapezoidal pulse chains [24], [47], [48] will lose accuracy in a certain frequency range without the accurate information of the rising and falling time. In practical cases, the changing slew rates are very difficult to obtain from device datasheets because device manufacturers usually only give the turn-on and turn-off time at one switching condition, which is often different from application cases. In recent research [78] - [82], gate drivers are carefully designed to shape the turn-on and turn-off transients, considering both EMI noise and switching loss.

2.1.2. EMI Noise Source Impedance

The EMI noise source impedance concept has been adopted in EMI filter design for an offline converter [41], [42], [83]. Since EMI filter performance depends not only on the filter itself but also the noise source impedance of the converter and the noise load impedance, all impedances of different components in the converter, such as the busbar, capacitors, inductors, load, and device parasitics, contribute to the converter-level noise source impedance, such as a motor drive system as shown in Figure 2-1. The general method to obtain the source impedance of a converter is to measure the input impedance of the off-line converter by either directly measurement [41] or by using the insertion loss method [42] [83]. All the source impedance measurements should be done after the entire converter has been built, which means the filter design cannot be carried out at the same time as the converter's other functions are designed. Although the noise source impedance of the converter will help to optimize the design of an EMI filter, it is difficult to help other possible EMI management at the design stage because noise source generation and propagation of the converter are not identified. The design and optimization of an entire converter at the design stage are very difficult because of the lack of models of the system's EMI emission.

Due to the physics of the device mechanisms, semiconductors cannot be turned on and off as ideal switches, as these have an infinite slew rate, infinite off resistance and zero on resistance. The semiconductor devices usually have a certain on and off resistance, junction capacitance and other parasitics. Furthermore, semiconductor device packaging also brings more parasitics inside of the device package such as lead inductances and stray capacitances. All the impedances of the device parasitics could interact with the impedances outside. Therefore, each switching device module includes not only equivalent noise sources but also impedances.

Some literature neglects the impedances and looks a switching device module only as a DM current source and a CM voltage source [18]. The omission cannot characterize the important high-frequency EMI noise. The device impedances impact on EMI noise can be shown in the following example. Figure 2-11 consists of the simulation circuits that illustrate the EMI effect of impedances in the device module. Figure 2-11 (a) is the device module with the parasitics, including the junction capacitance, lead inductance and resistance. Figure 2-11 (b) is the simulation with only switches. In the simulation, the devices are the switches in the Saber parts gallery, which provide some power semiconductor devices' characteristics, such as turn-on and turn-off resistance, as well as turn-on and turn-off time. A practical electrolytic capacitor is used as the DC-link capacitor. Two standard artificial networks required by international EMI regulations – line impedance stabilization networks (LISNs) – are inserted between the input source and the circuit. The device is switched at 200V/40A.

Figure 2-12 shows the spectra of EMI noise on the LISN of two simulation circuits. In the low-frequency range, the EMI noises of two simulation circuits are no difference. But when the frequency moves towards a higher frequency, the resonance involved with the device module's impedances appears. The resonance is between the junction capacitor, the lead inductance and the parasitic inductance of the electrolytic capacitor. Compared with the case of no impedance, the noise level at 22 MHz is 16 dBμV higher, which is difficult to mitigate in practice. Therefore, without the module's impedances, the important EMI noise phenomenon will be ignored.

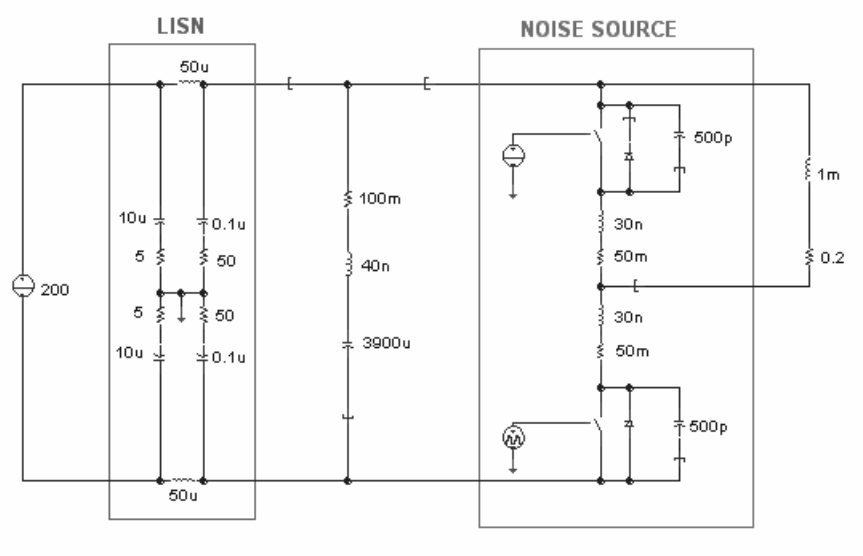

(a) Simulation with Impedances inside the module

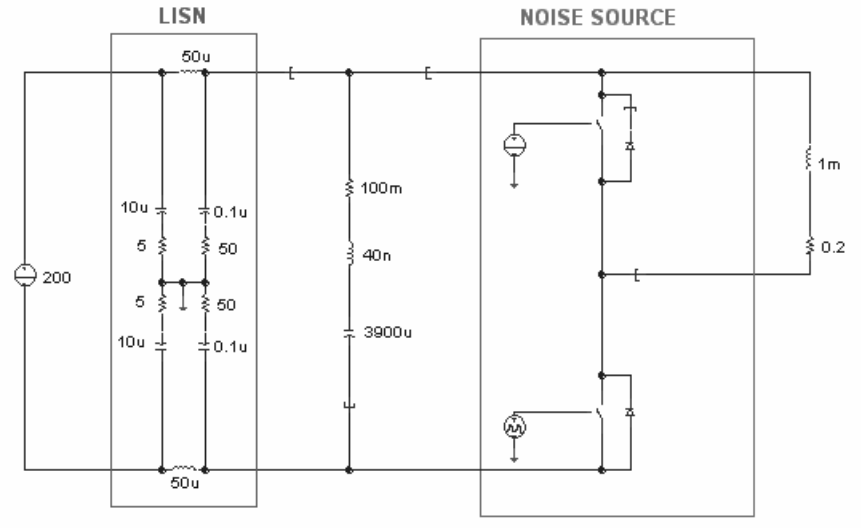

(b) Simulation without Impedances inside the module

Figure 2-11 Illustration of EMI effect of Impedances inside the Device Module

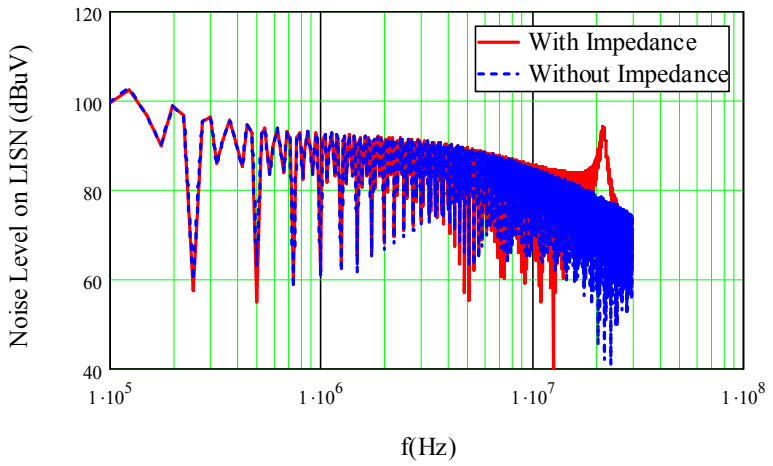

Figure 2-12 Spectrum Comparison of with and without Device Impedances

From above analysis, the impedances inside the module have significant impact on EMI noise spectrum, though device parasitics are small compared with other propagation paths. Some research work has gone as far as to model and characterize device parasitics [26], [55], [59]. Some research also shows that there are EMI noise prediction errors in the high-frequency range due to inaccurate impedance models or measurements [30], [35], [47], [48], and [50]. However, there are two major drawbacks of the state-of-the-art impedance modeling methods:

1) Since the noise sources are separated to CM and DM noise source, the impedances of the device module have to be separated to CM and DM source impedance. In the literature, the impedances of the device module except the impedance between the module and the ground are modeled as the DM noise source impedance and the impedance between the module mid-point and the ground is only considered as the CM impedance. However, this impedance separation is arbitrary and based on two assumptions: a) The interaction between the device module and propagation path shown in Figure 2-12 will not affect the CM noise; b) There is no noise transfer between the two modes. In power converters, these assumptions may not be valid, especially for the high-frequency EMI noise. In fact, in terms of EMI noise generation a device module is a four-terminal device, which includes three electrical terminals and ground. Strictly speaking, the conventional CM and DM separation cannot be used in the EMI noise source because

of the module four-terminal structure. The more detailed analysis will be presented in Chapter 3.

2) Most commercial devices are already packaged, which makes it difficult to measure or simulate an individual parasitic, whose geometry information is not provided by the manufacturers. In fact, in terms of EMI noise emission each individual component value is not necessary if the entire device terminal impedance characteristics can be known.

In summary, the traditional EMI noise source modeling methods – two-terminal DM and CM noise source and impedances are not accurate and cannot characterize the EMI noise generated by the switching device.

2.2. MTB Equivalent EMI Noise Source Modeling Approach

From above analysis, noise source and source impedances play important roles in EMI noise generation and the separation of different noise modes cannot accurately represent the noise source. Since commutations are considered as noise sources and exist between the top devices and the bottom devices inside of a device module, two current sources or voltage sources between three electrical terminals can be used to represent the noise sources of the switching phase-leg module.

In general, there is an impedance between every two terminals of all terminals in the device module. However, some impedances are significantly affected by the device physical connection, such as the ground connection of the module. In this dissertation, the impedances between electrical terminals and ground are not modeled in the equivalent noise source model and are characterized as parts of the propagation path. In addition, the direct impedance between the terminals, which connect to the bus, is neglected because of the module physical structure.

Therefore, the terminal characteristics of a module from an EMI standpoint are the characteristics of equivalent sources and impedances, which can be illustrated as Figure 2-13. There are two forms of the source and impedance model: one is current sources with impedances Figure 2-13 (a); the other is voltage sources with impedances Figure 2-13 (b). These two forms can transform to each other. In this dissertation, EMI noise current sources are used to represent EMI noise source. From the model structure, the proposed model is a modular-terminal-behavioral (MTB) equivalent EMI noise source model. It has same terminals of a phase-leg module and is dependent on the operating conditions, which shows the behavioral characteristics.

In fact, one device module is not simply one noise source pair. In a device module, there are four devices. Each switching transient involves two devices – the top IGBT and the bottom diode or the top diode and the bottom IGBT. Therefore, there are two noise source pairs in one module. Since there is a known relationship between these two pairs, it is only necessary to model one pair. The detailed analysis will be presented in Chapter 4.

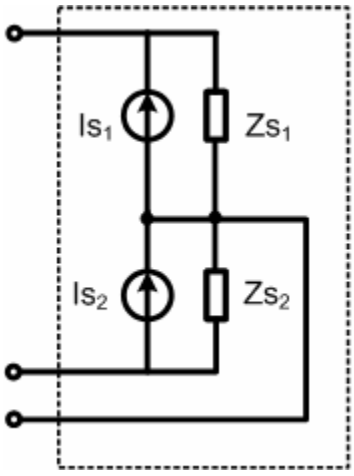

(a) Current Sources and Impedances

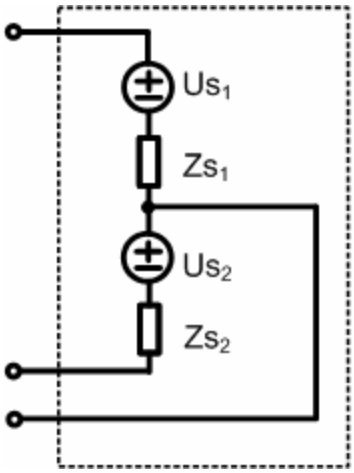

(b) Voltage Sources and Impedances

Figure 2-13 Equivalent EMI Noise Sources and Impedances of Each Phase Leg

In order to derive the entire converter EMI model, each EMI noise source and its impedance should be obtained first. Strictly speaking, there are no identical EMI noise source pairs since there are no identical device modules. But it is practical to assume the devices are the same and to model one device module switching under a certain condition as an EMI noise source pair. To obtain the EMI noise source pair, a circuit with one module will be selected as a testbed. As an example, a chopper circuit as shown in Figure 2-11. The bottom IGBT and the top diode are involved during the transient period. Therefore, the chopper circuit can be used to derive one EMI noise source pair. The similar EMI model of the chopper circuit can be shown as Figure 2-14 (a). There are four independent parameters to be solved: Is_1, Is_2, Zs_1, and Zs_2.

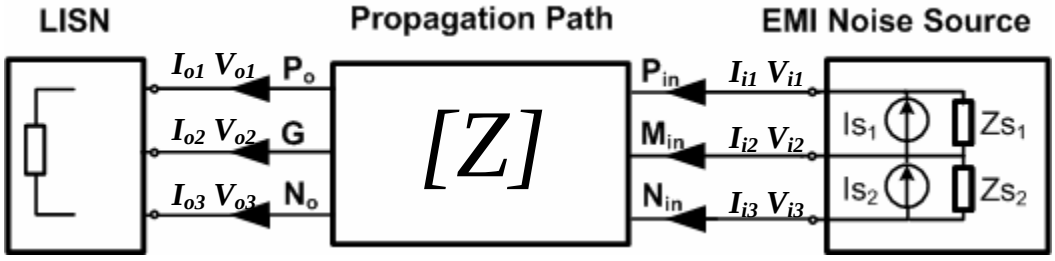

(a) Circuit I

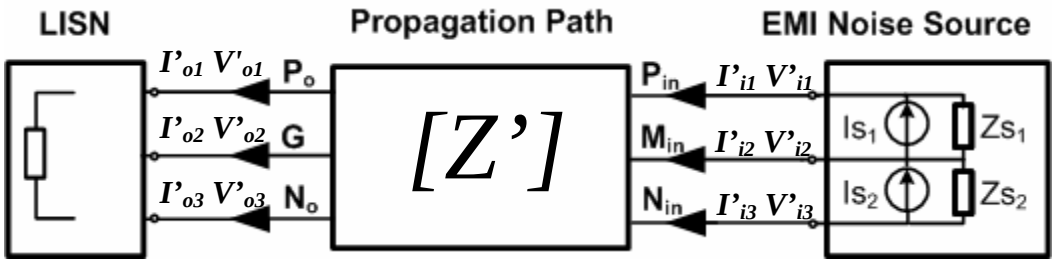

(b) Circuit II

Figure 2-14 Circuits Used to Derive EMI Noise Source Pair

The concept used to solve EMI noise current sources and source impedances is based on the Norton equivalent circuit theory. Normally, open-circuit and short-circuit conditions are used to solve equivalent source and impedance. But in the process of obtaining an EMI noise source pair, open-circuit and short-circuit conditions are very difficult to obtain. For example, to create the open-circuit condition requires the switching conditions of the devices to be the same as the normal condition, which means the power delivery path is the same. But for EMI noise propagation, the circuit should be open. Because the power delivery path and EMI propagation path involve the same components, it is difficult to insert components to create the pure open-circuit and short-circuit conditions for EMI noise source pair derivation while the operating conditions of the devices are unchanged. Hence the proposed approach in this dissertation is to change noise propagation paths, which slightly affect circuit operating condition, to obtain different currents and voltages on the device terminals in terms of conducted EMI. With enough propagation paths, the noise source pair can be solved. This approach can avoid dramatic change of the circuit operation caused by creating open-circuit and short-circuit conditions.

In Figure 2-14 (a), three parts of the entire converter EMI model are shown: the LISN, the propagation path and the EMI noise source. The LISN is a standard EMI noise receptor required by EMI regulations, whose impedance characteristics are known. In the EMI noise source pair, there are four unknown parameters Is_1, Is_2, Zs_1, and Zs_2. From circuit theory, one circuit alone cannot solve all the parameters. As a result, more circuits are needed. Changing the propagation path and keeping the device module under the

same switching condition can create another circuit with the same noise source pair, as shown in Figure 2-14 (b).

Because of module package and circuit connection, it is not easy to directly measure the EMI noise on the device module terminals. One indirect method used to obtain the EMI noise on the module side is to measure the noises on the LISNs and then calculate the EMI noise on the terminals with the impedance characteristics of the propagation path. The impedance of the propagation path can be measured by an impedance analyzer or simulated by software [21], [24].

Assuming that the impedance matrices for the two propagation paths are $[Z]$ and $[Z']$ respectively, and the corresponding noises measured on LISNs are $U_o = [V_{o1} \quad V_{o2} \quad V_{o3}]^T$, $I_o = [I_{o1} \quad I_{o2} \quad I_{o3}]^T$ and $U_o' = [V_{o1}' \quad V_{o2}' \quad V_{o3}']^T$, $I_o' = [I_{o1}' \quad I_{o2}' \quad I_{o3}']^T$. Let us also define the EMI noise voltage and current vectors at the input port of the propagation path to be $U_i = [V_{i1} \quad V_{i2} \quad V_{i3}]^T$ and $I_i = [I_{i1} \quad I_{i2} \quad I_{i3}]^T$, corresponding to $[Z]$ network, and $U_i' = [V_{i1}' \quad V_{i2}' \quad V_{i3}']^T$ and $I_i' = [I_{i1}' \quad I_{i2}' \quad I_{i3}']^T$, corresponding to $[Z']$ network. The output and input voltages and currents should satisfy Eq. (2-6).

$$\begin{bmatrix} U_o \\ U_i \end{bmatrix} = [Z] \cdot \begin{bmatrix} I_o \\ I_i \end{bmatrix} \quad \text{and} \quad \begin{bmatrix} U_o' \\ U_i' \end{bmatrix} = [Z] \cdot \begin{bmatrix} I_o' \\ I_i' \end{bmatrix} \tag{2-6}$$

From (2-6), two sets of voltage and current vectors, U_i and U'_I and I_i and I'_i, can be obtained based on U_o and U'_o and I_o and I'_o, as well as $[Z]$ and $[Z']$. With these terminal voltages and currents for the Norton equivalent source, the parameters of the source can be determined. For circuit in Figure 2-14, it can be found that

$$Z_{s1} = \frac{(V_{i1} - V_{i3}) - (V'_{i1} - V'_{i3})}{I'_{i1} - I_{i1}} \tag{2-7}$$

$$I_{s1} = \frac{(V'_{i1} - V'_{i3}) \cdot I_{i1} - (V_{i1} - V_{i3}) \cdot I'_{i1}}{(V'_{i1} - V'_{i3}) - (V_{i1} - V_{i3})} \quad \textbf{(2-8)}$$

$$Z_{s2} = \frac{(V_{i2} - V_{i3}) - (V'_{i2} - V'_{i3})}{I'_{i2} - I_{i2}} \quad \textbf{(2-9)}$$

$$I_{s2} = \frac{(V'_{i3} - V'_{i2}) \cdot I_{i2} - (V_{i3} - V_{i2}) \cdot I'_{i2}}{(V_{i3} - V_{i2}) - (V'_{i3} - V'_{i2})} \quad \textbf{(2-10)}$$

In the modeling process, all the calculations are carried out in the frequency domain. Compared with the time-domain method, this approach is more efficient, accurate and straightforward due to the following reasons: 1) It avoids the tedious device physics model extraction and time-consuming simulation; 2) It is more accurate than methods with approximate device impedances and unknown device packaging effect; and 3) Since the EMI noise standard is in the frequency domain, the proposed method can directly obtain the noise frequency spectrum.

With the EMI noise source current and source impedance of each device module, a power electronic circuit can have its EMI noise generation and propagation form, as shown in Figure 2-15. It is more convenient and straight-forward to study EMI characteristics. Since EMI noise generation is closely linked with device operating conditions, such as switching voltage, current, gate circuit and switching frequency, one device module can have many EMI noise current source and source impedance pairs. But the EMI noise pair can be used in different topologies as long as switching conditions stay the same.

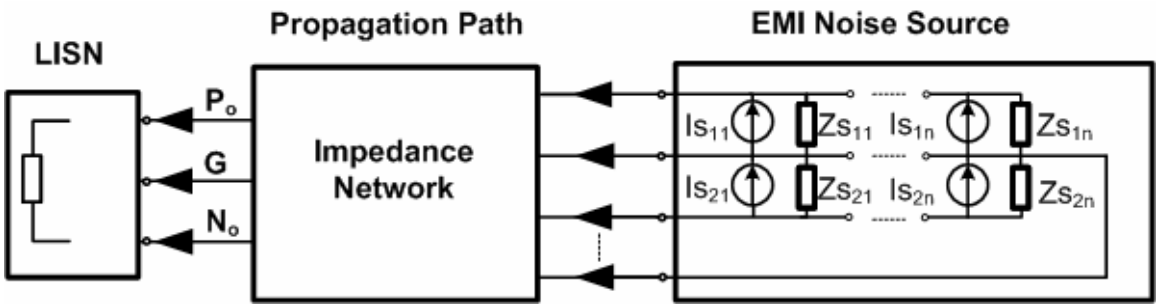

Figure 2-15 EMI Noise Generation and Propagation with Noise Current Sources and Source Impedances

Once the device module EMI source model under a certain operating condition is obtained, it can be easily applied to the circuit with a different propagation path. With the source model and a new propagation path impedance matrix, the EMI noise on the LISNs can be calculated. The change of the propagation path is a parametric study. The EMI management based on accurate source model can be carried out and minimize the EMI noise before designing the input EMI filter. The MTB noise source model together with the propagation path can derive the entire converter EMI noise model, which includes converter-level noise current sources and noise source impedances. Therefore, one type of EMI management, the EMI filter, can be designed with the knowledge of the noise source and source impedance information at the design stage, which can make the filter more efficient and favorable. The entire converter optimization program can be developed while considering the EMI noise in the system.

In addition, in a power conversion system there are different power converters. They have various functions and work in different switching conditions. The converter-level EMI model of each converter in the system provides the possibility of studying EMI interactions between converters. Based on the converter-level models, the entire system-level EMI management structure can be designed and optimized.

2.3. MTB Equivalent Source Experimental Procedure

This section illustrates the detail of the MTB modeling process using again the IGBT-based chopper circuit as example. Experimental verification is provided for the testing circuit.

2.3.1. Standard Testbed

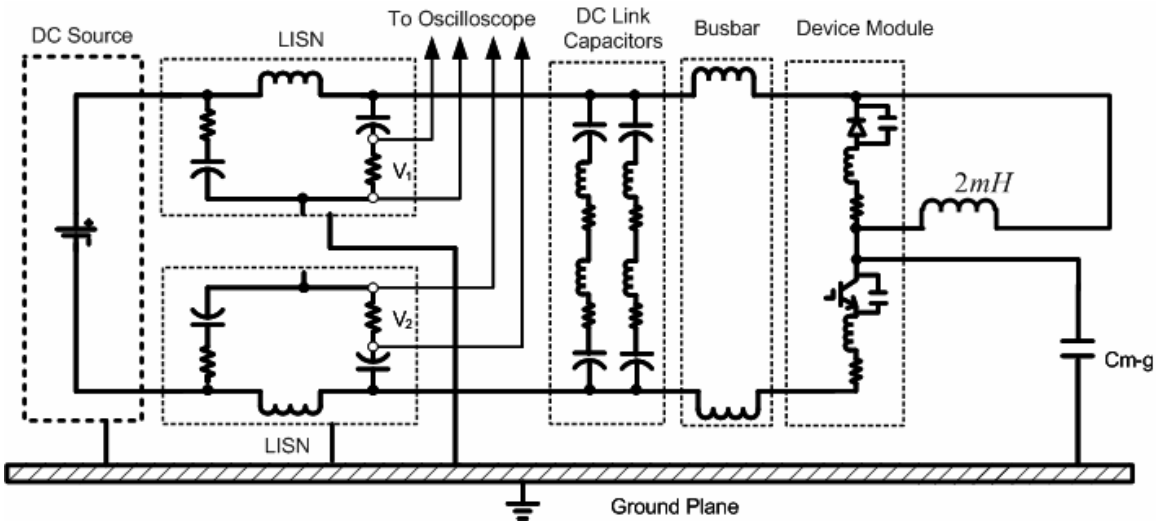

(a) Test Circuit

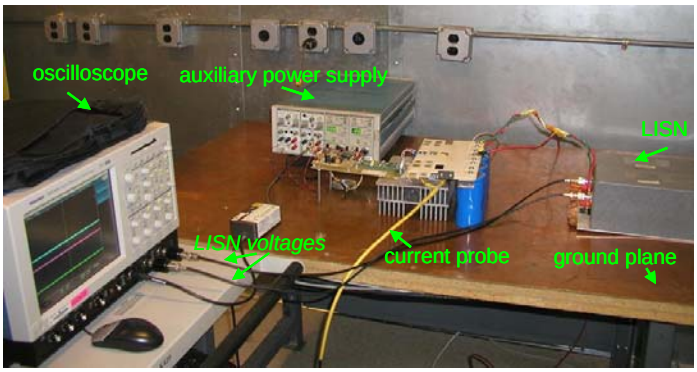

(b) Implementation

Figure 2-16 Chopper Circuit Testbed

To establish the equivalent MTB EMI source model for a switching module, a standard testbed can be used to conveniently control the switching conditions and propagation paths. A chopper circuit testbed and its implementation are shown in Figure 2-16 (a) and (b). It consists of the switching module under test, a controllable DC power supply, DC-link capacitors, LISNs, and the bus to connect them together. In the testbed, the switching module is a dual-pack IGBT module, but only one IGBT switch is tested at a time. In this case, the switching on and off of the bottom IGBT is controlled while the top switch remains open. Four DC-link capacitors are connected between the terminals of the bus. A large inductor (2 mH in Figure 2-16) is connected between the positive DC bus and the switching module mid-point as the load. A large ground plane is used as the reference earth ground. In addition to the major components, Figure 2-16 (a) also includes parasitic impedances of the bus, DC-link capacitors, ground plane and heatsink, as well as the device module internal connections.

Since the EMI emission is a result of device switching, the test focuses on the turn-on and turn-off periods of the IGBT. Standard double-pulse switching is used for the investigation. The first pulse allows the current through the tested (bottom) switch to build up to and turn off at the desired current level. With a short off period, the second pulse will turn the switch on again at practically the same current. The time-domain switching waveform and EMI noise can be measured with an oscilloscope, and the frequency-domain data can be obtained through off-line data processing. The EMI noise voltages V_1 and V_2 are obtained directly from LISN noise measurements.

2.3.2. Data Processing

Spectrum analyzers or EMC receivers are widely used for EMI measurements [90]. A spectrum analyzer displays a spectral distribution of RF energy. Essentially, a spectrum analyzer is a swept-tuned heterodyne receiver. The signal being measured is received from a transducer, such as an antenna or probe. From here, the signal travels to the analyzer's mixer stage and is mixed with a voltage-tuned local oscillator swept at the

same rate as the horizontal deflection of the cathode ray tube (CRT) by means of a saw-tooth generator. This gives a frequency-related horizontal display on the screen. The output of the mixer is amplified and sent to the vertical deflection stage. Thus, a spectrum analyzer sweeps frequency while an oscilloscope sweeps time.

A heterodyne type of spectrum analyzer, it cannot provide the phase information. Since the derivation and calculations of the MTB source models are all in the frequency domain, both the noise magnitude and phase information are required. Furthermore, for the double-pulse test with very short pulse width (e.g. 20 μs) repeating with a long pause in between (e.g., 100 ms), it is difficult to obtain the correct frequency-domain data with a spectrum analyzer [88]. For this reason, the off-line discrete Fourier transformation (DFT) [89] was used to process the data from the time-domain measurement to obtain the frequency-domain EMI noise levels.

Figure 2-17 illustrates the process of obtaining the frequency-domain characteristics from the time-domain test results. The repeating frequency in the process is 1/T, meaning that the equivalent switching frequency is 1/T. In the test, the sampling window is 40 μs, corresponding to an equivalent switching frequency of 25 kHz. When changing the sampling window, it is straightforward to determine the relationship between the switching frequency and the EMI noise level. The frequency between the center of a DFT filter and its first null response is equal to the reciprocal of the total time for data collected for the DFT input. The data processing used in this dissertation has been verified through comparisons with the test results obtained for standard signals using a spectrum analyzer. A further analysis of the accuracy of off-line calculations will be discussed in the next chapter.

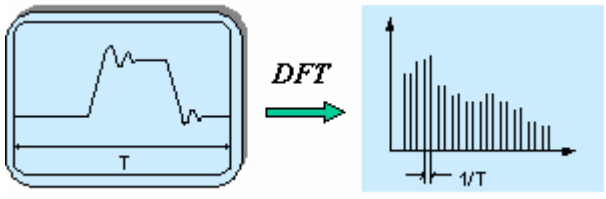

Figure 2-17 Illustration of Data Processing

2.3.3. Model Extraction

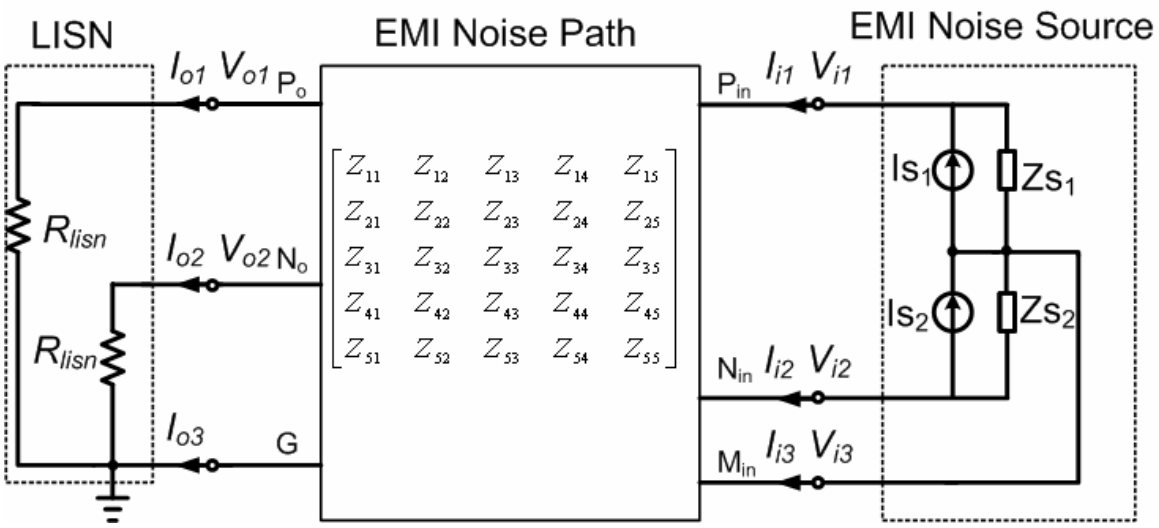

Figure 2-18 Equivalent EMI Noise Emission Model

For the testbed chopper circuit, the equivalent noise source model, in the form of a Norton equivalent source, is shown in Figure 2-18. Because G is the reference ground point, the number of input terminals and output terminals for the propagation path network are 3 and 2, respectively. The impedance matrix $[Z]$ is therefore (5×5), and Eq. (2-6) becomes

$$\begin{bmatrix} V_{o1} \\ V_{o2} \\ V_{i1} \\ V_{i2} \\ V_{i3} \end{bmatrix} = \begin{bmatrix} Z_{11} & Z_{12} & Z_{13} & Z_{14} & Z_{15} \\ Z_{21} & Z_{22} & Z_{23} & Z_{24} & Z_{25} \\ Z_{31} & Z_{32} & Z_{33} & Z_{34} & Z_{35} \\ Z_{41} & Z_{42} & Z_{43} & Z_{44} & Z_{45} \\ Z_{51} & Z_{52} & Z_{53} & Z_{54} & Z_{55} \end{bmatrix} \cdot \begin{bmatrix} I_{o1} \\ I_{o2} \\ I_{i1} \\ I_{i2} \\ I_{i3} \end{bmatrix} \quad \textbf{(2-11)}$$

The $[Z]$ matrix can be obtained through off-line measurements of the propagation path using an impedance or network analyzer. Some parameters, such as transfer impedances Z_{12}, Z_{23}, etc., are more difficult to measure than others at high frequencies. For example, in order to measure the transfer impedance between terminal P_o and N_o, all terminals expect P_o and N_o will be open. According to the definition of Z_{12} as shown in

Eq. (2-12), the open circuit voltage V_{i1} should be measured. In practice, it is difficult to obtain an accurate result at a high frequency due to the parasitic capacitance shorting terminal 1 (P_o) to ground. This dissertation adopts the method that uses driving-point impedances Z_{11}, Z_{22}, Z_{33}, Z_{44}, and Z_{55} and attenuation of the network to calculate these transfer impedances [25]. An illustration of measuring the attenuation of the network is shown in Figure 2-19. Using a gain-phase/network analyzer can measure the attenuation of the network. The impedance of Z_{12} can be calculated by Eq. (2-13) with Z_{11}, Z_{12}, and the attenuation A_T. Since the passive network is a reciprocal network, it is only necessary to measure the impedances of the up diagonal or down diagonal matrix. Therefore, 15 impedances need to be measured.

$$Z_{12} = \left.\frac{V_{i1}}{I_{i2}}\right|_{I_{i3}=I_{i4}=I_{i5}=0} \tag{2-12}$$

$$Z_{12} = -R/A_T + \sqrt{(R/A_T)^2 + R^2 + R(Z_{11}+Z_{22}) + Z_{11}Z_{22}} \tag{2-13}$$

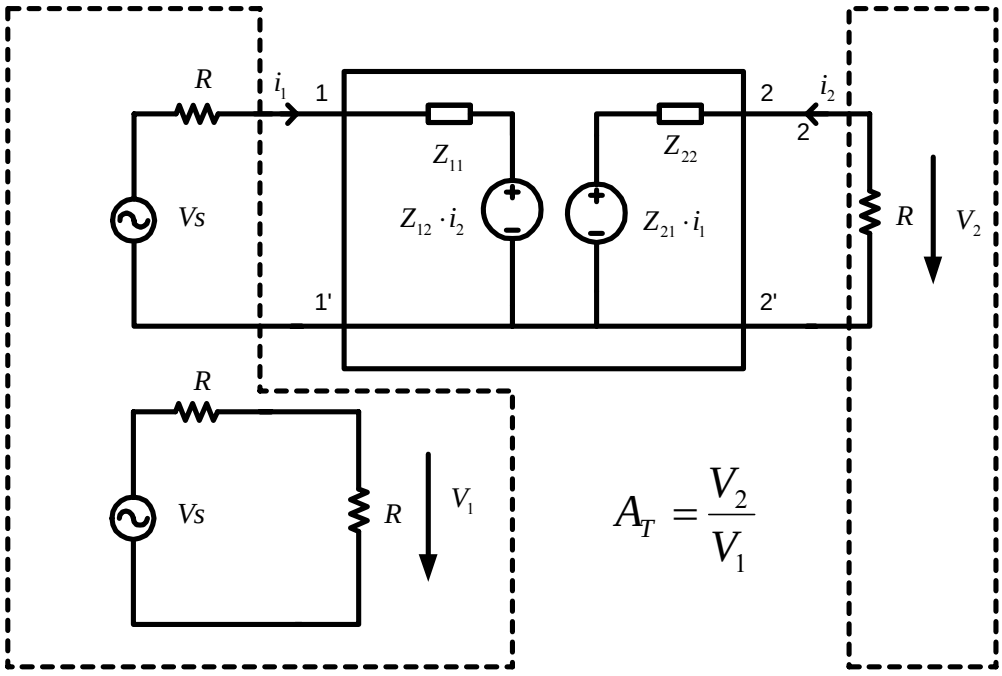

Figure 2-19 Illustration of Measuring Attenuation of Impedance Network

Using Eq. (2-11) and the relationships below,

$$I_{i1} + I_{i2} + I_{i3} = 0 \tag{2-14}$$

$$I_{o1} = \frac{V_{o1}}{R_{lisn}} \tag{2-15}$$

$$I_{o2} = \frac{V_{o2}}{R_{lisn}} \tag{2-16}$$

where $R_{lisn} = 50ohm$ is the equivalent resistance of the LISN, one can determine the relationships for the Norton equivalent source parameters as Eqs. (2-17) and (2-18).

$$I_{s1} = I_{i1} + \frac{V_{i1} - V_{i3}}{Z_{s1}} \tag{2-17}$$

$$I_{s2} = -I_{i2} - \frac{V_{i2} - V_{i3}}{Z_{s2}} \tag{2-18}$$

As presented in Section II, in order to solve for the EMI source currents Is_1 and Is_2 and the source impedances Zs_1 and Zs_2, another propagation path with a different impedance matrix $[Z']$ is needed for establishing a similar relationship to (2-11). By using Eqs. (2-7) and (2-10), Is_1 and Is_2 and Zs_1 and Zs_2 can be solved. All the calculations are carried out in the frequency domain, which is efficient, and also convenient for EMI standards compliance testing and for filter design.

A key to the MTB equivalent model extraction using a testbed is to obtain two different propagation paths, with their influence on the device switching conditions essentially the same. One way to obtain two different paths is to change the bus structure. In the impedance matrix, there are 15 independent impedances. Some of the impedances

can significantly affect EMI noise. For example, the impedance Z_{34}, which is the transfer impedance between device positive terminal (P_{in}) and negative terminal (N_{in}), can be directly involved in the resonance between the device module and the propagation path. In the example, the inductance of the original bus (Network I) is lower than that of the altered bus (Network II), as shown in Figure 2-20. The physical structure of two different networks is shown in Figure 2-21 (a) and (b), respectively. The impedance Z_{34} of two networks, which is affected by the bus structure, results in different magnitudes. It can contribute to the resonance between the noise source impedance and the propagation path significantly.

Selecting propagation paths is very important for the modeling process. The basic rule for the selection is to keep the switching conditions the same when changing the propagation paths. When keeping the converter under a specific switching condition, including operating voltage, current, gate drive circuit condition, switching frequency, and to a lesser extent, temperature, the EMI noise source will not change. The validation analysis will be presented in next chapter.

For the chopper circuit in Figure 2-16, the switching conditions are generally determined by DC voltage, load current, gate control, and propagation path. On the other hand, it is possible to slightly vary the propagation path in such a way that the variation will have negligible effect on the switching conditions. This is especially true if the difference in path characteristics mainly lies in the high-frequency range. Under the condition that the propagation paths chosen will not change the switching conditions, it can be straightforward to obtain the equivalent EMI source parameters Is_1, Is_2, Zs_1, and Zs_2, shown in Figure 2-18, with two sets of propagation paths and corresponding noise measurements.

Figure 2-22 and Figure 2-23 show the DM and CM noises of two different propagation paths. The DM and CM noise of Network I both have a noise peak at 7.2 MHz. The two noises of network II have a noise peak at 5.8 MHz. Since Network I has a lower inductance shown in Figure 2-20, the device and the path resonate at a higher

frequency. Changing the bus structure results in a change of the DM and CM noises in the high-frequency range (5 MHz – 30 MHz) simultaneously.

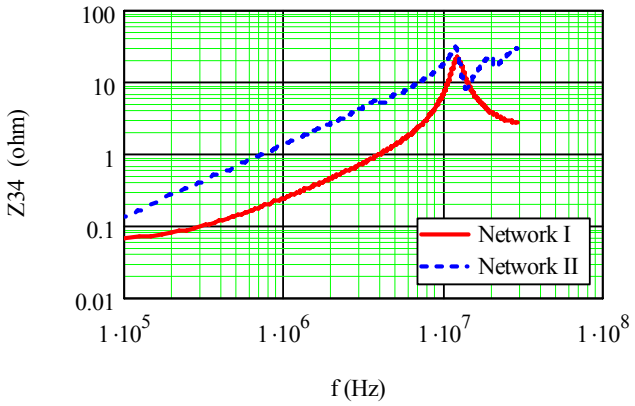

Figure 2-20 Comparison of Different Propagation Path Impedance Z_{34}

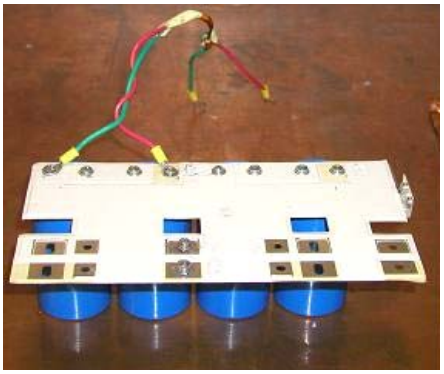

(a) Network I

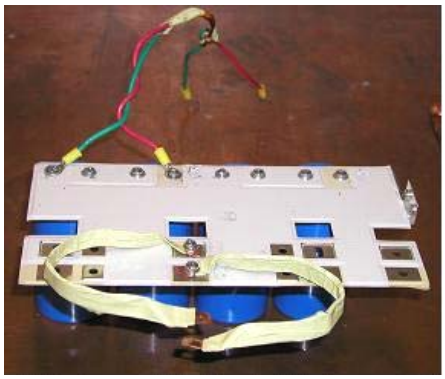

(b) Network II

Figure 2-21 Physical Structure of Network I and Network II

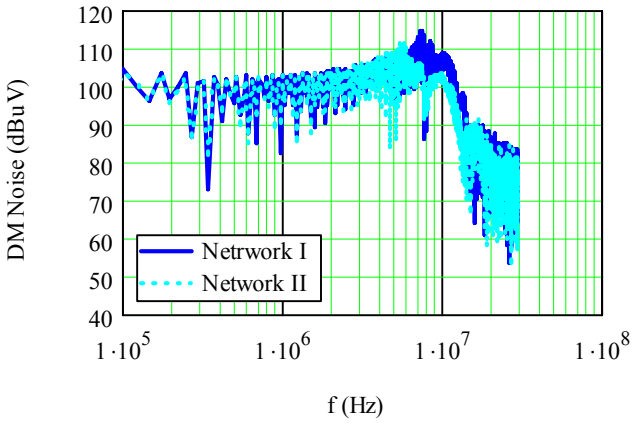

Figure 2-22 DM Noise Comparison for Two Different Paths

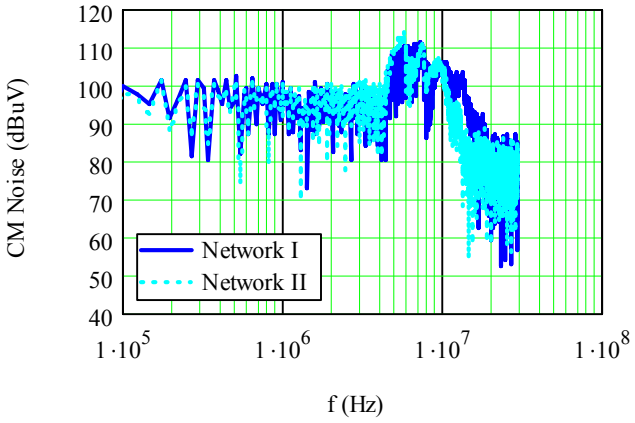

Figure 2-23 CM Noise Comparison for Two Different Paths

2.3.4. Experimental Verification

In order to verify the proposed frequency-domain EMI source modeling approach, a third propagation path network is built and tested with the same IGBT module. Again, the bus structure is modified for a different impedance matrix, as shown in Figure 2-24 and Figure 2-25. The third propagation path has a higher inductance. Therefore, the EMI noise should have a lower noise peak. With the EMI noise source currents, source impedances obtained previously, and the new path network impedance matrix $[Z'']$.

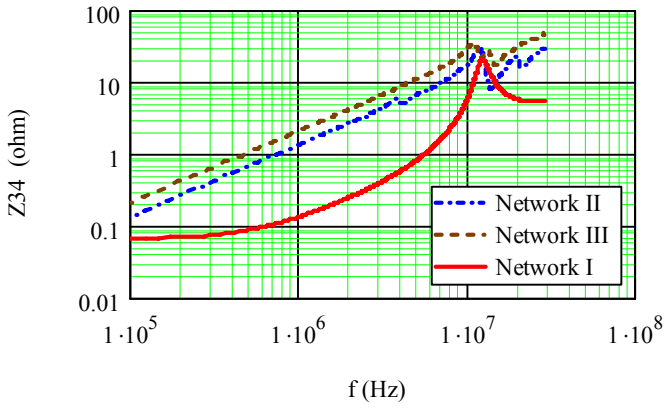

Figure 2-24 Comparison of Different Propagation Path Impedance Z_{34}

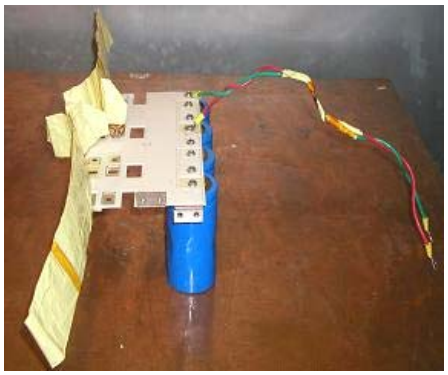

Figure 2-25 Physical Structure of Network III

The EMI test and predicted results are shown in Figure 2-26 (DM) and Figure 2-27 (CM). The noise peak is at 5 MHz, which is lower than Network I and Network II. The prediction and test results match closely throughout the entire frequency range. The maximum discrepancy is about 2 dBμV, and the frequency peaks can be accurately predicted.

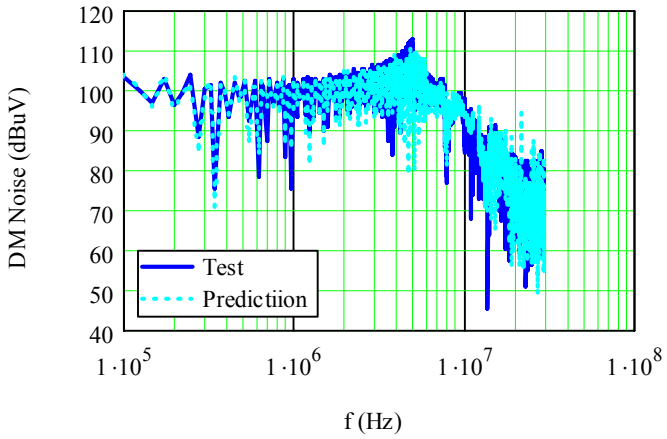

Figure 2-26 DM Test and Prediction Results with the Third Propagation Path Setup

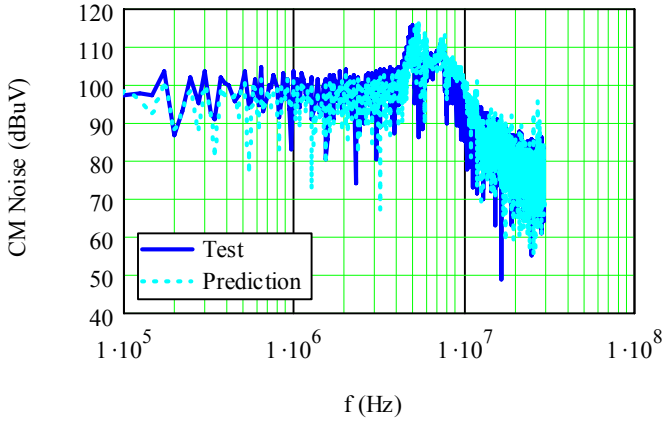

Figure 2-27 CM Test and Prediction Results with the Third Propagation Path Setup

2.4. Summary

In this chapter, the concepts of an EMI equivalent source and source impedance are systematically presented. The basic characteristics of the EMI noise source are analyzed first. As shown in the example, the source impedance is essential to describe the device module's high-frequency EMI characteristics. A linear circuit theory – the Norton equivalent circuit – is used to derive the source currents and source impedances. In next chapter, the validity of applying linear circuit theory will be analyzed in detail.

The major contribution presented in this chapter is the proposed modular-terminal-behavioral (MTB) equivalent EMI noise source modeling methodology, which is based on the EMI noise source and source impedance concepts. The methodology is to model a device switching behavior as a three-terminal active network along with current sources and source impedances. Since the model has modular and terminal characteristics, it can be easily used to derive an equivalent EMI noise emission model in a phase-leg based power converter. It also has the advantages of behavioral models. A chopper circuit, used as an example, demonstrates the modeling and prediction process. The experimental results show that the model can accurately predict EMI noise in the entire conducted EMI range.

In summary, the proposed MTB equivalent source modeling methodology forms the foundation of this dissertation.

Chapter 3 MTB Equivalent Source Model Analysis and Evaluation

Chapter 3 continues the analysis of the MTB equivalent EMI noise modeling methodology. The validity of the model and the prediction errors existing in the process and the measurement are discussed. The EMI noise characteristics based on the MTB model are analyzed in detail. A unified MTB CM and DM model is proposed and analyzed in detail, which can be used to predict DM and CM noise simultaneously. At the end of the chapter, the state-of-the-art methodologies and the proposed methodology are compared and evaluated according to the evaluation criteria discussed in Chapter 1.

3.1. MTB Equivalent Source Model Validation Analysis

Although the MTB EMI model has been experimentally shown to be very accurate in a test system, it is inherently an approximate model. Just like other frequency-domain behavioral modeling approaches, the MTB modeling concept is fundamentally a linear system technique. Of course, the Norton equivalent source model is also a concept for linear time-invariant (LTI) system. Generally, in power converters all the components are nonlinear [84], [85]. For instance, the semiconductor devices are nonlinear based on their physics and time-varying. In order to analyze the validity of applying LTI circuit theories to the noise source modeling, the key factors that cause device-switching nonlinearity should be known first. There are several key parameters that determine the state of a semiconductor device [64]: 1) Bus voltage – the device equivalent capacitances are changed with different voltages. 2) Gate circuits – different gate circuit changes the device turn-on and turn-off trajectory. 3) Load current – different currents change the device switching speed.

Since the semiconductor devices have nonlinear and time-varying characteristics, there are restrictions on how the MTB model should be applied. The basic requirement is

that the switching conditions should be kept the same for the MTB model, since the device characteristics change with different switching conditions. In general, the device switching conditions are mainly determined by gate circuit, voltage, and current. As a result, when using the MTB source model for a converter, the switching conditions for the modeled device module should not be affected by the connecting propagation paths. For example, changing bus structures, as shown in Chapter 2, normally will not change switching conditions. Although different buses can cause different resonances during switching, those resonances that are resulted from the switching transition should already be damped before the next switching event, keeping the device switching conditions essentially unchanged for different propagation paths.

Therefore, the validation process includes two steps: 1) validate the LTI theory in a time-varying circuit, and 2) keep the nonlinear circuit in a linear range. In [110], the theoretical spectral analysis of periodically time-varying linear networks is given. It concludes that the ideas used in the conventional linear time-invariant two-port network theory can be extended to the case of linear two-port networks consisting of both time-invariant and periodically time-varying lumped elements. It also can be used in a one-port network. The most important condition to apply LTI theory to a time-varying circuit is periodically time-varying behavior of the system. When assessing and modeling EMI of a switching circuit under a certain condition, the switching behavior of devices is periodically repeated. Therefore, the LTI theory is valid for these circuits.

Since semiconductor devices can operate under any switching conditions, in theory there should be an EMI source model for each condition. However, it is impractical and unnecessary to derive hundreds of EMI source models for one device, because the nonlinearity of the device may not significantly affect the EMI noise generation in certain operating ranges. As a result, dividing all the device's operating conditions into several zones and using the derived EMI model to predict the noise is a practical and efficient way to study EMI issues in power converters. During the modeling process of one operating condition, the gate circuit, load current and bus voltage are not changed.

Although the operating condition of the device is fixed, the voltage on the device terminals and the current through the device change during the switching transients, which the nonlinearity of semiconductor devices exists. For example, the semiconductor p-n junction theory shows the non-linear capacitive effect. The p-n junction capacitance represents the modulation of the space-charge during the transition with respect to the change of the junction voltage. Usually, semiconductor device manufacturers publish the diode datasheet of capacitance vs. reverse voltage, as shown in Figure 3-1 [86]. The junction capacitance is decreased when the reverse voltage increases. The change of the junction capacitance is small when the voltage is higher than a certain value. Equation (3-1) is used to define the small-signal junction capacitance associated with the charge in the depletion layer. The result is valid irrespective of the junction profile and is equivalent to the capacitance of the parallel plate condenser of dielectric constant *k* and thickness *l*, which means the junction capacitor can be treated as a constant capacitor when the reverse voltage is higher than a certain value. The other semiconductor devices, such as IGBTs, have similar characteristics of nonlinear capacitances. An example of the capacitance vs. applied voltage is shown as in Figure 3-2 [87].

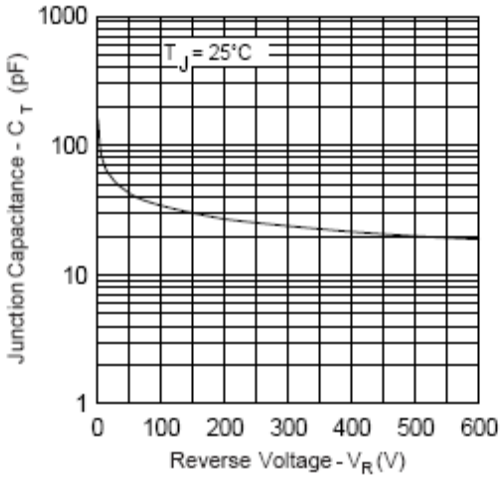

Figure 3-1 Typical Junction Capacitance vs. Reverse Voltage of a Diode

$$C_j = \frac{dQ}{dV} = \frac{k}{4\pi d} \quad \textbf{(3-1)}$$

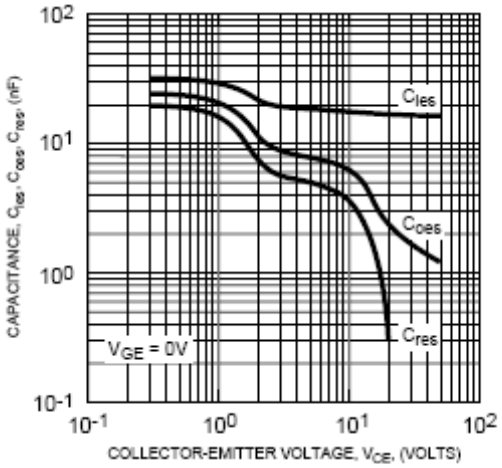

Figure 3-2 Typical Capacitances vs. Collector-emitter Voltage of an IGBT

Since nonlinearity is an intrinsic characteristic of semiconductor devices, the validity range of the modeling methodology is dependent on the effect of nonlinearity on device switching. Figure 3-3 is a simplification of a chopper circuit during switching transients. It is used to illustrate the nonlinear effect on commutation between the top and bottom device in a module. Since the DC link capacitance and load inductance are big enough, voltage on the DC link capacitor and load current can be replaced by the voltage and current source during the switching transients. The input current I and mid-point voltage U_m are shown in Figure 3-4. The waveform has four different zones: rising edge (I), ringing (II), falling edge (III) and ringing (IV). It can be decomposed as three major parts as in Figure 3-5. These include the ideal square waveform, the slope and ringings.

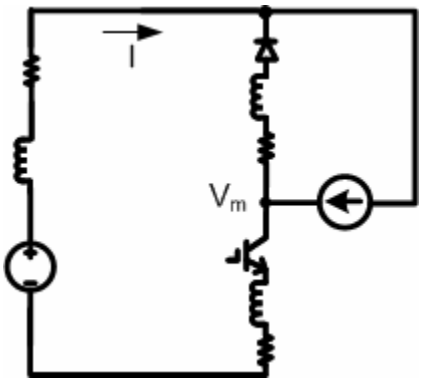

Figure 3-3 Illustration of Commutation between Devices in a Module

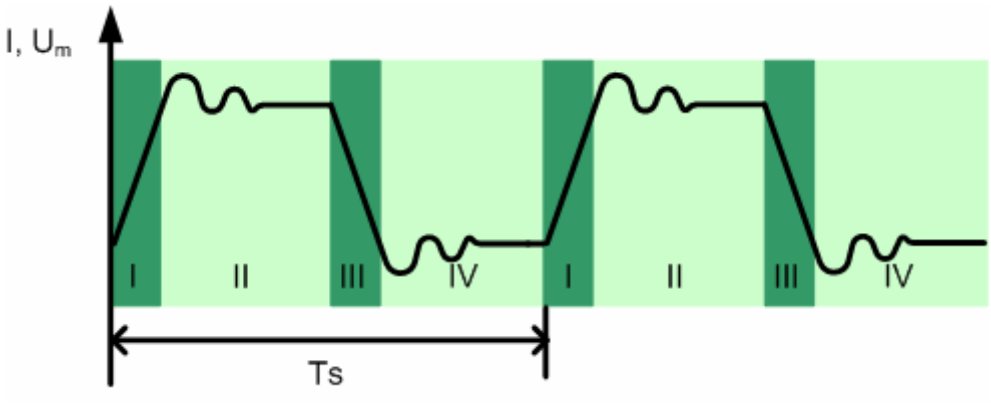

Figure 3-4 Input Current and Mid-point Voltage Waveforms

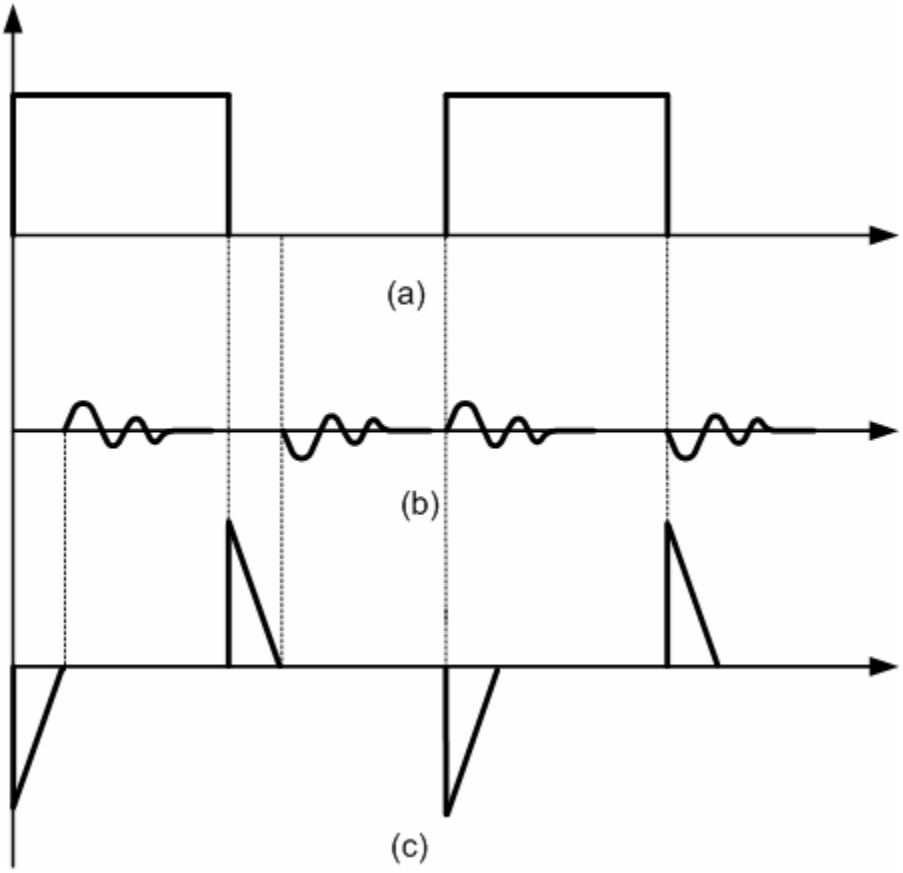

Figure 3-5 Decomposition of Input Current and Mid-point Voltage Waveforms (a) Ideal Square Waveform; (b) Slope; (c) Ringing

Figure 3-5 (a) is the ideal square waveform. As an assumption of the proposed modeling methodology, the operating condition, which determines the bus voltage and load current, stays constant. In addition, the duty cycle of the square waveform is controlled by the converter's functional design and is not changed by the device switching characteristics. Therefore, the square waveform is a linear part of the source model.

Figure 3-5 (b) is the illustration of resonances in the circuit. The ringings are caused by the resonance between the junction capacitor and the inductors, including the lead inductor of the device module and the parasitic inductor of the DC-link capacitor. In the structure shown in Figure 3-3, the inductance of the bus structure is not considered for the sake of simplification. In an actual case, such as the testbed used in Chapter 2, the equivalent bus inductance also involves in the resonance.

The resonances start at the time when the current or voltage is higher than the load current or bus voltage, which indicates that the initial condition of the resonance is the load current or bus voltage. As shown in device datasheets, when the applied voltage on the device terminal is the same as the bus voltage, the junction capacitance is reduced to a small value and stays almost constant if the resonant voltage does not resonate back to a low voltage. For example, when the bottom IGBT fully turns on, the voltage on the diode is about the same as the DC bus voltage though there are some voltage drops on parasitic inductors. The junction capacitance of the diode is a small value and undergoes almost no change. The ringings result in the resonance between the capacitor and parasitic inductors. The same phenomenon occurs in the IGBT when diode fully conducts. The equivalent circuit causing ringings can be shown as Figure 3-6 (a). It is a linear circuit.

Although the voltage on the device terminals can be changed due to the resonance, it is usually high enough to maintain the same capacitance. In practice, the voltage ringings are damped quickly, ending by the next switching transition, which is required by the unchanged switching conditions for MTB modeling. In Figure 3-5 (b), the ringings at Zone II and IV are the same frequency. This may not actually be true since the diode junction capacitance may be different from the IGBT output capacitance, which causes

different resonant frequencies. But during this ringing period, both cases can be represented by the same equivalent linear circuit in Figure 3-6 (a), except for the different capacitances.

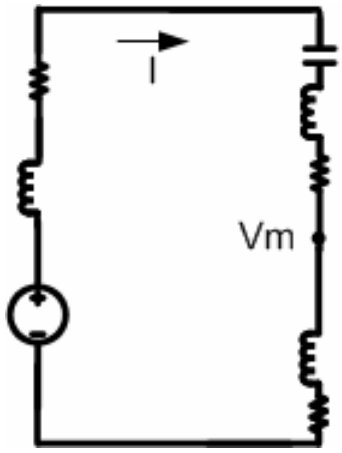

(a) Range I and III

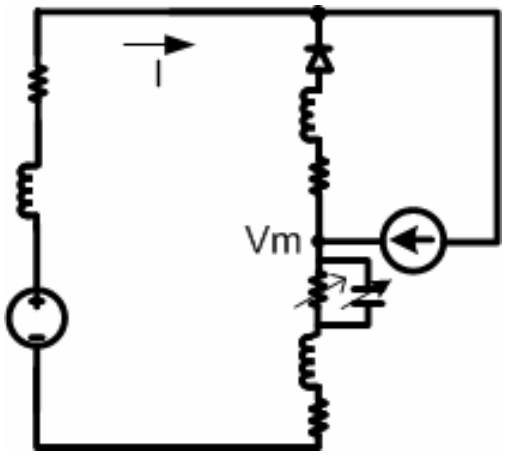

(b) Range II and IV

Figure 3-6 Equivalent Circuit for Different Switching Range

Figure 3-5 (c) is the illustration of the commutation between the diode and the IGBT. It describes the current and voltage change between two devices. During this process, the device equivalent parameters change, such as junction capacitance and resistance. When the IGBT turns on, it can be described by Figure 3-5 (b). The equivalent circuit of the diode turn-on period is similar to the IGBT turn-on, except the diode parameters change

instead of the IGBT. From the equivalent circuit and device datasheets, the major characteristics affecting the nonlinearity of the semiconductor device is the junction capacitance, and this could affect this commutation process.

Therefore, devices' nonlinearity during this period may affect the validity of the proposed MTB modeling methodology. In linear circuits, the equivalent source and impedance are not changed no matter what external circuit parameters change. But for a nonlinear circuit, there could be more than one pair of equivalent source and impedance when other circuit parameters change. In other words, one pair of the equivalent source and impedance is only valid for one condition in nonlinear circuits. When the effect of nonlinearity is small, the nonlinear circuit can be simplified as a linear circuit.

Figure 3-7 (a) and (b) are the simulation schematics of a linear and nonlinear circuit during the switching period. The schematic is based on the model shown in Figure 3-3. The external inductance is 100 nH. In Figure 3-7 (b), the nonlinear capacitor model is from the Saber simulation library. When the voltage on terminal P and M is high, which is the same situation as when there is no gate signal and the IGBT is added to the forward voltage, the nonlinear capacitance is small. When the terminal voltage V_{PM} is reduced, the capacitance will be increased. In the example, the maximum capacitance is 3 nF. At the reference voltage 50 V, the capacitance is 0.5 nF. And when voltage is higher than 50 V, the capacitance is reduced to 0.4 nF.

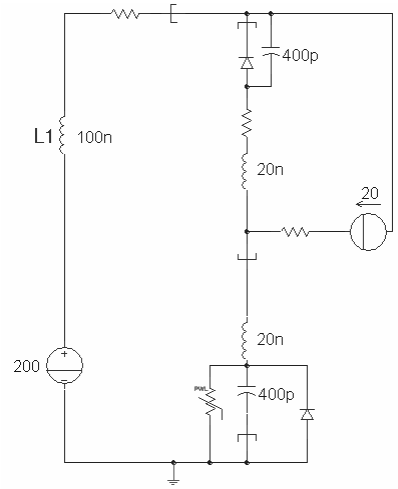

(a) Linear Circuit

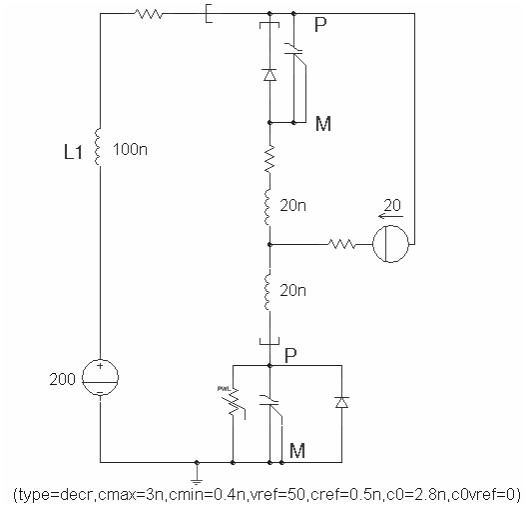

(b) Nonlinear Circuit

Figure 3-7 Simulation Schematics of Linear and Nonlinear Circuit

From the simulation results in Figure 3-8, it can be observed that the input current and mid-point voltage have similar slope and ringings as the linear circuit during the turn-off period. But for a nonlinear circuit, the voltage rising is very slow due to the big capacitance when the bottom device starts being turned off. Once the voltage increases, the behavior of the nonlinear circuit is same as the linear circuit, which can also be shown in the frequency-domain waveform in Figure 3-8 (b). Although there is a discrepancy in the time-domain waveform during device turn-off period, it causes very little difference between the linear and nonlinear circuit. Except for the waveforms' shifting, the current and voltage have the same frequency spectrum. Therefore, the linear circuit can be used to represent the nonlinear case and the linear circuit theory can be applied.

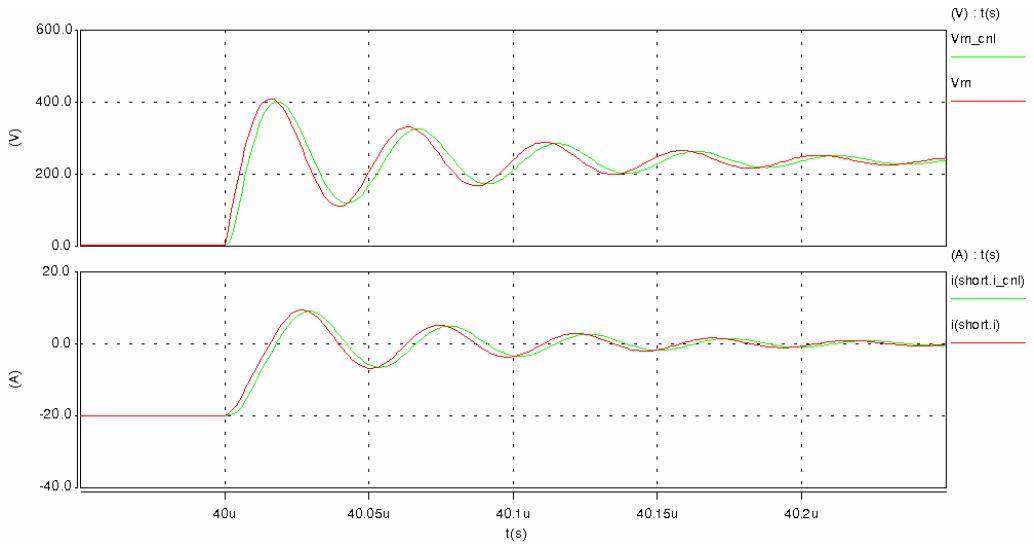

(a) Time-domain Waveform
(Vm_cnl, i_cnl: mid-point voltage and input current in nonlinear circuit;
Vm, i: mid-point voltage and input current in linear circuit)

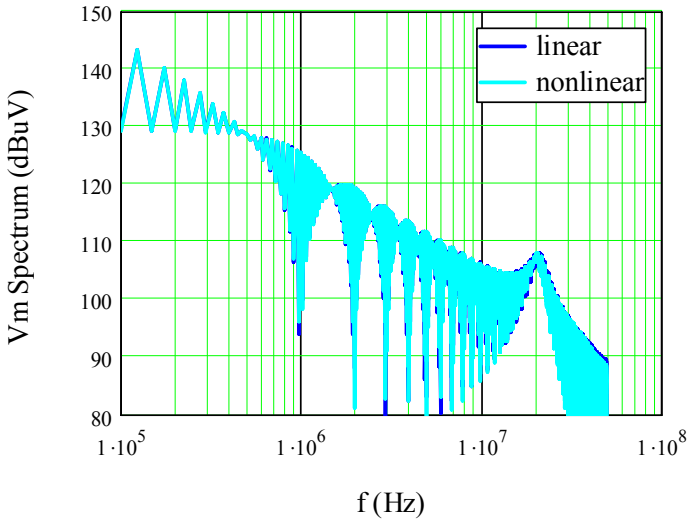

(b) Mid-point Voltage Frequency Spectrum Comparison

Figure 3-8 Simulation Comparison of Linear and Nonlinear Circuit (L1=100 nH)

When changing the propagation path, such as paralleling a snubber capacitor (2 nF) with devices and keeping the same L1, the conclusion is the same as the results shown in Figure 3-9 (a) and (b). Because of the large capacitance, the resonance frequency is lower. As a result, the snubber capacitors (2 nF) will not affect the validity of applying linear circuit theory in this case.

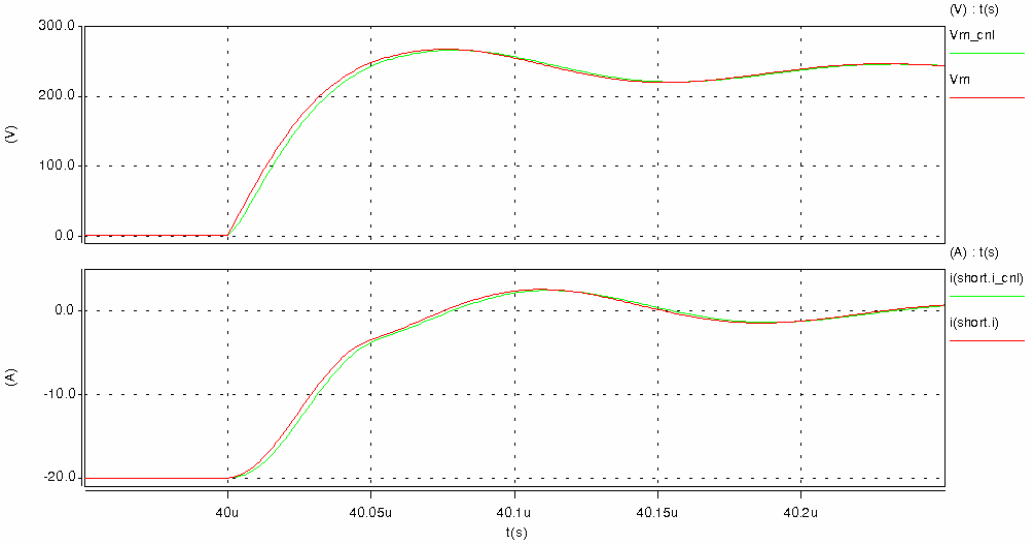

(a) Time-domain Waveform
(Vm_cnl, i_cnl: mid-point voltage and input current in nonlinear circuit;
Vm, i: mid-point voltage and input current in linear circuit)

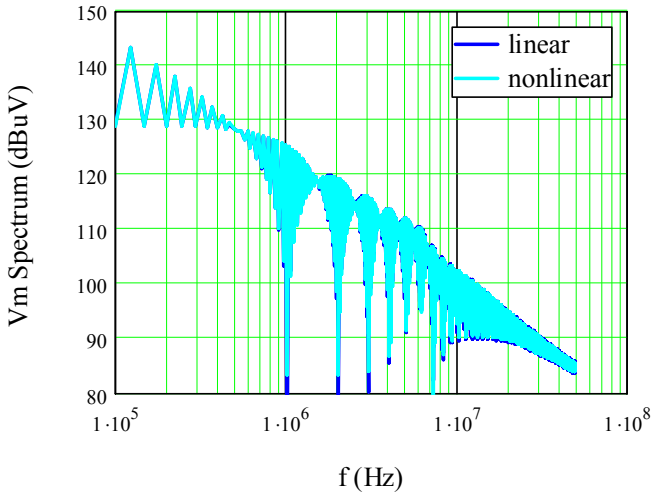

(b) Mid-point Voltage Frequency Spectrum

Figure 3-9 Simulation Comparison of Linear and Nonlinear Circuit (L1=100 nH, snubber = 2nF)

When continually increasing the snubber capacitance (10 nF), the nonlinear circuit still can be replaced by the linear circuit, as the results show in Figure 3-11 (a) and (b). Because of the big snubber capacitance, the rising edge is mostly affected by the snubber capacitor instead of devices' nonlinear capacitance. Therefore, the MTB modeling process is valid when the propagation path is changed due to the change of snubber capacitors.

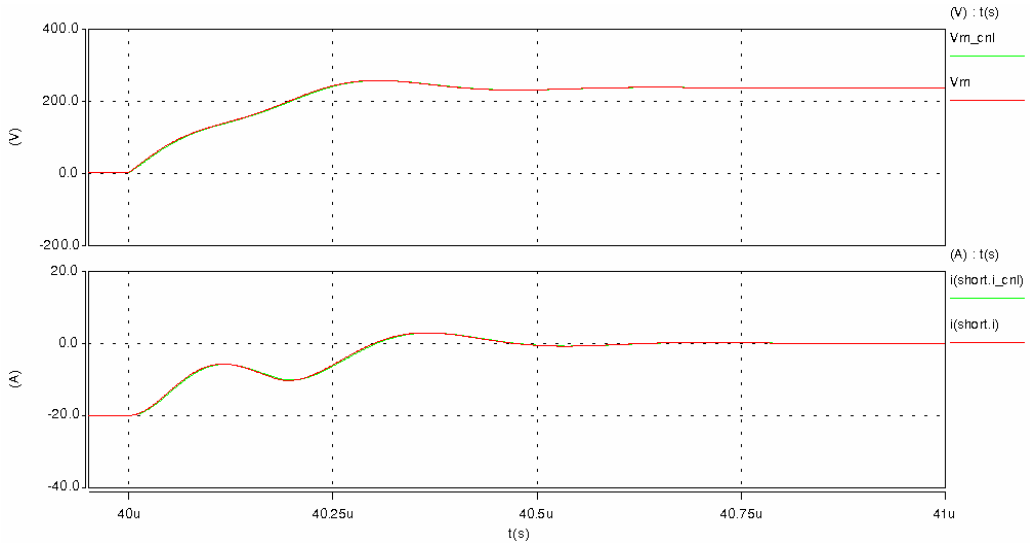

(a) Time-domain Waveform
(Vm_cnl, i_cnl: mid-point voltage and input current in nonlinear circuit; Vm, i: mid-point voltage and input current in linear circuit)

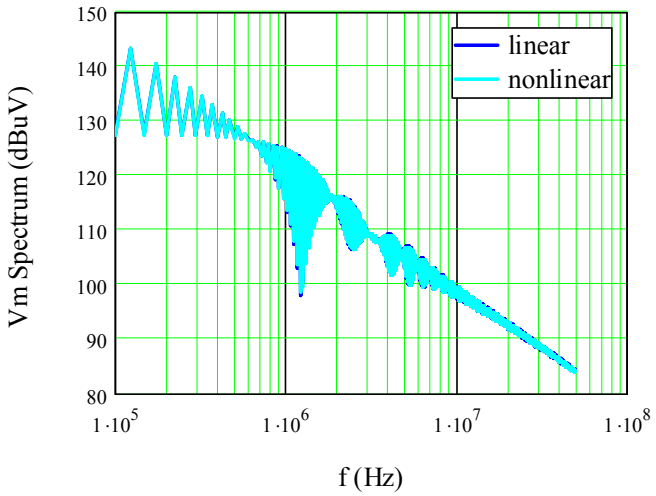

(b) Mid-point Voltage Frequency Spectrum

Figure 3-10 Simulation Comparison of Linear and Nonlinear Circuit (L1=100 nH, snubber = 10nF)

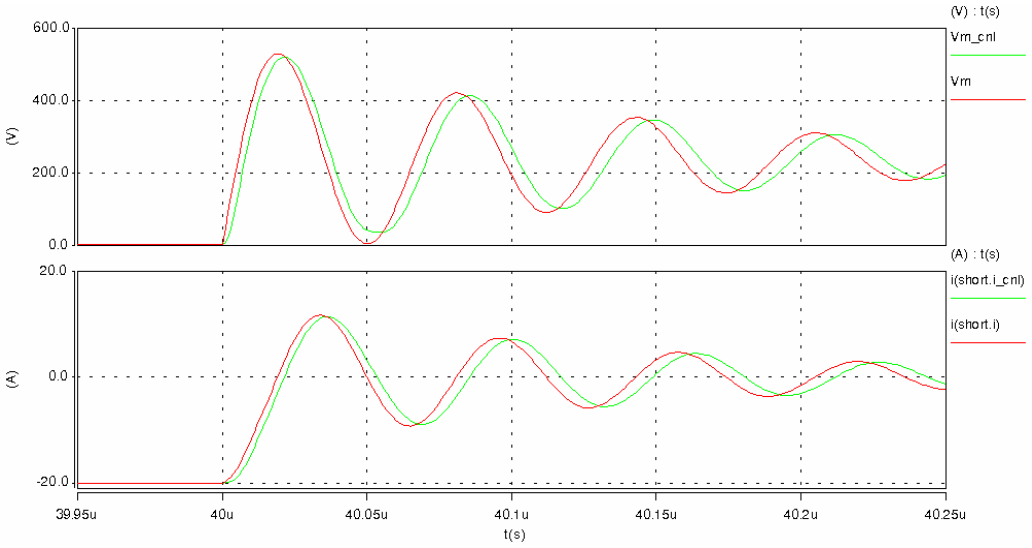

(a) Time-domain Waveform
(Vm_cnl, i_cnl: mid-point voltage and input current in nonlinear circuit;
Vm, i: mid-point voltage and input current in linear circuit)

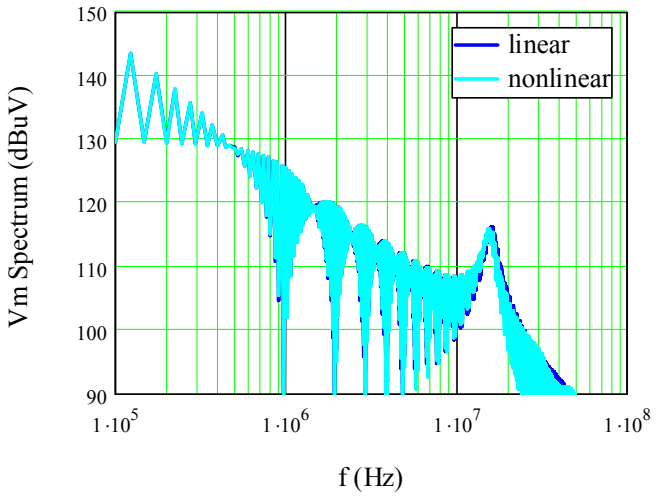

(b) Mid-point Voltage Frequency Spectrum

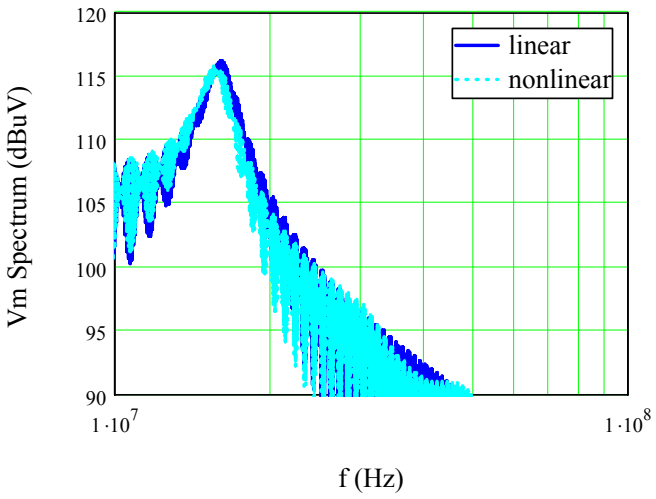

(c) Zoomed Mid-point Voltage Frequency Spectrum

Figure 3-11 Simulation Comparison of Linear and Nonlinear Circuit (L1=200 nH)

Another possible variation is changing the inductance in the loop, such as L1. The simulation results of increasing L1 to 200 nH is shown in Figure 3-11 (a) and (b). Both the time-domain and frequency-domain waveforms show that the slope does not change much when changing L1. But the ringings of nonlinear and linear circuit are different. Because of the nonlinear capacitance, the circuit can resonate with different frequencies. For example, when the voltage resonates to a small value, the capacitance becomes bigger, which results in low-frequency ringing, as shown in Figure 3-11 (a). Therefore, the linear and nonlinear circuit frequency-domain waveform in Figure 3-11 (b) and (c) are different. The resonant frequency in the nonlinear circuit moves toward to the lower frequency. The frequency difference is about 300 kHz and the magnitude difference is about 1 dBμV. Because of the damping effect of the circuit, the voltage resonant amplitude becomes small and is not severely nonlinear. The difference between the linear and nonlinear circuit is not severe.

When continually increasing L1 (L1=400 nH), the ringing amplitude is increased accordingly, as shown in Figure 3-12. The frequency-domain waveforms of a linear and nonlinear circuit are different, especially their different resonant peaks. The difference starts from 7 MHz. The resonance peak of the nonlinear circuit moves to 11.5 MHz and

the magnitude is 122.8 dBμV, which is 500 KHz lower and 3 dBμV higher than the peak of the linear circuit. The noise level and shape also change from the linear circuit.

There are two reasons for the discrepancies. One reason for this is the same as in the previous analysis. The large amplitude resonant voltage and small damping effect caused the nonlinear capacitor to return back to the nonlinear region, which results in the different resonant frequency and magnitude. Because of the low voltage, the nonlinear capacitance becomes very large (3 nF) and the resonance frequency is very low. The other reason is that when the Vm resonates to zero, the anti-parallel diode clamps the voltage to zero, which is also a nonlinear effect and change the resonance abruptly. This phenomenon widely exists in circuits with soft-switching techniques. Therefore, the nonlinear circuit with large resonant amplitude and diode-clamping cases cannot be applied the linear circuit theory.

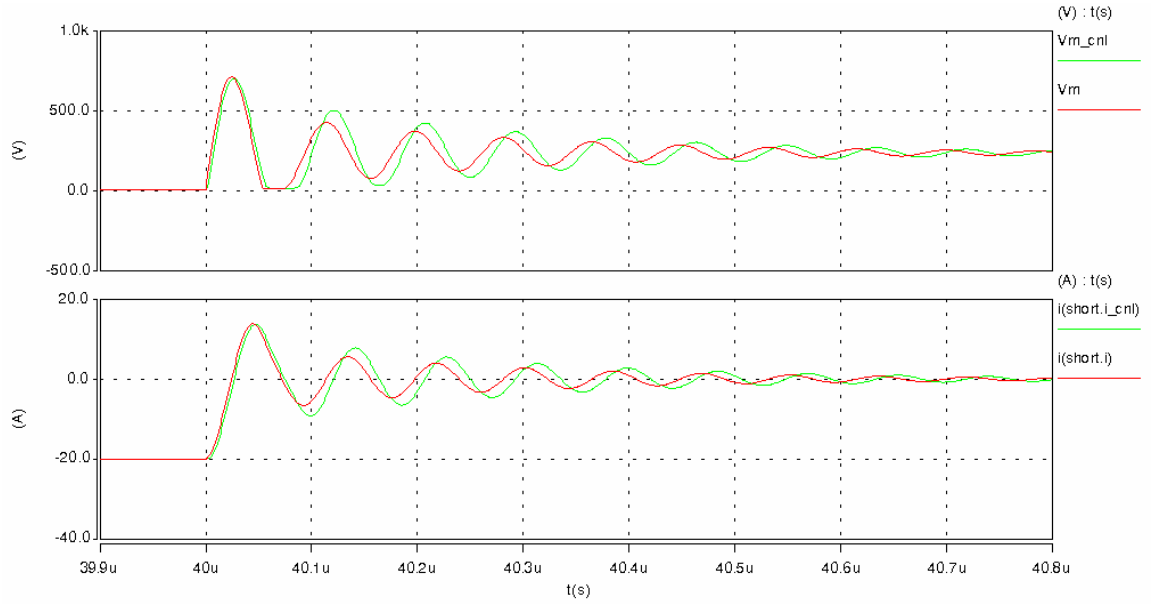

(a) Time-domain Waveform
(Vm_cnl, i_cnl: mid-point voltage and input current in nonlinear circuit;
Vm, i: mid-point voltage and input current in linear circuit)

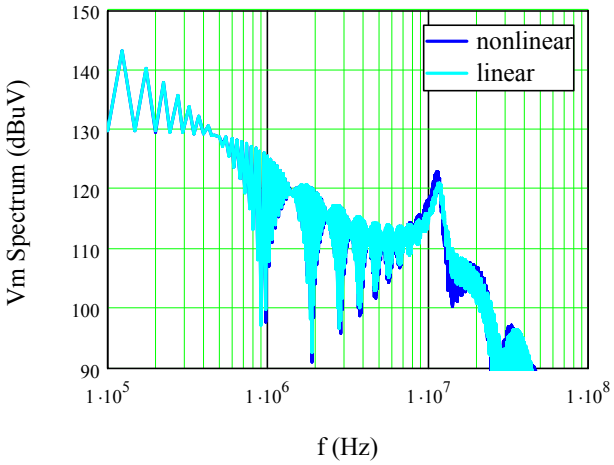

(b) Mid-point Voltage Frequency Spectrum

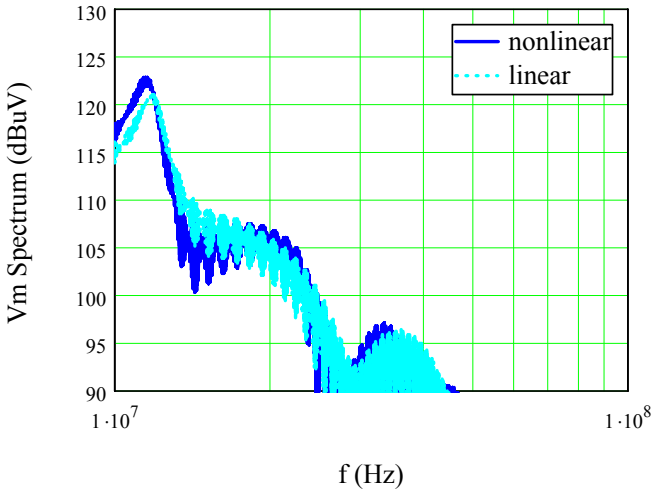

(c) Zoomed Mid-point Voltage Frequency Spectrum

Figure 3-12 Simulation Comparison of Linear and Nonlinear Circuit (L1=400 nH)

The above analysis shows that the nonlinearity during switching transients can affect EMI noise generation. As shown in Figure 3-5, the mid-point voltage and input current can be decomposed as three parts. The nonlinearity can affect the rising and falling slopes and the ringings. But the nonlinear capacitance will not affect the rising and falling part significantly, because the nonlinear period is short. When adding snubber capacitors, the dominant factor is not the nonlinear capacitor. Therefore, the circuit can still be treated as a linear circuit. In terms of the ringings, the effects from the nonlinear capacitor are

determined by the resonance amplitude and the damping factor. The larger the resonance amplitude, the more nonlinear effects including the diode-clamping situation could happen. In order to reduce the nonlinear effects, an attempt should be made to keep the device terminal voltage from resonating back to the nonlinear region.

As discussed above, the important EMI noise generation period – device switching transients – involves the nonlinear effect. Since the MTB EMI equivalent source modeling concept is fundamentally a linear system technique, there are restrictions on how the MTB model should be applied. The basic requirements are summarized as follows:

1) The switching conditions should be kept the same for the MTB model, since the device characteristics change with different switching conditions. In general, the device switching conditions are mainly determined by gate control, voltage, and current. As a result, when using the MTB source model for a converter, the switching conditions for the modeled device module should not be affected by the connecting propagation paths.

2) During the modeling process, changing the propagation path should not change switching conditions. Although different propagation paths can cause different resonances during switching, those resonances that result from the switching transition should already be damped before the next switching event, keeping the device switching conditions essentially unchanged for different propagations.

3) The device terminal voltage resonating back to the severe nonlinear region should be avoided when selecting a propagation path. In practice, the resonant voltage is usually controlled because a large voltage resonance may destroy devices and the damping effect in the high-frequency range is large. With increasing frequency, the AC resistance of the circuit loop can help reducing the resonance in the circuit. In order to valid the MTB model the propagation path should be designed carefully.

In short, the MTB modeling methodology based on the linear circuit theory is valid when certain conditions are satisfied. In the modeling process, the propagation paths and switching conditions should be kept the device in the linear region.

3.2. EMI Noise Prediction Analysis

As presented in Chapter 2, the modeling process is carried out in the frequency domain, except for measuring time-domain noise waveforms on LISNs. Since the purpose of the modeling is to extract the device switching behavior under certain operating conditions, it is not necessary and may not be possible to use the tests required by the EMI standards to obtain the model. During the modeling process, there are two major error sources in making a prediction: 1) Data processing, and 2) Measurements.

3.2.1. Data Processing Error

In Chapter 2, instead of the EMC analyzer, a digital storage oscilloscope (DSO) – the Tektronix TDS7054 [91] – is used to collect EMI noise data on LISNs due to the modeling process of the proposed MTB method. There are several characteristics to consider in choosing the right oscilloscope, including: 1) Sampling rate; 2) Bandwidth; 3) Input impedance.

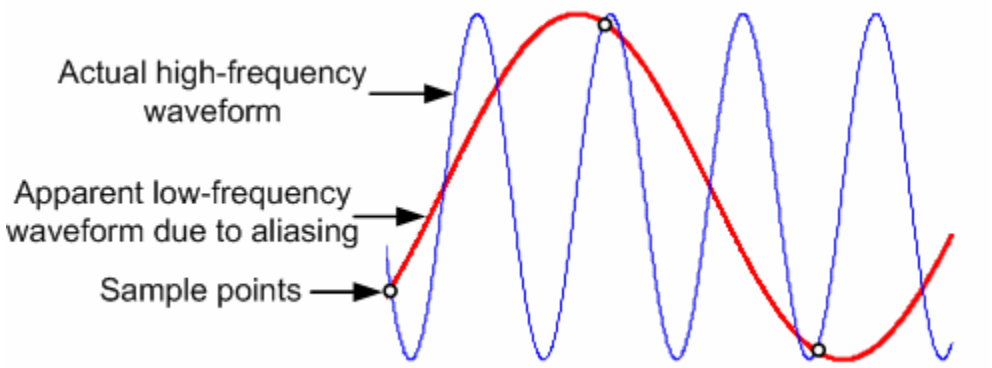

Figure 3-13 Illustration of Aliasing Effect

The sampling rate is an important parameter in choosing a DSO, since it determines the accuracy of the following DFT. When the oscilloscope is not sampling the signal fast enough, the aliasing effect occurs, as shown in Figure 3-13. The phenomenon of aliasing means that two continuous sinusoids of different frequencies appear at the same frequency when sampled. Therefore, they cannot be distinguished based on their samples alone.

Aliasing is a distortion of the signal being measured shifted to a frequency lower than the original frequency. The Nyquist criterion [89] or sampling theorem [92] requires two or more samples per measured signal cycle to prevent the aliasing phenomenon. But the sampling theorem also requires that the noise be band-limited, which means all frequency above half of the sampling frequency is zero. In the experiments, the sampling rate in the test is 250 M/s and the highest noise frequency of interest is 30MHz. Regarding the EMI noise characteristics, noise higher than the half of the sampling frequency measured from LISNs will be attenuated significantly and the quantity of those frequencies is small, therefore the experiment sampling rate is still reasonable for good accuracy. In addition, to minimize the error caused by the aliasing effect, it is standard practice to precede the sampling operation by a low-pass anti-alias filter that will remove substantially all spectral content above the half-sampling frequency.

The bandwidth of an oscilloscope is another important factor in choosing a DSO. The bandwidth must be sufficiently wide to reproduce the signal faithfully. A rough approximation is to use the 'rule-of-thumb' equation $f=1/(\pi t_r)$ of the signal being measured. Above this bandwidth frequency, the spectrum envelope rolls off by 40 dB/dec. Therefore, in measuring a 1-ns rise-time pulse, the oscilloscope must have an absolute minimum bandwidth of 350 MHz. The bandwidth of the oscilloscope used is 500 MHz.

For accuracy in signal acquisition, the impedance of the oscilloscope must match that of the coax and probe. Using a 75-Ω coax with a 50-Ω scope input will produce significant error in measurement data. In the experiment, a 50 Ω terminator is connected with a LISN output, and a high-input impedance input is selected (typically 1 MΩ).

Though the digital oscilloscope can store the data and calculate the signal's frequency spectrum, the function of performing DFT is not used because there are other frequency-domain calculations in the modeling process. Therefore, post-processing after collecting data by the oscilloscope is necessary. A piece of commercial mathematical calculation software, Mathcad®, is used to process the data. A simple linear circuit, as shown in Figure 3-14 (a), is used to examine the accuracy of the software for all frequency-domain

calculations. A trapezoidal current source shown in Figure 3-14 (b) and some impedances are included in the noise source block. The rest of the circuit is the propagation path. The modeling process is the same as that presented in Chapter 2. By changing propagation paths, as shown in Figure 3-15, the noise source and source impedance can be obtained, as described in Figure 3-16 and Figure 3-17. The source impedance can also be drawn directly by the known impedances in the circuit, shown by the dotted line in Figure 3-17. From the results, it can be seen that the calculation using Mathcad has no significant error for the entire conducted EMI frequency range. Since the process is only done in Mathcad, other effects, such as sampling, are not included.

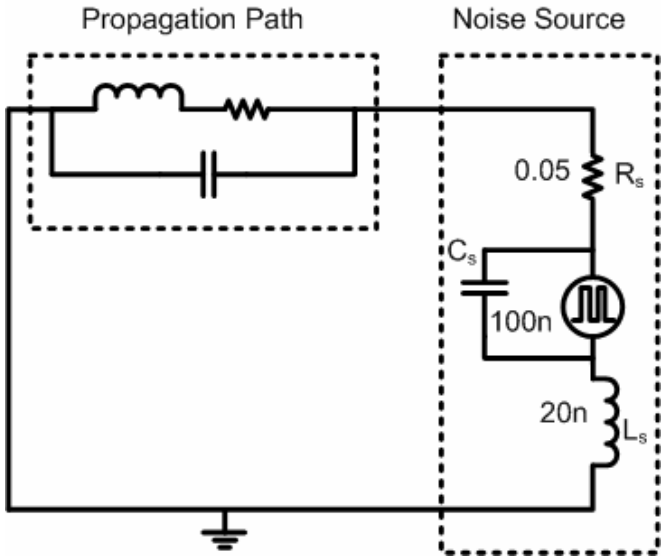

(a) Circuit

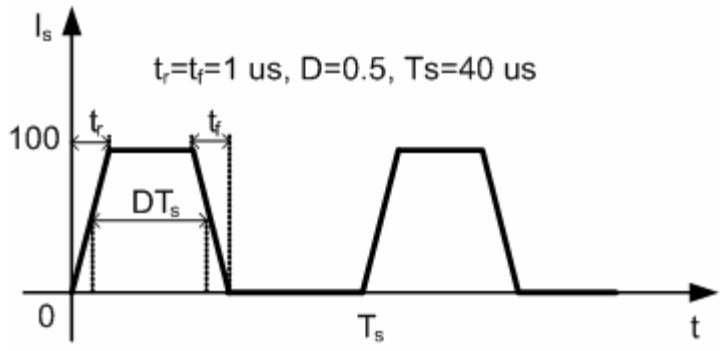

(b) Current Source Waveform

Figure 3-14 A Linear Circuit for Verifying Post data-processing Accuracy

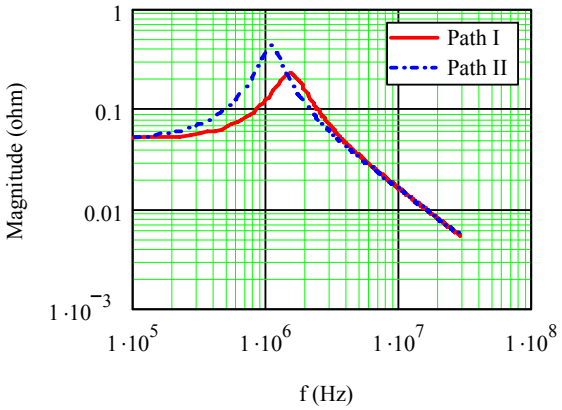

Figure 3-15 Two Different Propagation Paths

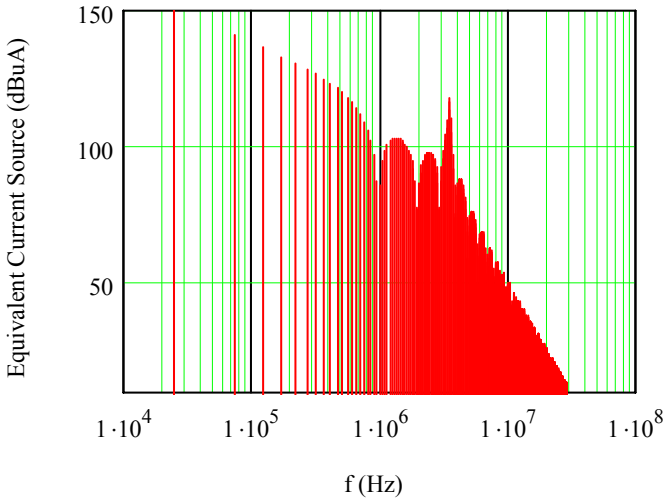

Figure 3-16 Equivalent Terminal Current Source

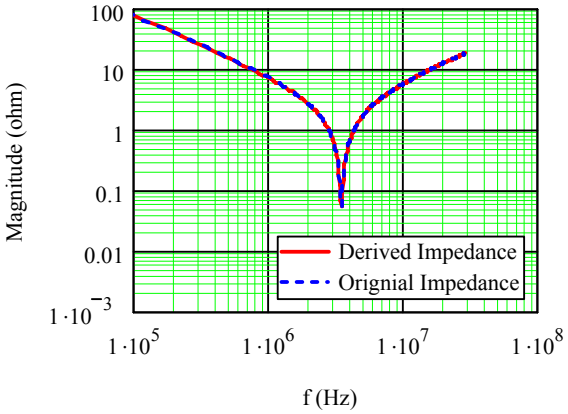

Figure 3-17 Equivalent Source Impedance

3.2.2. Experimental Error

From the above analysis, it can be seen that the accuracy of the source derivation is high when the process is only carried out in the Mathcad. In experiments, there are other factors which may affect the accuracy of the modeling process. In the modeling process, the oscilloscope digitizes the noise waveform and exports the noise data for data processing. Because of the limitation of the oscilloscope, the sampled data can produce some other errors in addition to aliasing effect. A simple example is given to analyze this problem briefly.

Figure 3-18 is a trapezoidal waveform with ringings, which is written in Mathcad with an analytical form. When sampling this waveform with different levels of accuracy (sampled data with different significant digits), the differences can be shown in Figure 3-19 (a), (b) and (c). The original spectrum of the trapezoidal waveform is from transferring the sampled data, which have 16 significant digits. When changing the sampling accuracy by 2, 3, and 6 significant digits respectively, the difference from the original spectrum is reduced with the increasing the digits. For the data with 2 significant digits, the difference starts from 2 MHz and increases with frequency. When increasing the significant digits to 6, the difference from the sampled data with 6 digits is very small during the conducted EMI frequency range.

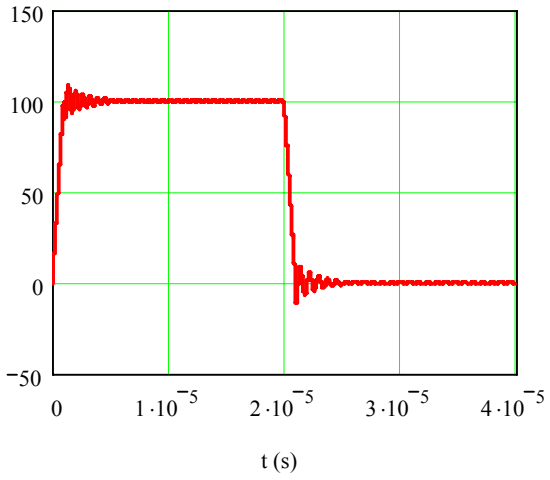

Figure 3-18 Trapezoidal Waveform with Ringings

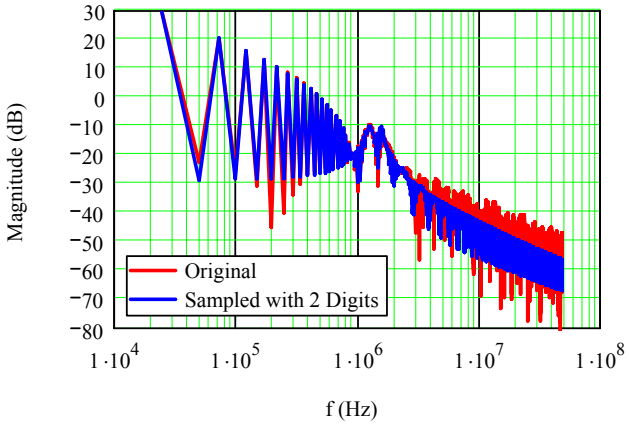

(a) Sampled Data with 2 Significant Digits

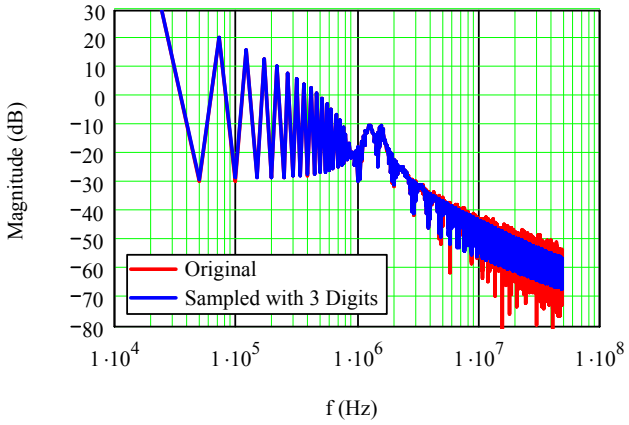

(b) Sampled Data with 3 Significant Digits

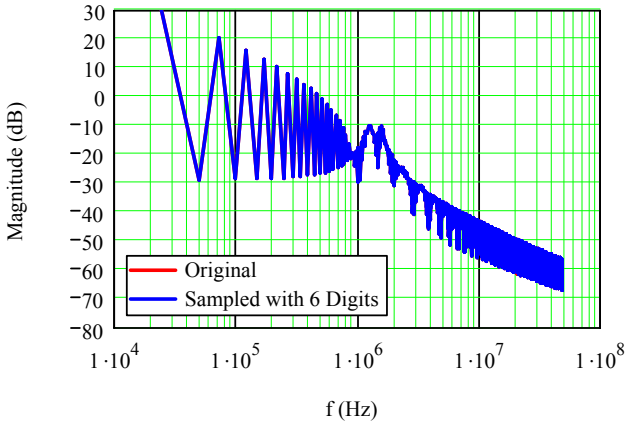

(c) Sampled Data with 6 Significant Digits

Figure 3-19 Comparison of Sampled Data with Difference Accuracy

In the experiment, the oscilloscope can only export the data with 3 significant digits. Therefore, the error from the sampled data starts from 5 MHz and is 4 dB at 30 MHz. Since sampling the data is the first step to derive the MTB in the frequency domain, the error from sampled data may cause a larger error in the high-frequency range. One of the solutions of reducing the MTB modeling error is to use a high-accuracy oscilloscope to collect the data. If the data have 6 digits, the error from sampling can be neglected for the entire conducted frequency range.

3.3. Unified MTB Equivalent DM and CM Source Model

As presented in Chapter 2, another important difference between the proposed method and most existing behavioral modeling methods is that the new method does not separately model CM and DM noise sources. A 5×5 impedance matrix is used to depict the propagation path of both CM and DM noise. Therefore, the derived source model is not separated into CM and DM noise source. To summarize, the proposed MTB equivalent source model is a unified equivalent CM and DM source model.

In the test circuit, as redrawn in Figure 3-20, the CM and DM noise on LISN terminals can be calculated by Eqs. (3-2) and (3-3) according to the definition.

$$V_{CM} = \frac{V_1 + V_2}{2} \tag{3-2}$$

$$V_{DM} = \frac{V_1 - V_2}{2} \tag{3-3}$$

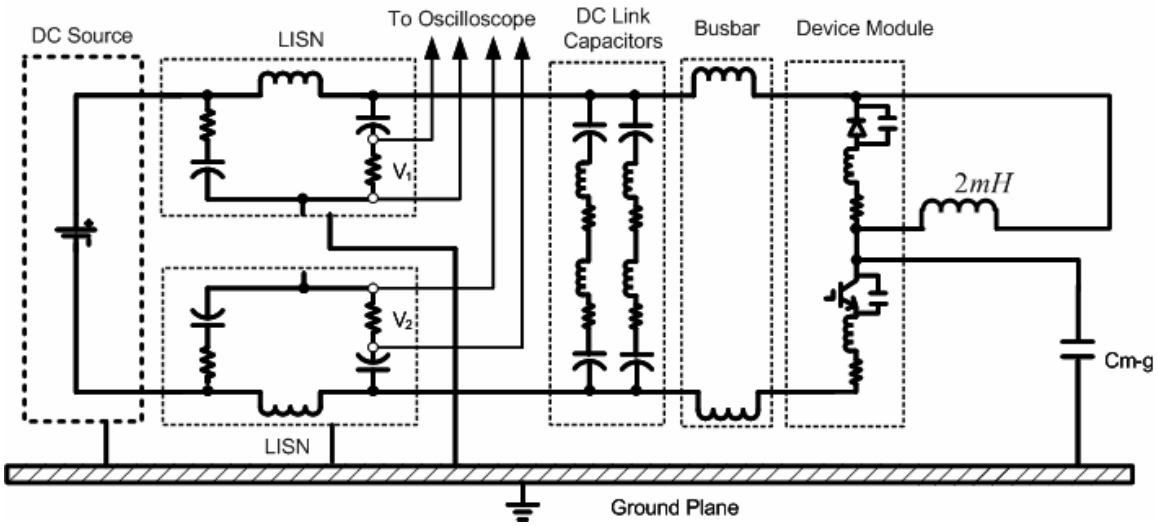

Figure 3-20 Chopper Circuit Test Circuit

The concept of CM and DM noise separation is widely used. For example, the two DC buses are considered equal-potential for CM noise in [39]. As a result, the two DC buses are shorted when modeling CM noise in a drive system. Although the separation of noise modes is very helpful for noise modeling and filter design, it is based on the assumption that the CM and DM noises are decoupled and the CM and DM propagation paths can be physically separated.

In the case of Figure 3-20, the CM and DM noises on the LISNs are generated from the same noise source – device switching – and propagate through the busbar and ground to the LISN side. Basically, the DM noise is caused by the discontinued input current and the CM current is induced by the voltage variation through the capacitors to the ground. When the device switches, the parasitics of the DC-link capacitor and busbar can resonate with the device module output capacitor, and the voltage change at the switching module mid-point induces the CM current flowing through the ground, as shown in Figure 3-21. The mid-point-to-ground voltage U_{mg} has a resonant frequency at 6.25 MHz, which is equal to the frequency which is roughly calculated by the inductances of the busbar and DC-link capacitor and the output capacitance of the device module. The resonance caused by the inductance of the busbar and the capacitance (280 pF) between the mid-point and the ground is around 20 MHz.

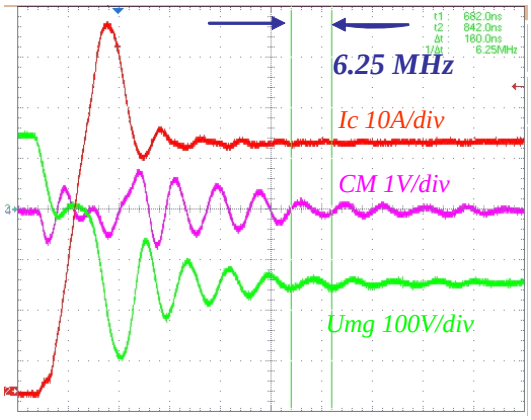

(a) Turn-on

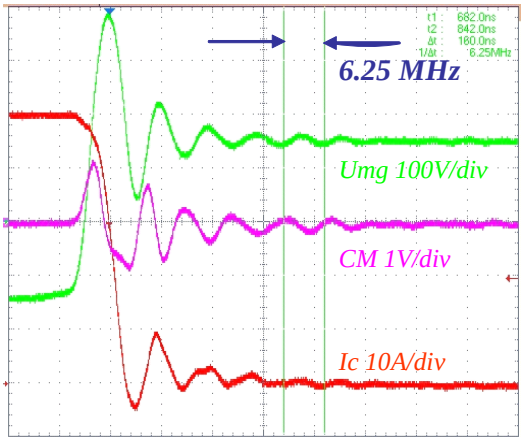

(b) Turn-off

Figure 3-21 Switching Waveform of the Test Circuit

In this case, the parasitic inductance of the DC-link capacitor affects the CM noise significantly, which in previous EMI research is usually considered to be only part of the DM noise path. When separating the DM and CM propagation path with traditional methods [35], [39], [41], [47], the effect from the parasitic inductance between two busbars is ignored. In the conducted EMI range, this effect described above is very important because missing the resonant peak could cause the whole converter to fail to pass EMI regulations. In addition, the resonance is usually at the high-frequency rang (> 5 MHz). It is not easy to attenuate this resonance by adding input EMI filters. Therefore, understanding and modeling the resonance is necessary for filtering the noise peak.

Since the propagation paths may not be decoupled, separating the CM and DM noise sources as well as the propagation path may not properly account for the interactions between CM and DM noises. Another concern of modeling CM and DM propagation at the same time is that the mode transformation exists when the propagation path is unbalanced [93], [68]. Therefore, the general modeling of the propagation path is a 5×5 matrix, as shown in Eq. (2-11) and Figure 3-23.

For the MTB EMI source modeling approach, both the noise current source and source impedance need to be modeled as discussed in Chapter 2. From the propagation path transfer impedance Z_{34} in Figure 2-20, there should be no resonance at 5.8 MHz for Network II, while DM and CM noises do show a resonance there (Figure 2-22 and Figure 2-23), indicating that the noise peak is caused by interactions between the propagation path and the noise source. Without the noise source impedances, the important EMI noise characteristics will be missing. Some of the previous research also showed that the inaccurate modeling of device module parasitics would result in prediction errors in the high-frequency range (> 5 MHz) [13]. Note also that in Figure 2-26 and Figure 2-27, the frequencies of DM and CM noise peaks are the same, showing again that DM and CM noises are caused by the same noise source via physically coupled propagation paths. The modeled source impedances affect both DM and CM noise generation, and it is more general not to model DM and CM noise source impedances separately because of the coupled noise paths.

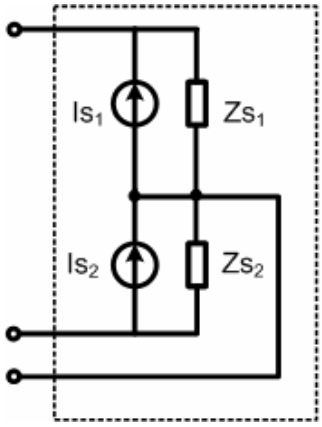

Figure 3-22 MTB Equivalent EMI Noise Source Model

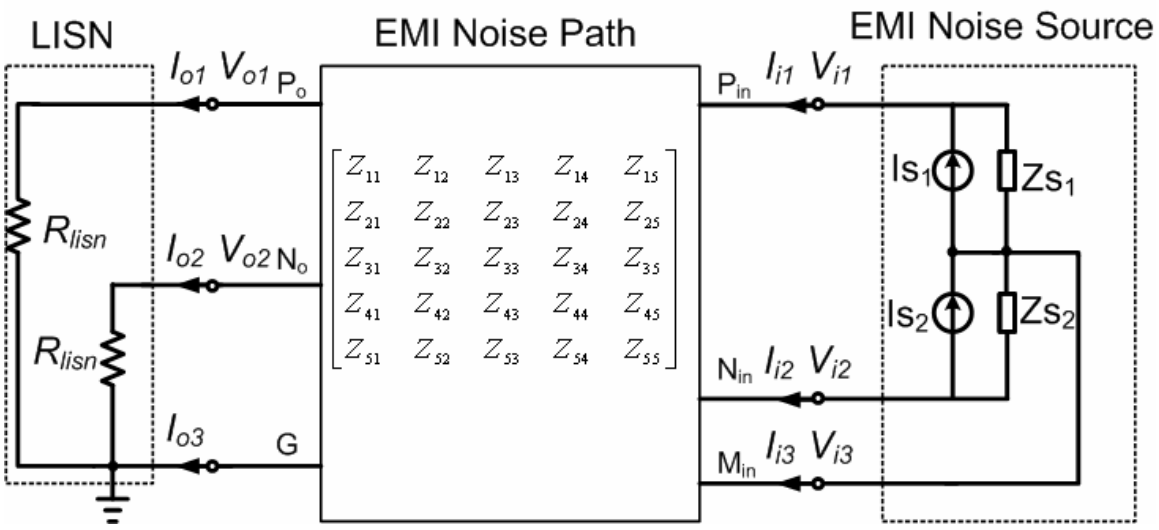

Figure 3-23 Unified MTB Equivalent EMI Noise Emission Model

From the modeling analysis, it is clear that the interaction between the MTB source and propagation path is an important EMI phenomenon in the high-frequency conducted EMI range. Since the device's switching behavior is the only noise source and the propagation path are inseparable, it is unnecessary and incorrect to model CM and DM noise sources individually. Therefore, the unified MTB equivalent noise source model is a 3-terminal active network, as shown in Figure 3-22 again. From the physical structure of MTB source model, three terminals in the model correspond to the terminals of the device module. The unified CM and DM propagation path is a 5×5 impedance matrix that connects with the noise source with three terminals. The rest of the terminals connect with LISNs and ground. Therefore, the entire system EMI noise emission model can be illustrated as Figure 3-23.

In the proposed MTB method, the EMI noise source will not be separated as DM and CM noise sources so that the approach will be more general and applicable to the coupled propagation paths. Therefore, the modeling method will directly predict the total noise for a converter system. On the other hand, if needed, the CM and DM noise can be calculated at the converter terminal according to Eqs. (3-2) and (3-3). The results can then be used for input EMI filter designs.

The modeling procedure described in Chapter 2 may seem too complicated and impractical as it involves many testing steps. The real significance of the method is establishing a "standard" procedure for building a terminal-behavioral model for a specific switching module under a specific switching condition. In principle, once a model is constructed, it can be used in any converter containing such a device module as long as the switching conditions match those for the specific MTB model. Further usage will be discussed in Chapter 4.

3.4. Evaluation of Different EMI Noise Modeling Methodologies

The proposed MTB method has accurate descriptions of switching transients. In principle, the MTB model is an approximate behavioral model, which has conducted EMI noise source frequency-domain characteristics. As mentioned in Chapter 1, in previous research, a current source with trapezoidal waveform was often used to represent the EMI noise source in power converters, which is an analytical modeling method and has its frequency-domain expressions. In order to illustrate the advantage of the proposed approach, a simulation of a chopper circuit in Figure 3-24 is used to demonstrate its difference with the trapezoidal current source modeling approach. The propagation path of the simulated circuit includes non-ideal capacitors, busbar inductances and LISNs. The device module includes some lead inductances and output capacitances.

For simplicity, only DM noise is simulated to analyze the two different modeling approaches. Figure 3-25 shows the simulation circuit that represents the switching device at a given working condition with a trapezoidal current source and parasitics. The parasitics inside the device module are kept the same as the values in the chopper circuit. The device turn-on and turn-off times are assumed to be 100ns, corresponding to the rising and falling time of the trapezoidal current source. Using the modeling approach described in Chapter 2, a corresponding MTB model can be established. Note that considering only the DM noise, the mid-point in the three-terminal MTB model can be

neglected and the model can be simplified into a two-terminal network and can be calculated by Eqs. (3-4) and (3-5).

$$I_s = \frac{I_{s1} \cdot Z_{s1} + I_{s2} \cdot Z_{s2}}{Z_{s1} + Z_{s2}} \quad \textbf{(3-4)}$$

$$Z_s = Z_{s1} + Z_{s2} \quad \textbf{(3-5)}$$

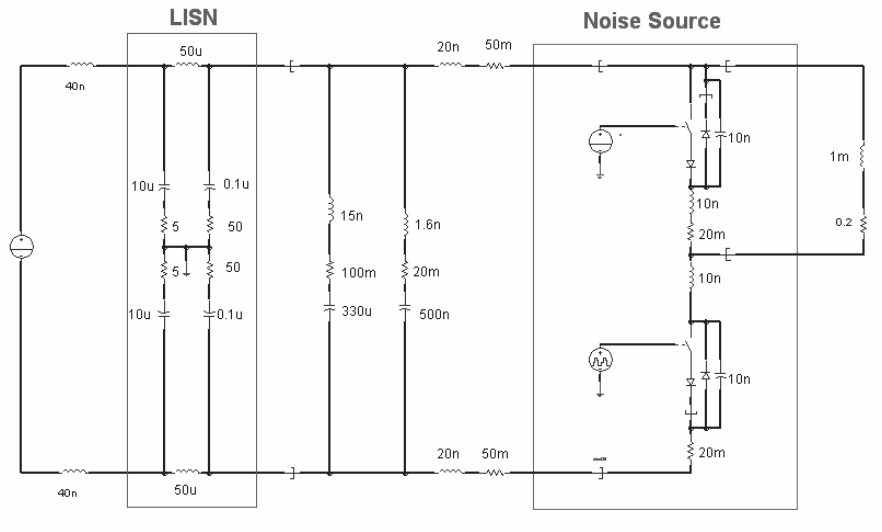

Figure 3-24 Simulation Circuit of Chopper Circuit

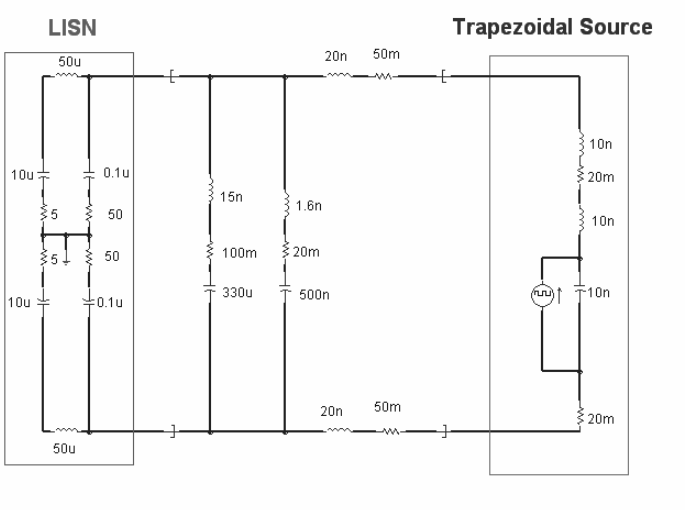

Figure 3-25 Simulation Circuit of Equivalent Circuit with Trapezoidal Current Source

Figure 3-26 shows the simulated noise levels on the LISN from three different approaches: the original simulated frequency-domain waveforms for the chopper circuit in Figure 3-24, the MTB equivalent model prediction, and the trapezoidal current source model prediction (Figure 3-25). The prediction results from the two models are close in the low-frequency range (<5 MHz) and match the original simulated result. However, the results in the high-frequency range are different. Using the trapezoidal current source as the DM noise source will result in a lower predicted DM noise on the LISN in the high-frequency range. As the frequency increases, the discrepancy between the prediction result based on the trapezoidal current source model and the simulated noise grows larger. Clearly, the MTB model can more accurately predict the noise for the entire frequency range.

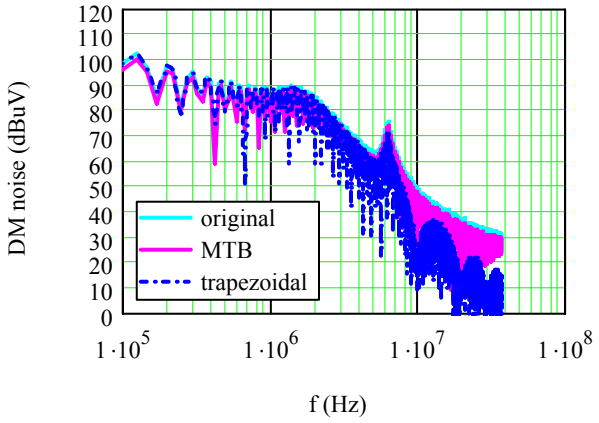

Figure 3-26 Prediction Results Comparison Based on Different Modeling Methods

To further understand the intrinsic differences between the MTB and trapezoidal current source approaches, the open-circuit voltages on the device terminals are derived and compared in Figure 3-27. Two noise sources have resonance at the same frequency, which are determined by the device module parasitics. In the low-frequency region (<5 MHz), the duty cycle of the noise source determines the noise spectrum. Therefore the two noise sources have little difference. In the high-frequency region, the spectrum of the noise should be determined by the on and off switching transients. Figure 3-28 shows the reconstructed time-domain waveform of the equivalent MTB model, with reconstructed details of the turn-on and turn-off transients in Figure 3-29 (a) and (b). The reconstruction

was through an inverse Fourier transform. There is no DC bias for these waveforms, since a DC bias will not affect the conducted EMI and DC component of the EMI noises. These are collected by LISNs and filtered by the required capacitors (0.1 μF) in LISNs. Clearly, the slopes of reconstructed turn-on and turn-off transients from the MTB model are not constant as they would be for a trapezoidal waveform, generally indicating a higher noise level at high frequencies. In other words, the trapezoidal current source representation will predict EMI that is lower than the actual EMI in the high-frequency region and the error will increase with frequency, as seen in Figure 3-26.

It should be pointed out that in the previous behavioral analytical equivalent model, it may not be sufficient to replace the trapezoidal waveform with actual switching waveforms to eliminate the error in high-frequency region. Another source of error may be the equivalent circuit topology itself, shown in Figure 3-25. The assumption that the device can be directly represented by an equivalent current source equal to its switching current is not necessarily valid. The MTB modeling approach does not rely on such an assumption.

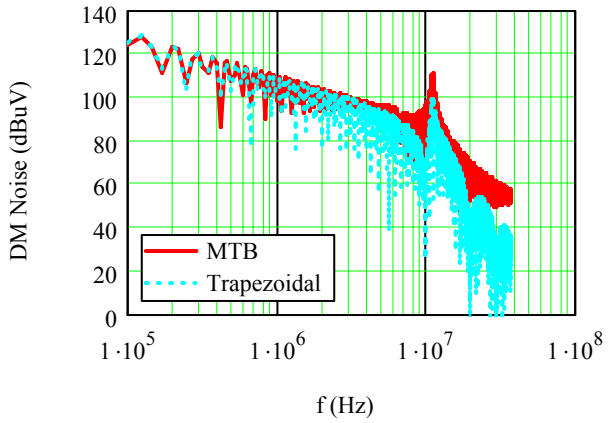

Figure 3-27 Terminal Noise Source Comparison

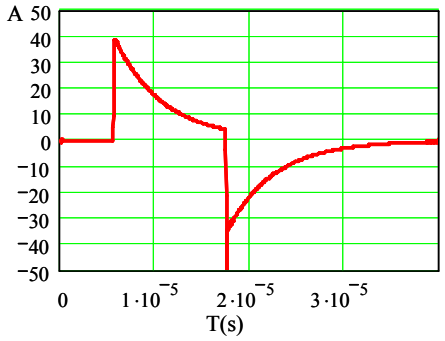

Figure 3-28 Reconstructed Time-domain Waveform of Equivalent MTB Noise Source

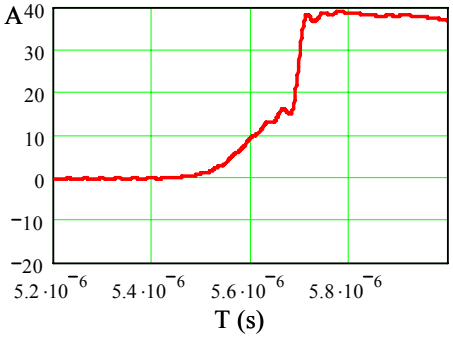

(a) Turn-on Period

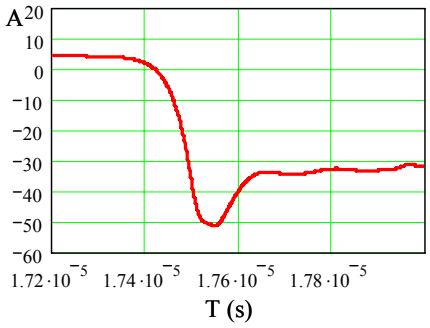

(b) Turn-off Period

Figure 3-29 Reconstructed Time-domain Waveform of Equivalent MTB Noise Source

This analysis shows that the MTB EMI model has more accurate descriptions than the analytical model under a given switching condition. For variable switching conditions, such as devices in a PFC circuit and a motor drive, the device physics behavior is changed due to semiconductor device nonlinearity. It is difficult for the analytical model

to integrate the different switching condition models into one expression and is therefore not accurate for variable switching conditions. But MTB models under each different switching condition can be derived easily with the standard testbed. In the next chapter, EMI modeling and prediction for a converter with variable switching conditions will be demonstrated. The MTB model application in a phase-leg-based converter is also described and experimentally verified.

The MTB model has other advantages over the device-based modeling methods. Using the three criteria for comparing modeling methodologies presented in Chapter 1, different EMI noise source modeling and prediction methodologies are summarized in Table 3-1. Although it has been shown that the analytical models are more suitable than the device-based model from EMI modeling standpoint, the evaluation is included the device-based model for the completeness.

Table 3-1 Comparison of Different Conducted EMI Modeling Methodologies

	Device-based Model				
	Physics-based Model	Models from Device Manufacturers	Simplified Device Model	Behavioral Analytical Model	MTB Model
Accuracy	Fair	Fair	Poor	Fair	Good
Feasibility	Poor	Poor (low-availability)	Fair	Fair	Good
Generality	Fair	Poor (low-availability)	Fair	Fair	Good
Parametric Study	Fair	Fair	Poor	Poor	Fair
Analysis Time	Long	Long	Short	Short	Short

One of the most important criteria of evaluating different modeling methodologies is accuracy. The good accuracy means that the frequency of the noise in the entire frequency range can be predicted and the error between the prediction and measurement result is less than 5 dBμV. Some of the device-based models, such as simplified device

model, have poor accuracy, and are only accurate up to 2 MHz. Other behavioral models can predict EMI noise lower than 5 MHz, which is defined as fair in the table. Although the physics-based models together with the packaging information can predict EMI noise accurately in principle, compromises are often made to have a less complicated modeling process. Another reason for unsatisfactory prediction results of behavioral models in the existing literature is that interactions between two-mode noises are not modeled. The arbitrary separation of two mode noises for simplifying the modeling process loses the insight of EMI noise generation, especially for the high-frequency noise. With a unified CM and DM propagation path and the MTB equivalent source impedance the high-frequency EMI noise emission and possible noise mode transferring can be predicted accurately in the entire frequency range.

Comparing the feasibility of different modeling methods, the analytical model and MTB models are better than physics-based and manufacturers provided models because they describe the device switching behavior under a certain switching condition and do not require intimate semiconductor physics information to derive the model and do not depend on the availability of the models. Therefore, physics-based model and the model provided by manufacturers have poor feasibility. Since the simplified and analytical models depend on the operating condition and the propagation path, it is difficult to apply those models in the applications different from the testbed or specific converters. As a result, these two types of models have fair feasibility. Although the MTB model is based on experiments, it can be conveniently derived by a certain “standard” testbed, as described in Chapter 2. There is no need of detailed information from manufacturers and only a few assumptions of avoiding severe nonlinearity should be made. The MTB model has best overall feasibility and can be applied to different converters when the switching conditions are met.

For a single converter, accuracy and feasibility are two critical criteria. In the design stage, the parametric study can be carried out based on EMI noise models. Since the device switching conditions are normally determined by converter functions, for certain selected devices changing the propagation path and using different filtering schemes can be used to control and manage EMI noises. Behavioral models used in the existing

literature depend heavily on propagation paths because the models are fine-tuned to satisfy one condition during the process. Nevertheless, those models with an omission of source impedance or a rough modeling of device module impedance are not suitable for parametric study. The physics-based model is good for parametric study because of less impact from the external circuit if the impedance due to the device packaging is known. The manufacturer's models have similar characteristics of the physics-based model. However, it is not fully based on the device physics, therefore the results of the parametric study will be less accurate than the physics-based model. For the MTB model, it is valid for study when the switching conditions do not cause large nonlinearity, as discussed in the first section of this chapter.

For a converter system, EMI phenomena are much more complex than for a single converter. To characterize and manage EMI noise in a large converter system that includes various converters, a generic modeling methodology is desirable. Complicated and inaccurate modeling methods are not suitable for system EMI research. Therefore, the easier the modeling process and the better accuracy for different converters, the better generality. Although the physics-based model is based on general semiconductor device theory, it is not convenient for a power electronic converter designer to use. And different types of devices in the converter system, such as the IGBT and MOSFET, cannot use the same parameter extraction method. The generality is limited except for semiconductor device experts. The worst generality among all the models is the manufactures' model because the availability of the model cannot be controlled by the users. Other models can be derived by users, which results in the fair to good generality. The MTB modeling method, it has certain physics bases and terminal characteristics, which can be easily used in a different converter. It demonstrates the good generality.

Another consideration for evaluating methodologies is the analysis time. Any model with good accuracy and short analysis time is more general than others from a system modeling point of view. In this case analytical models are superior to the physics-based and the manufacturer provided models, especially when the system is large and includes different types of converters. The simulation time of the three-phase converter with physics-based model could take hours or days to obtain the results, while simulations with

behavioral models only take minutes or hours. The analytical and MTB model have the shortest analysis time (minutes) because their equations are much simpler and the number of equations are less than the modeling methods involving the device physics equations.

3.5. Summary

This chapter builds on ideas expressed in the previous chapter. The validity of the proposed MTB model and prediction errors existing in the process and measurement are analyzed first. The necessary conditions for the MTB modeling process are discussed. Once the switching conditions, including bus voltage, load current, gate driver, and temperature are kept constant and the severe nonlinear effects are avoided, the MTB model can precisely predict EMI noise as verified in Chapter 2. The possible errors during the modeling process are studied, and it is found that the oscilloscope measurement is one major error source.

One of the contributions in this chapter is the analysis of the high-frequency EMI noise generation mechanism. The inseparable CM and DM noise characteristics are described in detail. The interaction between the source impedance and the propagation path is further analyzed. A general and unified CM and DM noise model structure is systematically proposed. At the end of this chapter, a comparison of the behavioral analytical model and the MTB model is presented. Different state-of-the-art methodologies and the MTB modeling are evaluated according to the evaluation criteria. The MTB model is shown to be more accurate, feasible and general than other models, and is therefore suitable for modeling EMI emission of a conversion system.

Chapter 4 EMI Noise Prediction for Power Converters Based on MTB Equivalent Source Model

This chapter applies the MTB equivalent source model to more complicated converters. Two application examples are presented. One example is to apply the MTB equivalent source model in a converter with variable switching conditions. The other example is to predict EMI noise of a full-bridge (FB) converter based on the MTB equivalent source model. The implementation procedure for each of these is described. The prediction results are verified by the experimental results. In addition, the possible industrial applications of the MTB model are discussed in this chapter.

4.1. EMI Noise Prediction for Converters with Variable Switching Conditions

In PWM AC converters, such as AC drives and PFC circuits, the switching conditions of devices change due to the varying input source or the output load. From EMI noise generation point of view, the EMI noise sources of the converters at each switching cycle are different, which is different from DC-DC converters. In the current literature, both device-based and behavioral analytical equivalent models are used to characterize and predict EMI noise in this type of converters. As discussed in Chapter 3, physics-based models are implemented in the simulation software, which require intimate knowledge of device physics. Furthermore, for a voltage-fed PWM AC drive, the load current changes with a low frequency, which leads a long system time constant (milliseconds). Therefore, the analysis time of the physics-based model is prohibitively long because the system should reach the steady-state operating condition and the simulation step is small (nanoseconds). Behavioral models are derived based on different operating conditions. They are not suitable for variable switching conditions. Although the analytical

behavioral model has a succinct expression of the noise source, it is not accurate in the high-frequency range and not easy to implement accurate turn-on and turn-off slopes in the noise source when operating conditions of the converter change, since the turn-on and turn-off slopes of the device are obtained under one operating condition.

As described in previous chapters, the MTB equivalent EMI noise source model represents a switching device under a given switching condition, with experimentally-obtained equivalent current sources and source impedances in the frequency domain. Since the MTB model is still a behavioral model, it has the same drawbacks as other behavioral models, that the model is only valid at a certain switching condition. But from the modeling process it is convenient to obtain MTB models at different switching conditions from a "standard" test, which can be used to predict the EMI noise for converters with variable switching conditions. The objective of this section is to extend the application of the equivalent MTB source model, originally developed for a single switching under a given operating condition, to characterization and prediction of the conducted EMI noise for converters with variable switching conditions, such as AC converters.

In Chapter 3, a unified CM and DM EMI noise modeling method is proposed to model the EMI noise in the entire frequency range. It is a general method, which can be used in converters with both coupled and decoupled propagation paths. In order to simplify the modeling process for a decoupled propagation path, CM and DM noise can be modeled separately. In the last section of Chapter 3, the DM noise current source and source impedance are derived based on the general model in the chopper circuit. Both the CM and DM noise source and the propagation path of the converter can be characterized as a one-port active network and a two-port passive network, respectively. The noise source model is made up of an equivalent noise source current $I_s(j\omega)$ and noise source impedance $Z_s(j\omega)$, as shown in Figure 4-1. All the parameters of the networks are modeled in the frequency domain.

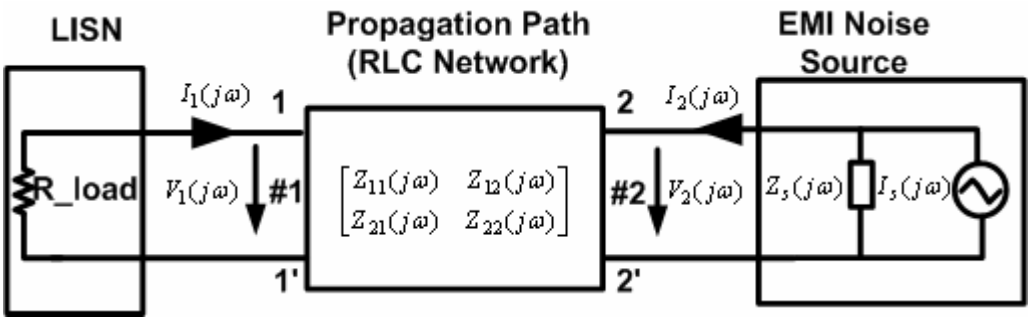

Figure 4-1 Equivalent EMI Noise Emission Model

The modeling process is the process described in Chapter 2, which involves obtaining two different sets of noises ($I_1(j\omega)$ and $V_1(j\omega)$) on the LISNs with two known but different propagation paths, characterized by impedance matrix $Z(j\omega)$. The noise on the device terminal ($I_2(j\omega)$ and $V_2(j\omega)$) can be calculated in the frequency domain using the impedance matrix of the propagation path. With two pairs of noise currents and voltages on the device terminals, the equivalent current source and source impedance can be obtained. Therefore, a set of DM and CM noise source and source impedance under a given condition can be obtained. It is valid for the same condition, such as a given current, voltage, gate signal and switching frequency.

Many power converters, particularly AC converters, have varying switching and operating conditions during an operating cycle, even at steady state, owing to time-varying load currents and voltages. In order to use equivalent MTB source models to predict the EMI noise generated by a switching device in converters with variable switching conditions, the EMI source modeling conditions must include the entire range of operating conditions of the device in converters. Without loss of generality, a simple IGBT-based half-bridge (HB) DC-AC converter with SPWM control is used as an example to illustrate the modeling process.

First, let us understand how to apply an equivalent MTB model of an IGBT device developed under a given condition to a HB converter using the device under the same condition. In the EMI noise prediction process, the EMI noise source and propagation

paths are modeled separately. The noise propagation path in the testbed is modeled as a two-port passive network. Figure 4-2 (a) shows the simulation circuit of the testbed for constructing the equivalent MTB source model of an IGBT device module. Note that while a totem-pole phase-leg with two IGBT-diode pairs is used in the testbed, for modeling purposes only one IGBT needs to be switched, and the phase-leg can be modeled with two identical equivalent sources due to the symmetry of the phase legs. For an asymmetrical case, the two sources would generally be different but the approach would remain the same. Figure 4-2 (b) shows the simulation circuit of a HB converter based on the same IGBT phase-leg. Although the topologies of the two circuits in Figure 4-2 are different, the propagation path of the HB converter, which is also a two-port network, can be modeled as the same structure as the testbed. For the chosen propagation paths shown in the two simulation circuits, the two-port networks have identical impedance characteristics. The levels of EMI noise produced in these circuits during one switching cycle are the same when the switch operating conditions are also the same, as shown in Figure 4-3 and Figure 4-4. In addition, while the connections of IGBT switches are different for the two circuits, they are equivalent for one switching cycle.

In the above example, the propagation path chosen for the HB converter has characteristics identical to the testbed for easy comparison. In the previous work, the equivalent MTB source model was proven to predict the EMI noise for different propagation paths in the modeling testbed. Therefore, the equivalent MTB source model can also be used to predict the EMI noise in a HB converter with different propagation paths as long as the model is built under the operating conditions of the HB converter.

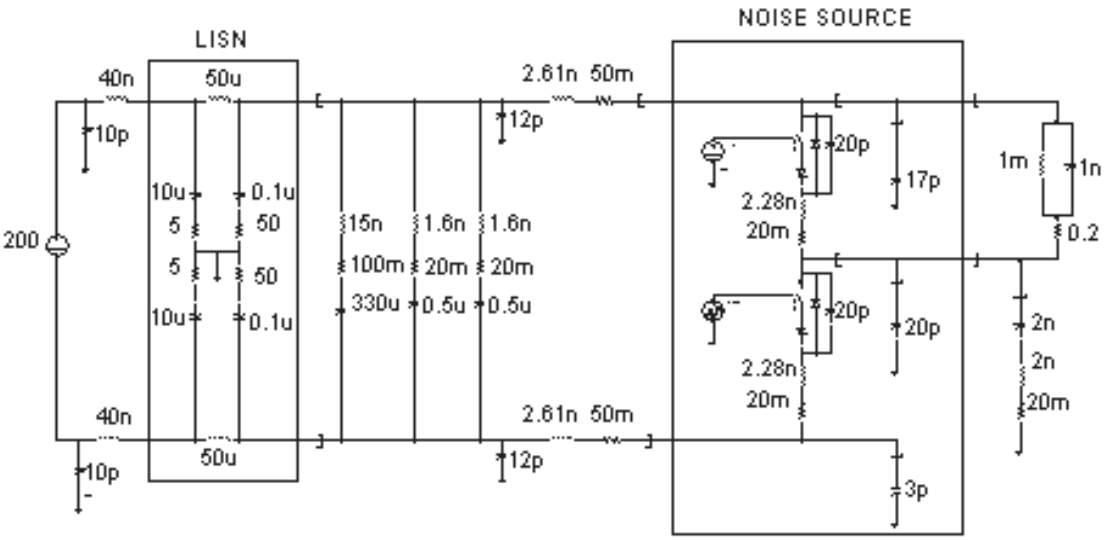

(a) MTB Model Testbed

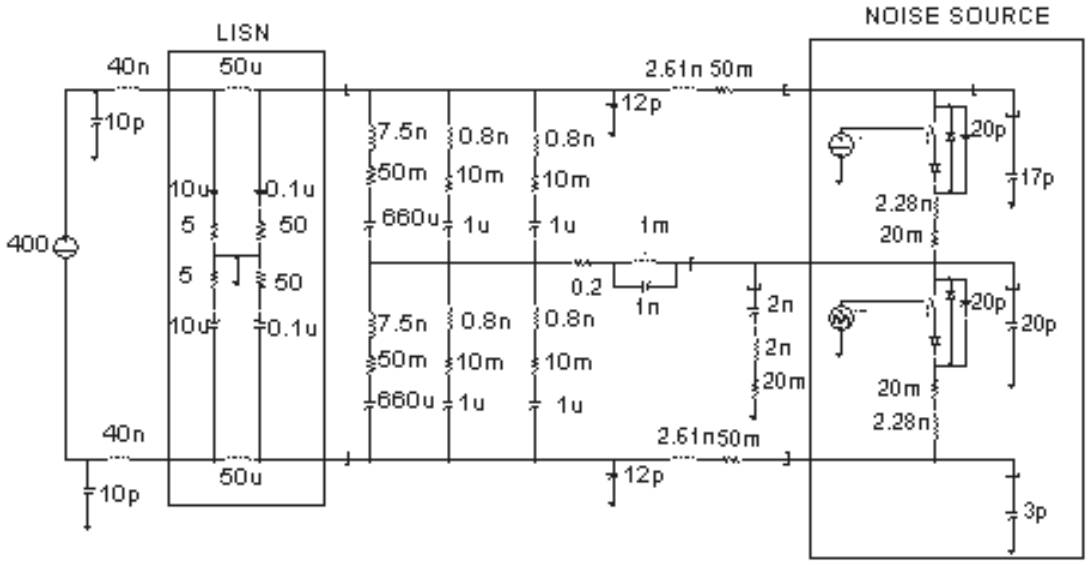

(b) Half-bridge Converter

Figure 4-2 Simulation Circuits of the MTB Model Testbed and HB Converter

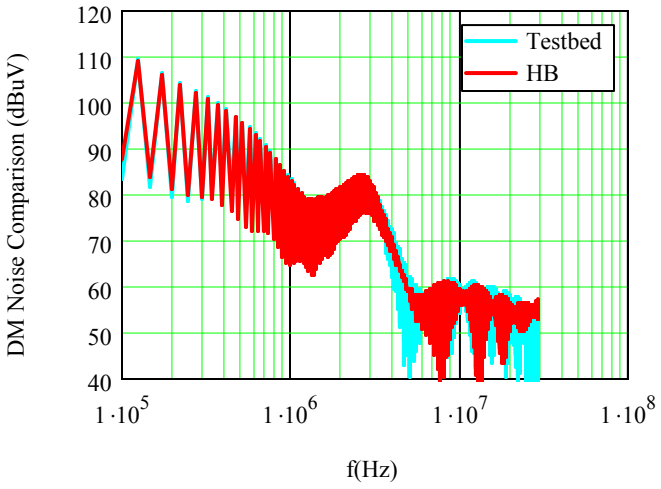

Figure 4-3 Simulation Results of DM Noises in the Modeling Testbed and the HB Converter for the Same Given Conditions

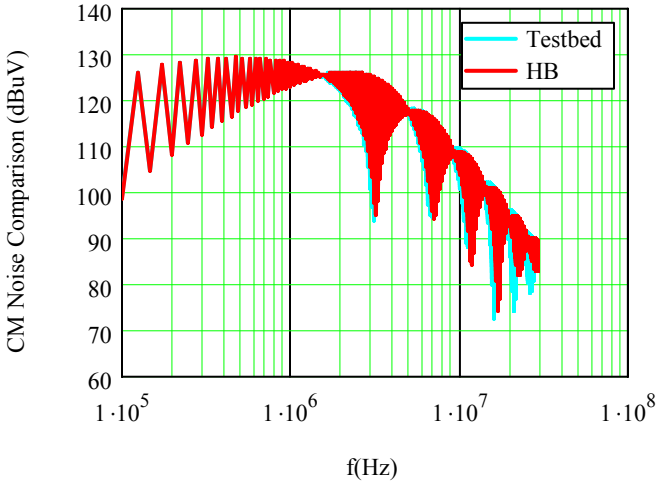

Figure 4-4 Simulation Results of CM Noise in the Modeling Testbed and the HB Converter for the Same Given Conditions

In a HB DC-AC converter, the load current will change during an operating period or a line cycle. The EMI noise will change along with the load current, as shown by time-domain waveforms in Figure 4-5. The DM noise increases with the load current. The CM noise changes less significantly.

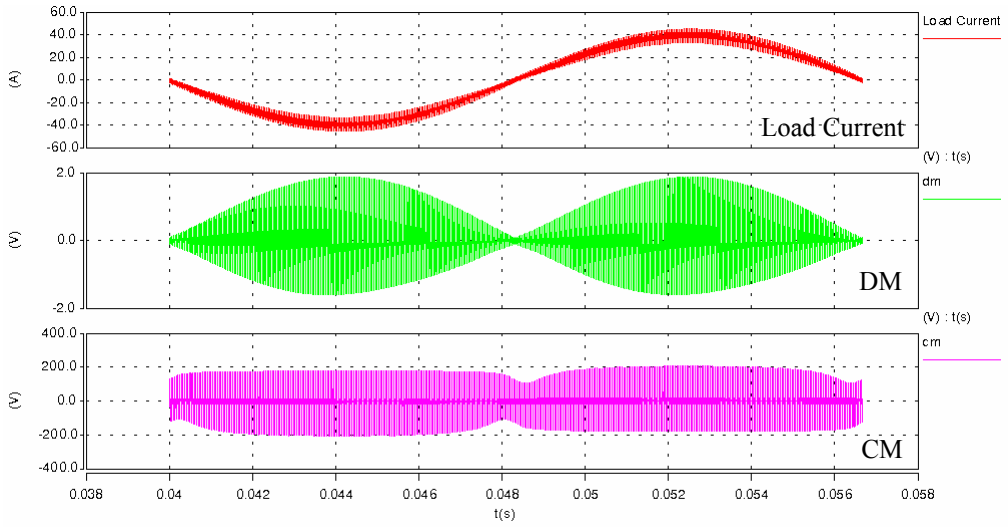

Figure 4-5 Time-domain Simulation Results of Load Current, DM Noise and CM Noise for the HB Converter

As described above, the equivalent MTB source model is built with data from one switching period, characterized by its turn-on and turn-off transients, as well as the duty cycle. The data processing for generating the frequency-domain model is based on the DFT. In a PWM HB DC-AC converter, switching events will change following the modulation requirement and in general will no longer have a repetitive pattern. In one special circumstance when the switching frequency is a multiple of the line frequency (or AC operating frequency), each switching event and the associated noise will repeat itself with the line frequency. Under this condition, there is a fixed relationship between the noise spectrum of a switching pulse based on the switching frequency and the noise spectrum based on the line frequency. Understanding the relationship will allow the MTB source model developed for one switching event (i.e., for the switching frequency) to be used for the line frequency.

Figure 4-6 is a simple illustration of this relationship, where the width of an ideal pulse is assumed to be one-fifth of the line period; or in other words, the switching frequency (SF) is $m=5$ times of the line frequency (LF). In this case, if considering the switching pulse and the associated noise for one switching cycle only, it is assumed that there are five (5) identical switching pulses in a line cycle. The signal can be treated as a

switching frequency signal. On the other hand, if considering the same switching event and the associated noise for the entire line cycle, there is only one switching pulse during each line cycle. The same signal can now be treated as a line frequency signal. Based on the DFT, in the frequency domain, the magnitude of the switching frequency signal will be *m* times greater than the magnitude of the line frequency signal at the switching frequency and its multiples. The phases of these two signals will be the same at the switching frequency and its multiples. The relationship can be seen clearly in Figure 4-7, where $m = 5$.

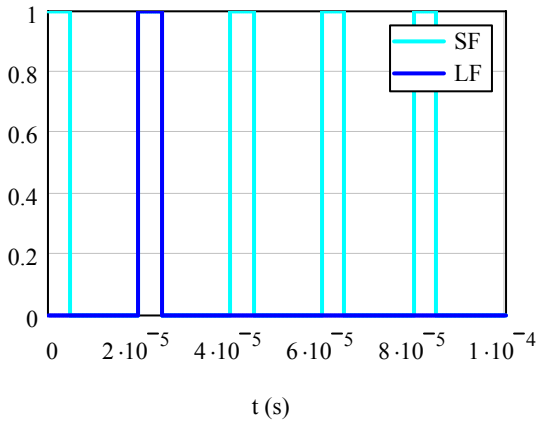

Figure 4-6 Time-Domain Waveform of Switching-Frequency (SF) Signal and Line-Frequency (LF) Signal

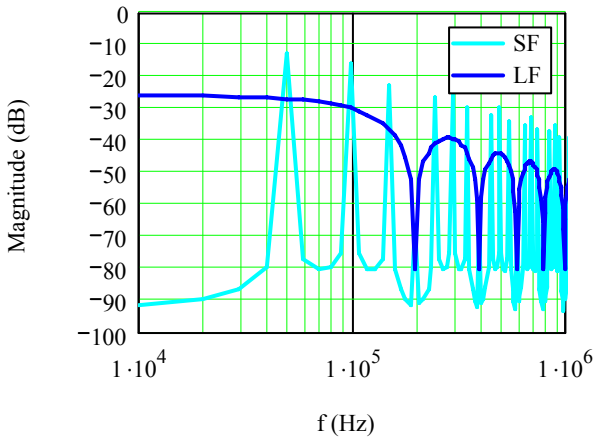

(a) Magnitude

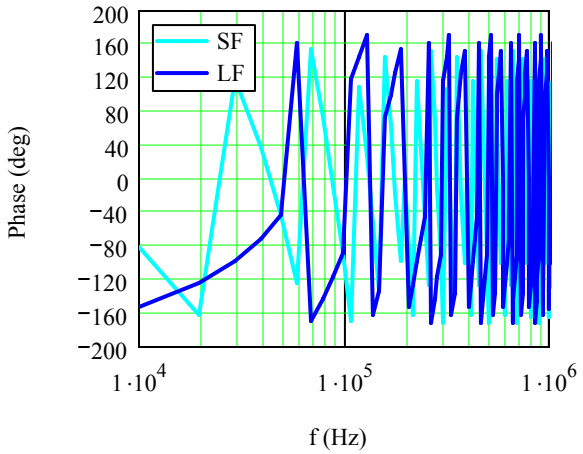

(b) Phase

Figure 4-7 Magnitudes and Phases of SF and LF Signal

The observations and relationships based on the simple examples described above can also be derived mathematically for more general cases. Again, under the assumption that switching frequency f_s is a multiple of line frequency f_l, the DFT results of the switching frequency signal $s(t)$ and the line frequency signal $s'(t)$ can be found as

$$EMI_{switching}(k) = \mathrm{DFT}[s(t)] = \frac{1}{N}\sum_{n=0}^{N-1} s(n)\cdot e^{-j\frac{2\cdot\pi}{N}nk} \quad \textbf{(4-1)}$$

$$EMI_{line}(l) = \mathrm{DFT}[s'(t)] = \frac{1}{m\cdot N}\sum_{n=0}^{m\cdot N-1} s'(n)\cdot e^{-j\frac{2\cdot\pi}{m\cdot N}nl} \quad \textbf{(4-2)}$$

where

N is the number of sampling points in one switching cycle,

f_s is the switching frequency;

f_l is the line frequency;

$m = \dfrac{f_s}{f_l}$ is an integer.

By definition, the switching cycle signal $s(t)$ and the line cycle $s'(t)$ are both periodic with periods T_s and T_l respectively.

$$\left.\begin{aligned} s(t) &= s(t + aT_s) \\ s'(t) &= s(t + aT_l) \end{aligned}\right\} \quad \text{for } a = 0,1,2,... \tag{4-3}$$

If the original switching signal occurs during the switching period $(aT_s, (a+1)T_s)$, then, within a line cycle,

$$s'(t) = \begin{cases} s(t), & aT_s < t < (a+1)T_s \\ 0, & t < aT_s, t > (a+1)T_s \end{cases} \quad \text{for } a = 0,1,2,...(m-1) \tag{4-4}$$

In discrete form, the equations (4-3) and (4-4) become

$$\left.\begin{aligned} s(n) &= s(n + aN) \\ s'(n) &= s(n + amN) \end{aligned}\right\} \quad \text{for } a = 0,1,2,... \tag{4-5}$$

$$s'(n) = \begin{cases} s(n), & aN < n < (a+1)N \\ 0, & n < aN, n > (a+1)N \end{cases} \quad \text{for } a = 0,1,2,...(m-1) \tag{4-6}$$

The spectrum of the line cycle signal at the switching frequency and its multiples will be

$$
\begin{aligned}
EMI_{line}(ml) &= \frac{1}{m \cdot N} \sum_{n=0}^{m \cdot N-1} s'(n) \cdot e^{-j\frac{2 \cdot \pi}{m \cdot N} n \cdot ml} \\
&= \frac{1}{m \cdot N} \sum_{n=aN}^{(a+1)N-1} s(n) \cdot e^{-j\frac{2 \cdot \pi}{m \cdot N} \cdot n \cdot ml} \\
&= \frac{1}{m \cdot N} \sum_{n=0}^{N-1} s(n) \cdot e^{-j\frac{2 \cdot \pi}{N} n \cdot l} \cdot e^{j \cdot a \cdot N \cdot \frac{2 \cdot \pi}{N}} \\
&= \frac{1}{m \cdot N} \sum_{n=0}^{N-1} s(n) \cdot e^{-j\frac{2 \cdot \pi}{N} n \cdot l} \\
&= \frac{1}{m} EMI_{switching}(l)
\end{aligned}
\tag{4-7}
$$

Note that frequency order *l* based on the switching frequency corresponds to frequency order *ml* based on the line frequency. It is clear from equation (4-7) that the spectrum of the line frequency signal is *1/m* of the spectrum of the switching frequency signal at the switching frequency and its multiples. The phase remains the same. This indicates that the frequency-domain equivalent MTB EMI source model obtained from a single switching event can be used for line cycle EMI prediction if the relationship in equation (4-7) is used. That is, if a switching event repeats every line cycle and there can be exactly *m* such switching events in a line cycle, then the contribution of the switching event to the total EMI noise is *1/m* of the EMI noise predicted by the frequency-domain equivalent MTB EMI source model obtained from the single switching event.

The above discussion is based on the assumption that *m* is an integer. Usually the switching frequency will not be an exact multiple of the line frequency. In this case, a switching event will not repeat exactly every cycle, and the relationship in (4-4) and (4-7) appears to be no longer relevant. Fortunately, when considering the conducted EMI in the frequency range of hundreds of kilohertz to tens of megahertz, the key parameters are switching turn-on and turn-off transients that mainly depend on switching conditions, not on duty cycles [1]. In other words, if the operating conditions for switching repeat every cycle, the discussions and the relationships in (4-4) and (4-7) still approximately apply. This is especially true when the switching frequency is much higher than the operating line frequency, a condition generally satisfied in modern PWM converters. For very high

power converters, a low switching frequency relative to operating frequency is often used, frequently together with synchronous switching schemes. For a synchronous switching scheme, it is obvious that equations (4-4) and (4-7) will hold. This dissertation focuses on more common asynchronous or carrier-based PWM converters with a switching frequency sufficiently higher than the operating frequency. In the HB DC-AC converter example used in the dissertation, the operating frequency is 60Hz and the switching frequency is 25 kHz such that $m = 416.7$. In this case, it can be assumed that a particular switching event will repeat in a 60 Hz cycle, and its contribution to the EMI noise of the whole cycle is approximately $\frac{1}{416}$ of the level predicted by the MTB model developed for the switching event, assuming a 25 kHz frequency.

Based on the equivalent MTB source model method, EMI source models vary for different load currents and different duty cycles. The effect of duty cycles is small and thus negligible considering the frequency range of interest. In the case of a VSC, as shown in Figure 4-2 (b), the EMI noise for every switching cycle can be calculated with the knowledge of EMI noise sources at different load currents and duty cycles. Since the noise levels generated by these switching events are independent, the total noise for one line cycle can be obtained through superposition in the frequency domain. As the equivalent MTB source modeling method relies on experimental characterization of each switching event, it is impractical to build an EMI noise source model as a continuous function of load current and duty cycle for a converter. A practical approach is to build source models for a family of selected current levels covering the whole operating range, as shown in Figure 4-8.

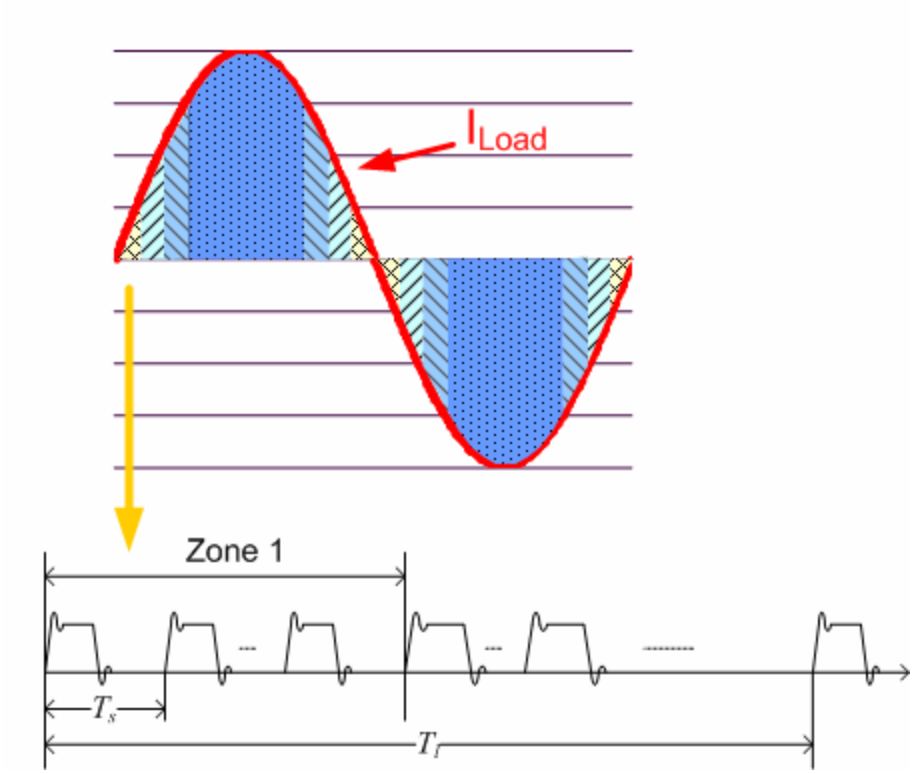

Figure 4-8 Illustration of Building Several Source Models at Different Load Current

For the example used in this dissertation, four DM and CM source models are built for load currents of 40A, 30A, 20A and 10A, with 40A being the maximum current for the HB converter. When the load current is between 30A and 40A, it is assumed that the EMI noise can be calculated by the 40A model. As a result, the whole line cycle is divided into four operating zones. Within each zone, the EMI noise can be calculated using one corresponding source model, and the noise for one line cycle can be calculated by combining the results of the four zones having four different source models but the same propagation path. Figure 4-9 and Figure 4-10 show the different source models at different load currents. Since the number of device switching events in each zone can be known, the total noise in one line cycle can be calculated by Eqs. (4-8) and (4-9).

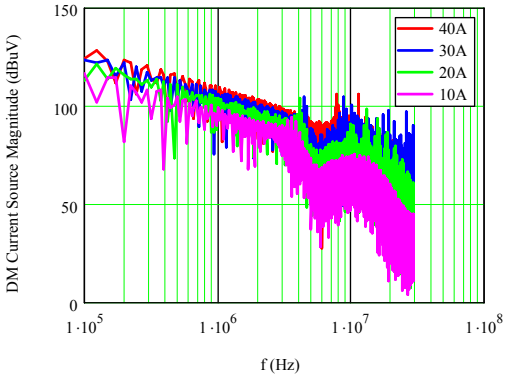

(a) Current Source Magnitude

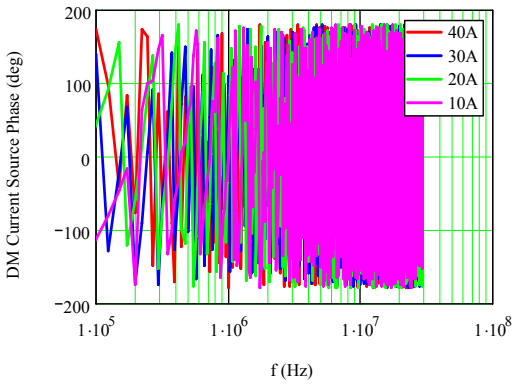

(b) Current Source Phase

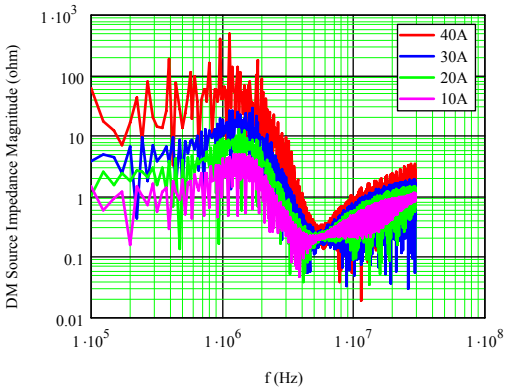

(c) Source Impedance Magnitude

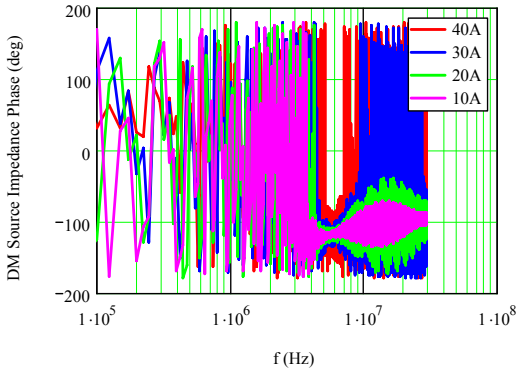

(d) Source Impedance Phase

Figure 4-9 DM Noise Current Sources and Source Impedances for Different Load Currents

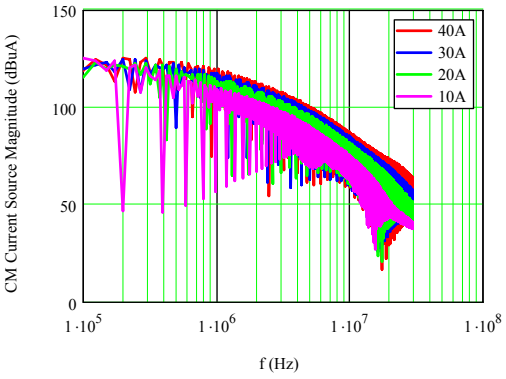

(a) Current Source Magnitude

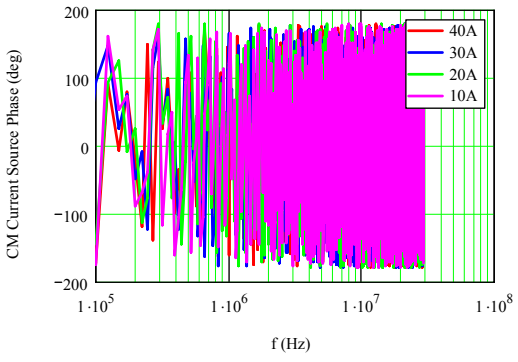

(b) Current Source Phase

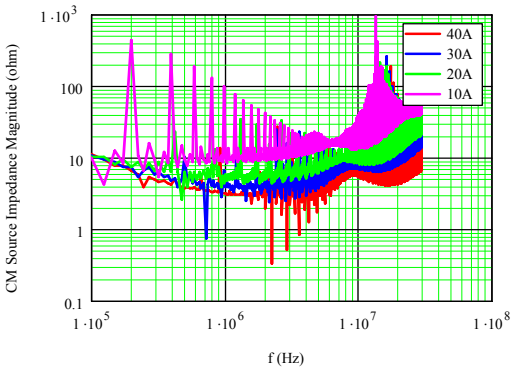

(c) Source Impedance Magnitude

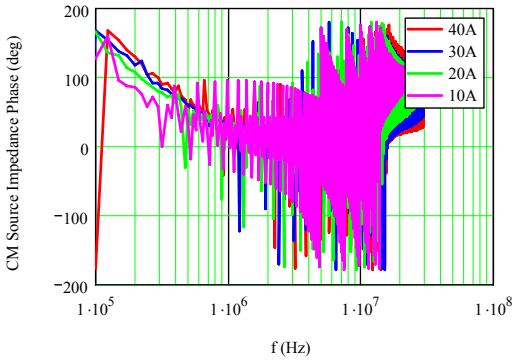

(d) Source Impedance Phase

Figure 4-10 CM Noise Current Sources and Source Impedances for at Different Load Currents

$$DM_{line} = \frac{N_{40A}}{N_{line}} \cdot DM_{40A} + \frac{N_{30A}}{N_{line}} \cdot DM_{30A} + \frac{N_{20A}}{N_{line}} \cdot DM_{20A} + \frac{N_{10A}}{N_{line}} \cdot DM_{10A} \quad \textbf{(4-8)}$$

$$CM_{line} = \frac{N_{40A}}{N_{line}} \cdot CM_{40A} + \frac{N_{30A}}{N_{line}} \cdot CM_{30A} + \frac{N_{20A}}{N_{line}} \cdot CM_{20A} + \frac{N_{10A}}{N_{line}} \cdot CM_{10A} \quad \textbf{(4-9)}$$

where N_{40A} , N_{30A} , N_{20A} and N_{10A} are the switching numbers for operating zones corresponding to currents of 40A, 30A, 20A, and 10A respectively in one line cycle; N_{line} is the total number of switching events in one line cycle; DM_{40A} , DM_{30A} , DM_{20A} and DM_{10A} are the DM noises calculated by the four source models in one line cycle; and CM_{40A}, CM_{30A} , CM_{20A} and CM_{10A} are the CM noises calculated by the four source models in one line cycle.

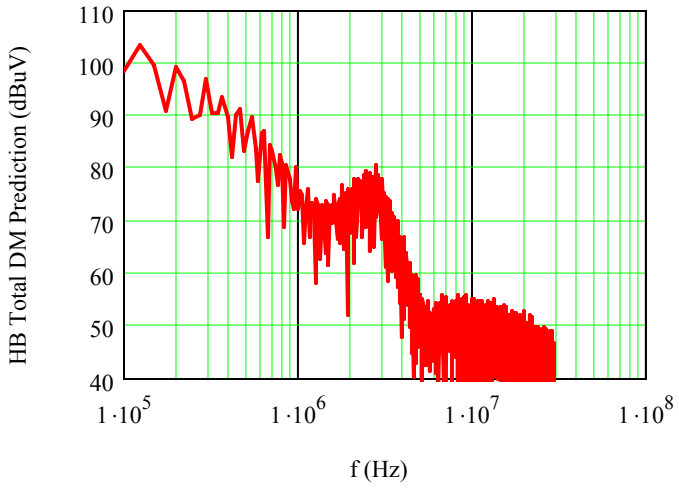

Figure 4-11 DM Noise Prediction Result for the HB Converter

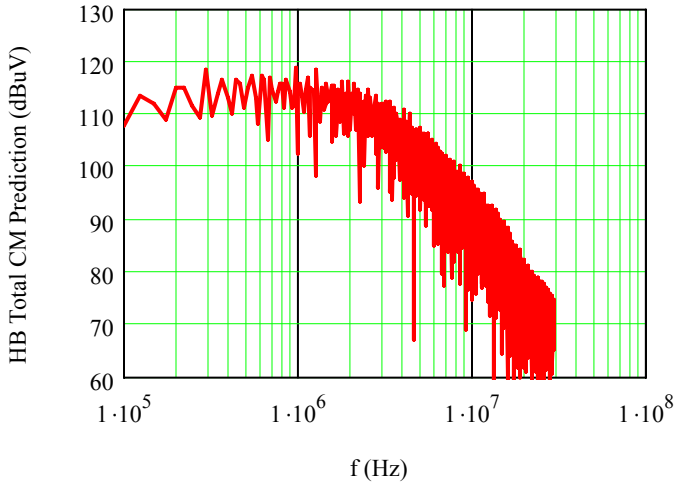

Figure 4-12 CM Noise Prediction Result for the HB Converter

Note again that only the number of the switching events is important, while the actual duty cycles of switching pulses are not important for EMI. Figure 4-11 and Figure 4-12 show the predicted DM and CM noise in the HB converter for one line cycle for a simulation circuit.

Comparing the predicted DM and CM noises in Figure 4-11 and Figure 4-12 with the time-domain simulation results shown in Figure 4-13 and Figure 4-14, it can be seen that the proposed method using MTB source models for operating zones can accurately

predict the frequencies of the noise peaks. The magnitudes of the predicted DM and CM noise are higher than the magnitudes of the simulated noise. In the time-domain simulation, the time-domain data for one line cycle is obtained first and then converted into the frequency-domain using the Fourier transform. This approach implies that a band-pass filter, whose bandwidth is the same as the line frequency, is used to obtain the frequency-domain waveform. In the proposed method, the MTB model is built at the switching frequency, and only the noise at the switching frequency and its multiple frequencies will be calculated. Without using any filters, the proposed prediction method should yield a higher noise level than results from time-domain circuit simulation and the subsequent Fourier transform.

Furthermore, the EMI results obtained with time-domain circuit simulation are also lower than the measurement results using a spectrum analyzer. The reason for this discrepancy is that a 9 kHz bandwidth band-pass filter is required to measure the conducted EMI noise (150 kHz - 30 MHz) such that all frequency components within the 9 kHz band around a given frequency are summed during the measurement, while simulation results contain side-band components due to modulation effects. Some literature [60]-[63] has discussed modulation effects on EMI measurements, and a method was even proposed to model the band-pass filter in time-domain simulation [63]. In this dissertation, the EMI noise level obtained through simulation, such as those shown in Figure 4-13 and Figure 4-14, cannot be directly compared to measured results or prediction results using MTB model-based measurements due to the lack of a 9 kHz band-pass filter in the simulation circuit.

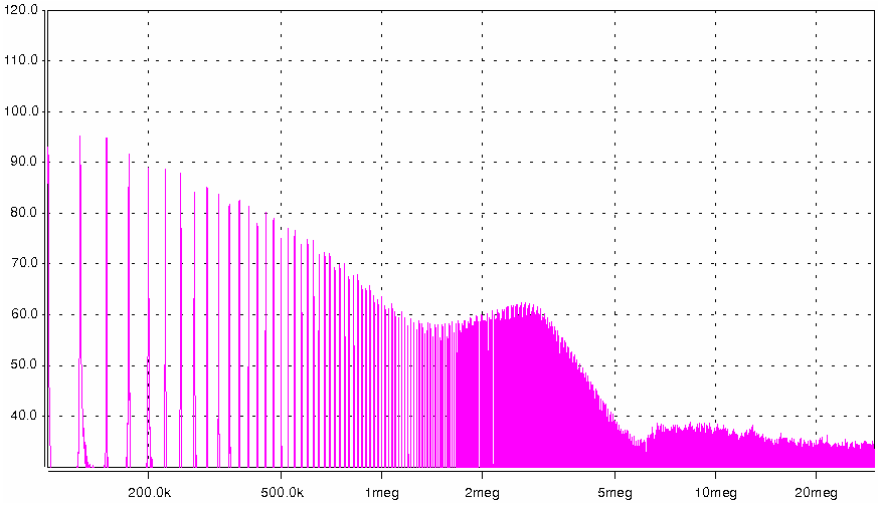

Figure 4-13 DM Noise Simulation Result for the HB Converter

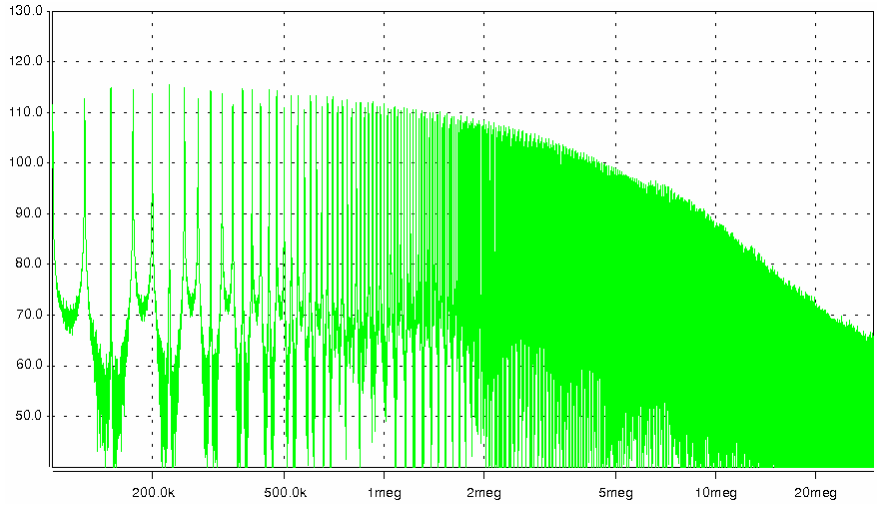

Figure 4-14 CM Noise Simulation Result for the HB Converter

On the other hand, the prediction results using MTB models should match the direct measurement using an EMC receiver or a spectrum analyzer. With the 9 kHz band-pass filter, the direct measurement of EMI will not be affected by modulation strategies [60]. The proposed MTB modeling method, considering the EMI noise only at the switching frequency and its multiples, has the equivalent effect of a narrow band-pass filter. This observation on the validity and accuracy of the proposed prediction method will be verified in the experimental results.

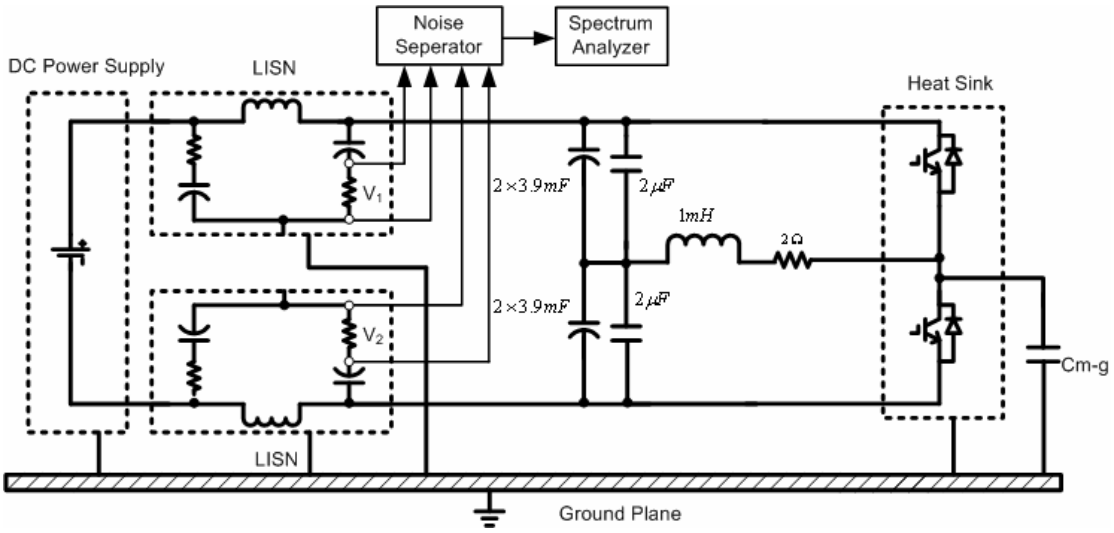

Figure 4-15 HB Converter Test Setup

Figure 4-15 shows the test setup for the HB converter. The IGBT device module used in the converter is the same as the module used in the modeling testbed. Four DC-link capacitors are connected between the terminals of the laminated busbar, four high-frequency capacitors are paralleled with the DC-link capacitors, and SPWM is used as the modulation scheme. During one half of the operating cycle or line cycle, the current commutation is between the top diode and the bottom IGBT; during the other half of the line cycle the commutation is between the bottom diode and the top IGBT. The test circuit is connected directly to an LISN, as required by EMC standards, for consistent and reproducible results. A ground plane is used as the reference earth ground. A noise separator is used to separate DM and CM noise. The operation conditions are as follows:

Switching frequency	25 kHz
Output line frequency	60 Hz
Peak output current	40 A
DC bus voltage U_{bus}	400 V

Using four DM and CM equivalent MTB source models derived from the modeling testbed shown in Figure 4-15 and equations (4-8) and (4-9), the DM and CM noise on the LISN side can be predicted, as shown in Figure 4-16 (a) and (b). Figure 4-17 (a) and (b) show the experimental results of the DM and CM EMI noise spectra. The prediction and

test results match closely, with both DM and CM prediction results having the same shapes as the test results. The noise peaks are predicted accurately.

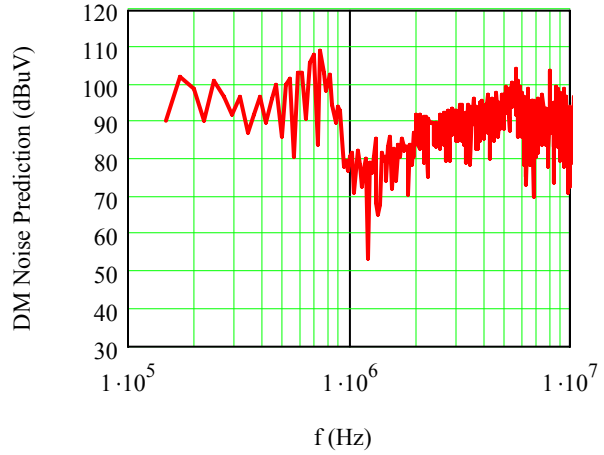

(a) Prediction

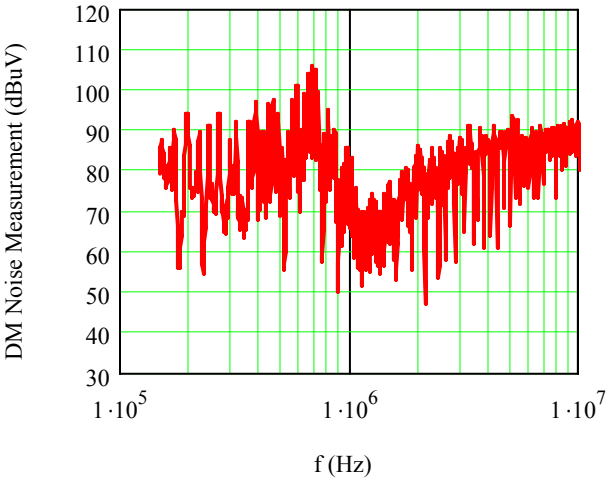

(b) Measurement

Figure 4-16 DM Noise Prediction and Measurement Results for the HB Converter

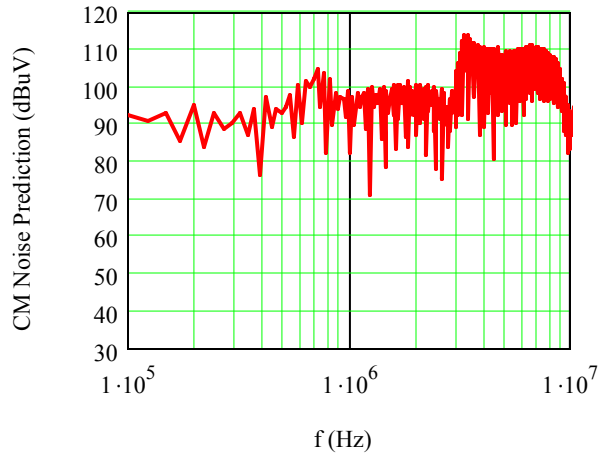

(a) Prediction

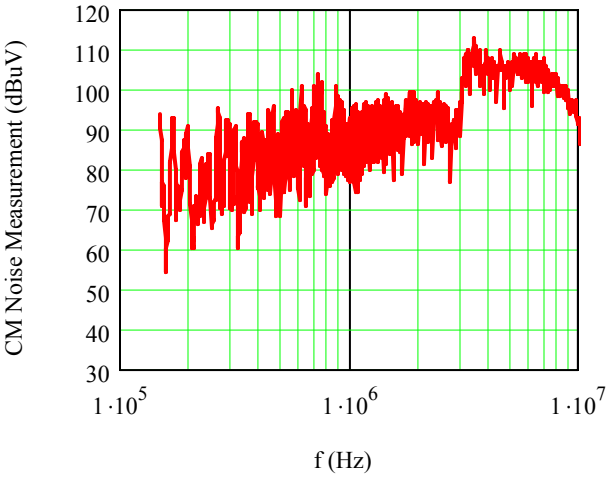

(b) Measurement

Figure 4-17 CM Noise Prediction and Measurement Results for the HB Converter

The prediction and measurement results for the HB converter example still show some discrepancies, with the maximum discrepancy around 5 dBμV for the test case. These discrepancies may be attributed to the differences between the instruments used for collecting the data for modeling and those used for measuring EMI noise. In the process of establishing the equivalent MTB source model, an oscilloscope is used to collect data for one switching cycle noise, since the equivalent MTB source model needs both noise magnitude and phase. The EMC analyzer is used to measure the line-cycle EMI noise

because of EMI regulation requirements and because of the limited sampling point capability of the oscilloscope.

In the prediction process for the HB DC-AC converter described above, the operating period is divided into four zones based on the load current. Generally speaking, the division of zones is dependent on device characteristics and the converter switching condition. Dividing into more zones and building more equivalent MTB source models will help improve EMI noise prediction accuracy, but too many zones are not practical and the resulted accuracy improvement is limited. For example, if the EMI noise level based on the source model is proportional to the load current, which means that the EMI noise level of the half load current is 6 dB smaller than that of the full load current, the prediction error of different zone numbers can be illustrated in Figure 4-18. When only using the EMI source model at maximum load current without dividing zones, the whole EMI level predicted will be about 4 dB higher than using 20 zones. With 4 zones, the noise error level is about 1 dB, well within the accepted range of accuracy.

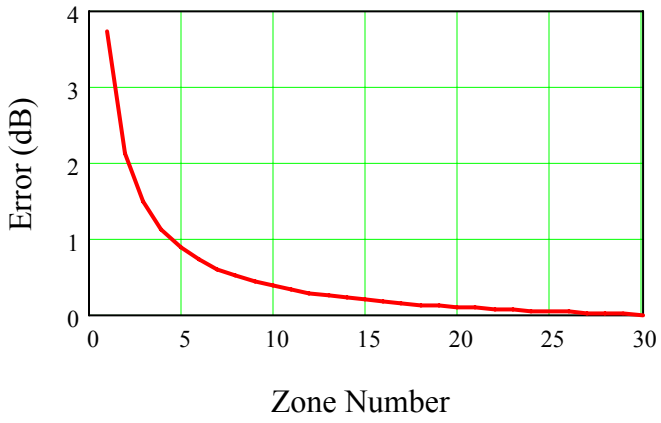

Figure 4-18 Illustration of Different Zone Effects

4.2. EMI Noise Prediction for Converters with Multiple Phase Legs

In Chapter 2, a chopper circuit was used as a testbed to model one half of a phase-leg module with a noise source pair consisting of two current sources and two impedances. In a simplest phase-leg based converter, the half-bridge converter shown in previous section, a phase-leg module includes two EMI noise source pairs. Each noise source pair works during half of the line cycle. In a multi-phase-leg converter, such as three-phase motor drive systems and FB DC/DC, each system includes more than two EMI noise source pairs.

For a converter with multiple phase-legs each switching transient involves at least two phase legs, which can be shown in Figure 4-19. This two-module structure is an extension of the one phase-leg module and is the simplest configuration with multiple phase-legs. In fact, it can represent a FB DC/DC converter, an AC/DC converter and a DC/AC converter. It also represents any two phase-leg transient in three-phase inverters or drive systems. Therefore, modeling this structure can help to understand and characterize EMI emission in multi-phase converters.

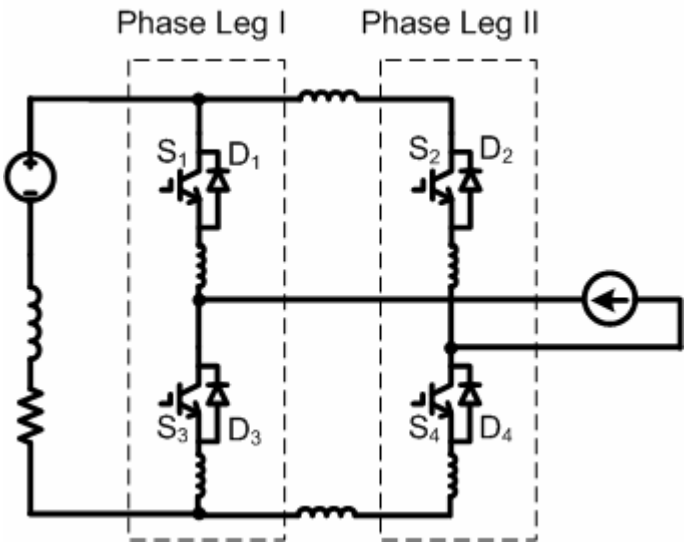

Figure 4-19 Two Phase-leg Structure

For each module, the commutation is still between the top IGBT and the bottom diode or the top diode and the bottom IGBT. But the commutating sequence of the two phase-legs is different, which is determined by the control scheme. Basically, there are two kinds of commutations in the two phase-leg structure: 1) two phase legs commutate at the same time; and 2) one of two phase legs commutates each time. In Case I, as shown in Figure 4-20 (a), the commutation of each phase leg starts at the same time. In the example, S_3 and D_1 commutate in Phase Leg I and S_2 and D_4 commutate in Phase Leg II. In Case II, as shown in Figure 4-20 (b), there is a phase shift of the commutations between two phase legs. At the time S_3 and D_1 commutate, S_2 and D_4 do not exhibit switching behavior. Both of the cases are widely used in DC/DC converters and motor drives, as well as other applications. Although the switching sequences of the two phase-legs are different, the basic commutation phenomenon is still the same for individual module. That is, it takes place between the top and the bottom device.

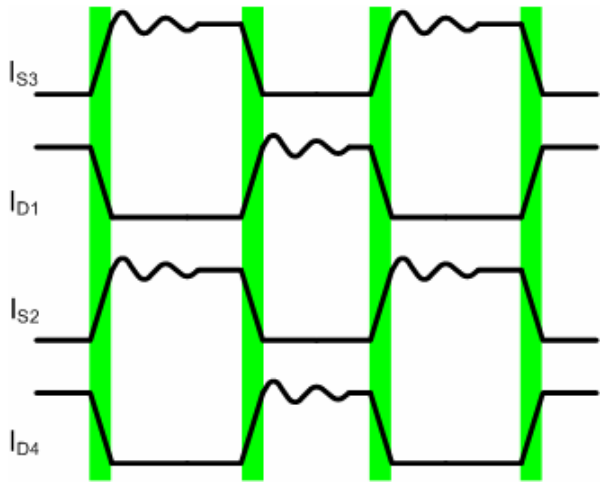

(a) Case I

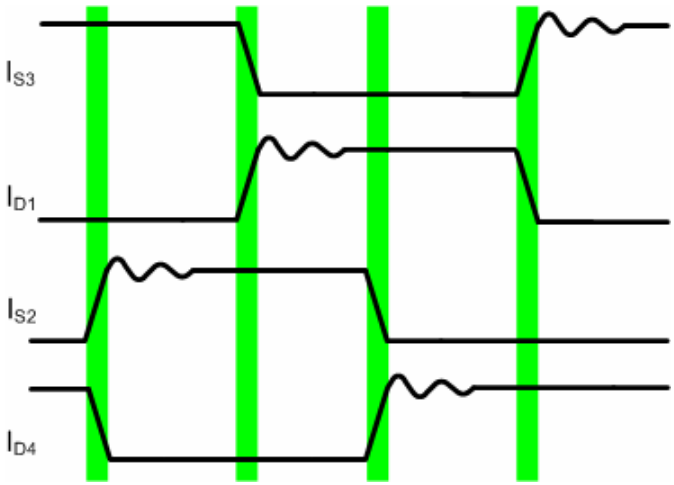

(b) Case II

Figure 4-20 Illustration of Commutating Sequence in Two Phase Legs

In the chopper testbed in Chapter 2, the commutation between the bottom IGBT and the top diode in one phase-leg was modeled. In a two phase-leg structure, one commutation is the same as the testbed (between S_3 and D_1), while the other is different (between the top IGBT S_2 and the bottom diode D_4). Although when using the same testbed with the different connection of the inductive load it is convenient to obtain the other noise source pair involving S_2 and D_4, it is unnecessary to repeat the modeling procedure if the same type of devices in one module have the same characteristics including their dies and packaging. That is, the two IGBTs are identical and the two diodes are identical. In the testbed, the switching behavior of one IGBT (S_3) and one diode (D_1) has been modeled as two current sources and two impedances, as shown in Figure 4-21 (a). Because the same type of devices has the same switching behavior, the source and impedance will not be changed. The change is that the noise current source and source impedance connect to different terminals of the propagation path. Therefore, the commutation between S_2 and D_4 can be modeled as Figure 4-21 (b).

When the circuit can be decoupled and CM and DM noise have no interaction, the two noise source pairs shown in Figure 4-21 can be simplified to CM and DM noise source, respectively. For the DM noise source, according to Eqs. (3-4) and (3-5), the DM noise current source and source impedance of the two cases are the same. In fact, when

only considering DM noise, the effect of chopping the circuit current is the same. As a result, the equivalent DM noise source of two modules is the same. When considering the equivalent CM noise source, the voltage jumping of the terminals of the two modules are different because the connections of the noise current sources are changed. If using the form of voltage source and source impedance shown in Figure 2-13 (b), the different voltage jumping directions will be clearly seen. Therefore, the CM equivalent noise sources are different, which is the same as the practical situation. In fact, the voltages on the mid-point of two modules jump toward different directions, which is good for reducing EMI noise. The results will be shown later.

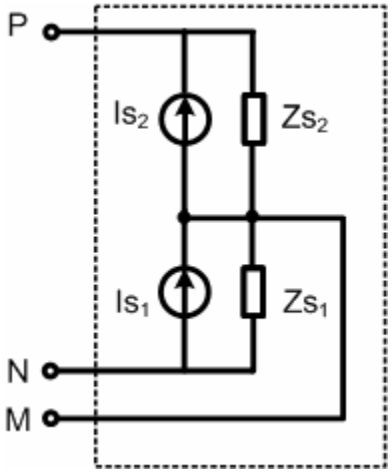

(a) Model I: Commutation between S3 and D1

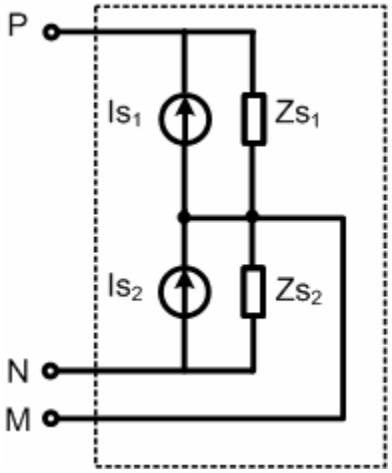

(b) Model II Commutation between S2 and D4

Figure 4-21 Source Model of Two Commutations

In the application of Case I, the two models can be used directly to predict EMI noise in the converter along with the propagation path model. But in Case II, there is a phase shift between two phase legs, which will affect the phase of the noise current source at each frequency in the frequency domain. In fact, Case I is a special case when the phase shift is zero in Case II. Therefore, Case II is more general.

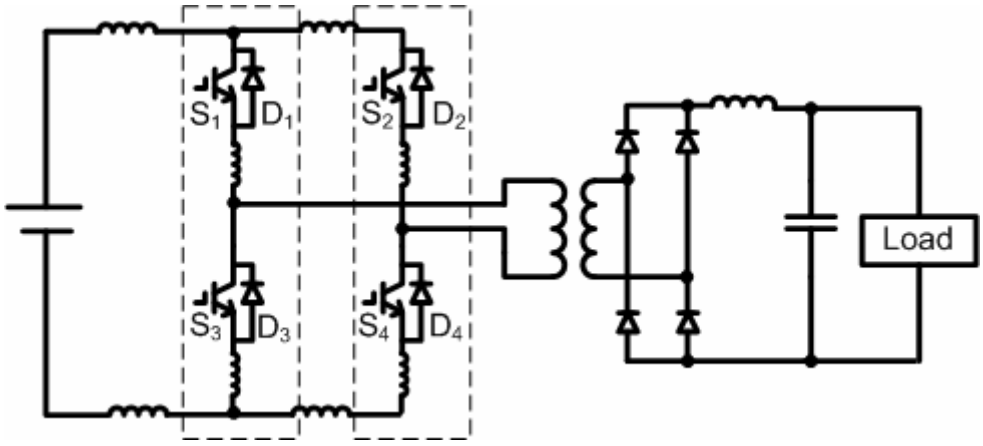

Figure 4-22 Full-bridge DC/DC Converter

In order to demonstrate and verify the application of the MTB equivalent source model in a multiple phase-leg converter, a converter with two phase-legs is implemented as shown in Figure 4-23 (a) and (b). It consists of two IGBT modules, a controllable DC power supply, DC link capacitors, LISNs, and the wires to connect them together. The test circuit will have two modules commutating at the same time, which is Case I. In a practical DC/DC full bridge converter, as shown in Figure 4-22, a transformer connects two modules. A rectifier bridge, an output filter and the load connect to the secondary side of the transformer. Since the purpose of this test is to verify the applicability of the MTB source model, the transformer along with the rest of the circuit could increase the complexity of modeling and prediction process. Therefore, an inductor is used to simplify the load structure. The inductive load normally will not affect the commutation process because the load current stays constant at the switching transients. The inductor can also represent the load of a voltage-fed motor drive. In the test circuit, two DC-link capacitors are connected between terminals of the DC inputs. A large ground plane is also used as

the reference earth ground. There are other parasitic impedances of all the major components included in the circuit.

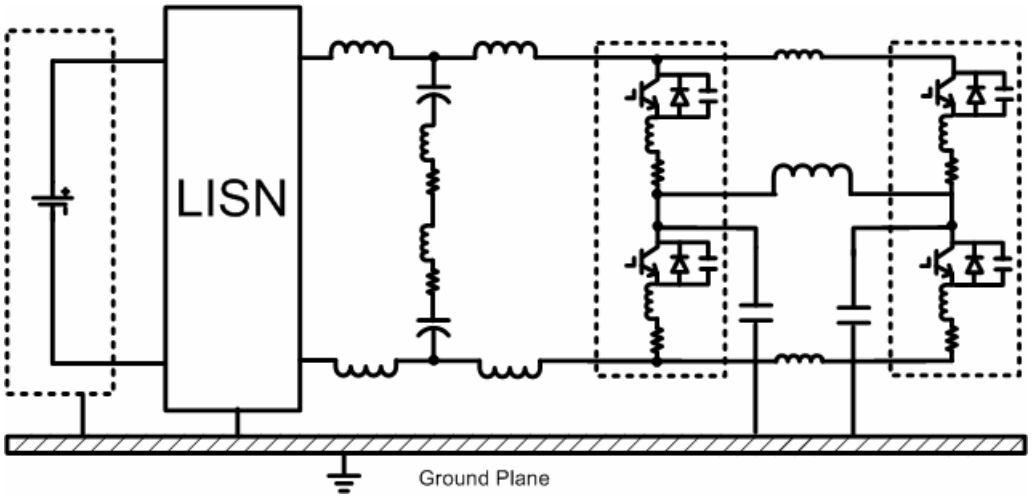

(a) Test Circuit

(b) Implementation

Figure 4-23 Full-bridge Converter (Two Phase-leg Converter)

In the test, the EMI noise of one switching cycle is characterized and predicted with the continuous switching and without changing the operating conditions. Therefore, the

modeling process can be directly used to predict EMI noise for a FB DC/DC converter. It also helps to understand the EMI characteristics of the converter without building a complex control circuit at the design stage. For converters with variable switching conditions the method presented in section 4.1 can be used to synthesize the EMI noise sources at different switching conditions. As a result, a double-pulse switching can be used for the investigation. Since it is a FB converter, the gate signals are sent to two IGBTs, for example S_2 and S_3, to allow the current to build up and be turned off at the desired current level. The current will continue flowing through D_1 and D_4. With a short off period, the second pulse turns on the S_2 and S_3 again at practically the same current. The process of data collecting and processing is the same as that presented in Chapter 2.

The test circuit will have the same commutating process as Case I from the above test description. Two EMI noise source pairs generate the EMI noise at the same time, which can be shown as Figure 4-24. The structure is very similar to the chopper testbed in Figure 2-18. It includes three parts: the noise collector – LISNs, the noise propagation path, and the noise source. The propagation path now is a 6×6 matrix. It satisfies Eq. (2-6). The input and output relationship can be described by (4-10). There is one more terminal in the whole impedance model due to the additional phase-leg module. Note the connections between two positive terminals and negative terminals of the modules have impedances. These impedances can be included into one module source model or modeled as another propagation path inserted between the two modules. In the test circuit, the connection buses between two modules are very short. During the modeling process, the impedances have been neglected.

$$\begin{bmatrix} V_{o1} \\ V_{o2} \\ V_{i1} \\ V_{i2} \\ V_{i3} \\ V_{i4} \end{bmatrix} = \begin{bmatrix} Z_{11} & Z_{12} & Z_{13} & Z_{14} & Z_{15} & Z_{16} \\ Z_{21} & Z_{22} & Z_{23} & Z_{24} & Z_{25} & Z_{26} \\ Z_{31} & Z_{32} & Z_{33} & Z_{34} & Z_{35} & Z_{36} \\ Z_{41} & Z_{42} & Z_{34} & Z_{44} & Z_{45} & Z_{46} \\ Z_{51} & Z_{52} & Z_{35} & Z_{45} & Z_{55} & Z_{56} \\ Z_{61} & Z_{62} & Z_{36} & Z_{46} & Z_{65} & Z_{66} \end{bmatrix} \cdot \begin{bmatrix} I_{o1} \\ I_{o2} \\ I_{i1} \\ I_{i2} \\ I_{i3} \\ I_{i4} \end{bmatrix} \quad \textbf{(4-10)}$$

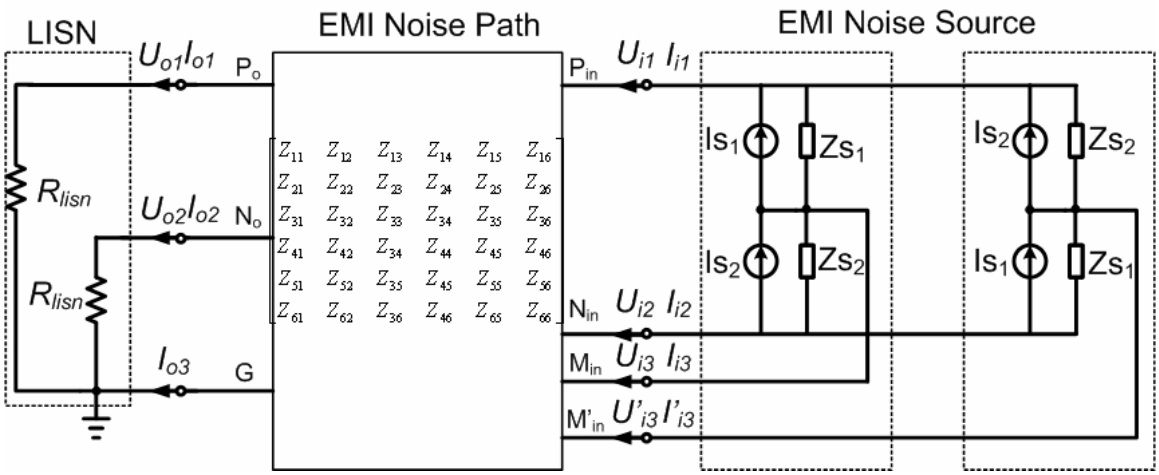

Figure 4-24 Equivalent EMI Emission Model of a FB Converter

Although the new impedance matrix is bigger than that of the testbed, it will not take much more time to measure the 6×6 impedance matrix due to the identical packaging and geometry of the two modules. For example, Z_{55} equals Z_{66}, which are the driving impedances from terminal M_{in} and M'_{in} respectively. And Z_{56} and Z_{65} are the impedances between M_{in} and M'_{in}, which represent the impedance of the load. In next section, the propagation path modeling procedure of a converter with more than two phase legs will be presented in detail. As discussed in Chapter 3, the MTB model has its validity range. The propagation path should be in the valid range and the operating condition should be the same as the modeling condition.

The MTB model derived in the "standard" testbed can be used to predict the EMI noise of the FB converter according to the EMI noise emission model in Figure 4-24. Figure 4-25 and Figure 4-26 show the DM and CM prediction and test results. The prediction results match the test results closely up to 20 MHz. The noise peaks can be accurately predicted with the maximum discrepancy is about 5 dBμV. The DM and CM prediction envelopes are several dBμV higher than the test results. When the frequency is higher than 20 MHz, the error is bigger. In fact, the test results show that there is no noise peak during 20 MHz - 30 MHz. The noises are flat, which are close to the noise floor. As discussed in Chapter 3, one of the major errors in predicting noise comes from the sampling process. Because of the limited sampling accuracy, the MTB equivalent model

at a high frequency cannot be as accurate as it is at a low frequency. In addition, more calculation steps in the FB converter noise prediction could cause more errors.

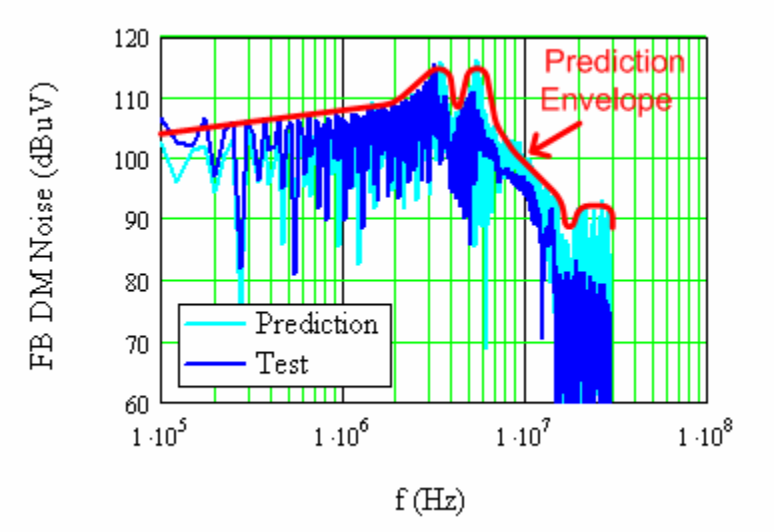

Figure 4-25 DM Test and Prediction Results of FB Converter

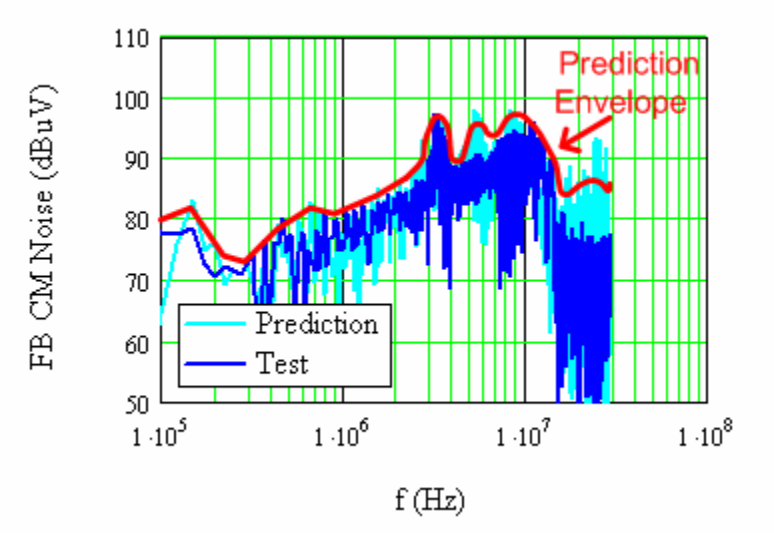

Figure 4-26 CM Test and Prediction Results of FB Converter

As discussed in previous chapters, both MTB noise current sources and source impedances are important for EMI noise prediction. In the FB structure, there are four sources and four impedances affecting EMI noise for one switching cycle. The effects of

source impedances can be observed from the comparison of the chopper circuit and the FB converter with the same propagation path.

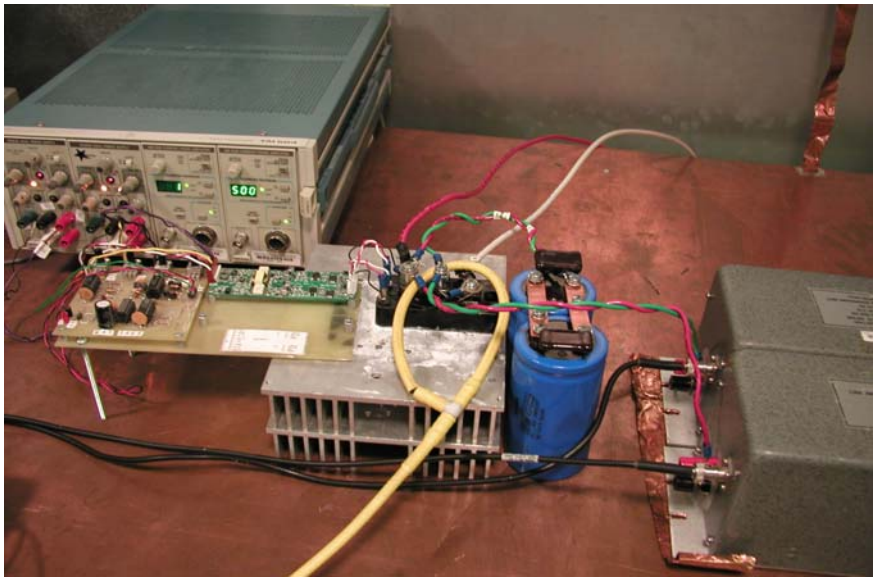

Figure 4-27 Tested Chopper Circuit

Figure 4-27 shows the chopper circuit with one device module. The propagation path is the same as the FB converter as shown in Figure 4-23 (b). The DM and CM noise comparison are shown in Figure 4-28 and Figure 4-29 respectively. It can be seen that the DM noise of the FB converter is 6 dBμV higher than the chopper circuit. The two switching modules at the low frequency are two current sources and the impedances do not affect EMI generation. As a result, the noise source of the FB circuit is 2 times bigger than the chopper circuit, which is 6 dBμV in the frequency domain. When the source impedances in the FB converter interact with the propagation path, the resonant peaks move toward the lower frequency, which is around $1/\sqrt{2}$ lower than those of the chopper circuit. In the high frequency range (>5 MHz), the FB structure has lower DM noise because of the steeper decreasing slope after a resonant peak. For the CM noise, the FB has lower EMI noise than the chopper circuit in the low-frequency range because the voltage jumping at the mid-points of two modules are toward opposite directions, which can cancel the CM noise. But in the high-frequency range, the voltage jumping behavior may not help because other stray capacitances between device modules and ground may

be dominant. In general, the FB converter with the switching pattern as Case I can help reduce the CM EMI noise emission

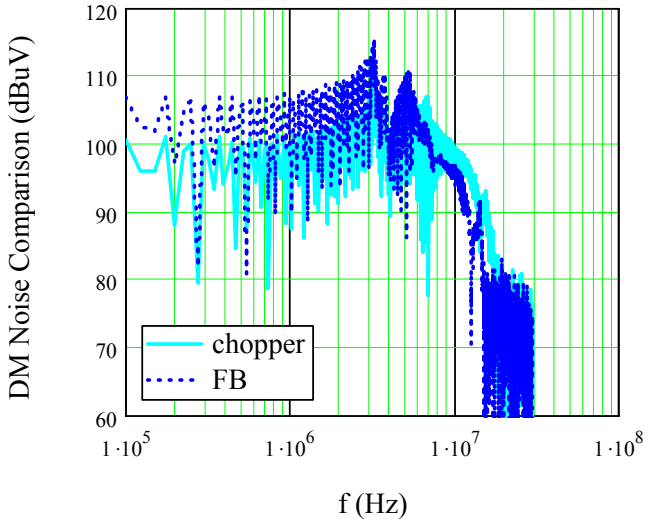

Figure 4-28 DM Noise Comparison of Chopper Circuit and FB with Same Propagation Path

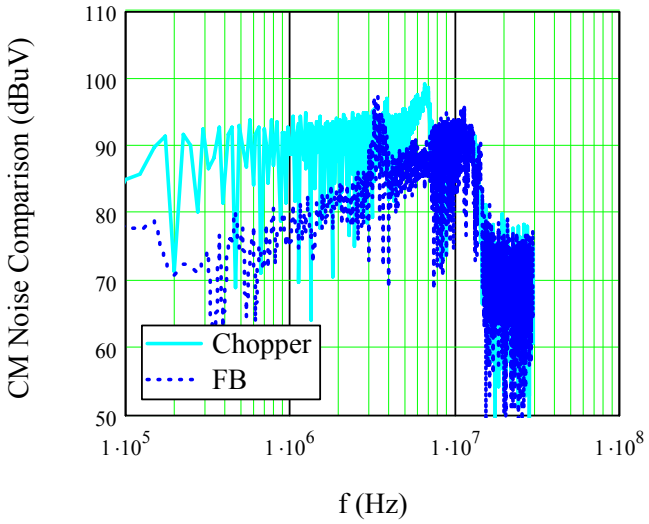

Figure 4-29 CM Noise Comparison of Chopper Circuit and FB with Same Propagation Path

In this section, the MTB equivalent source model is applied in a converter with two phase legs. The experiment, using a FB converter as the example, verifies the model application. The MTB model has the modular characteristics and can be applied in

converter with two phase-legs. In next section, a three-phase motor drive application will be analyzed.

4.3. Discussion on MTB Equivalent Source Model Application

In a three-phase voltage-fed motor drive system with SPWM control scheme shown in Figure 4-30, the switching is more complicated than the FB converter, as each switching period can involve three commutations and the switching conditions change with the load conditions. Since the MTB equivalent source model has modular and terminal characteristics, it can be used to predict the EMI noise while taking the load condition into consideration. The load condition includes two aspects: 1) phase current amplitude; and 2) phase current direction.

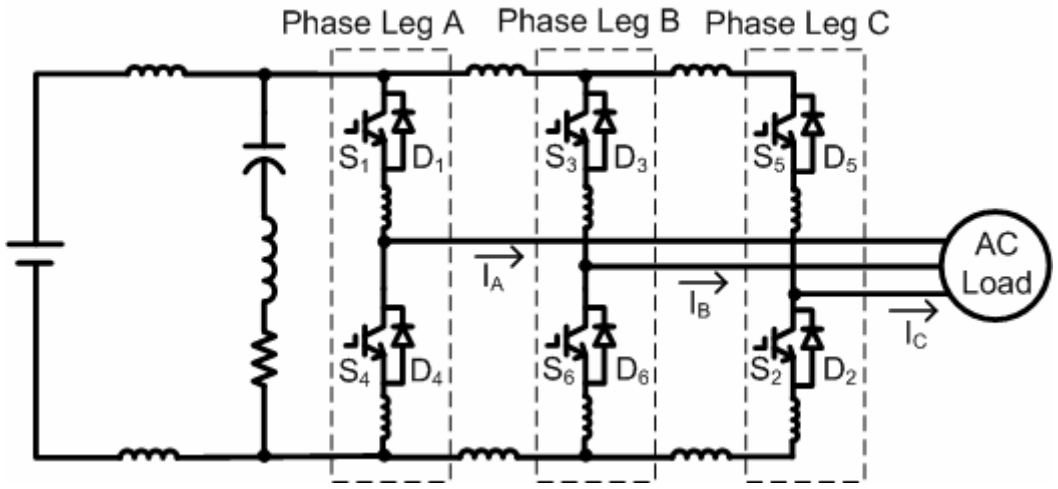

Figure 4-30 Three-phase Motor Drive System

In the previous section, MTB equivalent source models are derived according to the current level. For example, the whole line cycle can be divided into four zones based on the load current for each phase, which is shown in Figure 4-31. Therefore, there are four basic MTB models, which represent the commutation between the top diode and bottom IGBT (Model I) or the top IGBT and bottom diode (Model II). Since Model I and Model

II have a certain relationship, as discussed in the previous section, it is enough to only have one model. The basic modeling concept for three-phase and multi-phase (more than three-phase) converters is to determine the composition of different MTB models for each phase. If we assume "+" to represent Model II and "-" to represent Model I, the four different MTB models for the commutation between the top IGBT and the bottom diode at different current levels can be described as M_{I1+}, M_{I2+}, M_{I3+}, and M_{I4+}. The entire line cycle can be divided into three areas, since the each phase current has the same amplitude and 120° phase shift.

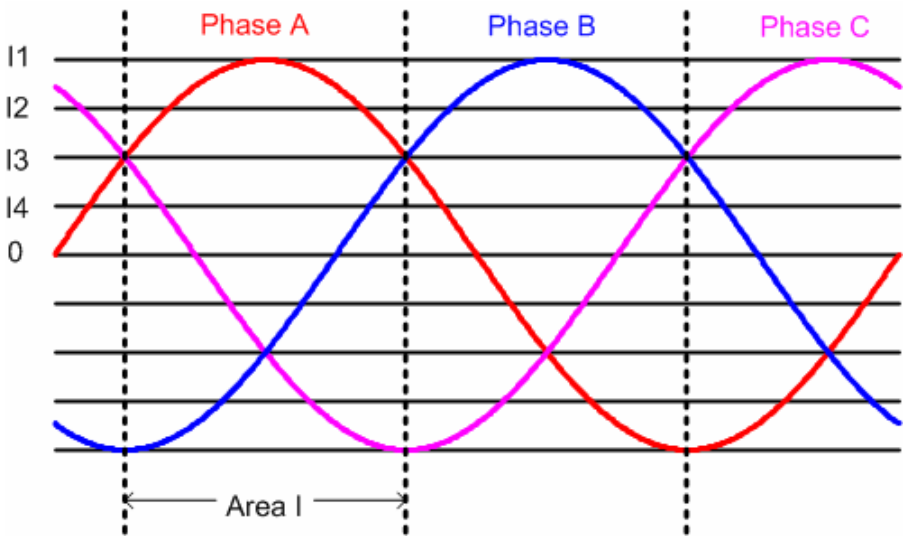

Figure 4-31 Illustration of Applying MTB Model in Voltage-fed Three-phase Motor Drives

Let us consider Area I first. In Area I, Phase A current is positive and is the largest current among all three phases. According to the Phase A current direction, the commutation in the Phase A module is between S_1 and D_4. As a result, there are two MTB models, M_{I1+} and M_{I2+}. The current in Phase C changes direction in Area I. When the current has a positive direction, M_{I3+} and M_{I4+} are used to model the EMI noise sources because the commutation is between S_3 and D_6. When the Phase C current goes in the negative direction, the commutation is between S_6 and D_3, and M_{I4-}, M_{I3-}, M_{I2-} and M_{I1-} are used to represent the EMI noise sources of Phase leg B. For Phase C, the current also changes the direction; here M_{I4-}, M_{I3-}, M_{I2-}, M_{I1-}, M_{I4+}, and M_{I3+} are used as the EMI

noise source models. All of the MTB models used in Area I according to the load current condition can be summarized in Table 4-1. By looking at the models in Area I, the EMI noise can be predicted along with the noise propagation path.

Table 4-1 EMI Source Models in Area I

Phase	Area I											
	1	2	3	4	5	6	7	8	9	10	11	12
A	M_{I2+}	M_{I2+}	M_{I1+}	M_{I1+}	M_{I1+}	M_{I1+}	M_{I1+}	M_{I1+}	M_{I1+}	M_{I1+}	M_{I2+}	M_{I2+}
B	M_{I1-}	M_{I1-}	M_{I1-}	M_{I1-}	M_{I2-}	M_{I2-}	M_{I3-}	M_{I4-}	M_{I4-}	M_{I4+}	M_{I4+}	M_{I3+}
C	M_{I3+}	M_{I4+}	M_{I4+}	M_{I4-}	M_{I4-}	M_{I3-}	M_{I2-}	M_{I2-}	M_{I1-}	M_{I1-}	M_{I1-}	M_{I1-}

As discussed in the previous section, the division of the zones is determined by the device module characteristics. Although Area I has twelve different source-model compositions, the calculations can be done very efficiently with the knowledge of the switching pattern. In a line cycle of a three-phase converter, there are three areas, which are the same in terms of EMI noise generation. The terminal characteristics of the different areas are identical. Therefore, the EMI noise of the entire system will be 3 times higher than that of a single area, which is 9.5 dBμV higher in the frequency spectrum.

In the example, the three-phase drive system is controlled with the SPWM scheme. The approach is independent of the control schemes and thus can be applied to other schemes, such as space vector modulation (SVM) and synchronous switching schemes. For more complex, non-symmetrical modulation schemes, such as a discontinuous PWM, a device may not switch uniformly within a line cycle, which will affect the zone selection and the contribution of each zone. For example, for a discontinuous PWM that switches a device for 2/3 of the period only, we can divide the entire period into 3n zones to facilitate the MTB modeling process, where n is a nonzero integer. In this case, 2n zones corresponding to continuous PWM switching can be modeled normally with the MTB modeling process, and the remaining n zones can be modeled with zero noise current source since they correspond to non-switching regions. The total EMI will be 2/3 of the EMI noise level when the devices switch continuously during the entire operating

period. In any case, the required parameters and information for the modeling and prediction process include the switching numbers in one line cycle, equivalent MTB source models for each zone, the source model compositions and the propagation path impedance matrix.

As the comparisons shown in Figure 4-28 and Figure 4-29, the FB structure with Case I switching pattern can effectively reduce CM noise in the low-frequency range. In a three-phase system, the different modulation schemes determine how many phase-legs are involved in a switching cycle. Therefore, the modulations with two-phase-leg switching at a time will help to generate less EMI noise.

It can be seen that the EMI noise source modeling of a multi-phase converter based on the MTB model can be easily derived. As shown in Figure 4-24, an additional phase leg results in at least one more terminal. Hence, the dimension of the propagation path impedance matrix increases by one if including the connecting impedances between two phase legs into a one phase-leg source model. However, the dimension increase is due to the function of the converter and the more complex load connection. A 6×6 impedance matrix is used for a two-phase structure and a 7×7 matrix is used for a three-phase structure. As shown in the previous section, Z_{56} and Z_{65} are the impedances between M_{in} and M'_{in}, which represent the load characteristics. Z_{55} and Z_{66} are the impedances between M_{in} and ground, and M'_{in} and ground respectively. For the three-phase converter, Z_{55}, Z_{66} and Z_{77} are the impedances between the load terminals and ground. Z_{56}, Z_{67}, Z_{57} are the impedances between different phases. Since the impedances between the module terminals and ground are not included in the MTB model, these impedances should be synthesized and included in the propagation path. Other impedances, such as Z_{17}, Z_{27}, etc. should be accurately modeled in theory. However, some of the impedances can be modeled in a simpler way if the connection and geometry information are known. For example, the impedance between one LISN terminal and M_{in} can be set with a very large impedance because there is no direct connection between them and the distance between these two terminals are relatively far. Therefore, the impedance matrix measurement can be simplified.

When the structure of the converter becomes more complex, more propagation path modeling and measurement should be carried out for other EMI modeling methods. The MTB modeling method is neither more time-consuming nor more complicated than other methods for the propagation path modeling from a path modeling perspective. Since the structure of each converter is different, the complexity of modeling the propagation path impedance matrix is varying.

Although the MTB model is the EMI noise source model for phase-leg based converters, the commutation characteristics of each phase leg are fundamentally similar to some non-phase-leg-based topologies, such as so-called single-switch converters, as shown in Figure 4-32. Single-switch buck and boost converters are widely-used topologies. Each converter includes one controlled device *S* and one diode *D*. For the boost converter, the commutation is occurs between bottom the device and the top diode, which is Model I in Figure 4-21 (a). For the buck converter, the commutation is between the top device and the bottom diode, which is the same as Model II shown in Figure 4-21 (b). The difference between a buck and boost converter, in terms of EMI noise emission, is the different propagation path. In fact, the chopper circuit used as the testbed is a buck converter. Since each phase-leg module has two controlled devices and two diodes, it is not used in a single-switch converter. However, the MTB source model extraction method can be used to characterize the different composition of the controlled device and the diode by using the standard testbed.

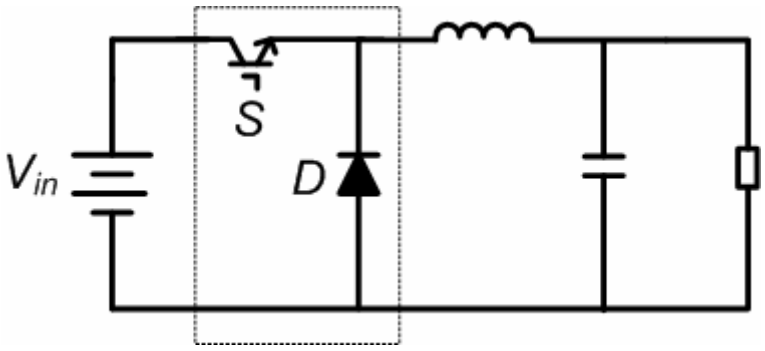

(a) Buck Converter

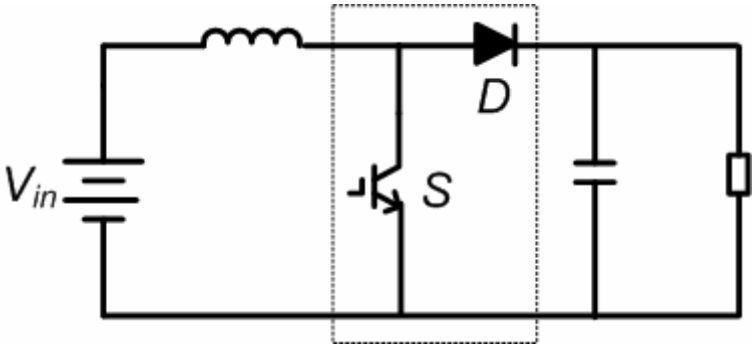

(b) Boost Converter

Figure 4-32 Single-switch Converter

As presented in the previous section, the two-phase structure, as shown in Figure 4-19, is the simplest structure in the multi-phase converters. It can also be a standard cell for other topologies, such as a multi-level converter [95] [96], as shown in Figure 4-33. The basic cell is a single-phase full-bridge inverter. Each phase-leg commutation is still between the IGBT and the diode, which can be represented by Model I and Model II, as shown in Figure 4-21. Although three full-bridge inverters are in series in order to obtain high voltage in each phase ($3V_{dc}$), the voltage change of each phase-leg mid-point is V_{dc}. As a result, the CM current contribution of each phase can be calculated by three separate full-bridge inverters. Applying MTB models under different load current conditions to a FB converter with the knowledge of the switching numbers of each phase leg will yield accurate EMI noise source models.

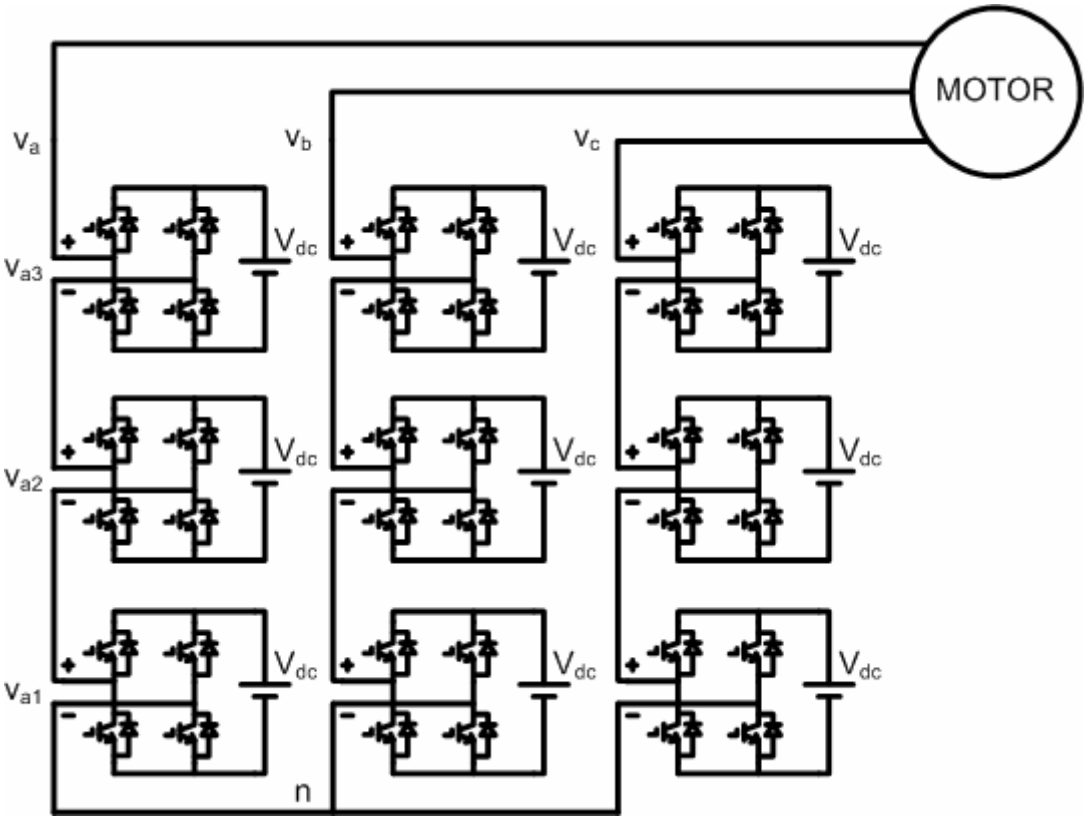

Figure 4-33 Five-level Cascaded Motor Drive

It should be pointed out that an active switch and a passive switch are lumped together in a single functional block called the PWM switch for the small-signal analysis of power converters [107] [108]. In terms of EMI source modeling, the same functional block is defined as a basic unit, which includes two noise sources and two impedances, as shown in Figure 2-13. The majority of basic non-isolated switching power converter topologies used today fall into the following categories: single-ended, half-bridge, full-bridge, multi-phase, and multi-level converters [109], as depicted in Figure 4-34. All of these topologies are based on this basic unit. For example, the single-ended topology is usually employed for single-quadrant DC-DC choppers, such as the single-switch buck and boost converter in Figure 4-32 and the chopper circuit in Figure 2-16. Half-bridge, full-bridge, three-phase and multi-phase converters are directly based upon the phase-leg structure, which is identical to the physical structure of the MTB model. In previous discussion an example of a multi-level converter, which cascades full-bridge converters, is given to show the applicability of the MTB model.

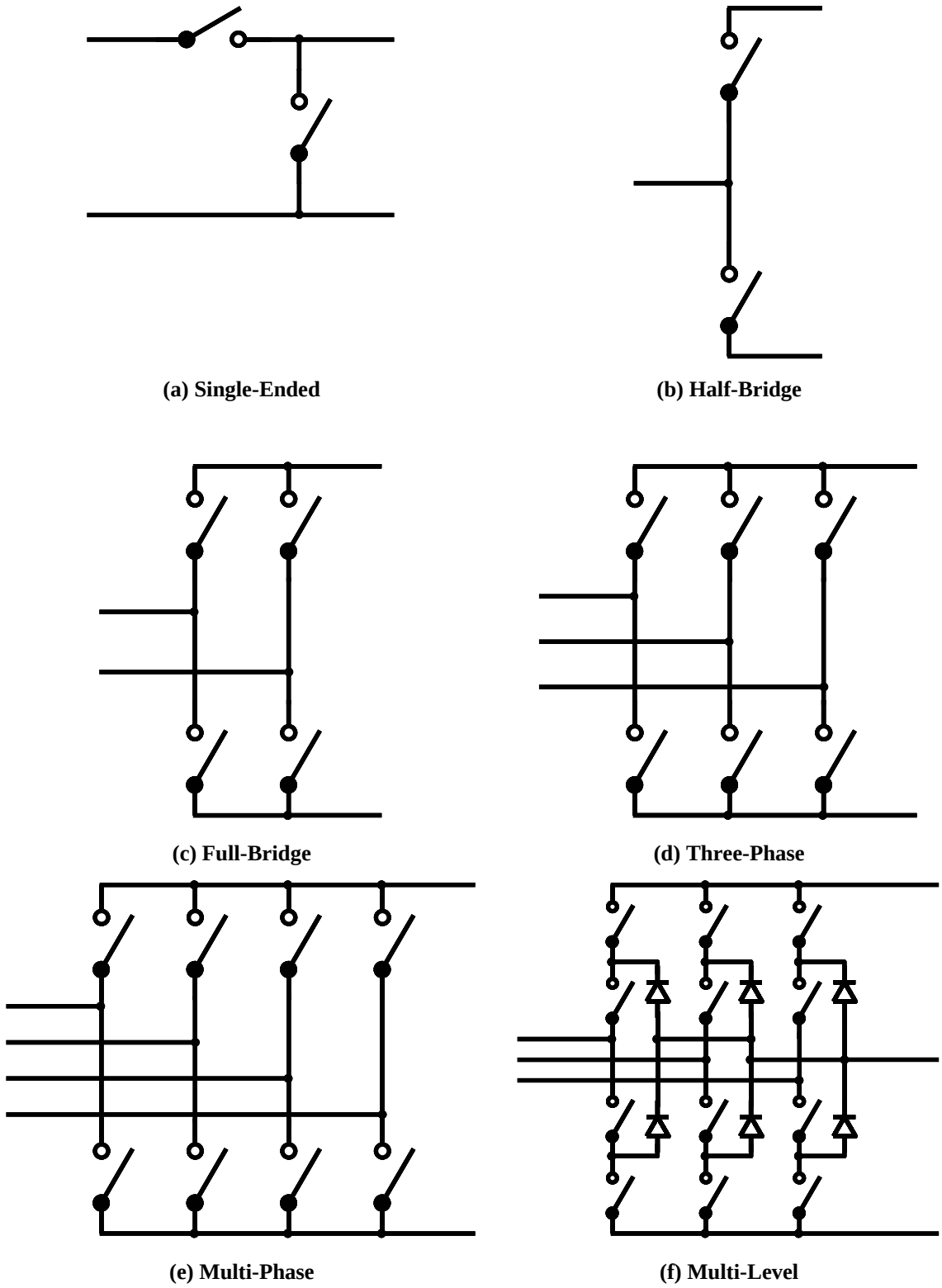

(a) Single-Ended **(b) Half-Bridge**

(c) Full-Bridge **(d) Three-Phase**

(e) Multi-Phase **(f) Multi-Level**

Figure 4-34 Major Non-isolated Switching Network Topologies

Essentially, the commutation between the active and passive device in the functional block is one of the most common behaviors in power electronics. Commutation exists in the examples given in this dissertation as well as other converters as shown in Figure 4-34. Selecting and modeling the EMI characteristics of this functional block can help understand the essence of EMI noise generation for converters based on this kind of commutation. Although the unit has two forms, consisting of Model I and Model II shown in Figure 4-21, they can be transferred to each other. With the modular and terminal characteristics of the MTB model, EMI emissions of a converter with a complex topology can be derived, as long as the commutation is the same as the basic unit. Therefore, it is important to obtain this basic unit for EMI noise emission characterization and prediction.

In this dissertation, the analysis is based on voltage-fed converters, whose commutation is between one IGBT and the other IGBT anti-parallel diode in one phase-leg module. There is another important category of converters, current-fed converters, as shown in Figure 4-35 (a). The three-phase buck rectifier has the same power stage as CSI except for the different input source and output load, as shown in Figure 4-35 (b). Each phase-leg includes two IGBTs and two diodes in series with the IGBTs. The phase-leg structure is different from that of a voltage source converter. Therefore, the MTB model derived from the VSC cannot be used in CSI or three-phase buck rectifier.

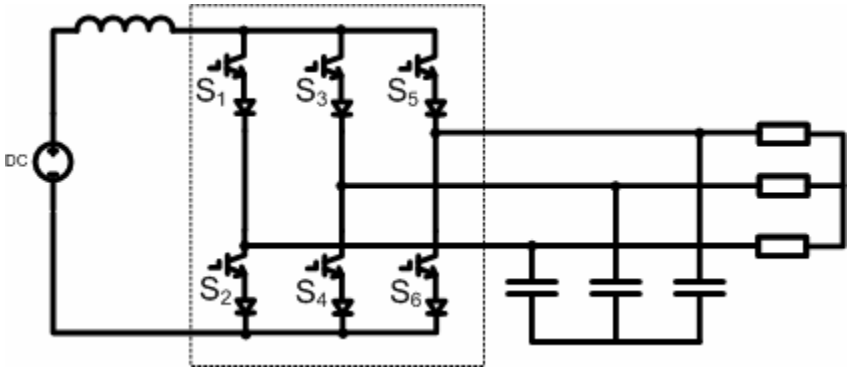

(a) Current Source Three-phase Inverter

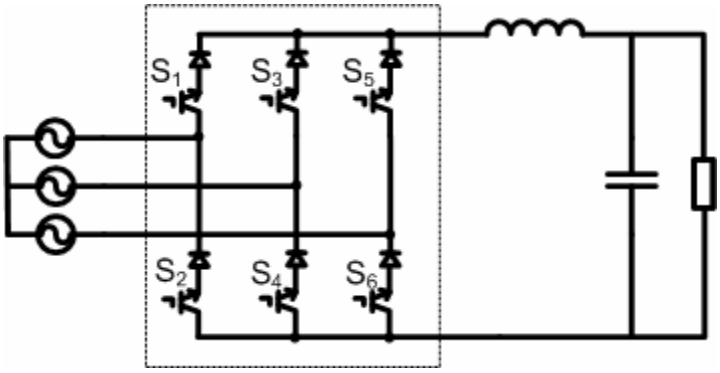

(b) Three-phase Buck Rectifier

Figure 4-35 Topology of Three-phase Buck Converter and Current Source Inverter

However, the MTB modeling concept can still be applied in a CSI and a buck rectifier. The commutation is not between the top and the bottom device. It is among the devices that have the same connectors, such as S_1, S_3, and S_5 or S_2, S_4 and S_6. Any two phases of the three-phase systems can be simplified as Figure 4-36. S_1 and S_3 consist of a new phase-leg. The MTB model could be derived for the composition of S_1 and S_3 or S_2 and S_4.

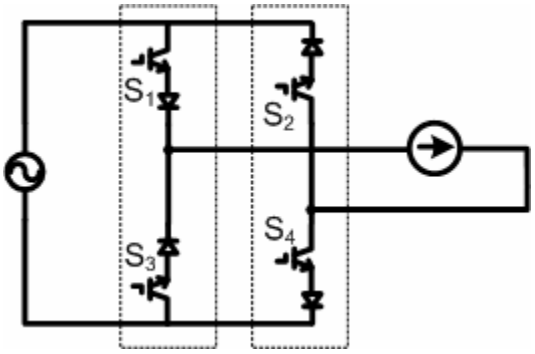

Figure 4-36 Standard Two-phase Cell of Buck Converter and CSI

As reviewed in Chapter 1, an accurate EMI noise source model for the entire conducted EMI frequency range is not available yet for power converter designers. From looking at the MTB EMI equivalent source model concept and modeling process, one can conclude that device module vendors can provide the MTB model characteristics for a

device module for various operating conditions, so the users can use the model in their converter design for EMI noise prediction and management.

Although device manufactures have the ability to obtain detailed and accurate models of devices, such as providing physics-based models, it is not efficient and convenient for users to apply in EMI research. However, the MTB modeling process does not require many details of devices. A simple-structure standard testbed can be used to derive the MTB models under different operating conditions. The modeling process is presented as in Chapter 2. It can be summarized as the following flow chart in Figure 4-37. Two different propagation paths are selected to obtain two sets of voltages and currents on the noise source side. Based on the Norton circuit theory, the MTB equivalent noise current and source impedance can be obtained.

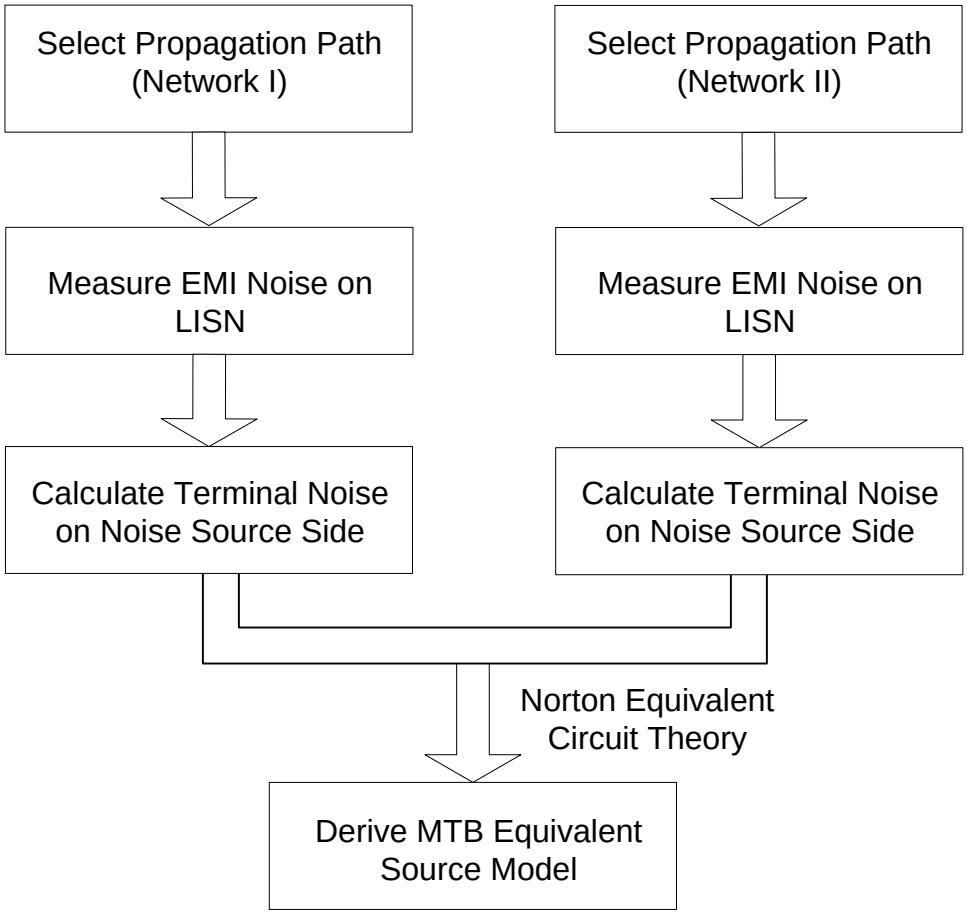

Figure 4-37 MTB Equivalent EMI Noise Source Modeling Process

During the process, there are a few requirements for the standard testbed: 1) The propagation path selections for the standard testbed should not beyond device validation range, which is discussed in Chapter 3; 2) The propagation path can interact with device module and be accurately characterized; 3) The data collection and processing should not affect the modeling accuracy.

MTB models are modeled under a certain condition, which includes a given bus voltage, load current, gate circuit, switching frequency and temperature. In general, when changing any of the above parameters, the MTB model is nonlinearly changed. However, the switching frequency and MTB noise source current have a fixed relationship, as shown in Figure 4-38. There are three different frequency signals: 25 kHz, 50 kHz, and 100 kHz in Figure 4-38 (a). They have same duty cycle and rising and falling time. From the frequency spectra shown in Figure 4-38 (b), three different frequency signals have the same envelope shape, but different amplitudes. When the frequency is doubled, there is 6 dB increase in the frequency domain. Based on the analysis, the MTB model derived at a certain switching frequency can be used for other switching frequency conditions since changing the frequency will not change the device physics characteristics. The spectra are linearly shifted to different levels. However, increasing the frequency will reduce the time for damping the resonance between the device module and the propagation path, which could change the switching condition of the device. Therefore, applying MTB models to predict EMI noise in the converter with higher switching frequency than the testbed should be careful to keep the same switching conditions.

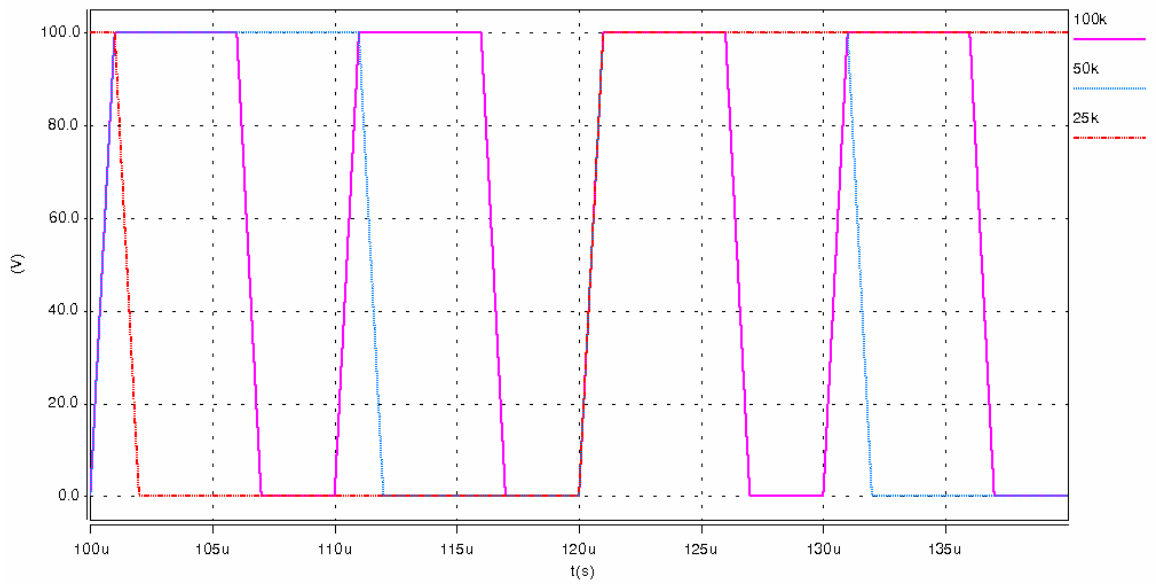

(a) Time-domain Waveforms of Three Different Frequency Signals

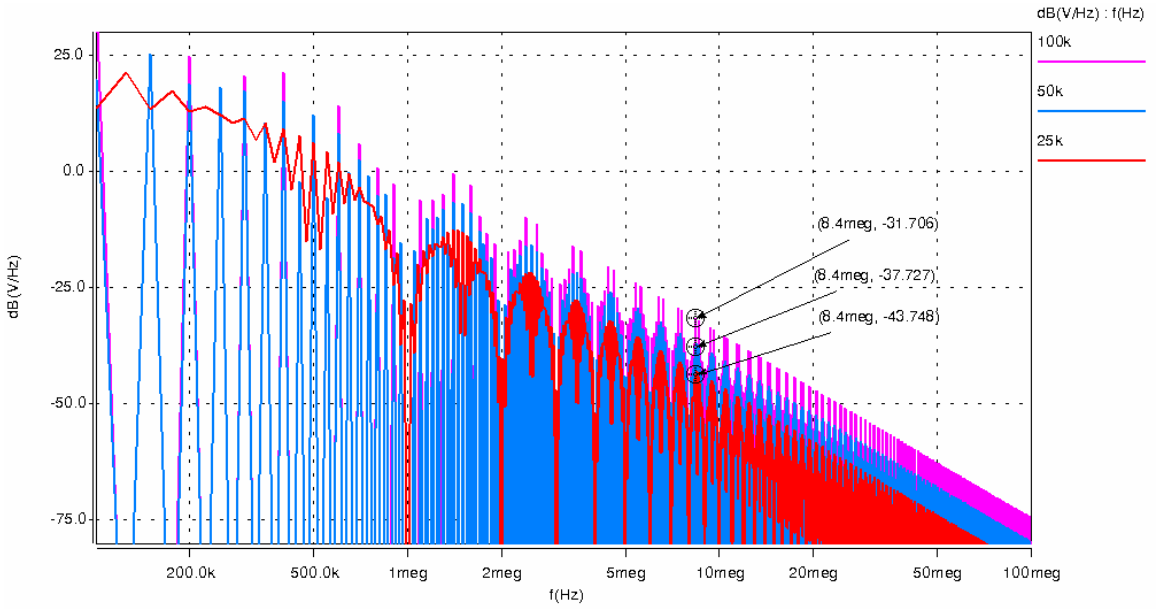

(b) Frequency-domain Waveforms of Three Different Frequency Signals

Figure 4-38 Illustration Switching Frequency Effect

The MTB models are modular and in principle can be applicable to any converters with the device modules, provided that the switching conditions in converters match those for the models. Under each switching condition, the MTB model basically consists of data arrays of noise current sources and source impedances in the conducted EMI range.

It is possible that manufacturers could provide a library of device EMI models under several switching conditions along with other characteristics included in the device datasheet.

So far, there are no existing EMI models from device manufacturer, except some behavioral device models. For power converter designers, due to the lack of easy-to-use and accurate EMI model for converters, EMI noise management is still a trial-and-error process and depends on the engineers' experience. For example, input EMI filters usually have to be designed and fine-tuned after a power electronics converter has been built. In addition, input filters may not attenuate high-frequency EMI noise because of the limitations of filter design, material, etc. Therefore, controlling and managing EMI noise at the converter function design stage is not available, which can often lead to a long design cycle and less-than-optimal system designs.

Some research has developed design tools for designing different parts of converters [69] - [71], [98] - [102]. For example, [69] demonstrates how to design an input EMI filter for voltage-fed motor drives, as shown in Figure 4-39. There are several design conditions, such as the total bare noise of the drive, CM bare noise, DM bare noise, CM noise source impedance, and DM noise source impedance. Without an accurate EMI noise model of the drive, the only way to obtain these conditions is to measure the noise after building the drive. However, the drive is built without systematic considerations of EMI aspects, such as selecting devices and designing the propagation path. As a result, the only method to comply with the EMI regulations is to design an input EMI filter as a "remedy" to solve EMI issues in the converter. Nevertheless, the source impedances are one of the conditions for the filter design, which can only be measured with a fully-functional drive.

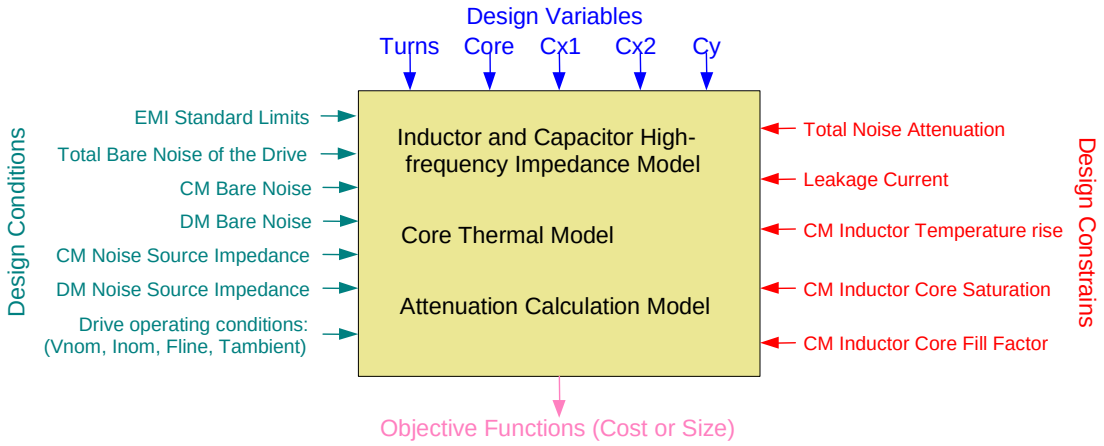

Figure 4-39 Optimization Program for Input EMI Filter Design

In fact, using the MTB equivalent source model and the propagation path model, the total bare noise, CM bare noise, and DM noise can be accurately predicted and both CM and DM noise source impedance of the entire drive can be derived. Therefore, the MTB modeling methodology can provide the required information for an EMI filter optimization program. In addition, the MTB model provides the possibility to control the EMI noise by means other than merely adding EMI filters. As presented in Chapter 1, cables, wires, DC-link capacitors, the busbar, parasitics of the system, etc. all belong to noise propagation path. With proper propagation path design, the EMI noise can be reduced or confined in the converter, which can reduce the size and the cost of the input EMI filter. The parametric study of the converter can be easily done with the MTB model.

There are some other optimization programs for an entire converter design, such as selecting devices from thermal point of view. All these design programs are dealing with one part of the converter design, which makes them local programs. In terms of a systematic design of a converter, basic functions, thermal issues, EMI issues, etc. should be included in one design program. For example, thermal and EMI characteristics are the two aspects of a semiconductor device. The design program can have both a library of different devices' MTB EMI noise source models and a library of the thermal (loss) models. The program can select a device while considering both EMI noise generation

and device loss. A global optimization program can be developed instead of using many local optimization programs for designing a power converter.

In addition, MTB models also provide the possibility for optimizing the design for a power conversion system, which includes multiple converters in the system. Each converter can have an EMI noise emission model characterized by the MTB modeling method. The interactions between different converters can be studied based on the converter-level models. The entire conversion system EMI management can be also designed based on the derived models.

Therefore, MTB models for switching device modules can conceivably be provided by module vendors, or a library of such models can be built through standard tests. Clearly, MTB EMI source models can potentially become a valuable part of the converter design tool for converter-level and system-level EMI modeling, prediction and management.

4.4. Summary

In this chapter, the MTB equivalent source model is applied in more complicated converters. The half-bridge DC/AC converter and full-bridge converter are used as examples to demonstrate the EMI prediction process with MTB models. The first example presented is applying the MTB equivalent source model in a converter with variable switching conditions. The operating cycle can be divided into operating zones based on the device operating conditions, such as load currents. Each zone can be characterized by an equivalent MTB noise source, based on the MTB model for one representative switching event and the number of switchings in the zone. By superposing the MTB models for all operating zones in the frequency domain, the conducted EMI noise for the entire operating period can be modeled and predicted. The prediction results using the proposed method match both simulation and experimental results on an IGBT based HB DC-AC converter. The next example that is presented is applying the MTB models in a FB converter. Although two different commutations in one phase-leg module

determine two different MTB models, it is only necessary to model one MTB noise source pair due to the relationship between two noise source pairs in the module. The detailed modeling process is presented. The experimental results prove the applicability of MTB models and the models' modular and terminal characteristics.

In the last part of this chapter, the possible industrial applications of the MTB model, such as three-phase voltage-fed inverter, multi-level converter, single-switch converter and CSI, are discussed. The MTB model derived in the voltage-fed circuit can be used to in the converters with the same commutation type (commutation between IGBT and diode). Since the phase-leg structure in the CSI is different from the derived MTB model, EMI prediction of CSIs cannot use the MTB model directly. However, the MTB modeling concept is still applicable.

Compared with other EMI noise source models, the MTB model is a modular and behavioral model and has simple modeling process, which makes it possible for device manufactures to provide devices' EMI models to users. A library of a device with several MTB models under different switching conditions can satisfy different users' applications. Furthermore, the MTB model provides a chance for power converter designers to develop a global design tool with the consideration of EMI noise emission. The EMI management can be designed along with other function design at the converter design stage. The MTB model can help optimize the EMI filter and reduce the design cycle. Different level EMI emission models – converter-level and system-level – can be derived based on the MTB models.

In summary, a MTB model can be applied in phase-leg based converters and is a basic unit of EMI noise emission modeling.

Chapter 5 EMI Noise Management for Power Converters Based on MTB Equivalent Source Model

Chapter 5 begins the analysis of EMI noise interactions and management based on the MTB model. In this chapter, the selection of DC-link decoupling capacitors in VSC is used as an example to demonstrate the parametric study based on the MTB model. The EMI noise effect and voltage overshoot of decoupling capacitors based on the MTB model is presented. Suppression methods that are effective in reducing the noise source level and containing EMI noise on the source side are discussed. A completed converter-level MTB equivalent EMI model procedure is presented, and applications of the model are discussed.

5.1. EMI Noise Interactions Analysis and Management of Converters Based on MTB Equivalent Source Model

In the design of a converter, the operating conditions of devices are normally determined by the converter's function. As a result, the EMI noise sources in the converter are known at the design stage after selecting devices if the devices' MTB models are available. As shown in Figure 5-1 (replication of Figure 2-14 (a)), the effect of the propagation path on the EMI noise, which is a kind of parametric study of the converter, can be analyzed based on the converter EMI noise emission model. The process of this parametric study can be carried out in following steps:

1) Obtain the MTB equivalent noise source model, which is demonstrated in Chapter 2. The modeling process can be experiment-based or simulation-based. As discussed in Chapter 1, it is time-consuming to perform parametric studies using physics-based models

and models provided by manufacturers. If those device models are available, extracting their MTB models is more convenient and time-saving to perform parametric study in simulations. The procedure in simulations is the same as the experimental procedure.

2) Obtain the propagation path model. As shown in the modeling process, the propagation path is modeled as an impedance matrix. If new components are added to the modeled propagation path, the impedance matrix of the new propagation path can be obtained by the matrix calculation of the original and new components' impedance matrix.

3) Calculate the EMI noise of different propagation paths. In addition, the effect of the propagation path on the device terminals, such as voltage overshoot of the device, can be predicted, since the terminal voltages and currents on the device terminals can be calculated by the MTB modeling approach. As mentioned in Chapter 3, changing propagation path may change the operating condition or cause severe nonlinearity. Therefore, the validity of the MTB model in the parametric study should be estimated first. In this section, selecting decoupling capacitors is used as an example to demonstrate the parametric study based on the MTB model

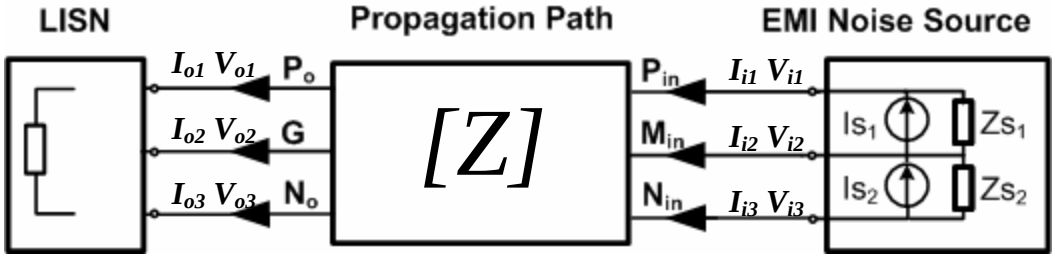

Figure 5-1 EMI Noise Emission Based on MTB Model

In order to operate devices safely decoupling capacitors are usually used on the DC-link in hard-switching VSCs. The basic function of the capacitors is placed between the device module and the rest of the circuit to minimize the voltage overshoot due to the abrupt current change in the parasitic inductors in the circuit. The decoupling capacitors together with other components, such as DC-link capacitors, busbars, connectors and parasitics, are all included in the propagation path. The voltage stress and EMI noise

impact can be analyzed by simulation, as shown in Figure 5-2. The device is operated with 200V bus voltage and 40A load current. In the simulated chopper circuit, the DC-link capacitors, decoupling capacitors and the device module are not ideal since their parasitics impact the device stress and EMI noise spectrum significantly.

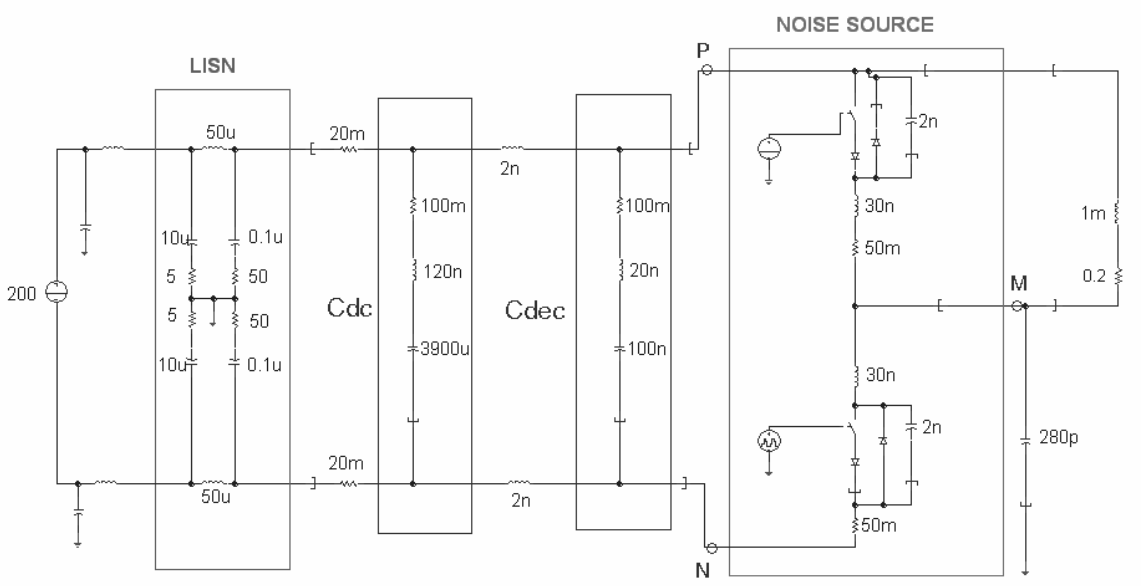

Figure 5-2 Simulation of Decoupling Capacitor Effects

Following the steps of the parametric study based on the MTB model, the DM and CM noise on the LISN side can be predicted accurately, as shown in Figure 5-3 and Figure 5-4. Since the MTB model is a terminal model, the voltage on the device terminal side can be calculated, as shown in Figure 5-5. Because there is no DC component in the terminal voltage prediction results, the result cannot be directly compared with the simulation result. However, the voltage overshoot of the device can still be calculated from the waveform in Figure 5-5 and is about 48 V. The simulation result in Figure 5-6 shows that the overshoot voltage is 51 V. The difference between the simulation and prediction result is about 3 V. In Figure 5-6, it also shows the voltage overshoot with and without the 100 nF decoupling capacitor. Without capacitor, the voltage overshoot is about 70 V higher. Both effects on the voltage stress and EMI noise can be predicted by the MTB model.

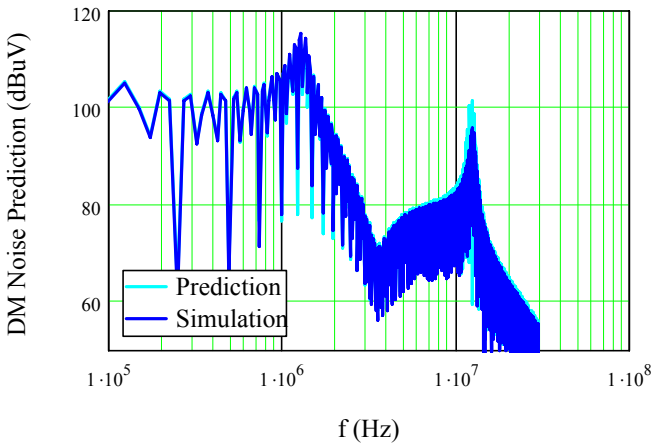

Figure 5-3 DM Noise Prediction Results and Simulation Results

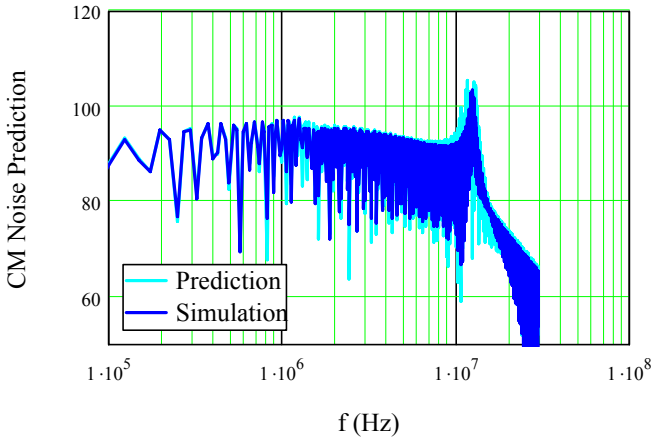

Figure 5-4 CM Noise Prediction Results and Simulation Results

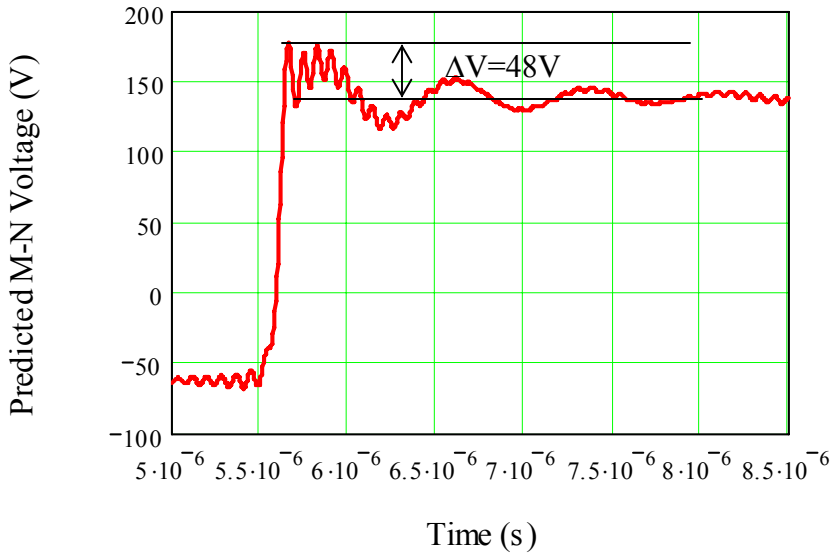

Figure 5-5 Predicted Terminal M-N Voltage

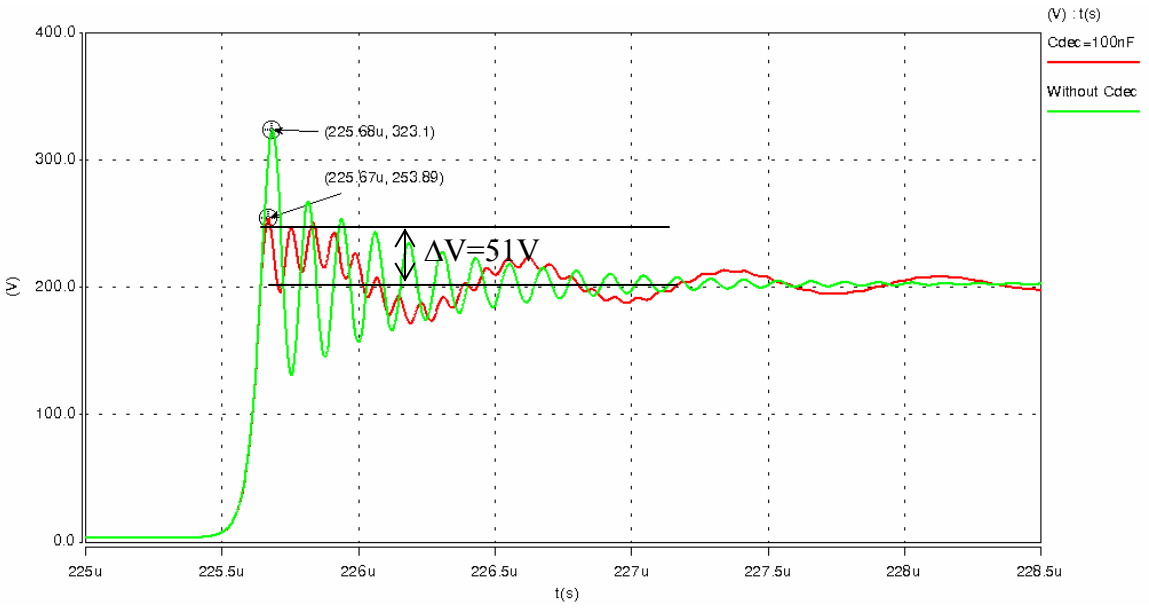

Figure 5-6 Voltage Stress Comparison between Without and 100 nF Decoupling Capacitor

When changing the decoupling capacitor C_{dec} from 0 nF to 20 nF, 50 nF, 100 nF, 500 nF to 1 uF, the voltage stress (voltage from mid-point (M) to negative bus (N)) is reduced from 323 V to 248 V, as shown in Figure 5-7. But there is not a big change (<5 V) when the capacitance is larger than 100 nF.

In the DM noise spectra, as shown in Figure 5-8, there is a high-frequency noise peak at 8.2 MHz and no low-frequency noise peak when there are no decoupling capacitors. When adding the decoupling capacitor, the high-frequency noise is reduced significantly and the noise peak moves toward a higher frequency (12.3 MHz), but there is another noise peak at a lower frequency. For the high-frequency DM noise peak, since the impedance of the DC-link capacitor and busbar parasitic inductance is larger than that of the decoupling capacitor, most DM noise current flows into the decoupling capacitors. As a result, the high-frequency noise is reduced by adding a decoupling capacitor. But adding a decoupling capacitor in the circuit could cause a new resonance between the decoupling capacitor and parasitic inductors of the busbar and the DC-link capacitor. When increasing the capacitance, the low-frequency noise peak is reduced and moves toward a lower frequency. Therefore, adding a decoupling capacitor to suppress voltage overshoot could cause higher EMI noise in the low-frequency range.

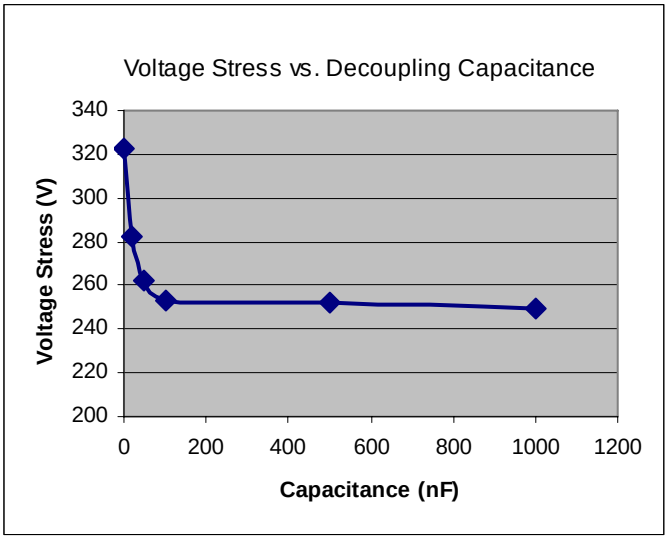

Figure 5-7 Voltage Stress vs. Decoupling Capacitance

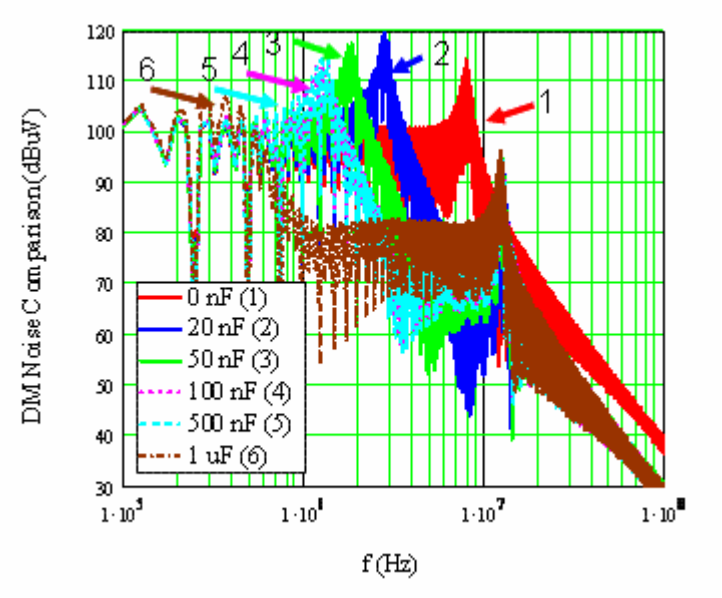

Figure 5-8 Different DM noise Comparison When Changing Decoupling Capacitance

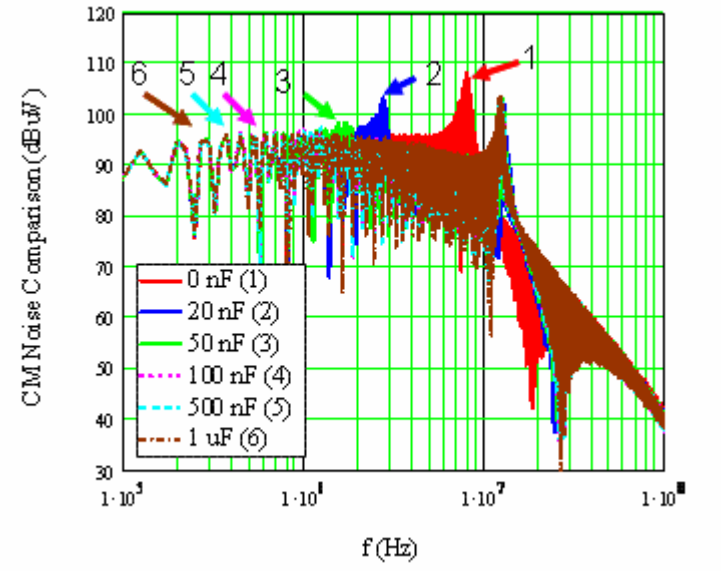

Figure 5-9 Different CM noises Comparison When Changing Decoupling Capacitor

For CM spectra, as shown in Figure 5-9, the CM noise, when there is no decoupling capacitor case has one noise peak, during which the frequency is the same as the DM noise. When adding a decoupling capacitor, the CM noise is also affected by the resonance between the device module and the propagation path. The high-frequency noise

is pushed to a higher frequency. The noise frequency is the same as the DM noise, which shows that the resonances existing in the DM noise path induce noise in the CM path. In the simulation circuit in Figure 5-2, a capacitor is placed between the device module middle point (M) and ground. Any voltage change on the terminal M could induce the current to the ground, which flows back to the LISNs. When the device switches, the resonances make the voltage at terminal M change. Therefore, the CM noise has the same frequency peaks as the DM noise, as analyzed in Chapter 3.

Since the decoupling capacitor is modeled in the propagation path matrix during the MTB modeling process, it is not easy to understand the interactions between the device module and the decoupling capacitor. Two simple models can be used to analyze the decoupling capacitor impact if the device parasitics, such as the lead inductance, are known. When choosing a large enough decoupling capacitance, the voltage on the capacitor V_{bus} stays constant, which can be illustrated as Figure 5-10. The overshoot voltage can be approximated by Eq. (5-1). The effect of a decoupling capacitor on the high frequency resonance can also be shown as the simplified model in Figure 5-10. The high-frequency noise is caused by the resonance between the device output capacitor, device parasitic inductor and the decoupling capacitor parasitic inductor. When taking inverse Laplace transformation of Eq. (5-1), the overshoot can be calculated by Eq. (5-2). The time of the maximum overshoot voltage occurs when the derivative of Eq. (5-2) is zero. From Eq. (5-2), the frequency of the noise peak and voltage overshoot is determined by the loop parasitic inductance and device output capacitance. But in practical design, the voltage on the decoupling capacitors can change within a certain range. The model shown in Figure 5-11 can calculate the voltage fluctuation on the decoupling capacitors. The voltage on the DC-link capacitor stays constant and the whole device is taken as a current source. The voltage on the decoupling capacitor ΔV_{bus} can be calculated by Eq. (5-3), which is similar to Eq. (5-2). The total voltage overshoot is determined by ΔV_{ds} and ΔV_{bus}. In practical design, choosing ω_0 to be 10 times higher than ω_1, the voltage overshoot caused by the resonance between the decoupling capacitors, and the parasitic inductance of the busbar and DC-link capacitance can be

neglected. In the simulation shown in Figure 5-2, the high-frequency noise peak is at 12.3 MHz, which is about 10 times higher than the low-frequency peak (1.35 MHz).

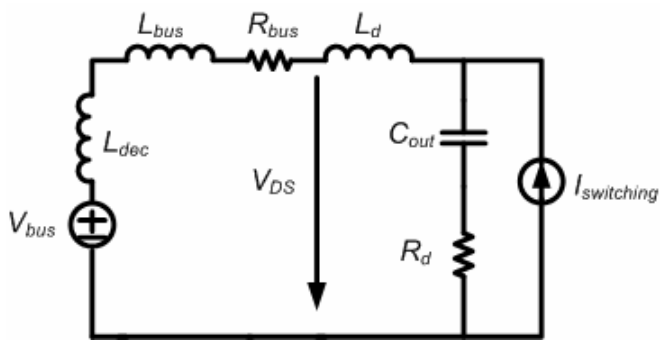

Figure 5-10 Model of Voltage Overshoot and High-frequency Resonance

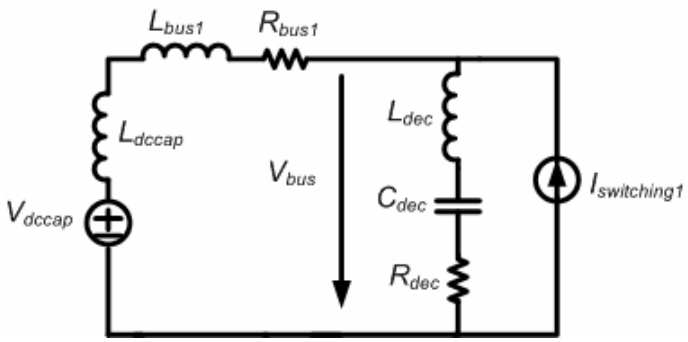

Figure 5-11 Model of Voltage Overshoot and Low-frequency Resonance

$$\Delta V_{ds}(s) = \frac{L_{bus} + L_{cap}}{L_{bus} + L_d + L_{cap}} \left[\frac{I_{switching}}{T_{off} \cdot C_{out}} \cdot \frac{1}{s(s^2 + \frac{R_d + R_{bus}}{L_{bus} + L_d + L_{cap}} \cdot s + \frac{1}{C_{out} \cdot (L_{bus} + L_d + L_{cap})}} \right] \cdot \left[1 - e^{-s \cdot T_{off}}\right] \quad \textbf{(5-1)}$$

Where: L_{bus} is the interconnection of the parasitic inductor between the decoupling capacitor and the device module.

R_{bus} is the parasitic resistance of the busbar and the decoupling capacitor parasitic resistance

L_{cap} is the parasitic inductance of the decoupling capacitor

C_{out} is the output capacitance of the device module

R_d is the parasitic resistance of the device module

L_d is the parasitic inductance of the device module, and

T_{off} is the turn-off time

$$\Delta V_{ds}(t) = \frac{I_{switching} \cdot (L_{bus} + L_{dec})}{T_{off}} \left[1 - \frac{1}{\sqrt{1-\zeta^2}} \cdot e^{-\zeta \omega_o t} \cdot \sin(\omega_o \sqrt{1-\zeta^2}\, t + \psi) \right] \quad \textbf{(5-2)}$$

where $\zeta = (\frac{R_{bus} + R_d}{2} \cdot \sqrt{\frac{C_{out}}{L_d}})$, $\omega_o = \sqrt{\frac{1}{(L_d + L_{bus} + L_{cap}) \cdot C_{out}}}$, $\psi = \arccos(\zeta)$

$$\Delta V_{bus}(t) = \frac{I_{switching} \cdot (L_{bus1} + L_{dccap})}{T_{off}} \left[1 - \frac{1}{\sqrt{1-\zeta_1^{\,2}}} \cdot e^{-\zeta_1 \omega_1 t} \cdot \sin(\omega_1 \sqrt{1-\zeta_1^{\,2}}\, t + \psi_1) \right] \quad \textbf{(5-3)}$$

where $\zeta_1 = (\frac{R_{bus1} + R_{dec}}{2} \cdot \sqrt{\frac{C_{dec}}{L_{dec}}})$, $\omega_1 = \sqrt{\frac{1}{(L_{dccap} + L_{bus1} + L_{dec}) \cdot C_{dec}}}$, $\psi = \arccos(\zeta)$

The overshoot voltage suppression could determine the minimum capacitance of the decoupling capacitor. But when considering the situation in terms of EMI noise, larger capacitance can result in less noise. In practical designs, low-ESL and high voltage-rating film capacitors are used as decoupling capacitors. It is not necessary to choose oversized capacitors to reduce EMI noise because doing so would unnecessarily increase size and cost. Nevertheless, an input EMI filter is required to attenuate low-frequency conducted EMI noise from 150 kHz up [14]. The EMI filter design is aimed at the low-frequency noise. After attenuating the low-frequency EMI noise to comply with EMI standards, the voltage transfer gain of the EMI filter will continue increasing in a certain range, which could bring higher attenuation at the decoupling capacitors' first resonant frequency. Therefore, there is no need to choose too large decoupling capacitance when the input EMI filter can be fully used. For example, in the simulation circuit, when choosing a 100

nF decoupling capacitor, the noise amplitude difference between the first peak at 1.35 MHz and the noise at 200 kHz is 9 dBuV (The noise at 150 kHz is lower than 200 kHz.). The requirement for the filter design is needed to provide 9 dB more attenuation at 1.35 MHz than 200 kHz. If a one-stage filter can be used to attenuate 200 kHz noise, it can have 40 dB more attenuation at 1.35 MHz, which is enough to attenuate the noise. As a result, the 100 nF decoupling capacitor can satisfy the suppression of overshoot voltage while not requiring a bigger EMI filter. Theoretically, from a filter design point of view, the attenuation can be higher and higher when frequency increases. But this is impossible in reality because of the parasitcs of the filter itself and core material property changes at high frequencies. Because of these changes, the filter can magnify the EMI noise instead of reducing the noise. Some research efforts have been carried out to eliminate the effect of filter parasitics [93]. Though adding a decoupling capacitor can reduce the high-frequency noise, it still causes another noise peak at the high frequency. Compared to the low-frequency noise peak, the high-frequency noise is more difficult to reduce with the input EMI filter. One way to reduce the high-frequency noise peak is to choose a low-ESL capacitor and use devices with lower lead inductance. In [93] a method to cancel the parasitic inductance in the capacitor was proposed, which provides good results for reducing the high-frequency noise peak.

Although analysis based on the two simple models above can help to understand the interactions between the decoupling capacitor and device modules, this understanding is difficult to apply to the converter design because the parasitics of devices are usually not available to users. However, the MTB model can be used to predict both the EMI noise and the voltage overshoot. This makes it easier for converter designers to select the optimal decoupling capacitors. Furthermore, selecting the decoupling capacitor demonstrates how to carry out a parametric study based on the MTB model. The whole process is similar to the EMI noise prediction of the converter. Since the parametric study based on the MTB model is accurate and fast, it is convenient for converter designers to use and optimize the propagation path design. Therefore, the EMI noise emission can be controlled and attenuated at the design stage, which can provide the lower bare noise for an input EMI filter design.

5.2. Converter-level EMI Model Based on MTB Equivalent Source Model

EMI management is required in order to comply with mandatory EMC standards. For this reason, EMI suppression components, such as EMI filters, are often necessary additions to power electronics products. In [35] [42] [49] and [69], the converter-level noise source impedance has been considered in EMI filter design. In fact, the source impedance is a design condition for the EMI filter design program [69]. The EMI filter performance depends not only on the filter itself but also on the noise source impedance of the converter and the noise load impedance at the noise collection site. The filter design guideline is mainly to maximize the impedance mismatch so that the noise energy delivered to the load is minimized. For industrial applications, the load impedance is the LISN. The state-of-the-art method to obtain the converter-level source impedance is based on the measurement of the existing converter. Once the converter is designed, the source impedance of the converter is determined; therefore the ability to maximize the impedance mismatch between the converter and the EMI filter is limited. The EMI filter design is still an afterthought of design instead of being involved in the converter functional design stage.

In terms of studying EMI interactions in a power conversion system, the converter-level EMI noise model is desirable. Since each converter is an EMI noise source unit in the power conversion system, without the converter-level model, the interaction is very difficult to characterize. As the EMI noise source model evaluation in Chapter 3 illustrates, other behavioral models cannot be extended to the power conversion system because of poor accuracy and the fact that the physics-based model is not practical for converter designers to use. So far, EMI research for the entire power conversion system has not been systematically studied.

Based on the MTB modeling approach, the terminal characteristics of the entire converter at the power input side can be as shown in Figure 5-12. P_o, N_o and G are the EMI noise output terminals, which connect other converters or LISNs when measuring EMI noise to comply with standards. The process of obtaining the equivalent converter-

level EMI noise source includes two steps: 1) Obtain the propagation path impedance network, and 2) Obtain the MTB noise source model of the converter. Because the MTB has modular, terminal characteristics, the MTB equivalent noise source model can be obtained by knowing the switching pattern, which has been demonstrated in a FB converter in Chapter 4. The MTB equivalent source model includes the source impedance network and the source current network. To derive the equivalent converter-level EMI noise source, one must calculate the short-circuit currents or open-circuit voltages and impedances at terminals P_o and N_o. Therefore, the converter-level EMI noise source model can be shown as Figure 5-13.

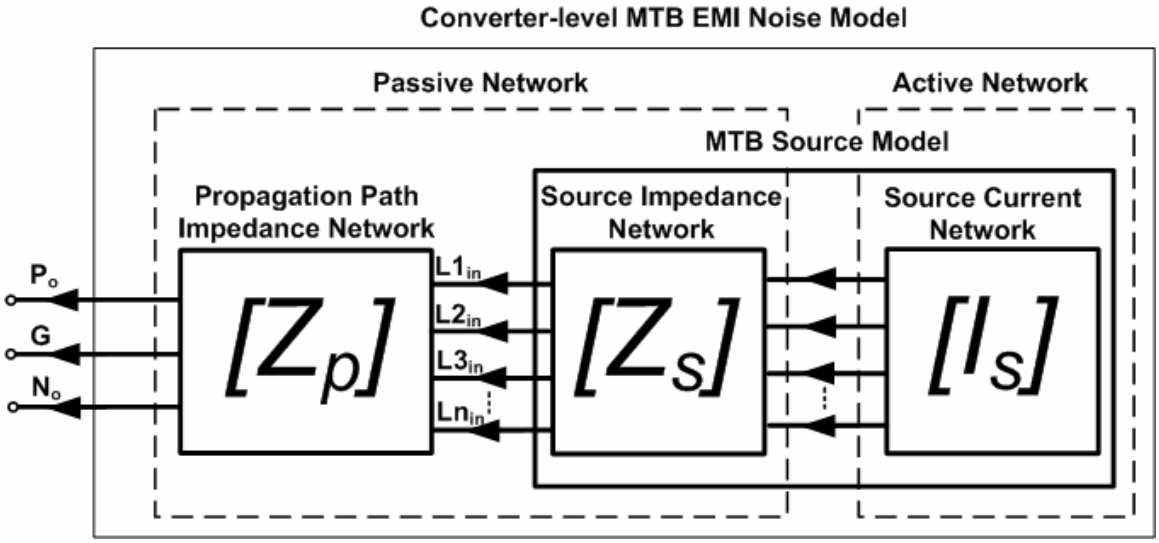

Figure 5-12 Illustration of Converter-level MTB EMI Noise Modeling Approach

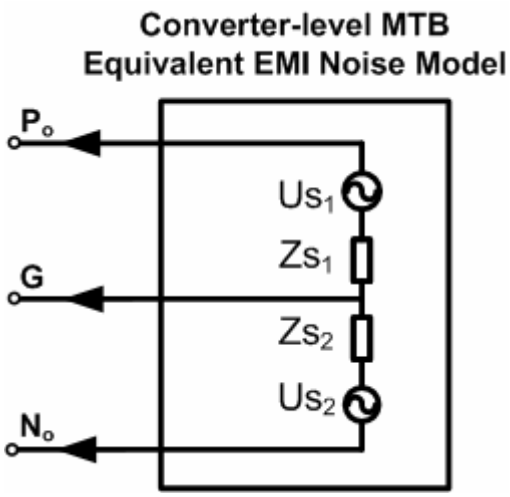

Figure 5-13 Equivalent Converter-level EMI Noise Source Model

From the definition of the equivalent source impedance, Zs_1 and Zs_2 are the driving impedances from terminals P_o and N_o respectively. They can be derived from the propagation path network and MTB noise source impedance network, which make up the entire passive network of the converter. The process of calculating the open-circuit voltage at terminals P_o and N_o is actually the same process as predicting the EMI noise for the converter. The difference is that LISNs are not placed at the terminals to collect the EMI noise. Therefore, the MTB noise source model together with the propagation path model can derive the converter-level equivalent noise source model.

As presented in Chapter 3, the MTB noise source modeling process does not separate CM and DM noise because of the coupling effect. The converter-level equivalent EMI noise model in Figure 5-13 follows the same modeling method and does not model CM and DM separately. As a result, the source model includes both CM and DM noise generated from the converter. In the existing literature, all the converter-level EMI noise source and source impedance separate CM and DM noise. For example, in [41], the method of obtaining the equivalent EMI source impedance is to short the devices' terminals and measure the impedance between the ground and the bus. It is obvious that the EMI noise impacts of devices' parasitics are neglected. This simplification causes an error in characterizing the converter EMI source model.

However, when designing an EMI filter for attenuating the low-frequency EMI noise, the CM and DM noise source and source impedance are useful. The converter-level EMI noise model based on the MTB modeling approach can have its DM and CM form, as shown in Figure 5-14. The derived CM and DM source model can be used as the EMI filter design program as shown in Figure 4-39. In addition, the converter CM and DM noise can be predicted as the bare noise for the filter design. The converter-level EMI noise source model based on the MTB modeling approach can be used for designing the EMI filter at the design stage and for the filter optimization with consideration of the entire converter.

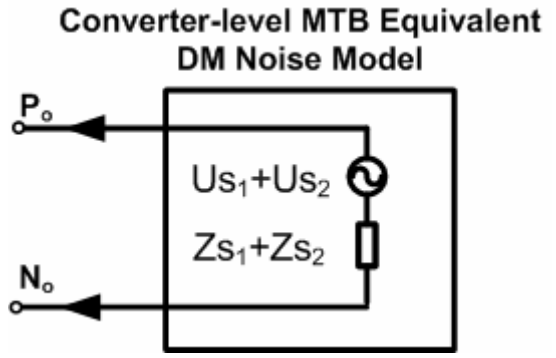

(a) Converter-level Equivalent CM Noise Model

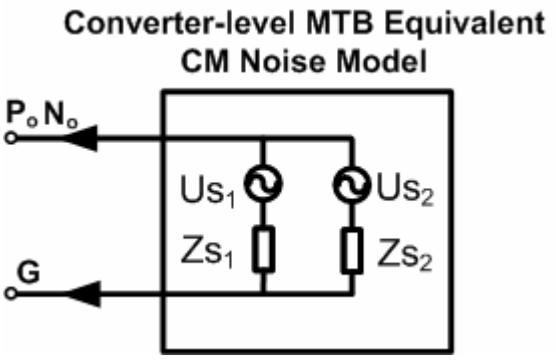

(b) Converter-level Equivalent DM Noise Model

Figure 5-14 Converter-level Equivalent CM and DM EMI Noise Model

Furthermore, in the power conversion system, the EMI noise mitigation scheme has not yet been studied, because the EMI interactions in the system are unknown. The state-of-the-art scheme is to manage EMI noise in converters individually, which is a non-

optimal approach. However, the converter-level MTB equivalent EMI noise model provides the capability of studying the interactions between different converters in the power conversion system because each converter can have the equivalent EMI noise source and source impedance determined, as shown in Figure 5-13.

5.3. Summary

In this chapter, the MTB source model is used to analyze the EMI noise interactions and management in a converter. The selection of the decoupling capacitor for a VSC converter demonstrates how to apply the MTB source model in a parametric study. The MTB modeling approach can predict both the EMI effect of the decoupling capacitor and the voltage stress of the device. Simple circuit models are used to further analyze the functions of the decoupling capacitor.

The MTB source model can also be used to derive the converter-level EMI source model, which is desirable for the input EMI filter design and EMI noise mitigation design in the power conversion system. The applications of the converter-level EMI model are discussed and the procedure for deriving the converter-level EMI noise source model based on the MTB source model is presented.

In summary, the MTB EMI noise source model can be used for parametric study and for deriving a higher-level EMI noise source model.

Chapter 6 Conclusions and Future Work

This chapter summarizes the entire dissertation and discusses some ideas for future work.

6.1. Conclusions

This work has studied the EMI noise source modeling issues for power switching converters. The major accomplishments and conclusions are summarized below.

- This work has proposed a modular, terminal, behavioral EMI noise source modeling approach. Each device module is modeled as pairs of equivalent noise current sources and source impedances. Although the importance of the parasitic impedances inside of device modules has been studied before by others for EMI noise generation, the source impedance concept is systematically developed in this work for the first time. The modeling methodology has both the feasibility of a behavioral model and good accuracy for predicting conducted EMI noise. Although the proposed MTB modeling approach applies the linear circuit theory to a semiconductor device, which has nonlinearity during switching transients, the analysis and experiments show that the nonlinearity does not affect the modeling methodology significantly. The conditions of using the MTB model are to keep the device's operating conditions constant and avoid the device terminal voltage resonating back to the dramatically nonlinear region.
- One of the most important features of the MTB model is that it does not separate CM and DM noise sources in the model, therefore automatically account for their interactions. In fact, the interaction of the CM and DM noise usually exists in all power converters. The inseparable high-frequency CM and DM noise characteristics contributed by the source impedance and

propagation path are analyzed. The MTB model can predict CM and DM noise simultaneously in the entire conducted EMI range.

- The modular and terminal characteristics of the MTB noise source model are verified in more complicated cases. A full-bridge converter with two device modules is used as the testbed. It clearly shows the applicability of the MTB source model in phase-leg-based converters. Although the MTB model is derived under a certain operating condition, the model can be combined with models derived under different conditions to predict the EMI noise for the converter with variable switching conditions, such as a VSI. Both applications are verified by experiment. Other possible applications of the MTB model are discussed. The conclusion is that the MTB model can be applied to any case that has the same switching condition as that of the MTB source model derivation.
- One research task of EMI study is to control and attenuate EMI noise. The EMI effect of a DC-link decoupling capacitor for a device's safe operation is analyzed based on the MTB model. Both the EMI noise and voltage overshoot are predicted. The analysis demonstrates the process of applying the MTB model to do parametric study. A completed converter-level EMI model can be derived based on the noise source model and propagation path model. This provides the possibility to study the EMI noise interactions between converters in a power conversion system.
- A comprehensive evaluation of different EMI noise source modeling approaches according to the criteria of accuracy, feasibility and generality has been presented. The comparison results show that the MTB modeling approach is more accurate, feasible and general than other state-of-the art modeling approaches.

6.2. Future Work

This work has developed a modular approach for studying EMI noise emission in power converters, which provides a basis for systematically studying EMI noise emission in power conversion system. Further studies can be carried out in the following directions.

- The proposed MTB EMI noise source model of each phase-leg module includes three terminals, which are the same as the electrical connectors of the module. However, there is another important terminal that significantly affects EMI noise, and which serves as the ground of each module. Normally, the device's direct-bond-copper (DBC) is treated as the module ground. The more general MTB source model should also include the earth terminal in the model, which could be as the structure shown in Figure 6-1. In this dissertation, the impedances between electrical terminals and ground have been considered during the EMI noise prediction by knowing the geometry structure and measuring them. In the future, one of the possible areas of study is to explore the more general four-terminal MTB equivalent source modeling approach to obtain these impedances.

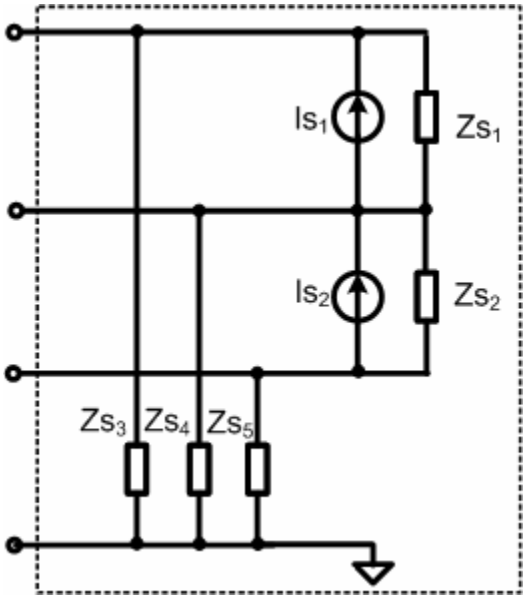

Figure 6-1 General MTB Equivalent EMI Noise Source Model

- The implementation of the proposed MTB source model in the converter design program can be studied. By doing so, the design and optimization of the converter can consider the converter functions, EMI and thermal aspects together at the design stage.
- The MTB model has its physics basis. The source impedances actually are the composition of the impedances inside the device module. In the future, the impact of device packaging technologies on EMI noise can be studied based on the MTB model. The possible measures can be used to contain EMI noise in the module. From comparing different MTB models of the same devices with different packaging, the insight of the EMI effects can be clear at the device design and manufacturing stage.
- As demonstrated and discussed in the dissertation, the MTB model can be used in converters with the same commutation characteristics. The applicability to different topologies, such as multi-level converters and CSI, need to be further analyzed.
- Since the MTB approach can be used in deriving the converter-level EMI noise source model, the EMI noise interaction and management in a power conversion system based on the MTB model can be researched further.

References

[1] C. Paul, “Introduction to Electromagnetic compatibility,” Wiley, 1992

[2] T. Williams, “EMC for Product Designers,” Newnes, 2001

[3] IEC61000: Electromagnetic compatibility, 2000.

[4] CISPR11: Industrial, scientific and medical (ISM) radio-frequency equipment - Electromagnetic disturbance characteristics - Limits and methods of measurement, International Special Committee on Radio Interference, 2004

[5] Federal Communications Commision (FCC) Part 18: Industrial, scientific, and medical equipment, 10-1-01 Edition

[6] MIL-STD-462D, Military Standard: Measurements on Electromagnetic interference characteristics, Department of Defense, USA, 1993

[7] F. Wang, S. Rosado, D. Boroyevich, “Open modular power electronics building blocks for utility power system controller applications,” In IEEE Proc. PESC’03, 2003, vol. 4, pp. 1792 – 1797

[8] T. Ericsen, N. Hingorani, Y. Khersonsky, “Power electronics and future marine electrical systems,” Petroleum and Chemical Industry Technical Conference, 2004, pp.163 – 171

[9] T. Ericsen, “Power Electronic Building Blocks-a systematic approach to power electronics,” IEEE Power Engineering Society Summer Meeting, 2000, vol. 2, pp. 1216 – 1218

[10] S. Wang, F.C. Lee and W.G. Odendaal, “Improving the performance of boost PFC EMI filters,” In IEEE Proc. APEC’03, 2003, vol. 1, pp. 368 - 374

[11] T. Farkas and M. F. Schlecht, “Viability of active EMI filters for utility applications,” IEEE Trans. on Power Electronics, vol. 9, pp. 328–337, 1994

[12] S. Ogasawara, H. Ayano and H. Akagi, "An active circuit for cancellation of common-mode voltage generated by a PWM inverter," IEEE Trans. on Power Electronics, vol. 13, Issue 5, pp. 835–841, 1998

[13] M. J. Nave, "Power line filter design for switched-mode power supplies," Van Nostrand Reinhold, 1991

[14] F. Shih, D.Y. Chen, Y. Wu, Y. Chen, "A Procedure for designing EMI filter for AC line applications," In IEEE Trans. on Power Electronics, vol. 11, Issue 1, pp.170 - 181, 1996

[15] R. Chen, "Integrated EMI Filters for Switch Mode Power Supplies," Ph. D Dissertation, 2004, Virginia Tech

[16] G. L. Skibinski, R. J. Kerkman and D. Schlegel, "EMI emissions of modern PWM AC drives," In IEEE Industry Applications Magazine, vol. 5, Issue: 6, pp. 47 - 80, 1999

[17] L. Yang; B. Lu; W. Dong; Z. Lu; M. Xu; F.C. Lee, W.G. Odendaal, "Modeling and characterization of a 1 KW CCM PFC converter for conducted EMI prediction," In IEEE Proc. APEC'04, 2004, vol. 2, pp. 763 – 769

[18] M. J. Nave, "The effect of duty cycle on SMPS common mode emissions: theory and experiment," In IEEE Proc. APEC'89, 1989, pp. 3 – 12

[19] B. Archambeault, A. E. Ruehli, "Analysis of power ground plane EMI decoupling performance using the partial element equivalent circuit technique," In IEEE Trans. on Electromagnetic Compatibility, vol. 43, Issue 4, pp.437 – 445, Nov. 2001

[20] J.-M Guichon, E. Atienza, E. Clavel, J. Roudet, V. Mazauric, "Automatic design of busbars considering electrical criteria," In IEEE Proc. Transmission and Distribution, 2001, vol. 2, pp.653 – 658

[21] M. T. Zhang, R. Watson, F. C. Lee, J. Roudet, J. L. Schanen, E. Clavel, "Characterization and analysis of electromagnetic interference in a high frequency AC distributed power system," In IEEE Proc. PESC'96, 1996, vol. 2 , pp.1956 – 1960

[22] G. L. Skibinski, D.M. Divan, "Design methodology and modeling of low inductance planar bus structure," In European Conference on Proc. Power Electronics and Applications, 1993, vol. 3, pp.98 – 105

[23] W. Zhang, M. T. Zhang, F. C. Lee, J. Roudet, E. Clavel, "Conducted EMI analysis of a boost PFC circuit," In IEEE Proc. APEC'97, 1997, vol. 1, pp. 223 – 229

[24] X. Huang, J.-S Lai, E. Pepa, "Analytical evaluation of modulation effect on three-phase inverter differential mode noise prediction," In IEEE Proc. APEC'04, 2004, vol. 2, pp.681 – 687

[25] D. Zhang; D. Y. Chen, D. Sable, "A new method to characterize EMI filters," in Proc. IEEE APEC'98, vol. 2, pp.929 – 933

[26] H. Zhu, A. R. Hefner, J. S. Lai, "Characterization of power electronics system interconnect parasitics using time domain reflectometry," IEEE Trans. on Power Electronics, vol. 14, Issue 4, pp. 622 – 628, July 1999

[27] L. Ran; S. Gokani, J. Clare, K. J. Bradley, C. Christopoulos, "Conducted Electromagnetic Emissions in Induction Motor Drive Systems Part I Time Domain Analysis and Identification of Dominant Modes," IEEE Trans. on Power Electronics, vol. 13, Issue: 6, pp. 757-766, 1998

[28] J. C. Crebier, M. Brunello, J. P. Ferrieux, "A new method for EMI study in boost derived PFC rectifiers," In IEEE Proc. PESC'99, 1999, vol. 2, pp. 855 - 860

[29] E. Zhong, T. A. Lipo, "Improvement in EMC performance of inverter-fed motor drives," IEEE Transactions on Industry Applications, vol. 31, Issue: 6, pp.1247 – 1256, Nov.-Dec. 1995

[30] S. Brehaut, J. C. Le Bunetel, D. Magnon, A.Puzo, "A conducted EMI model for an industrial power supply full bridge," In IEEE Proc. PESC'04, 2004, vol. 2, pp. 3227 - 3231

[31] S. Wang, F. C. Lee, W. G. Odendaal, "Using scattering parameters to characterize EMI filters," In IEEE Proc. PESC'04. 2004, vol. 1, pp. 297 – 303

[32] Q. Liu, W. Shen, F. Wang, D. Boroyevich, V. Stefanovic and M. Arpilliere, "Experimental evaluation of IGBTs for characterizing and modeling conducted EMI emission in PWM inverters," in Proc. IEEE PESC'03, 2003, vol. 4, pp. 1951 – 1956

[33] J. He, J. Jiang, J. Huang, W.Chen, "Model of EMI coupling paths for an off-line power converter," In IEEE Proc. APEC'04, 2004, vol. 2, pp. 708 - 713

[34] C. Serporta, G. Tine, G. Vitale, M. C. Di Piazza, "Conducted EMI in power converters feeding AC motors experimental investigation and modeling," In IEEE Proc, ISIE'00, 2000, vol. 2, pp.359 - 364

[35] S. Gokani, J.C. Clare, K. J. Bradley, C. Christopoulos, L. Ran, "EMC measurements and simulation in variable speed drives," Power Electronics and Variable Speed Drives, 1996, pp. 558 – 563

[36] H.-K. Yun, Y.-C. Kim, C.-Y. Won, Y.-R. Kim, Y.-S. Kim, S.-W. Choi, "A study on inverter and motor winding for conducted EMI prediction," In IEEE Proc, ISIE'01, 2001, vol. 2, pp.752 – 758

[37] E. Zhong, T. A. Lipo, J. R. Jaeschke, D. Gritter, "Analytical estimation and reduction of conducted EMI emissions in high power PWM inverter drives," In IEEE Proc. PESC'96, 1996, vol. 2, pp.1169 – 1175

[38] P. F. Okyere, L. Heinemann, "Computer-aided analysis and reduction of conducted EMI in switched-mode power converter," In IEEE Proc. APEC'98, 1998, vol. 2, pp. 924 – 928

[39] L. Ran, S. Gokani, J. Clare, K. J. Bradley, C. Christopoulos, "Conducted Electromagnetic Emissions in Induction Motor Drive Systems part II: Frequency Domain Models," IEEE Trans. on Power Electronics, vol. 13, Issue 6, pp. 768 – 776, 1998

[40] A. Consoli, C. Oriti, A. Testa, A. L. Julian, "Induction motor modeling for common mode and differential mode emission evaluation," In IEEE Proc. IAS'96 1996, vol. 1, pp.595 – 599

[41] L. Ran, J. C. Clare, K. J. Bradley, C. Christopoulos, "Measurement of conducted electromagnetic emissions in PWM motor drive systems without the need for an LISN," IEEE Trans. on Electromagnetic Compatibility, vol. 41, Issue 1, pp. 50 – 55, Feb. 1999

[42] D. Zhang, D. Y. Chen, M. J. Nave, D. Sable, "Measurement of noise source impedance of off-line converters," IEEE Trans. on Power Electronics, vol. 15, Issue 5, pp. 820 – 825, Sept. 2000

[43] C. Chen, X. Xu, "Modeling the conducted EMI emission of an electric vehicle (EV) traction drive," In IEEE Proc. Electromagnetic Compatibility, 1998, vol. 2, pp. 796 - 801

[44] H. Zhu, J. S. Lai; A. R. Hefner, Y. Tang, C. Chen, "Modeling-based examination of conducted EMI emissions from hard and soft-switching PWM inverters," IEEE Trans. on Industry Applications, vol. 37 , Issue 5, pp.1383 – 1393, Oct. 2001

[45] C. Chen, "Novel EMC debugging methodologies for high-power converters," In IEEE Proc. Electromagnetic Compatibility, 2000, vol. 1, pp. 385 – 390

[46] P. R. Mugur, J. Roudet, J. C. Crebier, "Power electronic converter EMC analysis through state variable approach techniques," IEEE Trans. On Electromagnetic Compatibility, vol. 43, Issue 2, pp. 229 - 238, May 2001

[47] D. Gonzalez, J. Gago, J. Balcells, "New simplified method for the simulation of conducted EMI generated by switched power converters," IEEE Trans. on Industrial Electronics, vol. 50, Issue 6, pp. 1078 – 1084, 2003

[48] J. C. Crebier, J. P. Ferrieux, "PFC full bridge rectifiers EMI modeling and analysis-common mode disturbance reduction," IEEE Trans. on Power Electronics, vol.19, Issue 2, pp. 378 – 387, March 2004

[49] J. Meng, W. Ma, L. Zhang Lei, "Determination of noise source and impedance for conducted EMI prediction of power converters by lumped circuit models," In IEEE Proc. PESC'04, 2004, vol. 4, pp. 4028 - 4033

[50] S. Brehaut, M. O. El Bechir, J. C. Le Bunetel, D. Magnon, A. Puzo, "Analysis EMI of a PFC on the band pass 150 kHz-30 MHz for a reduction of the electromagnetic pollution," In IEEE Proc. APEC'04, 2004, vol. 2, pp. 695 - 700

[51] C. Chen, "Characterization of power electronics EMI emission," In IEEE Proc. Electromagnetic Compatibility, 2003, vol. 2, pp. 553 - 557

[52] G. Grandi, D. Casadei, U. Reggiani, "Analysis of common- and Differential-Mode HF Current Components in PWM Inverter-Fed AC Motors," In IEEE Proc. PESC'98, 1998, vol. 2, pp. 1146 - 1151

[53] B. Revol, J. Roudet, J. L. Schanen, P. Loizelet, "Fast EMI prediction method for three-phase inverter based on Laplace transforms," In IEEE Proc. PESC'03, 2003, vol. 3, pp. 1133 – 1138

[54] J. S. Lai, X. Huang, S. Chen, T. W. Nehl, "EMI characterization and simulation with parasitic models for a low-voltage high-current AC motor drive," In IEEE Proc. IAS'02, 2002, vol. 4, pp. 2548 - 2554

[55] X. Huang, E. Pepa, J. S. Lai, S. Chen, T. W. "Three-phase inverter differential mode EMI modeling and prediction in frequency domain," In IEEE Proc. IAS'03, 2003, vol. 3, pp.2048 – 2055

[56] J. S. Lai, X. Huang, E. Pepa, S. Chen, T. W. Nehl, "Inverter EMI modeling and simulation methodologies," In IEEE Proc. IECON '03, 2003, vol. 2, pp.1533 – 1539

[57] X. Pei, K. Zhang, Y. Kang, J. Chen, "Prediction of common mode conducted EMI in single phase PWM inverter," In IEEE Proc. PESC'04, 2004, vol. 4, pp. 4060 – 4065

[58] S. Chen, T. W. Nehl, J. S. Lai, X. Huang, E. Pepa, R. De Doncker, I. Voss, "Towards EMI prediction of a PM motor drive for automotive applications," IN IEEE Proc. APEC'03, 2003, vol.1, pp. 14 – 22

[59] W. Dong, "Analysis and evaluation of soft-switching inverter techniques in electric vehicle applications," Ph. D Dissertation, 2003, Virginia Tech

[60] A. Santolaria, J. Balcells, D. Gonzalez, J. Gago, "Evaluation of switching frequency modulation in EMI emissions reduction applied to power converters," In IEEE Proc. IECON'03, 2003, vol. 3, pp. 2306 – 2311

[61] A. Santolaria, J. Balcells, D. Gonzalez, "Theoretical and experimental results of power converter frequency modulation," In IEEE Proc. IECON'02, 2002, vol. 1, pp. 193 – 197

[62] A. Santolaria, J. Balcells, D. Gonzalez, J. Gago, S. D. Gil, "EMI reduction in switched power converters by means of spread spectrum modulation techniques," In IEEE Proc. PESC'04, vol. 1, pp. 292 – 296

[63] M. Rahkala, T. Suntio, K. Kalliomaki, "Effects of switching frequency modulation on EMI performance of a converter using spread spectrum approach," In IEEE Proc. APEC'02, 2002, vol.1, pp. 93 – 99

[64] F. Klotz, J. Petzoldt, H. Volker, "Experimental and simulative investigations of conducted EMI performance of IGBTs for 5-10 kVA converters," In IEEE Proc. PESC'96, 1996, vol. 2, pp. 1986 – 1991

[65] A.R. Jr. Hefner, "Analytical modeling of device-circuit interactions for the power insulated gate bipolar transistor (IGBT),", IEEE Trans. on Industry Applications, vol. 26, Issue 6, pp. 995 – 1005, Nov.-Dec. 1990

[66] A.R. Jr. Hefner, "An improved understanding for the transient operation of the power insulated gate bipolar transistor (IGBT)," IEEE Trans. on Power Electronics, vol. 5, Issue 4, pp. 459 – 468, Oct. 1990

[67] D. Zhang, D. Chen; D. Sable, "Non-intrinsic differential mode noise caused by ground current in an off-line power supply," In IEEE Proc. PESC'98, 1998, vol. 2, pp.1131 – 1133

[68] S. Qu, D. Y. Chen, "Mixed-mode EMI noise and its implications to filter design in offline switching power supplies," In IEEE Proc. APEC,'00, 2000, vol. 2, pp. 707 - 713

[69] W. Shen, F. Wang, D. Boroyevich, V. Stefanovic, M. Arpilliere, "Optimizing EMI filter design for motor drives considering filter component high-frequency

characteristics and noise source impedance," In IEEE Proc. APEC'04, 2004, vol. 2, pp. 669 – 674

[70] G. Chen, M. Rentzch, F. Wang, D. Boroyevich, S. Ragon, V. Stefanovic, M. Arpilliere, "Analysis and design optimization of front-end passive components for voltage source inverters," In IEEE Proc. APEC'03, 2003, vol. 2, pp. 1170 - 1176

[71] S. Busquets-Monge, G. Soremekun, E. Hertz, C. Crebier, S. Ragon, J. Zhang, D. Boroyevich, Z. Gurdal, D. K. Lindner, M. Arpilliere, "Design optimization of a boost power factor correction converter using genetic algorithms," In IEEE Proc. APEC'02, 2002, vol. 2, pp. 1177 - 1182

[72] J. D. van Wyk, F. C. Lee, D. Boroyevich, "Power electronics technology: present trends and future developments," In IEEE Proceeding. Vol. 89, Issue 6, pp. 799 - 802, June 2001

[73] F. C. Lee, J. D. van Wyk, D. Boroyevich, G. Q. Lu, Z. Liang, P. Barbosa, "Technology trends toward a system-in-a-module in power electronics," IEEE Circuits and Systems Magazine, vol. 2, Issue 4, pp. 4 – 22, 2002

[74] B. K. Bose, "Energy, environment, and advances in power electronics," Power IEEE Trans. on Electronics, vol. 15, Issue 4, pp. 688 - 701, July 2000

[75] G. Skibinski, J. Pankau, R. Sladky, J. Campbell, "Generation, control and regulation of EMI from AC drives," In IEEE Proc. IAS'97, 1997, pp. 1571-1583

[76] G. Skibinski, B. Wood, J. Nichols, L. Barrios, "Effect of adjustable-speed drives on the operation of low-voltage ground-fault indicators," IEEE Trans. on Industry Applications, 2001, vol. 37, Issue 5, pp. 1423 - 1437

[77] R. J. Kerkman, "Twenty years of PWM ac drives: When secondary issues become primary concerns," In IEEE Proc. IECON'96, 1996, pp. 1vii-1xiii

[78] M. H. Nagrial, A. Hellany, "Conducted emission improvement of AC variable speed drives," In IEEE Proc. Electromagnetic Compatibility'97, 1997, pp. 41 – 46

[79] A. Consoli, S. Musumeci, G. Oriti, A. Testa, "An innovative EMI reduction design technique in power converters," IEEE Trans. on Electromagnetic Compatibility, vol. 38, Issue: 4, pp. 567 – 575, 1996

[80] S. E. Cho, F. Kang, C. Kim, "Optimal design and minimization of conducted EMI noise in elevator inverter system by customized IPM," IEEE Prod. on IECON '03., 2003, vol. 3, pp. 2320 - 2325

[81] S. Takizawa, S. Igarashi, K. Kuroki, "A new didt control gate drive circuit for IGBTs to reduce EMI noise and switching losses," IEEE Proc. On PESC'98, 1998, vol. 2, pp. 1443 - 1449

[82] S. Musumeci, A. Raciti, A. Testa, A. Galluzzo, M. Melito, "Switching-behavior improvement of insulated gate-controlled devices," IEEE Trans. on Power Electronics, vol. 12, Issue 4, pp. 645 – 653, 1997

[83] J. Meng, W. Ma, L. Zhang, "Determination of noise source and impedance for conducted EMI prediction of power converters by lumped circuit models," In IEEE Proc. PESC'04, 2004, vol. 4, pp. 4028 – 4033

[84] A. K. Jonscher, "Principles of semiconductor device operation," John Wiley & Sons, 1960

[85] J. S. Yuan, J. J. Liou, "Semiconductor device physics and simulation," Plenum Press, 1998

[86] 30ETH06S datasheet, International Rectifier Inc.

[87] CM150DY-24H datasheet, Powerex Inc.

[88] Agilent Spectrum Analysis Basics, Application Note 150, Agilent Technologies

[89] A. V. Oppenheim, R. W. Schafer, "Discrete-time Signal Processing," Prentice Hall Inc., 1989

[90] M. I. Montrose, E. M. Nakauchi, "Testing for EMC compliance," John Wiley & Sons, 2004

[91] TDS7000 Series Digital Phosphor Oscilloscopes User Manual, Tektronix, www.tektronix.com

[92] F. F. Franklin, J. D. Powell, M. Workman, "Digital control of dynamic systems," Third Edition, Addison Wesley Longman, 1998

[93] S. Wang, "Characterization and Cancellation of High-Frequency Parasitics for EMI filters and Noise Separators in Power Electronics Applications," Ph. D Dissertation, Virginia Tech, 2005

[94] A. M. Trzynadlowski, M. Zigliotto, S. Bolognani, M. M. Bech, "Reduction of the electromagnetic interference conducted to mains in inverter-fed AC drives using random pulse width modulation," In IEEE Proc. on IAS'98, 1998, vol. 1, pp. 739 - 744 vol.1

[95] L. M. Tolbert, F. Z. Peng, T. G. Habetler, "Multilevel inverters for electric vehicle applications," In IEEE Proc. on Power Electronics in Transportation, 1998, pp. 79 – 84.

[96] D. G. Holmes, T. A. Lipo, "Pulse width modulation for power converters," John Wiley & Sons, 2003

[97] H. Zhang; A. Von Jouanne, S. Dai; A. K. Wallace, F. Wang; "Multilevel inverter modulation schemes to eliminate common-mode voltages," In IEEE Trans. on Industry Applications, 2000, vol. 36, Issue: 6, pp. 1645 – 1653

[98] A. Nagel, R. W. De Doncker, "Systematic design of EMI filter for power converters," In IEEE Proc. on IAS'00, 2000, vol. 4, pp. 2523 - 2525

[99] E. R. Magnus, J. C. M. de Lima, V. M. Canalli, PJ. A. omilio, F. S. Dos Reis, "Tool for conducted EMI and filter design," In IEEE Proc. on IECON '03, 2003, vol. 3, pp. 2326 - 2331

[100] M. C. Caponet, F. Profumo, A. Tenconi, "EMI filters design for power electronics," In IEEE Proc. on PESC'02, 2002, vol. 4, pp. 2027 - 2032

[101] Sergio Busquets-Monge, "Application of Optimization techniques to the design of a boost power factor correction converter," Master Thesis, Virginia Tech, 2001

[102] Erik Hertz, "Thermal and EMI modeling and analysis of a boost PFC circuit designed using a genetic-based optimization algorithm," Master Thesis, Virginia Tech, 2001

[103] C. R. Paul, "Effectiveness of multiple decoupling capacitors," In IEEE Trans. on Electromagnetic Compatibility, vol. 34, Issue 2, 1992, pp. 130 – 133

[104] W. Teulings, J. L. Schanen, J. Roudet, "MOSFET switching behaviour under influence of PCB stray inductance," In IEEE Proc. on IAS'96, 1996, vol. 3, pp. 1449 – 1453

[105] H. J. Beukes, J. H. R. Enslin, R. Spee, "Busbar design considerations for high power IGBT converters," In IEEE Proc. on PESC'97, 1997, vol. 2, pp. 847 - 853

[106] Z. Chen, "Integrated electrical and thermal modeling, analysis and design for IPEM," Ph. D Dissertation, Virginia Tech, 2004

[107] V. Vorperian, "Simplified analysis of PWM converters using model of PWM switch Part I: Continuous conduction mode," In IEEE Transactions on Aerospace and Electronic Systems, Vol. 26, Issue 3, pp. 490 – 496, 1990

[108] V. Vorperian, "Simplified analysis of PWM converters using model of PWM switch Part II. Discontinuous conduction mode," In IEEE Transactions on Aerospace and Electronic Systems, Vol. 26, Issue 3, pp. 497 – 505, 1990

[109] D. Boroyevich, R. P. Burgos, "PEBB-oriented generalized representation of switching power converters," In IEEE Proc. on Power Engineering Society General Meeting, 2003, vol. 3, pp. 1344 – 1349

[110] B Bardakjian, M. Sablatash,"Spectral analysis of periodically time-varying linear networks,", IEEE Trans. on Circuits and Systems, vol. 19 , Issue: 3, pp. 297 – 299, 1972

Appendix

This program is to derive MTB equivalent EMI noise source model in simulation

LISN Characteristics:

$$j := 1..2000$$

$$C_{lisn1} := 0.1 \cdot 10^{-6}$$

$$C_{lisn2} := 10 \cdot 10^{-6}$$

$$L_{lisn} := 50 \cdot 10^{-6}$$

$$R_1 := 50$$

$$R_2 := 5$$

$$Part1(s) := R_1 + \frac{1}{s \cdot C_{lisn1}}$$

$$Part2(s) := R_2 + \frac{1}{s \cdot C_{lisn2}} + s \cdot L_{lisn}$$

$$Z\_part1_j := Part1(j \cdot 250002 \cdot \pi \cdot i)$$

$$Z\_part2_j := Part2(j \cdot 250002 \cdot \pi \cdot i)$$

$$Zlisn\_1(s) := \frac{\left(R_1 + \frac{1}{s \cdot C_{lisn1}}\right) \cdot \left(R_2 + \frac{1}{s \cdot C_{lisn2}} + s \cdot L_{lisn}\right)}{\left(R_1 + \frac{1}{s \cdot C_{lisn1}}\right) + \left(R_2 + \frac{1}{s \cdot C_{lisn2}} + s \cdot L_{lisn}\right)}$$

$$Zlisn_j := Zlisn\_1(j \cdot 250002 \cdot \pi \cdot i)$$

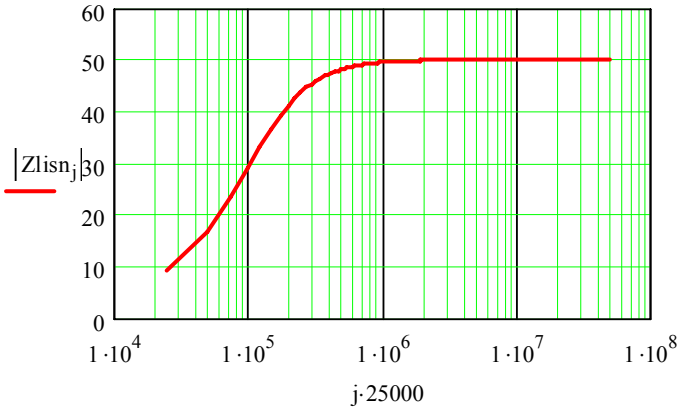

Load CM/DM Noise - Network I

Lisn1 := READPRN("lisn1_N1_5n_nsource.txt")

Lisn2 := READPRN("lisn2_N1_5n_nsource.txt")

i := 1.. 19999

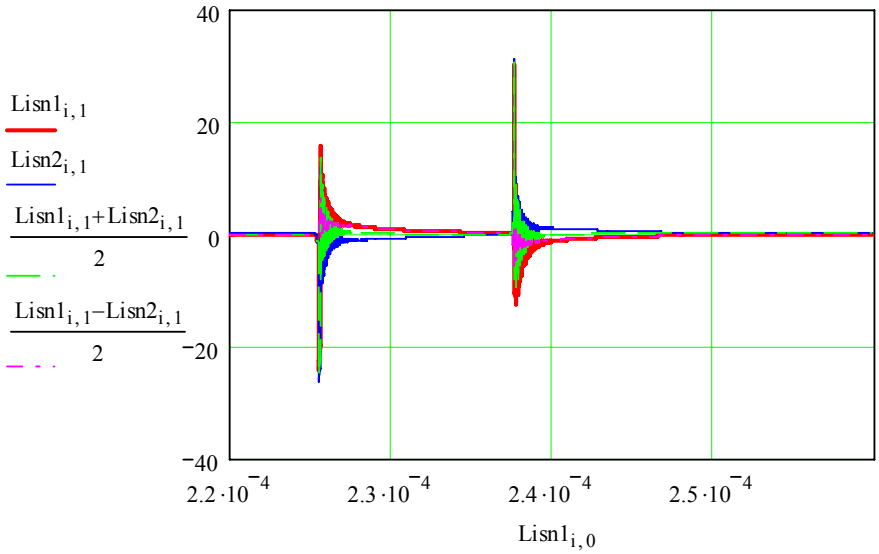

Transfer Time Domain Waveform to Frequency Domain

$L1_i := Lisn1_{i,1}$

Lisn1_net1 := CFFT(L1)

$L2_i := Lisn2_{i,1}$

Lisn2_net1 := CFFT(L2)

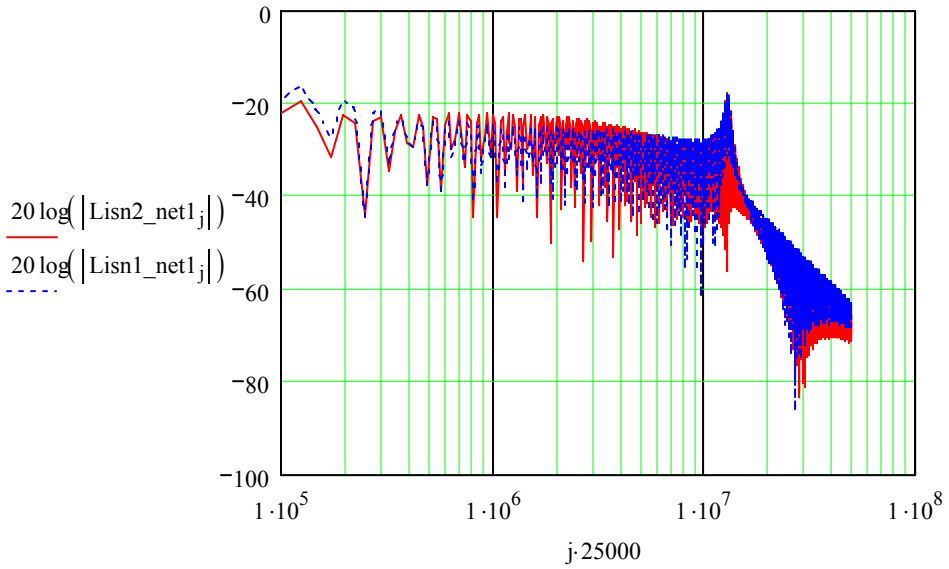

$$DM\_net1 := \frac{Lisn1\_net1 - Lisn2\_net1}{2}$$

$$CM\_net1 := \frac{Lisn1\_net1 + Lisn2\_net1}{2}$$

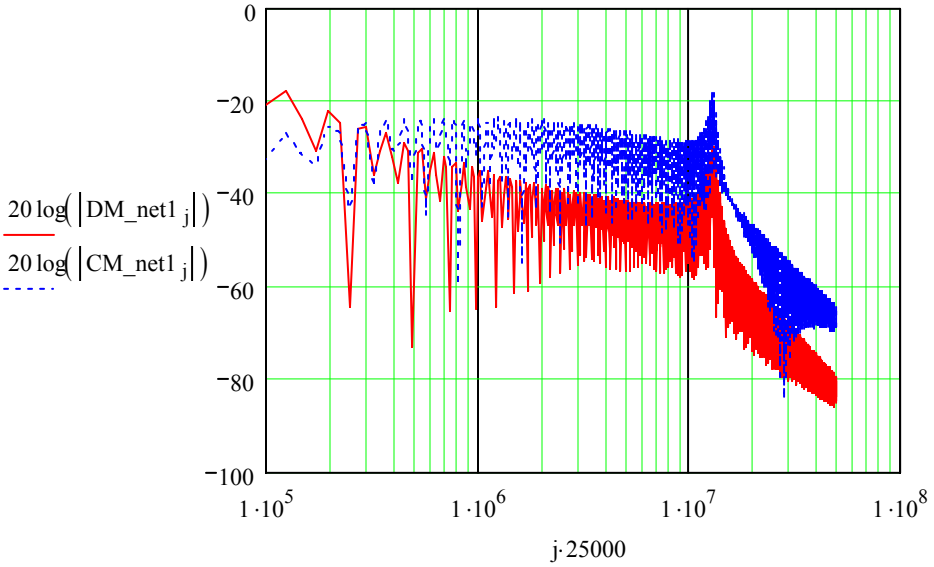

$R1\_cm := 0 \cdot 10^{-3}$

$L1\_cm := 0 \cdot 10^{-9}$

$C1\_cm := 280 \cdot 10^{-12}$

$$Zcm(s) := R1\_cm + s \cdot L1\_cm + \frac{1}{s \cdot C1\_cm}$$

$Zcm_j := Zcm(j \cdot 25000\, 2 \cdot \pi \cdot i)$

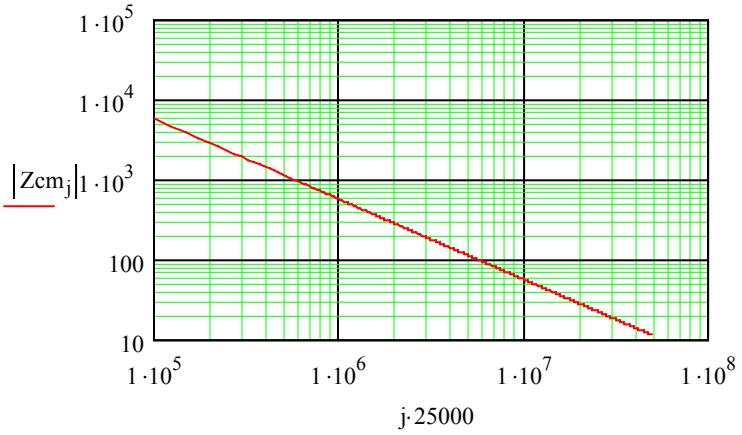

$$U1\_net1_j := \left(Z\_part1_j\right) \cdot \frac{Lisn1\_net1_j}{50}$$

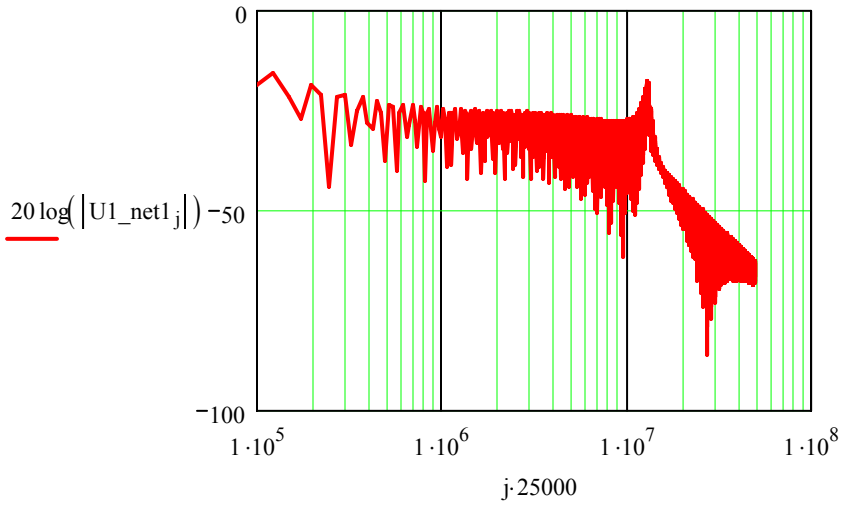

$$U2\_net1_j := \left(Z\_part1_j\right) \cdot \frac{Lisn2\_net1_j}{50}$$

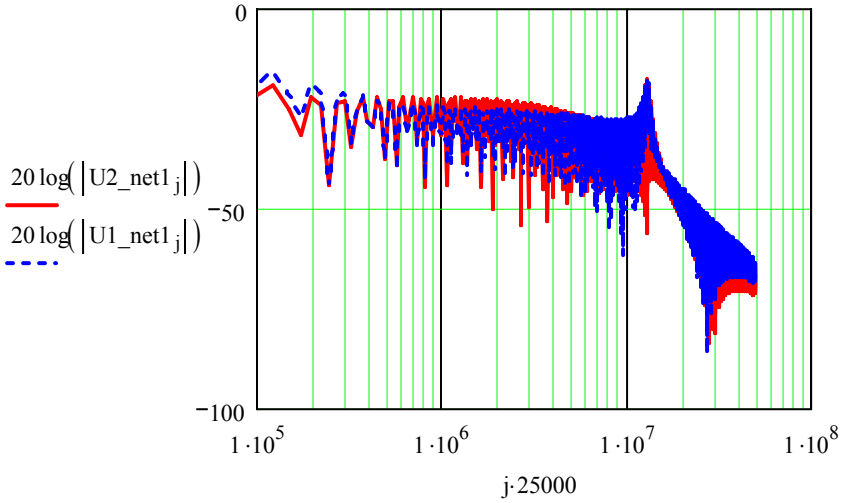

$$U3\_net1_j := -\left[\frac{CM\_net1_j}{25} \cdot \left(1 + \frac{Z\_part1_j}{Z\_part2_j}\right) \cdot Zcm_j\right]$$

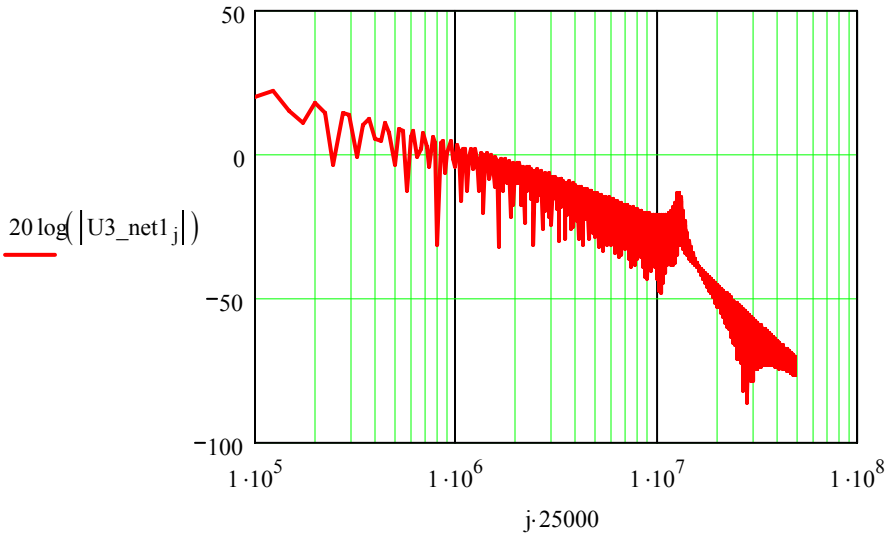

Propagation Path Impedance Network I

$R1 := 100 \cdot 10^{-3}$

$L1 := 10 \cdot 10^{-9}$

$C1 := 3900 \cdot 10^{-6}$

$$Z11\_DM\_v11(s) := R1 + s \cdot L1 + \frac{1}{s \cdot C1}$$

$Z11\_DM\_v1_j := Z11\_DM\_v11(j \cdot 25000 2 \cdot \pi \cdot i)$

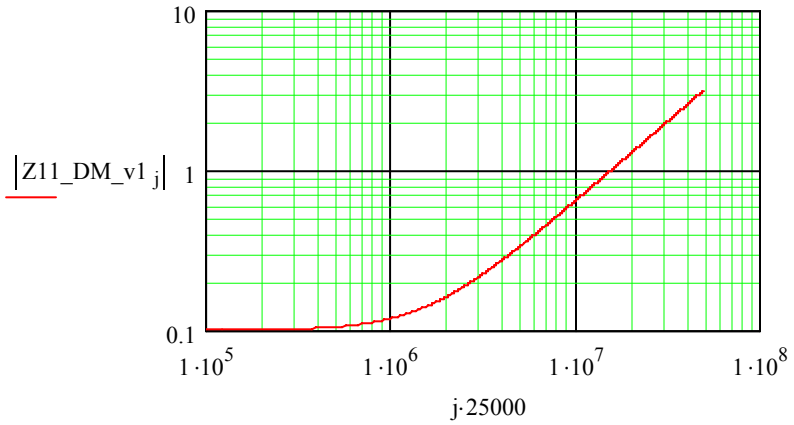

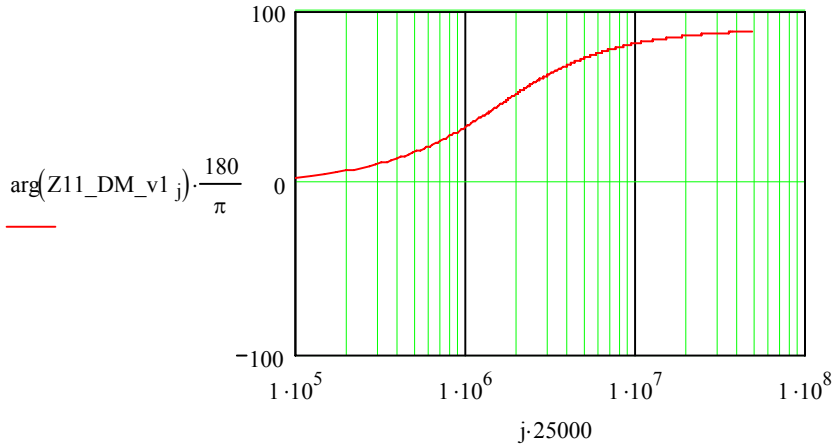

$$Z22\_DM\_v11(s) := R1 + s \cdot L1 + \frac{1}{s \cdot C1}$$

$$Z22\_DM\_v1_j := Z22\_DM\_v11(j \cdot 250002 \cdot \pi \cdot i)$$

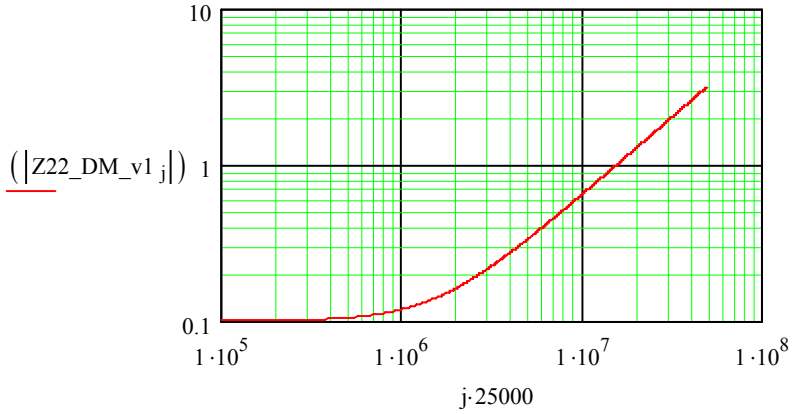

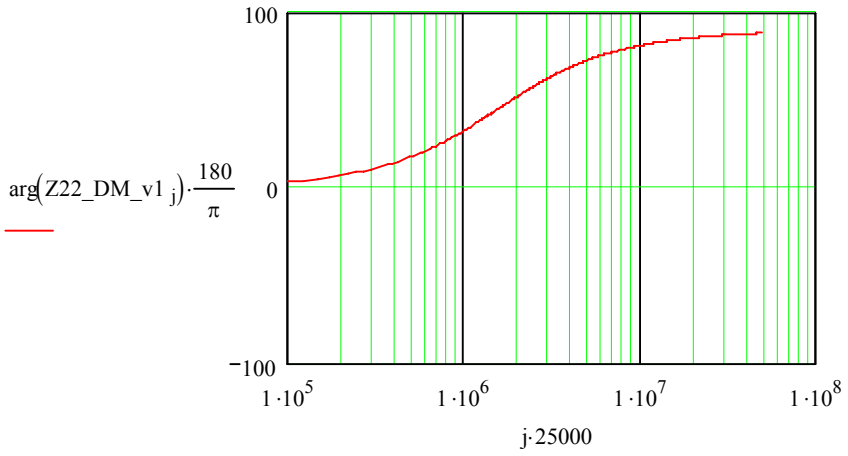

$$Z21\_DM\_v11(s) := R1 + s \cdot L1 + \frac{1}{s \cdot C1}$$

$$Z21\_DM\_v1_j := Z21\_DM\_v11(j \cdot 250002 \cdot \pi \cdot i)$$

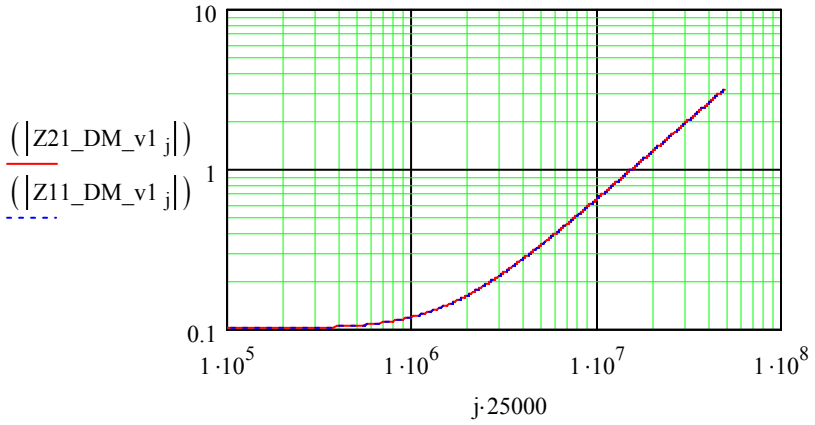

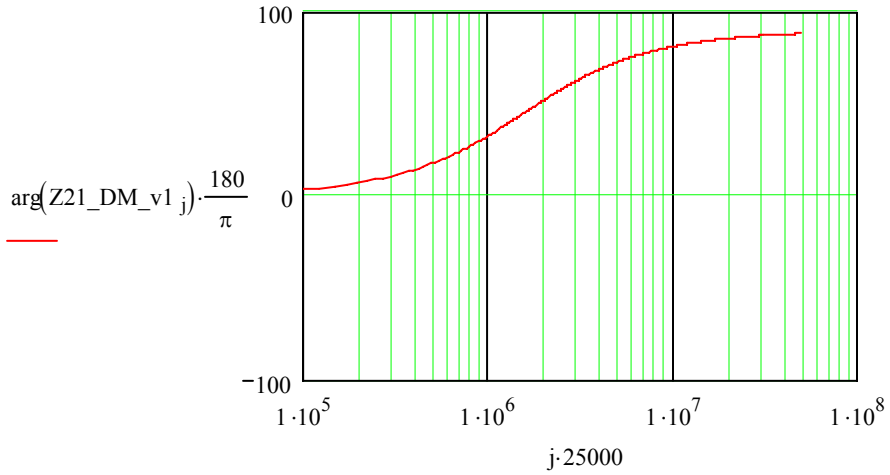

Load CM/DM Noise - Network IV

Lisn11 := READPRN("lisn1_N2_5n_nsource.txt")

Lisn22 := READPRN("lisn2_N2_5n_nsource.txt")

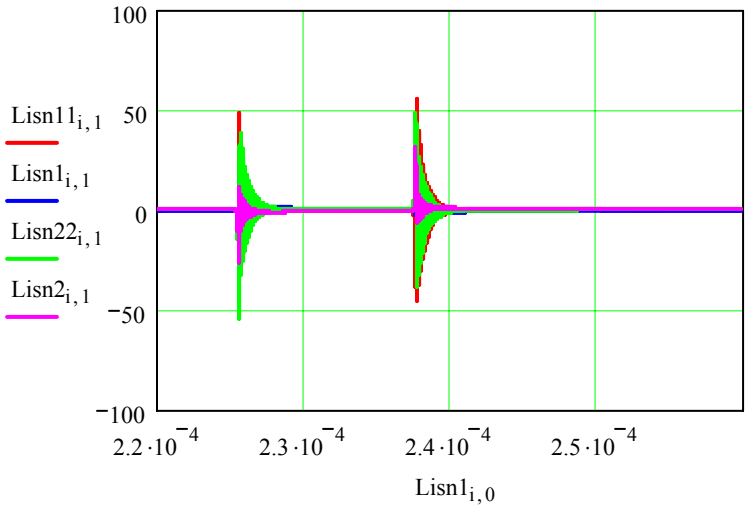

Transfer Time Domain Waveform to Frequency Domain

$L11_i := Lisn11_{i,1}$

Lisn1_net2 := CFFT(L11)

$L22_i := Lisn22_{i,1}$

Lisn2_net2 := CFFT(L22)

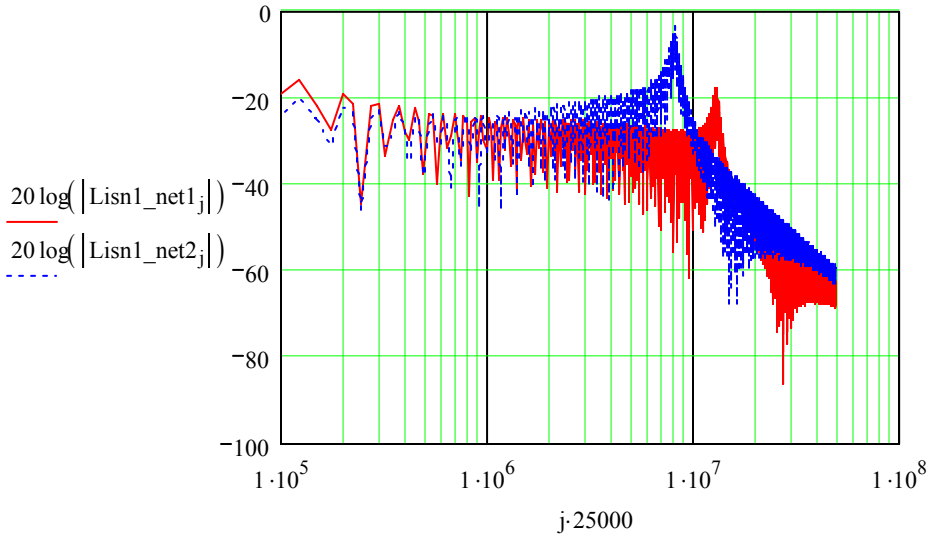

$$DM\_net2 := \frac{Lisn1\_net2 - Lisn2\_net2}{2}$$

$$CM\_net2 := \frac{Lisn1\_net2 + Lisn2\_net2}{2}$$

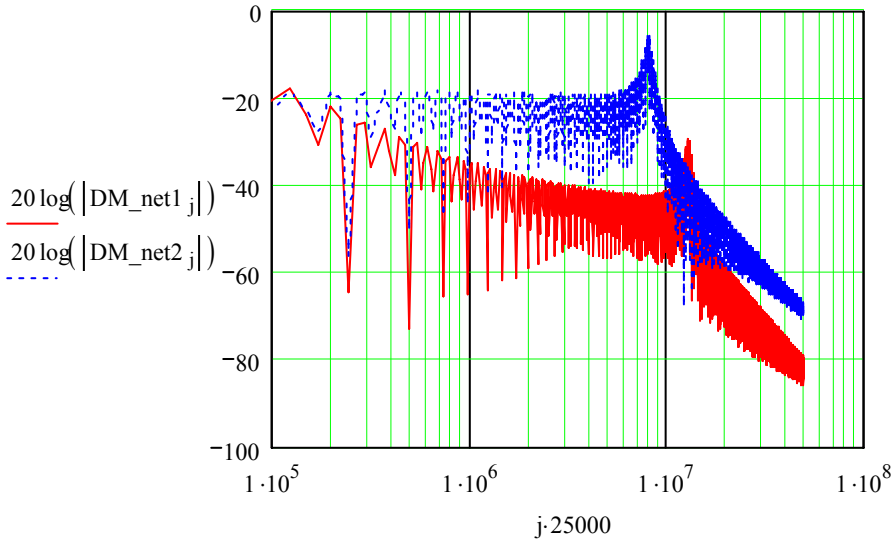

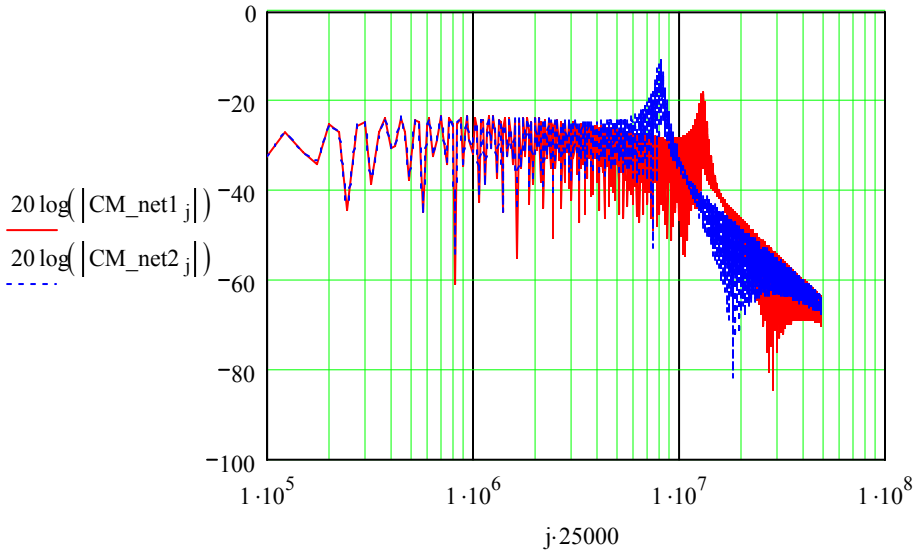

$$U1\_net2_j := \left(Z\_part1_j\right) \cdot \frac{Lisn1\_net2_j}{50}$$

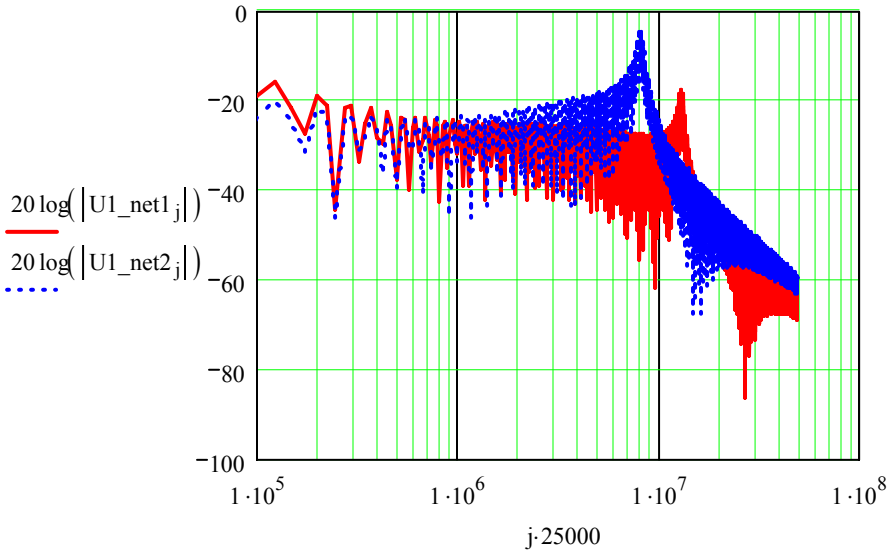

$$U2\_net2_j := \left(Z\_part1_j\right) \cdot \frac{Lisn2\_net2_j}{50}$$

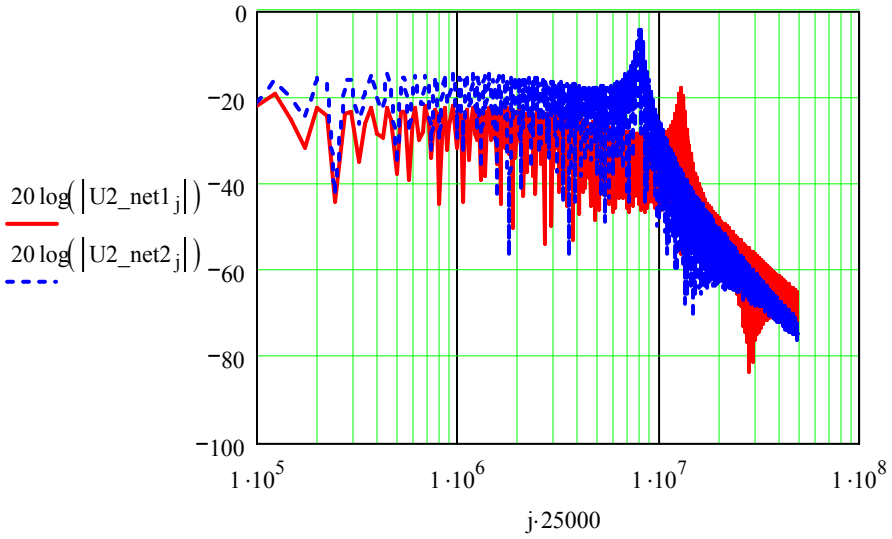

$$U3\_net2_j := -\left[\frac{CM\_net2_j}{25}\cdot\left(1+\frac{Z\_part1_j}{Z\_part2_j}\right)\cdot Zcm_j\right]$$

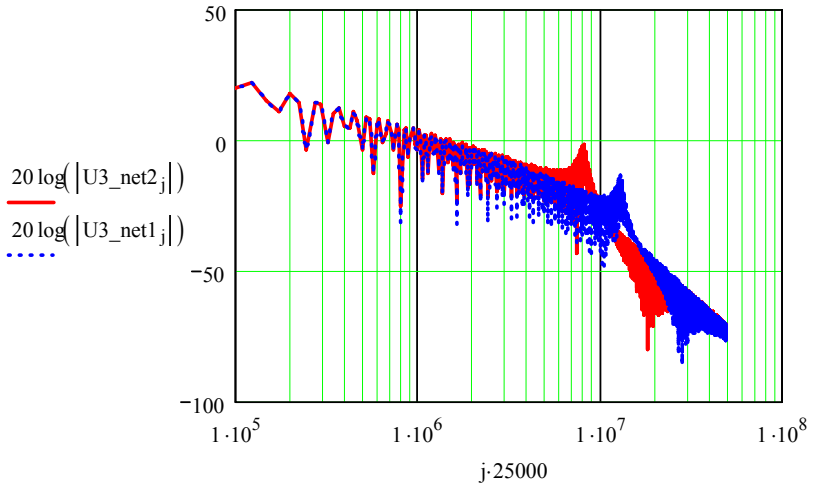

Propagation Path Impedance Network IV

$R1 := 10\cdot 10^{-3}$

$L1 := 120\cdot 10^{-9}$

$C1 := 3900\cdot 10^{-6}$

$$Z11\_DM\_v44(s) := R1 + s\cdot L1 + \frac{1}{s\cdot C1}$$

$$Z11\_DM\_v2_j := Z11\_DM\_v44\left(j\cdot 25000\,2\cdot\pi\cdot i\right)$$

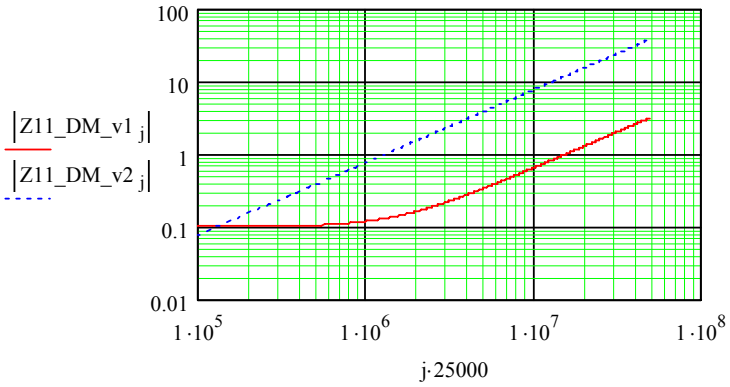

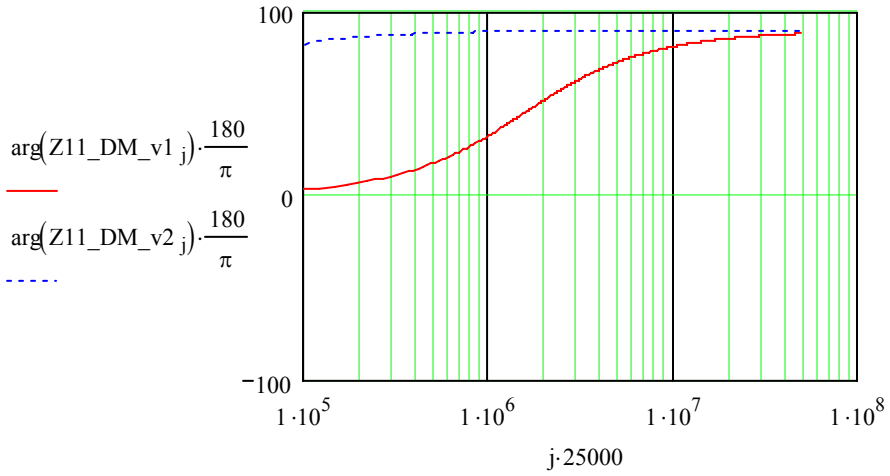

$$Z22\_DM\_v44(s) := R1 + s \cdot L1 + \frac{1}{s \cdot C1}$$

$$Z22\_DM\_v2_j := Z22\_DM\_v44(j \cdot 250002 \cdot \pi \cdot i)$$

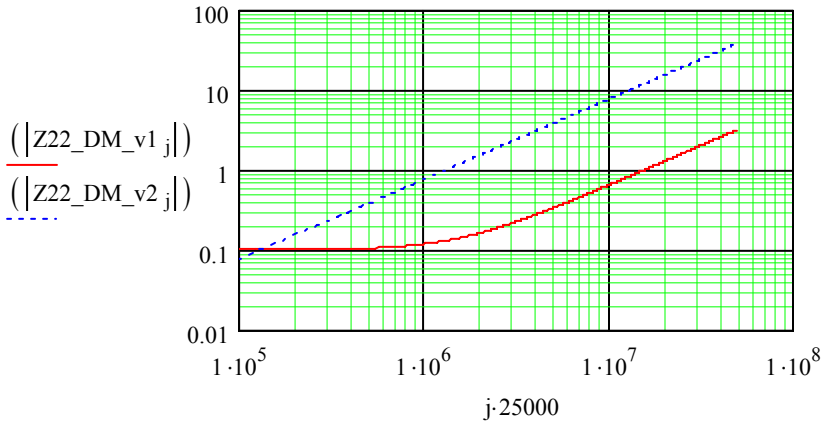

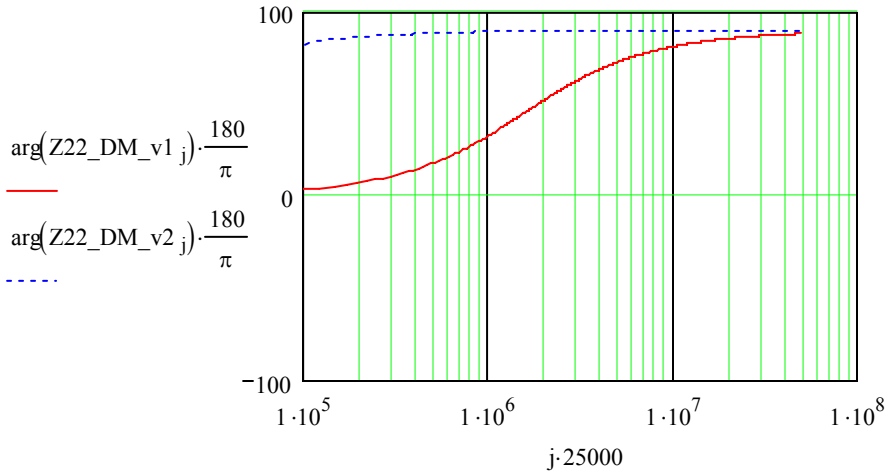

$$Z21\_DM\_v44(s) := R1 + s \cdot L1 + \frac{1}{s \cdot C1}$$

$$Z21\_DM\_v2_j := Z21\_DM\_v44(j \cdot 250002 \cdot \pi \cdot i)$$

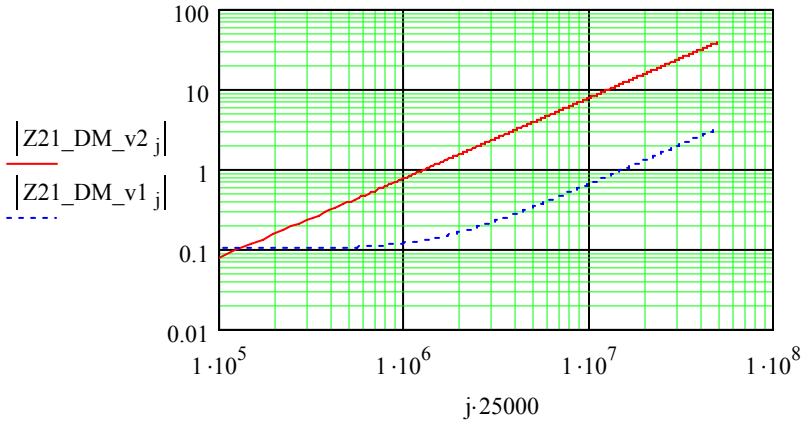

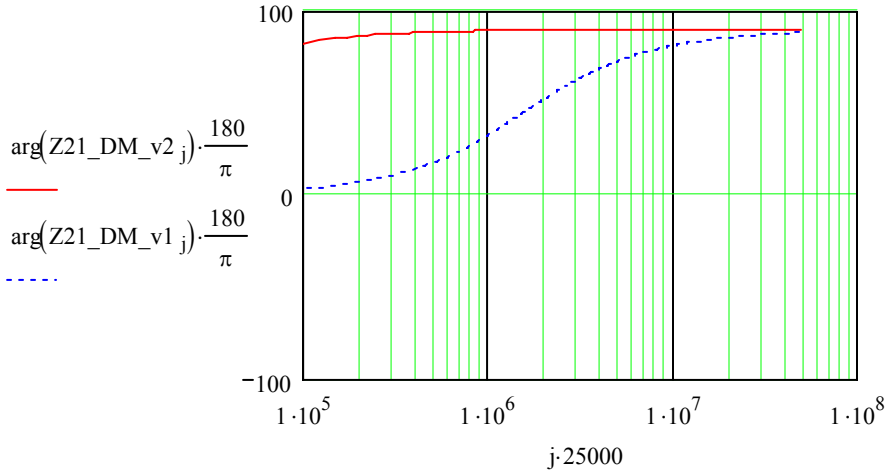

Source Model Derived from Net1and Net4

$$Zs1_j := \frac{\left(U3\_net1_j - U1\_net1_j\right) - \left(U3\_net2_j - U1\_net2_j\right)}{U1\_net1_j \cdot \left(\frac{1}{Zlisn_j} + \frac{1}{Z11\_DM\_v1_j}\right) - U1\_net2_j \cdot \left(\frac{1}{Zlisn_j} + \frac{1}{Z11\_DM\_v2_j}\right) + U2\_net2_j \cdot \left(\frac{1}{Z11\_DM\_v2_j}\right) - U2\_net1_j \cdot \left(\frac{1}{Z11\_DM\_v1_j}\right)}$$

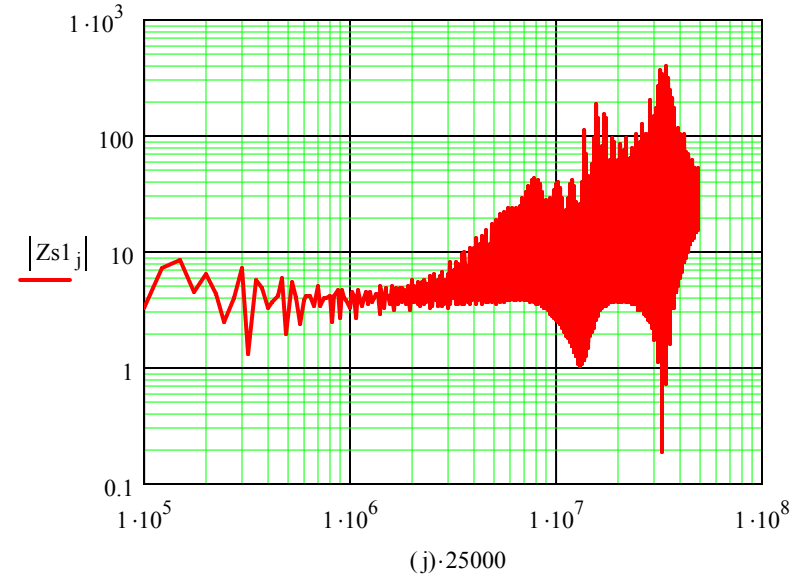

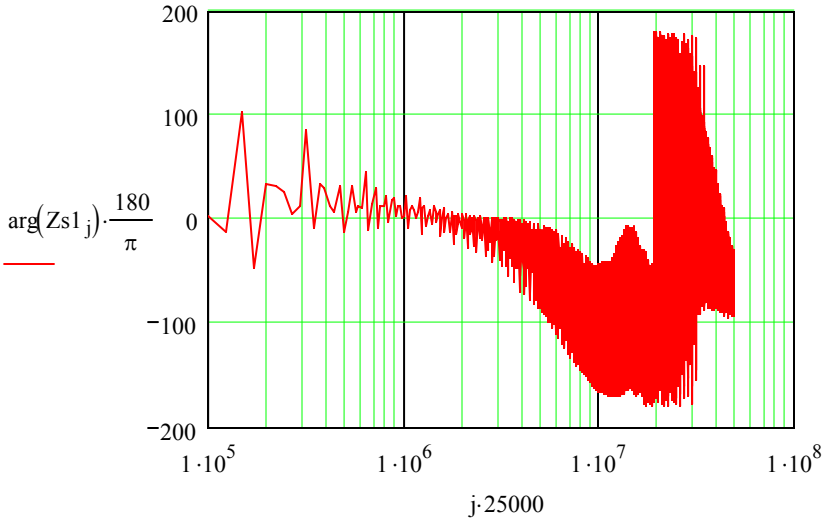

$$Is1_j := U1\_net1_j \cdot \left(\frac{1}{Zlisn_j} + \frac{1}{Z11\_DM\_v1_j} \right) - U2\_net1_j \cdot \left(\frac{1}{Z11\_DM\_v1_j} \right) + \frac{U1\_net1_j - U3\_net1_j}{Zs1_j}$$

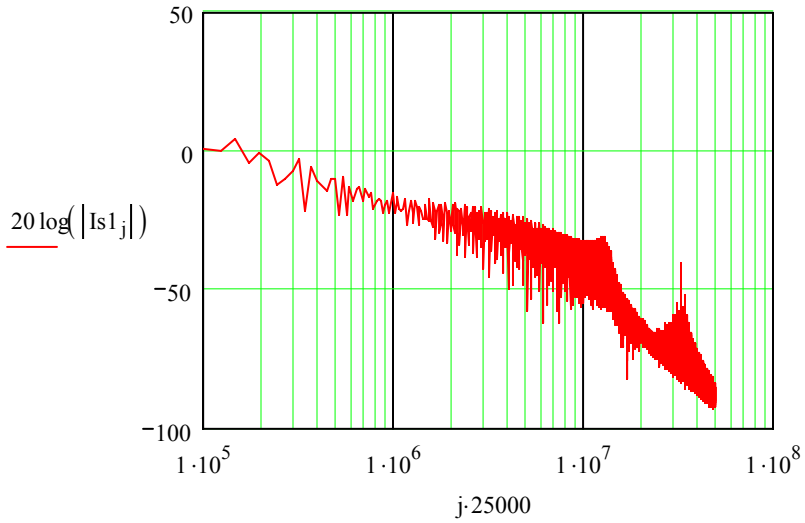

$$Zs2_j := \frac{\left(U3\_net1_j - U2\_net1_j\right) - \left(U3\_net2_j - U2\_net2_j\right)}{U2\_net1_j \cdot \left(\frac{1}{Zlisn_j} + \frac{1}{Z11\_DM\_v1_j}\right) - U2\_net2_j \cdot \left(\frac{1}{Zlisn_j} + \frac{1}{Z11\_DM\_v2_j}\right) + U1\_net2_j \cdot \left(\frac{1}{Z11\_DM\_v2_j}\right) - U1\_net1_j \cdot \left(\frac{1}{Z11\_DM\_v1_j}\right)}$$

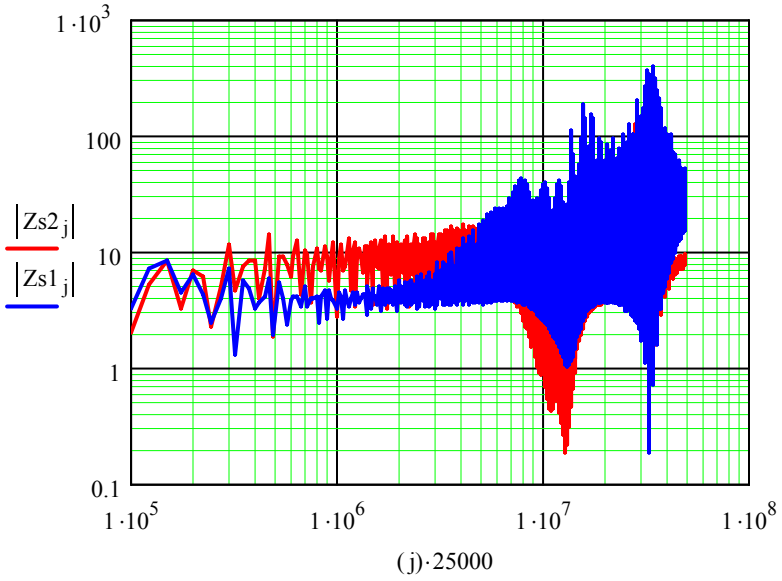

$$Is2_j := -\left[U2\_net1_j \cdot \left(\frac{1}{Zlisn_j} + \frac{1}{Z11\_DM\_v1_j}\right) - U1\_net1_j \cdot \left(\frac{1}{Z11\_DM\_v1_j}\right) + \frac{U2\_net1_j - U3\_net1_j}{Zs2_j}\right]$$

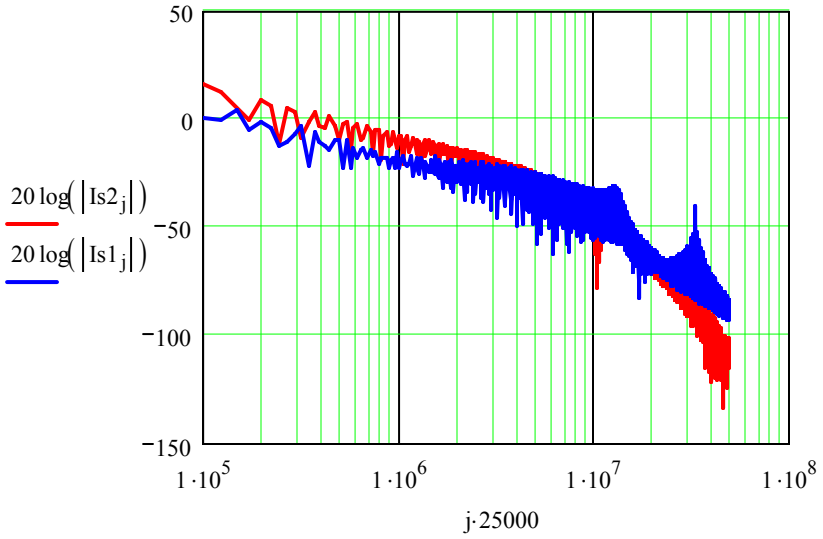

$$Is\_total_j := \frac{Is1_j \cdot Zs1_j + Is2_j \cdot Zs2_j}{Zs1_j + Zs2_j} \qquad Zs\_total_j := Zs1_j + Zs2_j$$

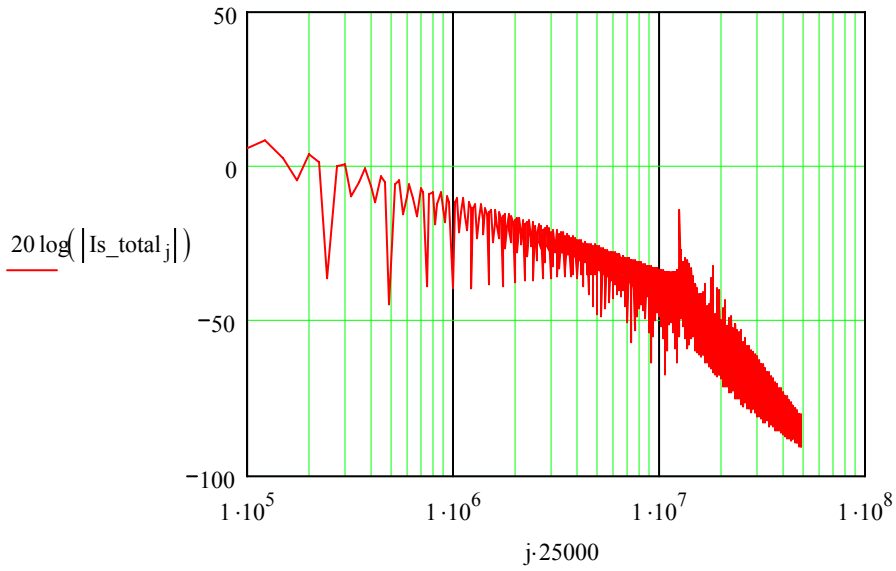

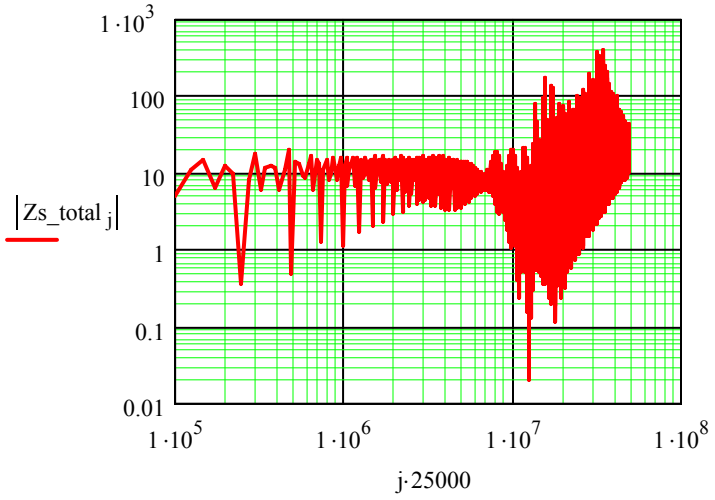

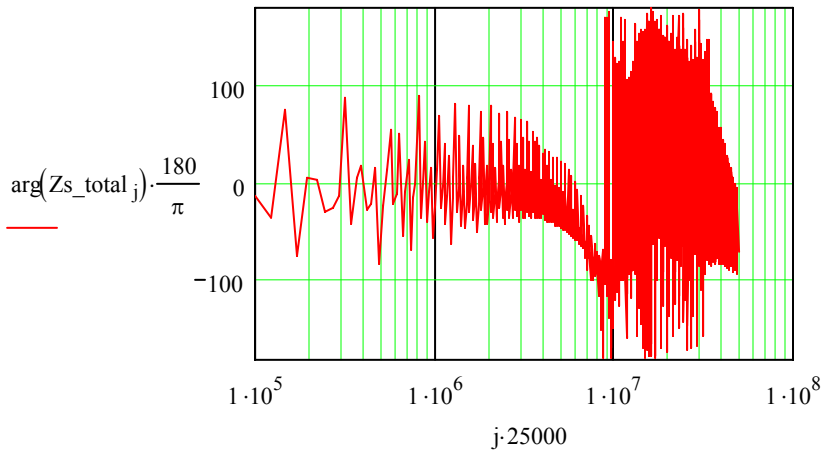

Load CM/DM Noise - Network V

Lisn111 := READPRN("pre_dmdec100n_20nH.txt")

Lisn222 := READPRN("pre_cmdec100n_20nH.txt")

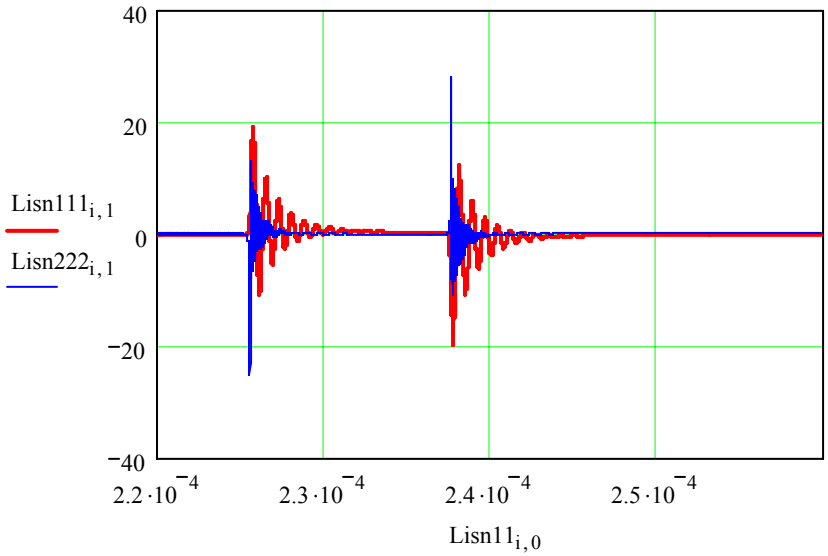

Transfer Time Domain Waveform to Frequency Domain

$L111_i := Lisn111_{i,1}$

DM_net3 := CFFT(L111)

$L222_i := Lisn222_{i,1}$

CM_net3 := CFFT(L222)

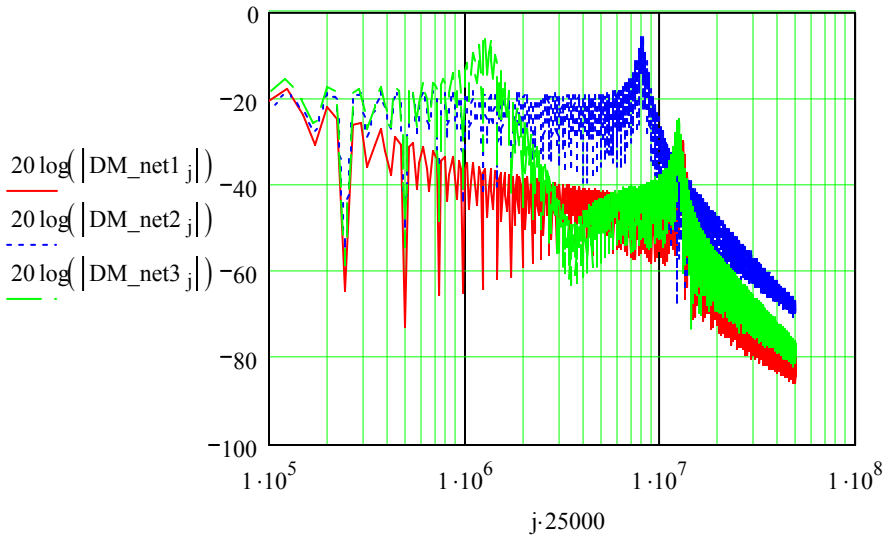

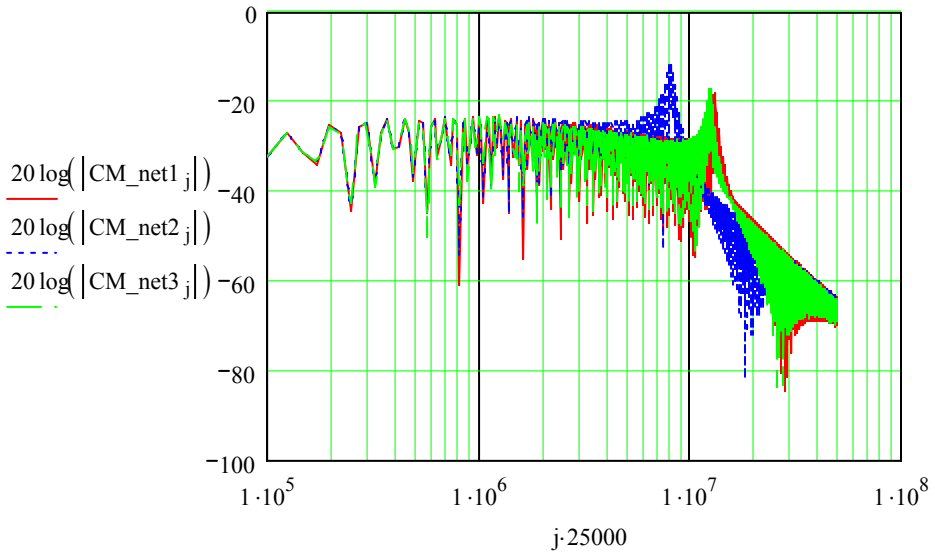

Propagation Path Impedance Network V

$R1 := 100 \cdot 10^{-3}$ $\quad Lbus := 4 \cdot 10^{-9}$ $\quad R2 := 100 \cdot 10^{-3}$ $\quad Rs := 100 \cdot 10^{-3}$

$L1 := 124 \cdot 10^{-9}$ $\quad Rlisn := 100$ $\quad L2 := 20 \cdot 10^{-9}$ $\quad Ls := 60 \cdot 10^{-9}$

$C1 := 3900 \cdot 10^{-6}$ $\quad Rbus := 40 \cdot 10^{-3}$ $\quad C2 := 100 \cdot 10^{-9}$ $\quad Cs := 1 \cdot 10^{-9}$

$$Z\_dec(s) := \left(R2 + s \cdot L2 + \frac{1}{s \cdot C2} \right)$$

$$Zdec_j := Z\_dec(j \cdot 250002 \cdot \pi \cdot i)$$

$$Z\_dc(s) := \left(R1 + s \cdot L1 + \frac{1}{s \cdot C1} \right)$$

$$Zdc_j := Z\_dc(j \cdot 250002 \cdot \pi \cdot i)$$

$$Z\_Lbus(s) := s \cdot Lbus$$

$$ZLbus_j := Z\_Lbus(j \cdot 250002 \cdot \pi \cdot i)$$

$$Z\_org(s) := \left(Rs + s \cdot Ls + \frac{1}{s \cdot Cs} \right)$$

$$Zs\_org_j := Z\_org(j \cdot 250002 \cdot \pi \cdot i)$$

$$Z11\_DM\_v55(s) := \left(R1 + s \cdot L1 + \frac{1}{s \cdot C1}\right)$$

$$Z11\_DM\_v3_j := Z11\_DM\_v55\left(j \cdot 250002 \cdot \pi \cdot i\right)$$

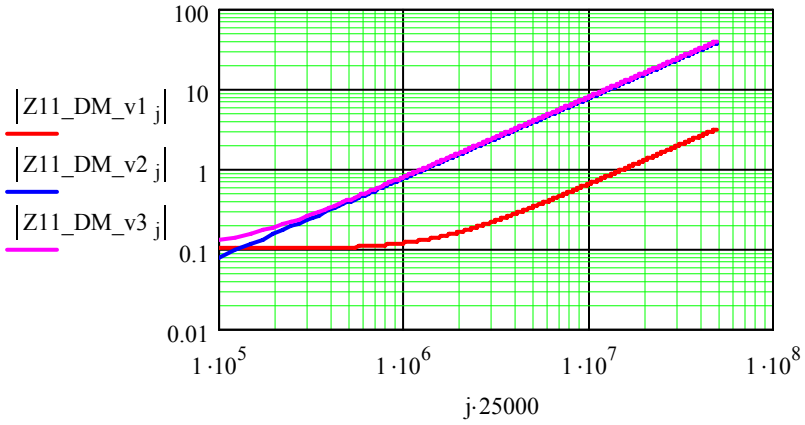

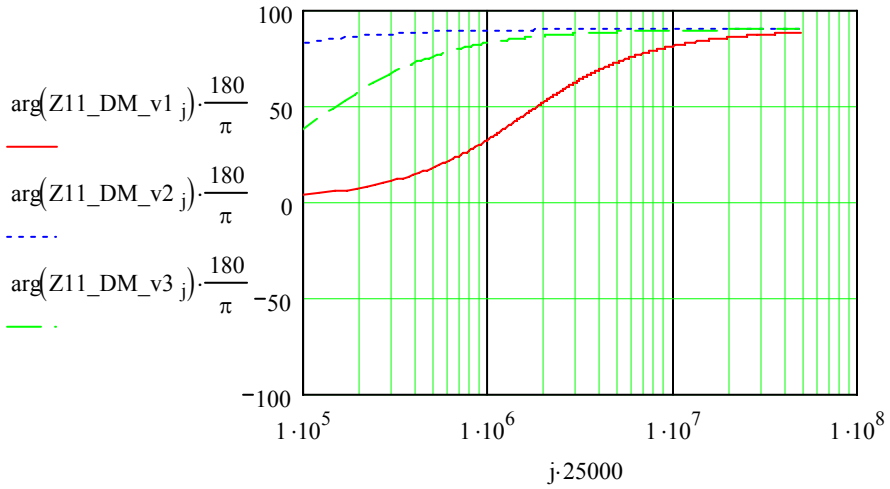

$$Z22\_DM\_v55(s) := \left(R1 + s \cdot L1 + \frac{1}{s \cdot C1}\right) + s \cdot Lbus$$

$$Z22\_DM\_v3_j := Z22\_DM\_v55\left(j \cdot 250002 \cdot \pi \cdot i\right)$$

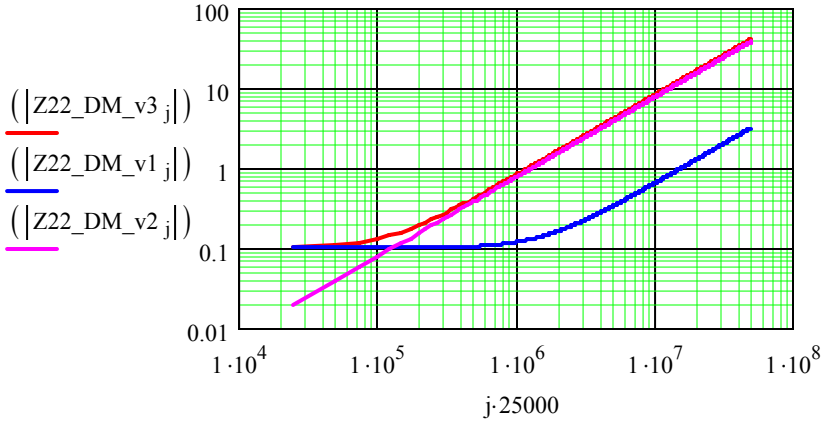

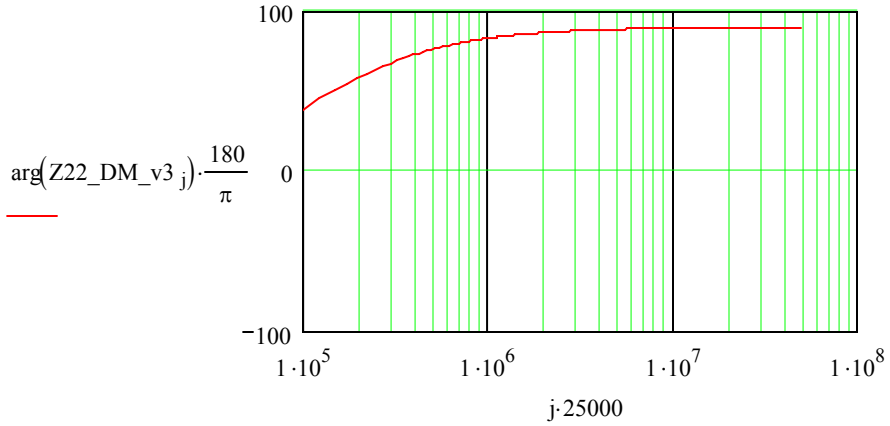

$$Z21\_DM\_v55(s) := \left(R1 + s \cdot L1 + \frac{1}{s \cdot C1}\right)$$

$$Z21\_DM\_v3_j := Z21\_DM\_v55(j \cdot 250002 \cdot \pi \cdot i)$$

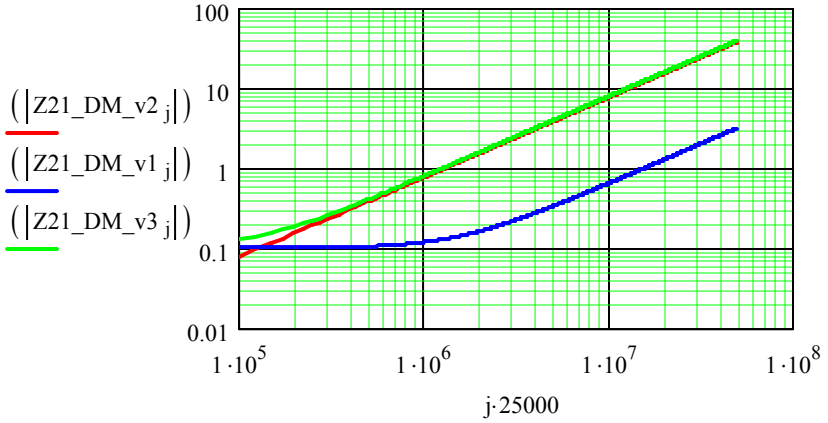

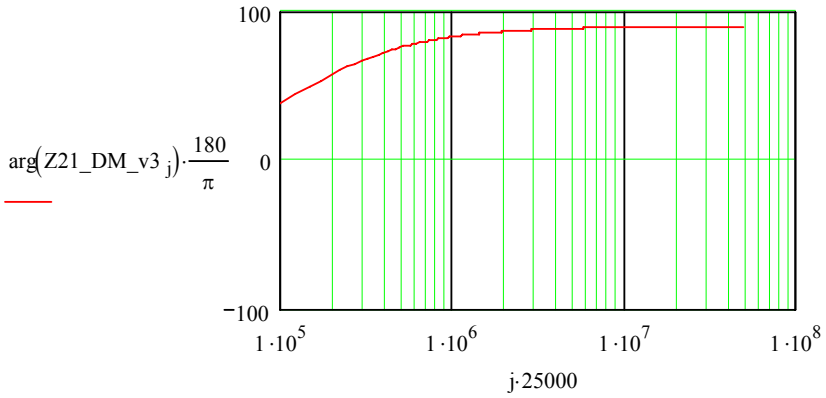

EMI Noise and Voltage Stress Prediction of Network V based on Derived MTB Source Model

$$T := 40\cdot 10^{-6}$$

$$a11_j := \frac{1}{Zlisn_j} + \frac{1}{Zdec_j} + \frac{1}{Zdc_j} + \frac{1}{Zs1_j} \qquad a12_j := \frac{-1}{Zdec_j} + \frac{-1}{Zdc_j} \qquad a13_j := \frac{-1}{Zs1_j}$$

$$a21_j := \frac{-1}{Zdec_j} + \frac{-1}{Zdc_j} \qquad a22_j := \frac{1}{Zlisn_j} + \left(\frac{1}{Zdec_j} + \frac{1}{Zdc_j}\right) + \frac{1}{Zs2_j} \qquad a23_j := \frac{-1}{Zs2_j}$$

$$a31_j := \frac{-1}{Zs1_j} \qquad a32_j := \frac{-1}{Zs2_j} \qquad a33_j := \frac{1}{Zs1_j} + \frac{1}{Zcm_j} + \frac{1}{Zs2_j}$$

$$A_j := \begin{pmatrix} a11_j & a12_j & a13_j \\ a21_j & a22_j & a23_j \\ a31_j & a32_j & a33_j \end{pmatrix}$$

$$A11_j := \left|\begin{pmatrix} a22_j & a23_j \\ a32_j & a33_j \end{pmatrix}\right| \qquad A21_j := -\left|\begin{pmatrix} a21_j & a23_j \\ a31_j & a33_j \end{pmatrix}\right| \qquad A31_j := \left|\begin{pmatrix} a21_j & a22_j \\ a31_j & a32_j \end{pmatrix}\right|$$

$$A12_j := -\left|\begin{pmatrix} a12_j & a13_j \\ a32_j & a33_j \end{pmatrix}\right| \qquad A22_j := \left|\begin{pmatrix} a11_j & a13_j \\ a31_j & a33_j \end{pmatrix}\right| \qquad A32_j := -\left|\begin{pmatrix} a11_j & a12_j \\ a31_j & a32_j \end{pmatrix}\right|$$

$$A13_j := \left| \begin{pmatrix} a12_j & a13_j \\ a22_j & a23_j \end{pmatrix} \right| \qquad A23_j := -\left| \begin{pmatrix} a11_j & a13_j \\ a21_j & a23_j \end{pmatrix} \right| \qquad A33_j := \left| \begin{pmatrix} a11_j & a12_j \\ a21_j & a22_j \end{pmatrix} \right|$$

$$B_j := \left| A_j \right|$$

$$U1\_net1\_ver_j := \frac{1}{B_j} \cdot \left[A11_j \cdot Is1_j + A21_j \cdot \left(-Is2_j \right) + A31_j \cdot \left(Is2_j - Is1_j \right) \right]$$

$$U2\_net1\_ver_j := \frac{1}{B_j} \cdot \left[A12_j \cdot Is1_j + A22_j \cdot \left(-Is2_j \right) + A32_j \cdot \left(Is2_j - Is1_j \right) \right]$$

$$U3\_net1\_ver_j := \frac{1}{B_j} \cdot \left[A13_j \cdot Is1_j + A23_j \cdot \left(-Is2_j \right) + A33_j \cdot \left(Is2_j - Is1_j \right) \right]$$

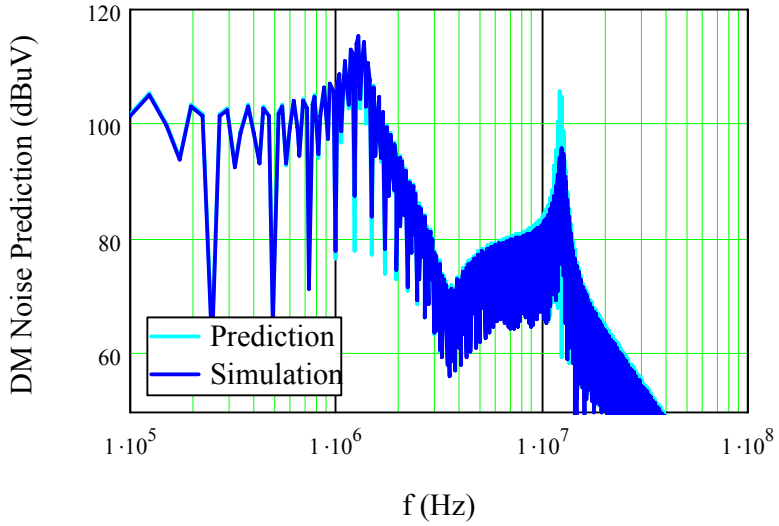

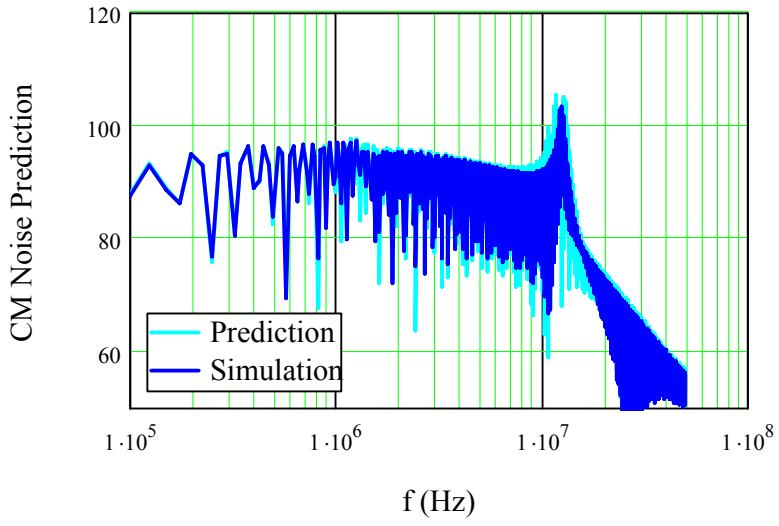

$$Ustress_j := U3\_net1\_ver_j - U2\_net1\_ver_j$$

$$ai\_Is\_non := Ustress + \overline{Ustress} \qquad bi\_Is\_non := \frac{\overline{Ustress} - Ustress}{i}$$

$$U_{MN}(t) := \frac{ai\_Is\_non_0}{2} + \sum_{k=1}^{2000} \left(ai\_Is\_non_k \cdot \cos\left(\frac{k \cdot \pi \cdot 2t}{T}\right) + bi\_Is\_non_k \cdot \sin\left(\frac{k \cdot \pi \cdot 2 \cdot t}{T}\right)\right)$$

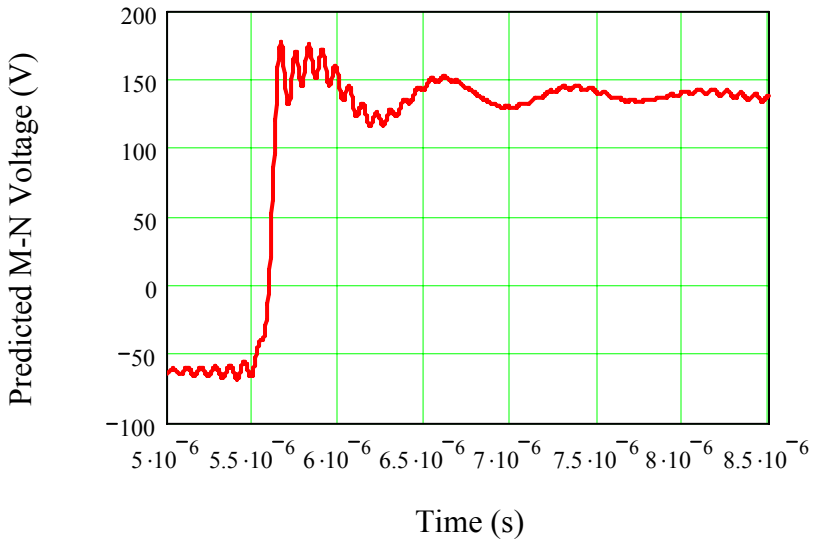

Vita

The author, Qian Liu, was born in Nanchang, Jiangxi Province, China in 1977. She received B. S. and M. S. degree from Zhejiang University in 1998 and 2001, respectively. Since August 2001, she has been working towards a Ph. D degree at the Bradley Department of Electrical and Computer Engineering, Virginia Polytechnic Institute and State University. Working as a research assistant at the Center for Power Electronics Systems (CPES), her research interests include EMI noise modeling and prediction, high-frequency high-power-density DC/DC converters, and optimization of motor drive systems.